INFORMATION TO USERS

This reproduction was made from a copy of a document sent to us for microfilming. While the most advanced technology has been used to photograph and reproduce this document, the quality of the reproduction is heavily dependent upon the quality of the material submitted.

The following explanation of techniques is provided to help clarify markings or notations which may appear on this reproduction.

1. The sign or "target" for pages apparently lacking from the document photographed is "Missing Page(s)". If it was possible to obtain the missing page(s) or section, they are spliced into the film along with adjacent pages. This may have necessitated cutting through an image and duplicating adjacent pages to assure complete continuity.

2. When an image on the film is obliterated with a round black mark, it is an indication of either blurred copy because of movement during exposure, duplicate copy, or copyrighted materials that should not have been filmed. For blurred pages, a good image of the page can be found in the adjacent frame. If copyrighted materials were deleted, a target note will appear listing the pages in the adjacent frame.

3. When a map, drawing or chart, etc., is part of the material being photographed, a definite method of "sectioning" the material has been followed. It is customary to begin filming at the upper left hand corner of a large sheet and to continue from left to right in equal sections with small overlaps. If necessary, sectioning is continued again—beginning below the first row and continuing on until complete.

4. For illustrations that cannot be satisfactorily reproduced by xerographic means, photographic prints can be purchased at additional cost and inserted into your xerographic copy. These prints are available upon request from the Dissertations Customer Services Department.

5. Some pages in any document may have indistinct print. In all cases the best available copy has been filmed.

University Microfilms International
300 N. Zeeb Road
Ann Arbor, MI 48106

Kuo, Chen-Chih

MORPHOLOGY AND PROPERTIES OF TRANS-1,4-POLYISOPRENE CRYSTALLIZED FROM SOLUTION

City University of New York PH.D. 1984

PLEASE NOTE:

In all cases this material has been filmed in the best possible way from the available copy. Problems encountered with this document have been identified here with a check mark _✓_.

1. Glossy photographs or pages ✓
2. Colored illustrations, paper or print _____
3. Photographs with dark background ✓
4. Illustrations are poor copy _____
5. Pages with black marks, not original copy _____
6. Print shows through as there is text on both sides of page _____
7. Indistinct, broken or small print on several pages ✓
8. Print exceeds margin requirements _____
9. Tightly bound copy with print lost in spine _____
10. Computer printout pages with indistinct print _____
11. Page(s) _____ lacking when material received, and not available from school or author.
12. Page(s) _____ seem to be missing in numbering only as text follows.
13. Two pages numbered _____. Text follows.
14. Curling and wrinkled pages _____
15. Other _____

MORPHOLOGY AND PROPERTIES OF TRANS-1,4-POLYISOPRENE CRYSTALLIZED FROM SOLUTION

By

CHEN-CHIH KUO

A Dissertation Submitted to the Graduate Faculty in Chemistry in Partial Fulfillment of the Requirements for the Degree of Doctor of Philosophy, The City University of New York.

1984

This manuscript has been read and accepted for the Graduate Faculty in Chemistry in satisfaction of the dissertation requirement for the degree of Doctor of Philosophy.

11/10/83
date

Arthur Woodward
Chairman of Examining Committee

10 November 1983
date

David C. Locke
Executive Officer

Harold Hoyer.

Jay C. Rummel

Supervisory Committee

The City University of New York

ABSTRACT

MORPHOLOGY AND PROPERTIES OF TRANS-1,4-POLYISOPRENE CRYSTALLIZED FROM SOLUTION

By

Chen-Chih Kuo

Adviser: Professor A.E. Woodward

Trans 1,4 polyisoprene (TPI) fractions with average number molecular weight ($\bar{M}_n$) from 4.7×10^3 to 2.5×10^5 and molecular weight distribution ($\bar{M}_w/\bar{M}_n$) of 2.0 to 1.3 were crystallized from solutions, mainly at a concentration of 1g per 100 cm^3, by cooling directly from 100°C to an apparent crystallization temperature (T_c) of -15 to +32°C, by precooling to 0°C, redissolving at 35-45°C and crystallizing at T_c, and by cooling to 0°C and heating to 10°, 20°, or 30°C. Most of the structures obtained were characterized, while suspended in the crystallization liquid, by interference contrast microscopy and with crossed polaroids; the crystalline fraction from the density, and the crystal form, from x-ray diffraction and differential scanning calorimetry, were determined for the dry products. The morphology obtained by direct crystallization was dependent on molecular weight, crystallization temperature and solvent with α- and β-hedrites, α- and β-spherulites and β-aggregates of cup-shaped lamellas being found. The precooling method yielded overgrown lamellas in most cases, however more

complex morphologies developed when the thermal history was changed. The density depended on molecular weight, concentration and crystallization temperature. The crystallinity was mainly a function of crystal form and molecular weight. The equation of Tseng, Herman, Woodward and Newman was used to explain the molecular weight dependence of the crystallinity at low $\bar{M}_n$ and to calculate the average number of monomer units per fold and interlamellar traverse. Epoxidation of some TPI structures suspended in amyl acetate at $0^{o}C$ was carried out. At high concentrations of the epoxidizing agent, metachloroperbenzoic acid, the fraction epoxidized approached or exceeded the non-crystalline fraction was obtained from density measurement.

ACKNOWLEDGEMENT

I am very grateful to my mentor, Professor A. E. Woodward for his excellent leadership during these studies and his patient assistance on this thesis. I would extend special thanks to Professor H. Hoyer and Professor J. Rennert for their helpful suggestions and discussion.

I would like to thank Professor G. Odian for his help in my early years at the City University of New York.

I wish to express my gratitude to the following organizations and individuals for their valuable assistance in this work.

To the Staten Island College for use of the differential scanning calorimetry and gel permeation chromatography, to the Chemistry and Biology Departments at the City College for use of proton NMR, X-ray diffraction, electron microscope and other instruments. Again I would like to thank Mr. H. G. Schimatz for the preparations and repairing of glass instruments, to Mr. P. Campione for the repairing of electronic instruments, to Mr. J. Downey for use of the electron microscope and to Mr. J. Bodnaruk for use of the dark room equipment.

Finally, I am deeply grateful to my preadvisors, Professor Y. Iwakura and Professor F. Toda in Japan for their previous encouragement and to my parents, Mr. and

Mrs. Y. C. Kuo in Taiwan, Republic of China, for their understanding and spiritual support.

TABLE OF CONTENTS

I. Introduction: 1

II. Experimental: 24

Preparation of Samples 24
Crystal Preparation 30
Optical Microscopy 32

1) Observation on a Cold Stage 32
2) Observation on a Hot Stage 33
3) Photography 33

Electron Microscopy 34
Wide Angle X-ray Diffraction 35
Density Measurement 36
Differential Scanning Calorimetry 39
Epoxidation and Proton NMR Analysis 39

III. Results: 41

Morphological Chracterization with Microscopy 41

1) The Influence of Crystallization Temperature and/or Molecular Weight 41

Type I: The Simplest Hedrites in Crystal Form 42
Type II: Sheaflike Hedrites with Weak Birefringence and α Form Structure 46
Type III and Type IV: Sheaflike Hedrites with Distinct Birefringence, Type III with β forms, and Type IV with α Form 50
Type V: Spherulites with Strong Birefringence in the β Form 66
Type VI: Cup-shaped Lameallar Aggregates with β Form 70

2) Effect of Concetration on TPI Crystallization 79

3) The Effect of Molecular Weight Distribution on TPI Crystallization 88

4) Effect of Solvent on TPI Crystallization 95

5) TPI Morphology Using Other Crystallization Methods 100

A. Precooling Method 100
B. Surface Crystallization By Solvent Evaporation from a Polymer Solution 106
C. Crystallization from Melt 109

Determination of Crystal Form 112

1) Wide Angle X-ray Diffraction 112
2) Differential Scanning Calorimetry Measurement 117

Stability of Cup-Shaped Lamellar Aggregates in Suspension 128

1) Annealing in Solution 131
2) Other Changes 139

Determination of Noncrystalline Content in TPI Structures from Solution 141

1) Density Measurements 141
2) Heat of Fusion Measurements 149
3) Epoxidation and Proton NMR Analysis 151

IV. Discussion: 163

The Morphologies of Multilayer Crystals 163
Influence of Crystallization Technique and Conditions on TPI 170
Crystal Form Determination 176
Density and Crystallinity 177
The Calculation of Average Number of Monomer Units in a Noncrystalline Chain Sequence 180
Epoxidation 188

V. Conclusion: 193

VI. References: 199

LIST OF FIGURES

Figure No.	Caption	Page
1.	Electron micrograph and electron diffraction pattern of polyethylene single crystals	2
	A). Electron micrograph of crystal from xylene	
	B). Electron diffraction pattern	
2.	Possible departures from strictly regular folding and defects in a single crystal	4
3.	Schematic representation of successive stages in the development of a spherulite from a chain folded precursor crystal	11
4.	Two electron micrographs of replicas of hedrites formed in the same melt crystallized thin film of poly(4-methyl pentene-1)	13
	A). An edge-on view of a hedrite	
	B). A plane view of a hedrite	
5.	Model of polymer spherulite with chain folded lamellae	14
	A). Spherulite consists of chain-folded lameallae radiating from central point	14
	B). Defect structure with high magnification between chain-folded lamellae	15
6.	Molecular structures of trans-1.4-polyisoprene	19
	A). β -structure from Bunn	
	B). α -structure from Bunn	
	C). α -structure from Takahashi et al.	
7.	Apparatus for column fractionation by solvent gradient elution	26
8.	Calibration curve for polyisoprene standards	29

Page

9. Shadowing used to determine lamellar thickness 34

10. Apparatus for density measurement 37

11. Typical calibration curve of density gradient 38

12. Photomicrographs for the simplest hedrites in α crystal form (Type I) 43

13. Photomicrographs for sheaflike hedrites with weak birefringence and α form structure (Type II) 47

14. Photomicrographs for sheaflike hedrites with distinct birefringence (Type III and Type IV) 52

15. Schematic drawing of 62

    a) Hedrites like those in Fig. 14 at two orientations with respect to analyzer (A) and polarizer (P) directions
    b) The birefringence patterns arising from them

16. Photomicrographs for α-TPI (Type IV) from 1% (w/v) amyl acetate solution, $\bar{M}_n$ = 2.5×10^5 at $T_C = 20°C$ 63

17. Photomicrographs from spherulites with strong bifringence in the β form 66

18. Photomicrographs of cup-shaped lamellar aggregates 72

19. Electromicrographs of cup-shaped lamellar aggregates at the edge grown from 1% (w/v) amyl acetate $\bar{M}_n = 2.5 \times 10^5$ at $T_C = -15°C$ 76

20. Optical micrographs of TPI crystals from dilute solution 80

21. Optical micrographs of β-TPI crystals from dilute solution 83

22. Optical micrographs of cup-shaped lamellar aggregates grown from 0.05% (w/v) amyl acetate TPI solution at 0°C with $\bar{M}_n$ = 2.5×10^5 85

23. Electron micrographs of TPI cup-shaped lamellar aggregates grown from 0.05% (w/v) amyl acetate solution at 0°C with $\bar{M}_n$ = 2.5×10^5 after O_sO_4 treatment 87

24. Optical micrographs of TPI crystals with a narrow molecular weight distribution 90

25. Optical micrograph of crystals grown from TPI blend of HMW fraction ($\bar{M}_n = 2.5 \times 10^5$ with 10% (w/w) LMW fraction ($\bar{M}_n = 2.4 \times 10^4$) in 1% (w/v) amyl acetate solution at 10°C 94

26. Optical micrographs of TPI crystals grown from dibutyl ether, heptane and n-butyl acetate 96

27. Electron micrographs of TPI single crystals grown from 1% (w/v) amyl acetate with $\bar{M}_n$ = 2.5×10^5 at T_D = 100°C, T_P = 0°C and T_R = 45°C, heating rate from T_P to T_R = 0.2°C/min 101

28. Electron micrograph of TPI single crystals grown from different precipitations temperature and redissolution temperature in 1% (w/v) amyl acetate with $\bar{M}_n = 2.5 \times 10^5$ 102

29. Optical micrograph of TPI crystals grown by the precooling method at higher redissolution temperature in interference contrast $\bar{M}_n = 2.4 \times 10^4$ in 1% (w/v) amyl acetate T_D = 100, T_P = 0, T_R = 45 and T_C = 20°C 103

30. Optical micrograph with hedrite structure by precooling method at a heating rate of 0.5-0.6°C/min from T_P to T_R $\bar{M}_n = 2.5 \times 10^5$ in 1% (w/v) amyl acetate at T_C = 20°C by interference contrast 106

31. Optical micrographs of thin films made by the evaporation of 1% (w/v) TPI amyl acetate solution 107

32. Optical micrographs of TPI crystallized from melt 110

33. Dependence of x-ray diffraction patterns on crystallization procedure 116

34. DSC scans for the HMW fraction from amyl acetate solution with $\bar{M}_n = 2.5 \times 10^5$ 118

35. Melting of hedrites grown from 1% (w/v) amyl acetate with $\bar{M}_n = 2.4 \times 10^4$ at T_c = 0°C from optical microscope 125

36. Thermograms of LMW TPI as a function of crystallization time 127

37. Micrographs of ether washed precipitate from cup-shaped lamellar aggregates 129

38. DSC thermograms for cup-shaped lamellar aggregates grown from amyl acetate solution with $\bar{M}_n = 2.5 \times 10^5$ at 0°C and treated with ether 130

39. Morphology of cup-shaped lamellar aggregates after annealing in amyl acetate suspension 133

40. Effect of annealing on the melting endotherms for TPI cup-shaped lamellar aggregates 134

41. Optical micrographs of cup-shaped lamellar aggregates, annealing to 35°C at a heating rate of 0.2-0.3°C min^{-1} 135

42. Morphological changes due to rapid heating rates from optical and electron microscopy 137

43. The effect of various treatments on the DSC 140

44. DSC scans for the crystallization from MMW fraction ($\bar{M}_n = 1.0 \times 10^5$) grown from 1% (w/v) amyl acetate 141

45. DSC thermograms of TPI crystals from different solvents 142

Page

46. DSC thermograms of TPI crystallized from the melt 143

47. Density at 25°C vs crystallization temperature, T_c, for TPI 146

48. ^{1}H NMR spectra of TPI and epoxidized TPI in $CDCl_3$ 155

49. Degree of epoxidation vs epoxidation time for TPI grown from amyl acetate solution 157

50. Electron micrographs of TPI single crystals before and after epoxidation 161

51. Erosive action of amyl acetate at 0°C on TPI spherulites grown from the melt 162

52. Crystalline fraction vs Log $\bar{M}_n$ for α-TPI structures from amyl acetate at T_C of 10, 20 185

LIST OF TABLES

Table No.	Caption	Page
1.	GPC Analysis: Experimental detail	27
2.	Molecular weight data for polyisoprene standards	28
3.	Morphological classification as a function of crystallization temperature and molecular weight	78
4.	Effect of molecular weight on crystal form for structures grown from 1% (w/v) heptane at T_C = 0°C	99
5.	The influence of heat rate on morphology	104
6.	d-spacing of α-TPI for the first six lines	113
7.	d-spacing of β-TPI for the first six lines	114
8.	DSC, density and x-ray diffraction results for TPI fractions crystallized from amyl acetate	120
9.	Effect of annealing cup-shaped lamellar aggregates in suspension	136
10.	Weight fraction crystallinity of TPI structure from solution	148
11.	Thermodynamic and density data of β and α-TPI grown by direct and precooling crystallization at T_C = 10°C	150
12.	Noncrystalline content from density and degree of epoxidation measurement for HMW fraction TPI crystals grown from amyl acetate solution	158
13.	Epoxidation data of TPI crystals grown from 1% (w/v) amyl acetate solution	160

14. Comparison between supermolecular structure of polyethylene and poly (ethylene oxide) 165

15. Average number of monomer units per fold and interlamellar traverse, U, for α-TPI from 1% (w/v) amyl acetate solution 185

16. Average number of monomer units per fold and interlamellar traverse, $\overline{U}$, for β-TPI from 1% (w/v) amyl acetate with $\overline{M}_n = 2.5 \times 10^5$ 188

I. INTRODUCTION

In the 1920's, it was discovered that some polymers yielded X-ray diffraction patterns. In contrast to metal and inorganic salts which exhibit well-defined patterns, these polymers produced only a few Bragg diffraction peaks superimposed on a diffuse, liquid like scattering pattern. The interpretation of these patterns, held for many years, was that small, relatively perfect crystallites existed in an amorphous matrix (1). The modern concept of polymer crystals resulted from the careful work of Keller (2) in 1957 following an earlier lead by Jaccordine (3), who showed that polyethylene molecules could form single crystals from dilute solution. Based on his studies of the properties of such crystals, Keller concluded that the polymer molecules in the crystals were folded back upon themselves. The evidence from which he drew his conclusion was supported by similar, independent observation of Fischer (4) and Till (5). This phenomenon has been reported for so many polymers (6) that its occurrence is considered to be universal. These single crystals are always grown by cooling a dilute solution from a temperature above the dissolution temperature to one below. For example, polyethylene single crystals can be grown isothermally from hot xylene ($\sim$135°C) in the range of concentration from 0.005 to 0.1% and the solution cooled to anywhere in the range of 75-85°C, the polymer crystallizes

anywhere in the range of 75-85°C, the polymer crystallizes in the form of thin platelets. An electron micrograph and a typical electron diffraction pattern of crystals from such a preparation (7) are shown in Fig. 1.

Fig. 1. Electron Micrograph and Electron Diffraction Pattern of Polyethylene Single Crystals.

A) Electron Micrograph of Crystal from Xylene, Crystal is ∿130Å Thick.

B) Electron Diffraction Pattern Shows That Chain Axes are Perpendicular to Large, Flat Faces of the Crystals.

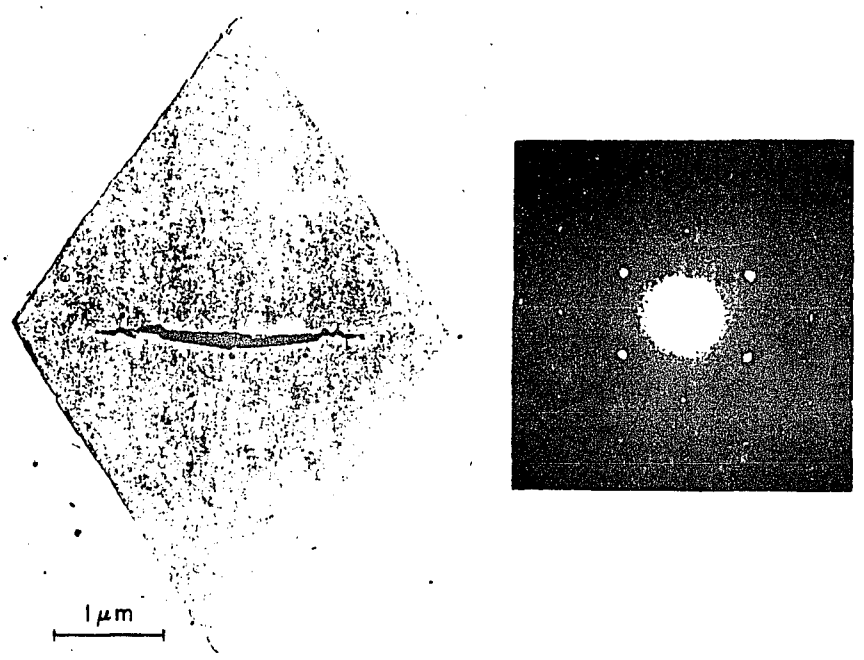

A B

Knowing the crystal structure of polyethylene from the work of Bunn (8), the electron diffraction experiments

on crystals formed in the general manner described on the previous page proved beyond any doubt that the polymer chain axes in the body of the crystals were essentially perpendicular to the large, flat faces of the crystal. The thickness of the crystals was in the vicinity of 100 - 200 Å, and this was far less than the contour length of the molecules in the preparation, the latter being at least 2000 Å on the average. On the basis of such information, the chains must be folded back and forth on themselves therefore, the upper and lower surfaces of the single crystals consisted of chain folds. A series of critical experiments followed this discovery, and it has become increasingly clear that the model for single crystals with chain folds is correct in its basic points.

Using polyethylene single crystals formed from mixtures of deuterated and the normal hydrogen-bearing chains, Banks and Krimm (9) have been able to show that the predominant type of folding involves reentry of the emergent stem into a adjacent position on the crystal face (adjacent reentry) as illustrated in Fig. 2.

Fig. 2. Possible Departures from Strictly Regular Folding and Defects in a Single Crystal.

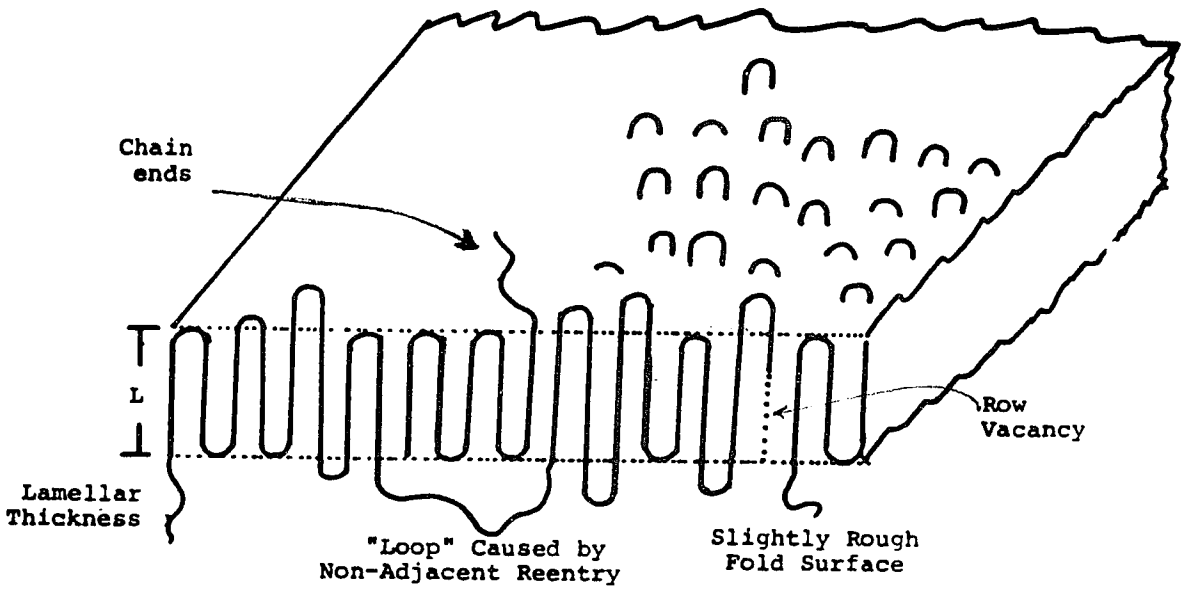

The density of polyethylene single cryst ls is somewhat lower than the theoretical crystal density (ρ = 1.003 g/cm^3) calculated from the dimensions of the unit cell. The observed values (9) are around (ρ = 0.97 g/cm^3 at 25°C, the exact value depending on the temperature of preparation and other factors. The observation of this

low density had led to considerable discussion and experimentation (10,11) but it is now commonly supposed that a portion of this density defect is associated with a slight roughness or irregularity of the chain-folded surface (see Fig. 2). Keller and coworkers (12) have shown by experiments in which the chain stems in chain-folded polyethylene single crystals were isolated after selective scission of the folds with ozone that the original crystals possessed a distribution of stem length corresponding to a somewhat rough fold surface. Probably some nonadjacent reentry folds or long loose folds occur in the growth plane and some chain ends (cilia) are thought to protrude from surface. Therefore, the lamella with a thickness L, includes a surface i.e. amorphous region (chain folds and chain ends) and the crystalline region with a crystalline thickness, L_c, is smaller than L.

It has been established that virtually all properties of bulk crystallized polymers are extremely dependent on the molecular weight and crystallization temperature. An extremely wide range in physical properties can be achieved by utilizing molecular weight fractions and varying the crystallization temperature under which crystallization takes place. These properties correlate with the level of crystallinity and the molecular structure of the lamellar crystallites and the associated interfacial and amorphous regions. Detailed studies of linear polyethylene

fractions have shown that in fact a variety of crystalline morphological forms can be obtained. These develop in a systematic manner as the molecular weight and crystallization temperatures are varied (13,14,15). The main work that has been reported on so far covered a molecular weight range from about 1×10^4 to 8×10^6, the complete isothermal crystallization range, as well as one rapid (quenched) crystallization procedure. The most perfectly developed spherulites, essentially of the classical type, are observed in the lower molecular weight quenched samples, $\overline{M}_w \leq 8.5 \times 10^5$. In constrast, the higher molecular weight samples do not display any well-defined morphology under any crystallization conditions. The lower molecular weight, isothermally crystallized samples developed either a poor spherulitic organization or rodlike forms, depending on the molecular weight and crystallization temperature. Recently, Allen and Mandelkern (16) also reported the crystalline morphology of poly(ethylene oxide) as a function of molecular weight and crystallization temperature. Molecular weight fractions, covering the range 6×10^3 to 1×10^7 were used over the range of accessible temperatures for isothermal crystallization as well as for a large set of controlled nonisothermal crystallization conditions. Three types of morphology, spherulites, an intermediate state and hedrites, were observed.

Polymers are known to exhibt several different types

of crystalline morphology while crystallized from very dilute solution in solvents. For example, polyethylene yields lamellar (chain-folded) single crystals in xylene (2) and from more concentrated (> 0.5% approximately) solution in the same solvent generally yields multilayer aggregates of such crystals (17). These aggregates are often found to consist of lamellae which diverge from a central spine or axis. When crystallized from the melt, on the other hand, polymer with high molecular weight almost always forms spherulites. However, thin films of the melt may also give rise, under certain conditions, to multilayer aggregates of lamellar crystals.

The crystallization technique is also an important factor in determing the morphology. Blundell, Keller and Kovacs (18) have described a self-seeding technique to grow uniform crystals from polymer solutions or the melt. The two essential advantages of self-seeding are preserved (19). First, the growth starts at the same time from crystallographically coherent nuclei and gives rise to crystalline units (single crystals, hedrites or spherulites) identical in shape and size. Second, the concentration of these nuclei (thus the final size of the crystalline units) can be controlled efficiently between large limits by an appropriate thermal treatment of the sample.

For the present discussion of crystallization one can thus suggest that perhaps the only change from solution to melt crystallization is an increase in interpenetration of molecules. Little is known at present about the degree of interpenetration of the molecules, the mechanism of disentanglement of the molecules on crystallization or the influence of short-range order on the overall melt structure and crystallization process.

The majority of studies on crystallization have been made using linear polyethylene. It is of interest to perform such investigations on other easily crystallizable polymers, such as trans-1,4-polyisoprene which includes double bonds in the polymer chain.

We mainly aim the study of crystal morphology at the influences on crystallization discussed above as summarized in the following:

1. Molecular weight of polymer.
2. Crystallization temperature.
3. Crystallization technique
4. Crystallization state - melt, concentrated or diluted solution.

It is very important to note that polymer spherulites do not grow in a spherically symmetric fashion from the moment of inception; rather, they evolve from simpler transitional precursor structures and the elucidation of

how and why these structures evolve into spherulites as they grow larger is of central importance to an understanding of the origins and mechanism of evolution of spherulites in polymers. Much has been learned during the last two decades about the nature of the early stages of the growth of polymer spherulites; there remain, however, some important aspects which it is fair to say still remain somewhat blurred. Our purpose is to crystallize some of the conspicuous morphological features which often characterize the early stages of growth of spherulites by changing the molecular weight and crystallization temperature in concentrated solution. The crystallization from solution is always advantageous for the morphological study, because, the three dimensional and isolated structures can be observed by floating and rotating the liquid with microscopy and it also shows less complicated morphological entities compared with melt crystallized specimens.

The development of a sheaflike precursor during the early stages of the growth of polymer spherulites is a feature which is very commonly observed in polymer spherulite growth studies. This feature has been known since the earliest investigation on the morphology of polymer spherulites. The early view was that the sheaflike precursors were similar in shape to a sheaf of wheat and consisted of a symmetric or twisted bundle of fibrillar structural units (20). Subsequent studies, which followed

upon the discovery of chain folding led to the realization first pointed out by Bassett et al., (17) that at an early stage in these seemingly sheaflike precursors are multilayered, chain-folded structures similar to the crystalline objects which have been variously and collectively referred to as axialites and/or hedrites and which are formed when polymers are crystallized from concentrated solutions under certain circumstances as well as from the melt at low undercoolings, i.e. at temperature above the wide range in which the evolution of spherulites prevails. The term "axialite" was first used by Bassett et al., (17) to describe multilayered objects grown in relatively concentrated solution of polyethylene in xylene. The term "hedrite" was first employed by Geil (21) to distinguish polygonal objects formed in melt-crystallized polymers from the more common spherulites. Geil subsequently extended his definition of a "hedrite" to include axialites (6).

According to Keith theory (22), the transitional multilayered hedrite structures which develop during the early stages in the growth of spherulites, and the spherulitic structures into which they ultimately evolve, represent respectively successive stages in the evolution of an initially formed lamellar chain-folded single crystal.

The idealized schematic representation of successive

stages in the evolution of a spherulite are summarized and depicted in Fig. 3.

Fig. 3. Schematic Representation of Successive Stages in the Development of a Spherulite from a Chain Folded Precursor Crystal.
Rows (a) and (b) Represent Respectively Edge-On and Flat-on Views of the Evolution of the Crystals.

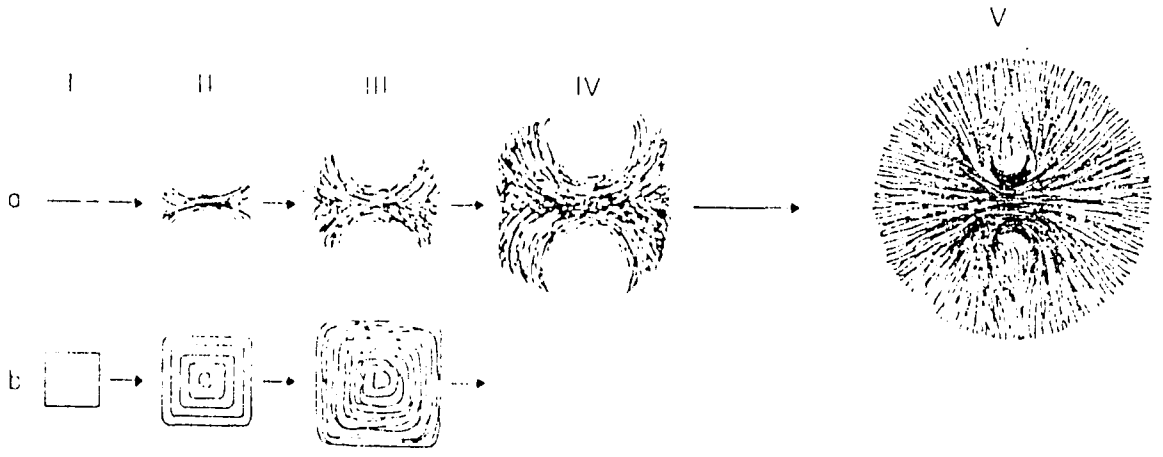

Column I shows a chain-folded, monolayered single crystal precursor as seen edge-on (column I, row a) and flat-on (column I, row b). Corresponding cross-sectional representations of the development of this precursor crystal as it evolves progressively into a spherulite consisting of a radiating array of ribbon like, chain-folded lamellae are shown in column II-IV, where column II and III represent the intermediate multilayered hedrite stages in the development of the spherulite. As indicated in

Fig. 3., the precursor (I) and the intermediate stages of development (II-IV) occur within a radial span beyond which growth progresses in a spherically symmetric fashion. It is pertinent to note at this juncture that the higher the crystallization temperature (and hence the slower the growth rate) the larger the radial span within which the transformation from single crystal to spherically symmetric (spherulitic) propagation is attained. Indeed, at high enough crystallization temperatures neighboring transitional structures (such as those shown in column II to IV) developing, for example, in a thin polymer film, impinge and hence stop growing further well before they attain the spherically symmetric growth stage.

An example is illustrated by the replica of poly(4-methyl pentene-1) hedrites shown in Fig. 4 (A) and 4 (B), respectively. These structures represent a stage in spherulite development which corresponds approximately to that in column III of Fig. 3. As described in Fig. 3, (column III, row b) and as can be readily judged from the replica of the flat-on cross section shown in Fig. 4 (B), the hedrite consists of a stack of superimposed lamellae which exhibit a trace of tetragonal lateral habit. Note the absence of any radiating fine texture emanating from the center of the structure as seen in this perspective. As can be seen from the replica of the edge-on cross section shown in Fig. 4 (A), the developing multilayer

hedrite exhibits a distinctly sheaflike appearance in this latter prospective, in which the constituent lamellae are oriented preferentially edge-on which respect to the field of view.

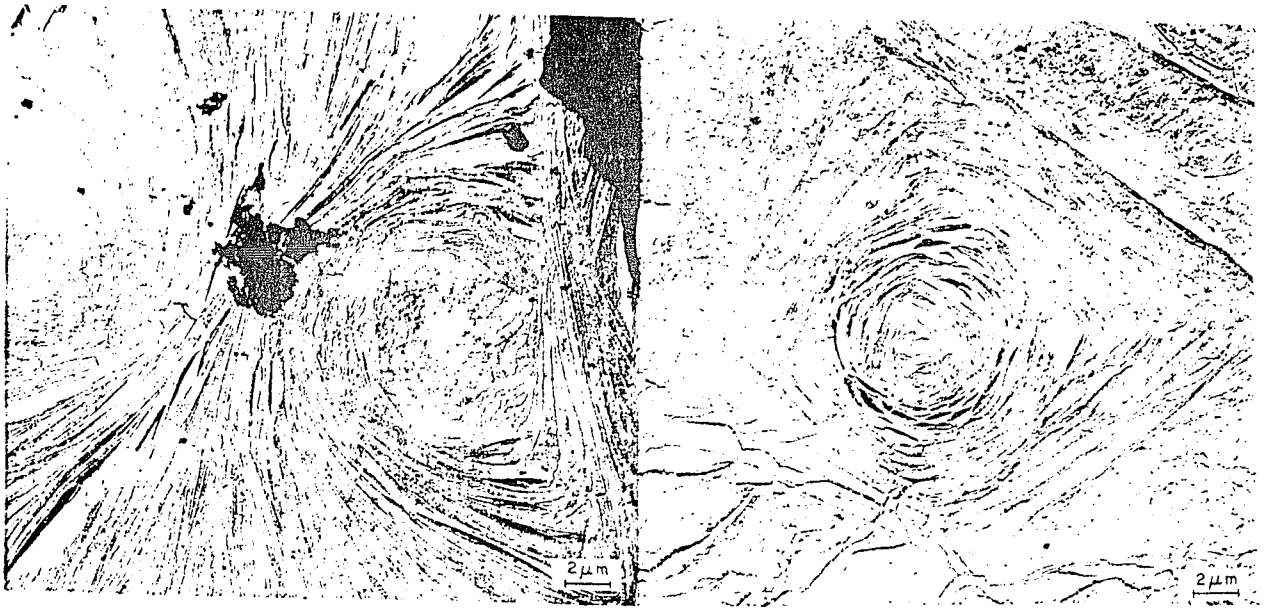

Fig. 4. Two Electron Micrographs of Replicas of Hedrites Formed in the Same Melt Crystallized Thin Film of Poly(4-Methyl Pentene-1)

(A) An Edge-On View of a Hedrite

(B) A Plane View of a Hedrite

Electron microscopy of melt crystallized polymers has shown that the spherulites are composed of lamellae radiating from a point in all direction (23,24) and measurements of physical properties like density, heat of fusion and mobility by NMR suggest that melt crystallized polymers have a considerable amount of amorphous materials (25,26,27) which should be between the lamellae.

Fig. 5 represents the spherulite as consisting of chain folded lamellae radiating from a central point, the polymer chain axes in lamellae are more or/less perpendicular to the radius of the spherulite. Small angle branching causes the spherulite to become spherical in shape, the smaller crystalline substructure to occupy the outwardly increasing volume after sufficient growth. Noncrystallizable material (not shown), when present, accumulates between lamellae and at the outer boundary. Interlamellar links, accompanying entanglements and chain ends can cause incomplete crystallization.

Fig. 5. Model of Polymer Spherulite with Chain-Folded Lamellae

A. Spherulite Consists of Chain-Folded Lamellae Radiating from Central Point (28)

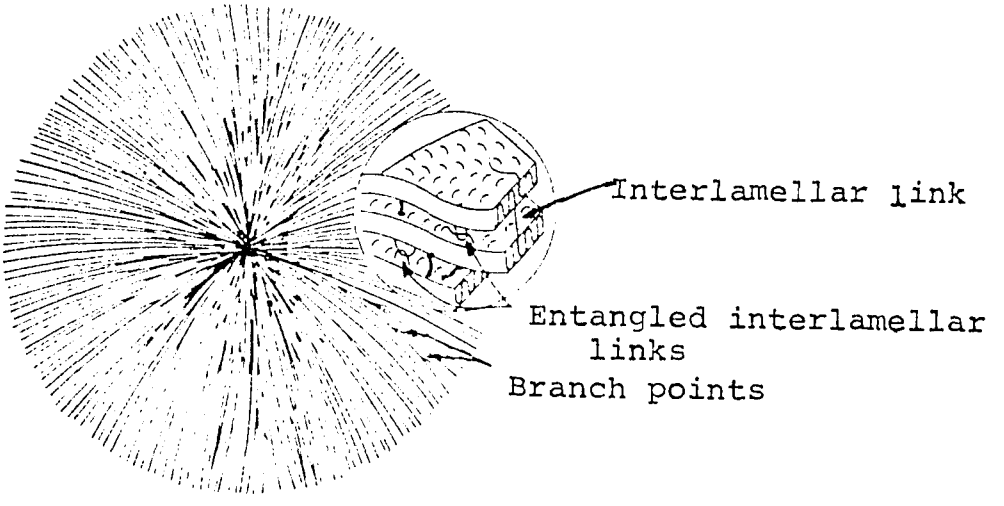

5B. Defect Structues with High Magnification between Chain-Folded Lamellae. Interlamellar Links, Chain Ends, Chain Folds and Entanglement Exist in the Noncrystalline Regions.

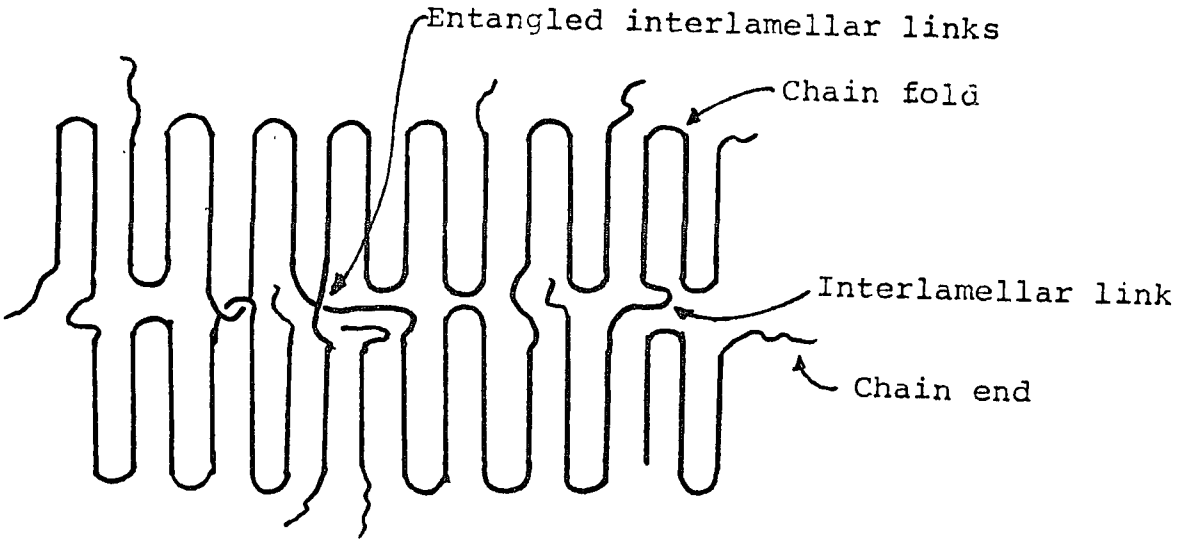

The concept of crystallinity arises natually from the observation that many physical properties of polymers are intermediate between those expected of a purely crystalline and of a purely liquid material. For example, using the floatation or density gradient method the observed densities of polyethylene are normally higher than those estimated for polymer liquids but are rarely as high as those calculated from X-ray crystallography (29).

Similarly, polymer X-ray diffraction patterns frequently contain many well-defined, sharp peaks which clearly arise from regions of three-dimensional order. However, there invariably appears broad, diffuse X-ray scattering which is attributed to the presence of liquid-

like material. A diffraction scan of a polymer crystal sample over a limited range of angle which contain most of the crystalline diffraction peaks and the major portion of amorphous halo can typically be separated; the crystallinity can be calculated from the resolved peak areas (30)

The heat of fusion as a function of crystallinity has been summarized for polyethylene (31). It shows that the heat of fusion is affected by both the crystallinity and the lamellar thickness.

Investigation of the surface region of spherulites by physical methods such as microscopy or crystallinity has not yielded a sufficient understanding of chain folding and interfacial regions. Therefore, a number of chemical methods such as etching (32,33), halogenation (34,35), dehydrohalogenation (36) hydrolysis (37,38), oxidation (39, 40) and epoxidation (41-45) were developed to study surfaces of polymer crystals. Depending upon their uses, chemical methods can be divided into two classes:

(1) techniques used to reveal the morphology of crystals buried in the polymer matrix and

(2) techniques used to study the nature of the crystal surfaces.

In class 1, the solvent-etching technique is used to reveal crystals embedded in the amorphous polymer matrix. Class 2, includes two types of techniques: (A) surface removal techniques like oxidation with HNO_3

and O_3 (polyethylene) and hydrolysis (cellulose, polyamides and polyester), and (B) surface modification techniques like halogenation (polyolefins), dehydrohalogenation (polyvinylidene chloride) and epoxidation (polydienes).

The studies of chain folding of dilute solution grown lamellae of trans-1,4-polybutadiene using chemical methods have been reported by Woodward and coworkers (41-45) and by Marchetti and Martuscelli (46). The double bonds of trans-1,4-polybutadiene in the noncrystalline region are reactive to the epoxidizing agent and bromine etc. by an addition reaction. For trans-1,4-polybutadiene (TPBD), it was shown earlier (41,42,43) that with an excess of epoxidizing agent, m-chloroperbenzoic acid (MCPBA) present the epoxidation reaction was completed within five days after only a fraction of the total number of monomer units had reacted. The kinetics of epoxidation was shown to follow the second order rate equation, i.e. the rate is proportional to the available double bond concentration and to the MCPBA concentration (43). In a more recent study (44) the noncrystalline component of self-seeded dilute heptane solution grown crystals of fractionated TPBD with $\bar{M}_n$ ranging from 4.7×10^3 to 1.5×10^5 was investigated by epoxidation of crystal surfaces using dried mats in contact with toluene solution at 6°C with an excess

amount of MCPBA present. The number of monomer units per fold was calculated from the fraction of double bonds epoxidized, the lamellar thickness and the number average molecular weight was found to be 2½ to 6½, increasing with increasing molecular weight and/or T_c while ΔT, the difference between the redissolution and final crystallization temperature, was held constant. An increase in ΔT led to a decrease in the number of monomer unit per fold. It was found in that work that the total noncrystalline fraction as calculated from density measurements for TPBD crystals is larger than the fraction available for epoxidation at the crystal surfaces. The bromination of suspensions of single crystals of TPBD is also selective at the fold surface (46). As the lamellar thickness of the single crystals is increased by increasing T_c, a larger number of double bonds per fold are brominated, i.e. a larger number of repeat units become accessible to bromine. This is consistent with an increase in the thickness of disordered surface layers with an increase in the crystallization temperature.

Turning to the studies of trans-1,4-polyisoprene (TPI) crystals with a similar chemical chain structure as TPBD, it is one of the first polymers to give recognizable crystals (47) and has been found to exist in two crystalline modifications, α and β. The β form can be described

by an orthorhombic unit cell with a = 7.78 Å, b = 11.7 Å and c = 4.72 Å from X-ray diffraction (48) or with a = 7.83 Å, b = 11.87 Å, c = 4.75 Å from electron diffraction. The structural parameters of the α form is a matter of dispute. Two different monoclinic unit cell have been proposed by Fisher (49) and by Takahashi, Sato, Tadokoro and Tanaka (50). The unit cell due to Fisher has a = 5.9 Å, b = 7.9 Å, c = 9.2 Å, α = β = 90° and γ = 94°, this cell corresponds to the γ-structure proposed by Bunn (48). The unit cell due to Takahashi et al., has a = 7.98 Å, b = 6.29 Å, c = 8.87 Å, α = γ = 90° and β = 102.0°. These two molecular models for the α-structure are shown in Fig. 6 in comparison with β structure.

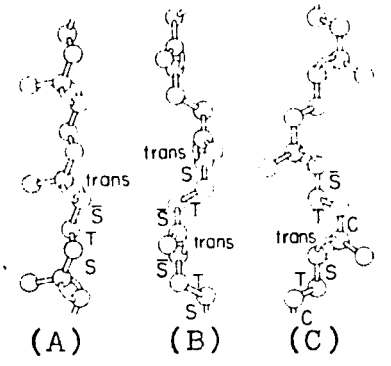

Fig. 6. Molecular Structures of Trans-1,4-Polyisoprene

(A) β-Structure from Bunn.

(B) α-Structure from Bunn.

(C) α-Structure from Takahashi et al.

For the melt crystallization of TPI, at temperatures below 35°C the spherulites which appear have a characteristic Maltese cross examined between crossed nicols; dendritic spherulites are observed if crystallization takes place above 45°C. In the intermediate temperature range, both types of spherulites are obtained (47,51). The Maltese Cross spherulites have the lower melting temperature and contain only β crystals. In addition to these spherulites, multilayer crystals with an elliptical shape were found at lower crystallization temperature (51,52). It was suggested that they were lamellar crystals with the molecular axis of the polymer oriented along the long axis of the ellipse.

The supermolecular structures of melt crystallized TPI have been studied by electron microscopy at early stages of crystallization (53) and by low-angle X-ray (54) at later stages, these methods measure the lamellar thickness and allow calculation of lamellar surface energies. The values of fold surface energy agree very well with those determined for solution grown crystals (55).

The crystallization of TPI from dilute solution has been carried out either by cooling (55,56,57) or by allowing a poor solvent to diffuse into the solution (59). It has been established that it leads to well shaped crystals. The geometry of the simplest monolayer forms has been

reasonably well explored, in the three particular types, Oval (55,57) hexagonal (56,57) and rectangular (57) lamellae have been observed.

However, much less is known of crystals containing more than one layer on crystallization from solution. The effect of molecular weight and crystallization conditions have been shown to have a strong influence on morphology of polyethylene melt crystallized samples (13-15) but has not been studied using trans-1,4-polyisoprene. There has also been little study of the contribution of lamellar crystallities and intervening amorphous regions.

The epoxidation method, used to evaluate the total noncrystalline content of trans-1,4-polybutadiene and trans-1,4-polyisoprene single crystals at the surfaces as a function of crystal thickness, the number of monomer unit per chain end and the number-average molecular weight (44,45,57), may be extended to the study of multilayer crystals grown from fractionated trans-1,4-polyisoprene in solution at different crystallization conditions. The results for the noncrystalline content at the crystal surfaces from epoxidation may also be compared with the results from density measurement for the total noncrystalline fraction to give information concerning the location of this component in TPI crystals.

The major goals for this investigation are the following:

1. To study the morphology of multilayered trans-1,4-polyisoprene crystals and the influence on morphology of:
    (a) molecular weight
    (b) crystallization temperature, and
    (c) crystallization technique.
2. To determine the noncrystalline fraction for TPI as a function of
    (a) molecular weight
    (b) crystallization temperature and other crystallization conditions and
    (c) crystal form.
3. To determine the surface fraction for selected TPI preparations.

The methods used were as follows:

1. Fractionation of Gutta percha (natural trans-1,4-polyisoprene) by a liquid-liquid phase separation method and on a celite support column.

2. Study of morphology as a function of molecular weight and crystallization temperature, using interference contrast and cross-polarized light microscopy and in some cases electron microscopy.

3. Determination of the crystal form by wide-angle X-ray diffraction and by differential scanning calorimetry.

4. The measurement of density to determine the non-crystalline fraction.

5. Epoxidation of lamellae in suspension and measurement of the fraction epoxidized by ^{1}H NMR to obtain the surface fraction.

II. EXPERIMENTAL

Preparation of Samples: Natural Gutta percha (Gubudam Prudusen Karet Indonesia) with $\overline{M}_w = 2.96 \times 10^5$, $\overline{M}_n = 7.91 \times 10^4$, $\overline{M}_w/\overline{M}_n = 3.75$ and natural Balata (Dunlop) with $\overline{M}_w = 2.75 \times 10^5$, $\overline{M}_n = 1.40 \times 10^5$, $\overline{M}_w/\overline{M}_n = 1.96$ were used. Purification proceeded by soaking the polymer in a soxhletextraction column with acetone for five days to remove impurities (59). The polymer chain sequence was determined as 100% 1,4 by 100 MHz proton NMR in $CDCl_3$. Two fractionation methods were used with Gutta percha, a liquid-liquid phase separation technique and a celite support column method, as described below.

A. Liquid-liquid phase separation method: The soaked samples were fractionated from toluene solution at 29°C. The solution contained approximately 1% by weight of polymer and 0.01 g/100 ml of 2,2'-methylene-bis(4-methyl-6-tertiary-butyl)phenol as antioxidant, with methanol as the nonsolvent. The separation was observed to involve two liquid phases as required. The polymer in the concentrated phase was precipitated by addition of a lot of methanol, filtered, washed several times with methanol, and then dried in vaccum at room temperature. Samples were stored in the refrigerator to reduce the possibilities of degradation and/or oxidation.

B. Fractionation from Celite Support Column: The apparatus as proposed by Francis, Cooke and Elliott (60) is shown schematically in Fig. 7.; all operations are carried out under nitrogen. Mainly it consists of a solvent holder, a packed column, a temperature control system, and equipment for sample collection.

The solvent used was amyl acetate, the nonsolvent was 2-ethoxyethanol. The mixtures contained 0.02 g/100 ml. of 2,2'-methylene-bis(4-methyl-6-teriary-butyl)phenol as antioxidant and were purged with nitrogen before use.

Gutta percha (30g) and antioxidant (0.3g) were dissolved in 1500 ml amyl acetate and 750g celite (a diatomaceous earth supplied by Sigma Chemical Co.) which was washed by N_2 purged amyl acetate were mixed at 65°C, and then cooled to room temperature. The polymer-coated support was washed with 2-ethoxyethanol to remove the amyl acetate. The column was preheated to the boiling point of methanol (64.5°C) by refluxing methanol about it. Simultaneously, the suspension of polymer-coated celite preheated to 64.5°C, was packed into the column on top of a layer of uncoated support.

Each fraction was extracted by allowing a solvent-nonsolvent mixture of increasing solvent power to pass through the column under gravity. A lot of nonsolvent (methanol) was added to the eluents to precipitate the fractionated polymer; the precipitate was filtered,

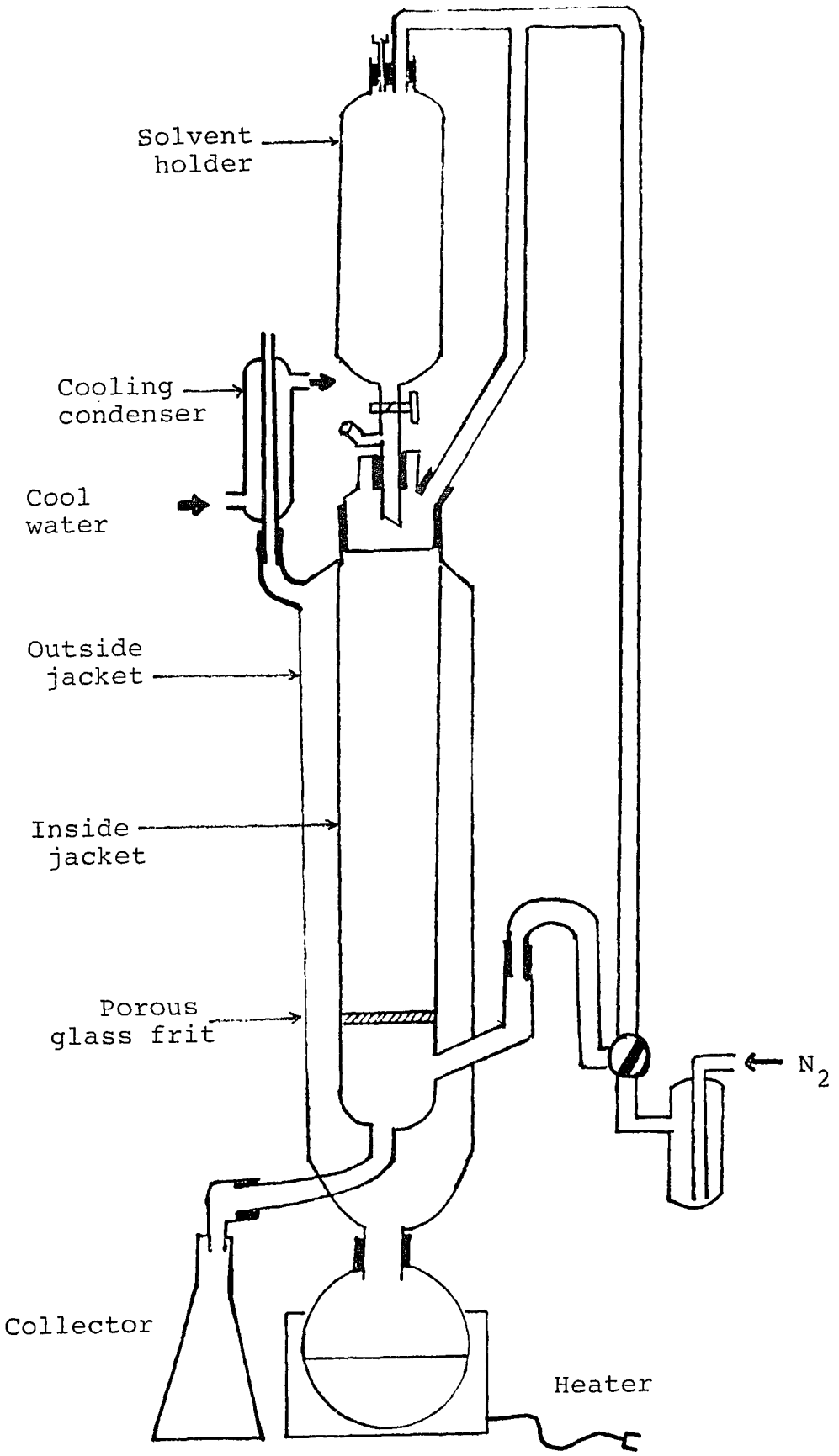

Fig. 7. Apparatus for Column Fractionation by Solvent-Gradient Elution.

washed and then dried under vaccum at room temperature.

The molecular weight distribution for each sample was determined by using gel permeation chromatography with a set of polystyrene columns. A Waters Model 200 Chromatcgraphy with a differential refractometer as detector was employed. Details of the experiment are shown in Table 1.

Table 1. GPC Analysis: Experimental Detail

Parameter	
Solvent	Toluene
Flow Rate ml/min	1.00
Sample Concentration % (w/v)	0.25
Oven Temperature °C	80-90
Upper porosity Rating of Column Å	
Column 1 (#39711)	500
Column 2 (#39714)	8.5×10^3
Column 3 (#39716)	10^5
Column 4 (#39718)	10^6

The system was calibrated by using various polystyrene, polyisoprene standards as well as squalene. Calibration in the 410 to 8.0×10^4 molecular weight range was carried out with six polyisoprene standards and squalene as described in Table 2. The elution volume for each peak maximum from GPC curve was plotted as a function

Table 2. Molecular Weight Data for Polyisoprene Standards

	Source	$\bar{M}_n$	$\bar{M}_w$	Elution Volume of Peak Maximum	$\bar{M}_w/\bar{M}_n$
CDS-I-2	Good Year Inc.	9.5×10^3 (VPO) 10.8×10^3 (MO)	10.2×10^3 (LS)	30.35	1.11
CDS-I-3	" " "	1.20×10^4 (VPO 1.33×10^4 (MO)	1.32×10^4 (LS)	30.10	1.13
CDS-1-5	" " "	1.65×10^4 (MO)	1.74×10^4 (LS)	29.75	1.12
CDS-I-6	" " "	2.12×10^4	2.84×10^4	29.30	1.14
#8281	Polymer Science Inc.	7.2×10^3	-	30.70	1.05
#8282	" "	8.0×10^4	-	27.60	1.05
Squalene ‡	Aldrich	410.7	-	34.75	-

‡ Molecular formula: $CH_3-\overset{CH_3}{\overset{|}{C}}=CH-CH_2\left(CH_2-\overset{CH_3}{\overset{|}{C}}=CH-CH_2\right)_4 CH_2-\overset{CH_3}{\overset{|}{C}}=CH-CH_3$

Fig. 8. Calibration Curve for Polyisoprene Standards

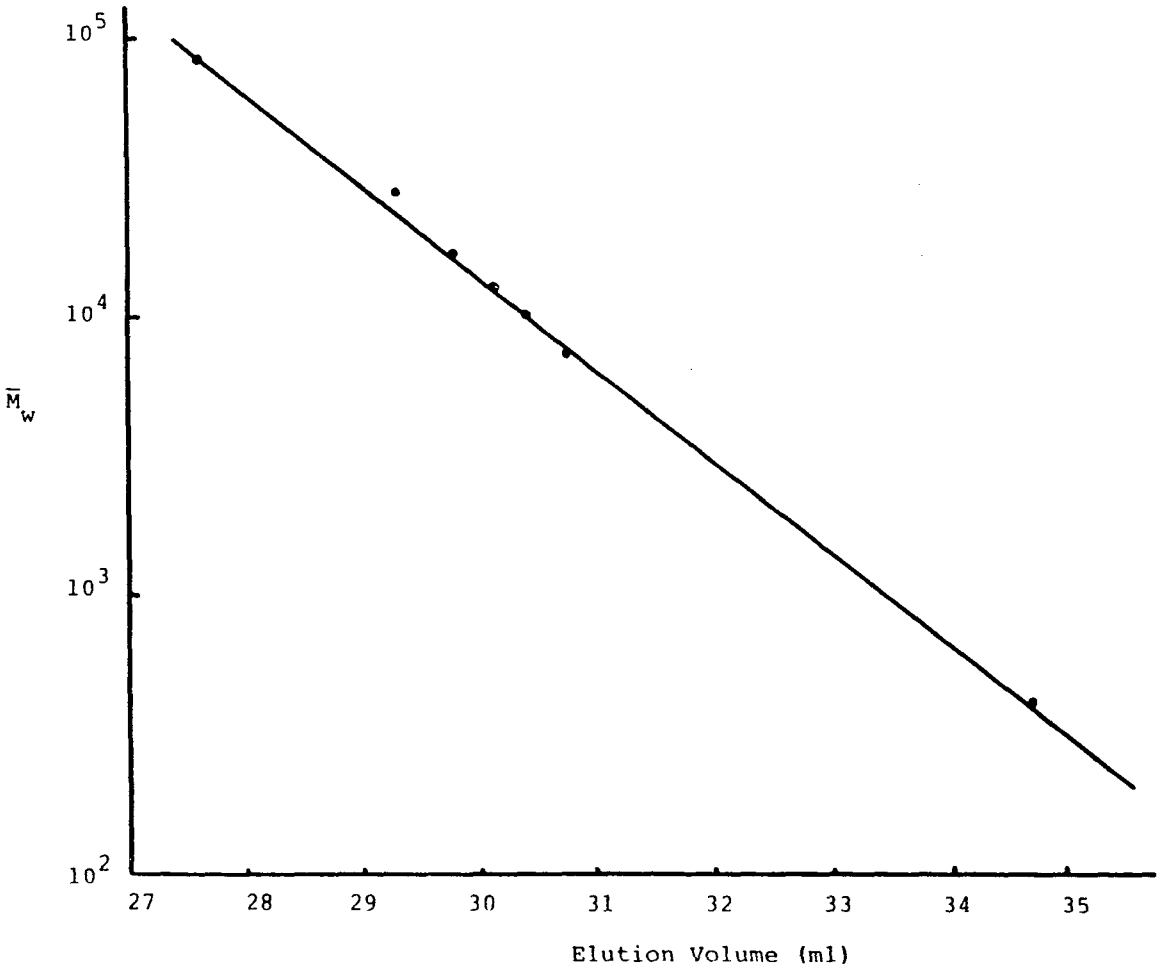

of $\overline{M}_w$ as shown in Fig. 8. For molecular weights above 2.8×10^4 the elution volume-molecular weight plot was assumed to parallel the curve obtained for a series of polystyrene standards.

Crystal Preparations: Four procedures for the growth of crystals were employed as described below:

1. Direct Crystallization from Solution: Solvents used included amyl acetate (Fisher Inc.) distilled under nitrogen purge, heptane (Fisher Inc.) n-butyl acetate (Fisher Inc.) and dibutyl ether (Eastman Inc.) used as received. A series of solutions of fractionated TPI at concentrations of 0.05,1,3 (two preparations) and 8% (w/v) (one preparation) were made by heating the polymer plus crystallization solvent to 100°C. The solution was filtered and held at the same temperature (100°C) for one hour, then removed to a constant temperature water bath in the range -15 to 32°C (±0.1°C) for one day. The precipitated polymer was separated from the mother liquor by filtration, the precipitate was washed with fresh solvent at the same temperature and then dried under vaccum.

2. Precooled Crystallization from Solution: A series of 1% (w/v) TPI solutions in amyl acetate were made by dissolving fractionated polymer at 100°C and filtering. The solutions were held at 100°C for one hour, then quenched

in ice water or a dry ice-acetone mixture (T_p), redissolved by increasing the temperature at a rate of 0.2°C min^{-1} approximately to a redissolution temperature (T_R) and finally cooled to the crystallization temperature(T_C) and held there for one day. T_R is found to increase with molecular weight; for a 1% (w/v) solution in amyl acetate it is 35°C for $\bar{M}_n$ of 4700 and 45°C for $\bar{M}_n$ of 2.5×10^5. In some other experiments the precipitated polymer-liquid mixture at 0°C was heated at various rates to a temperature below the redissolution temperature. Separation of the precipitate was as given in 1) above.

3. Melt Crystallization: Thin films of purified unfractionated Balata and fractionated Gutta Percha were prepared by pressing about 0.01g of sample between aluminum foil on a Carver press. A pressure of 5-7 metric ton was used to keep the film bubble free at 80°C. Such films were controlled at 0.02-0.04 mm (20-40 μm) thickness as measured by a micrometer caliper. Samples were crystallized by placing them between foils in glass tubes evaluated to less than 0.01 mm Hg and filled with nitrogen gas repeatly to exclude oxygen. The tubes were heated at 100°C for one hour to ensure complete melting of the polymer and the removal of any thermal history on subsequent crystallization. The sample tubes were then transferred to an oil bath at the desired crystallization

temperature (±0.1°C); after 14 days the tube was slowly cooled to room temperature.

4. Crystallization by Surface Evaporation: 1% (w/v) TPI solutions in amyl acetate at 100°C were cooled to 20 or 30°C for one or two hours respectively. A few drops of this solution were put on a glass slide and the solvent evaporated at room temperature (∿ 22°C).

Optical Microscopy: The crystals grown by direct crystallization were washed with a lot of crystallization solvent at the same temperature at T_c to remove material remaining in the solution and then the morphology was studied in suspension under the optical microscope using both interference contrast optics and crossed nicols (to observe the birefringence). A photomicroscope (Zeiss) with magnification from 500 to 800 was used. Both cold and hot stages were used.

1. Observation on a Cold Stage: A cold stage was designed as follows: a copper plate with 0.25 cm thick, about 10 cm by 10 cm and with a 0.25 cm hole in the center was attached to an insulated copper tube with 0.5 cm diameter. A fluid from an isothermal water-ethylene glycol and ethanol bath (±0.1°C) was circulated to the copper plate to maintain a temperature below that of the room.

2. Observation on a Hot Stage: To observe the phenomena of melting with the optical microscope, a Thomas Model 40, micro hot stage with its own condensing lens was set on the microscope stage. The optical path of the stage was adjusted until it was coaxil with the optical path of the microscope. The heating current was controlled by means of a variable transformer at a heating rate of 10°C min^{-1}.

3. Photography: Photographs of the structures observed with optical microscope were recorded with a 35 mm camera connected to the instrument on Kodak technical pan film 2415 with Estar AH base. When the reflecting system is in the exposure position, the object is imaged in the film plane and on the focusing reticle. The image will be sharply focused on the film if it is seem sharply defined on the focusing reticle. The image scale on the film depends on the position of the projective (3.2 x and 6.3 x). It is computed as the product of:

$$\text{Image scale on the film} = \begin{matrix}\text{Scale factor} \\ \text{of objective}\end{matrix} \times \begin{matrix}\text{Optovar}‡ \\ \text{factor} \\ \text{(magnification} \\ \text{changer)}\end{matrix} \times$$

x Scale Factor of Projective

‡: A cylindrical extension is in the optical system and gives a further magnification of 1.25 x, 1.6 x and 2 x.

Electron Microscope: The crystals obtained by the pre-cooling method were washed with a lot of crystallization solvent at T_C. A drop of the suspension was deposited on a carbon coated copper grid (200 mesh/in^2) and checked by optical microscopy. Solvent was evaporated in the refrigerator. The crystals were shadowed with Pt/Pd vapor in vaccum ($\leq 10^{-4}$ mm Hg) to increase image contrast at a shadowing angle of $\alpha = \tan^{-1} 1/3$ and observed in the transmission mode with a Philip EM 300 electron microscope at 80 KV. Photographs of these crystals were recorded with a plate camera connected to the instrument. The thickness of crystals was also calculated by measuring the shadow distance along the shadowing direction with high magnification as shown in Fig. 9.

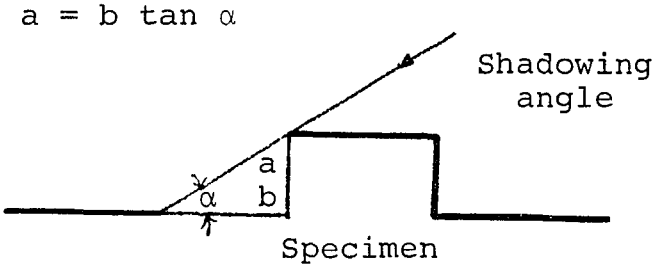

Fig. 9. Shadowing Used to Determine Lamellar Thickness

OsO_4 saturated amyl acetate solution was used to fix or harden the crystal aggregates with curved lamellar structure to prevent shrinkage in the drying process. Not only does the osmium tetroxide react with double

bonds of the TPI crystals in the amorphous regions but also the staining of osmium enhance the electron scattering ability and therby improves the contrast.

Wide Angle X-ray Diffraction: A Norelco X-ray generator (Philips Inc.) and a cylindrical camera of 57.3 mm diameter were used. The dried crystals were pressed to 10-20 mm thick sheets. Exposures were made with nickel-filtered (Cu - Kα) radiation using an accelerating potential of 35 KV and filament current of 15 MA for one and half hours. Black paper was commonly used to prevent light from exposing the film. For a random polycrystalline sample, diffraction from all the crystals in the sample having (hkl) planes making the proper Bragg angle with incident beam produces a cone of radiation with semiapex angle 2θ, which intersects the film of the camera. The most accurate measurements are made along the equator. The measured 2χ (the diameter of the diffraction ring) equatorial values may be converted into 2θ values by the equation

$$2\theta = 180^\circ \ (2\chi)/_{\pi D}$$

where D is the diameter of the camera. These 2θ values may be converted to d spacing for the diffracting planes by the equation

$$d = \frac{1}{2 \sin \frac{180\chi}{\pi D}}$$

Density Measurement: The form of the apparatus as shown in Fig. 10 consists of two 250 ml Erlenmeyer flasks connected by glass tubing to a vertical glass column. A density gradient was set up by mixing various proportion of high density liquid, water and less dense liquid, ethanol, so that the density at either end of the vertical column was controlled by the density of the original liquids in the reservoirs and an essentially linear density gradient developed in 5-7 hours, which was stable for 1-2 days only, through the process of mutual diffusion of the liquids. The gradient was determined with calibrated float (hollow glass beads) accurate to four decimal places at 25°C. A calibration curve, as shown in Fig. 11 is calculated each time by linear regression.

All samples were pressed at 3.4×10^7 P_a to eliminate air, cut in small pieces and dropped into the column. The densities were measured from the flotation level. The weight fraction crystallinity was calculated by using an amorphous density ρ_a of 0.905 g/cm^3 (61), crystalline density for the α form, $\rho_c(\alpha)$, of 1.05 g/cm^3 (48-50) and crystalline density for the β form, $\rho_c(\beta)$, of 1.02 g/ cm^3 (48,49).

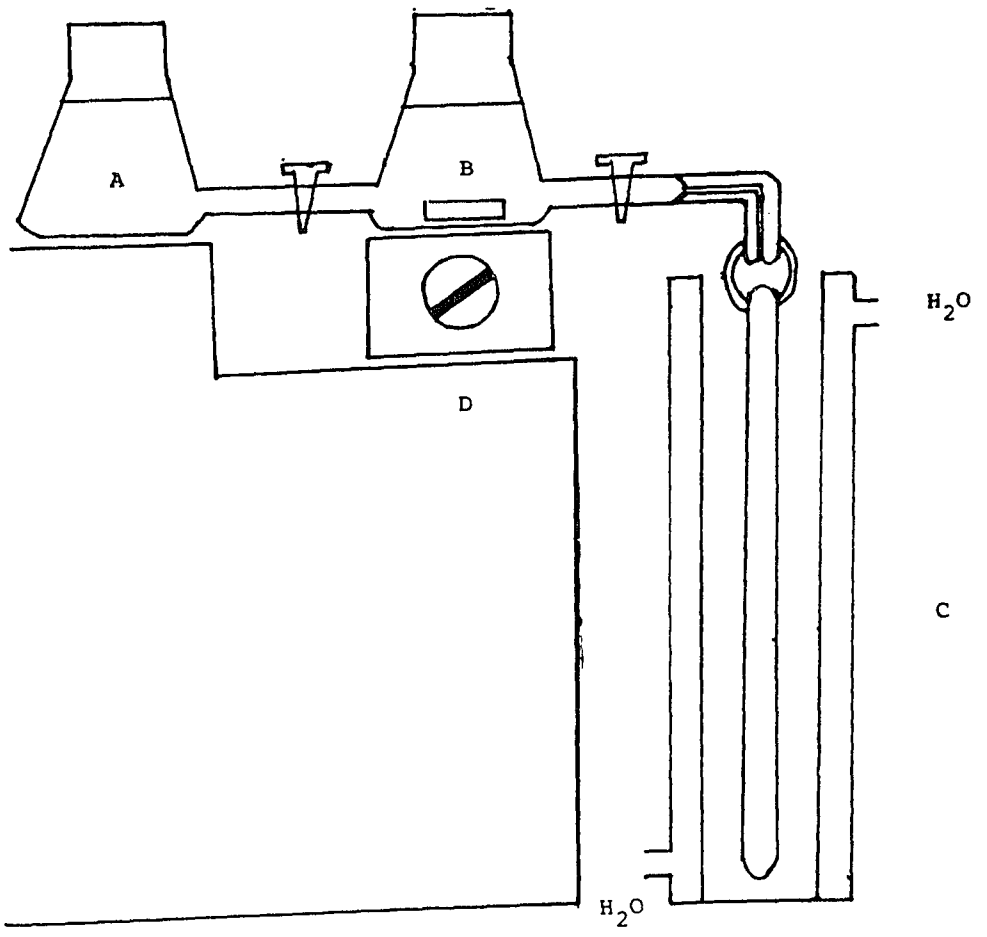

Fig. 10. Apparatus for Density Measurement

A. Low Density Solvent Reservoir

B. High Density Solvent Reservoir

C. Column with Temperature Controlling Outside Jacket

D. Magnetic Stirring Set

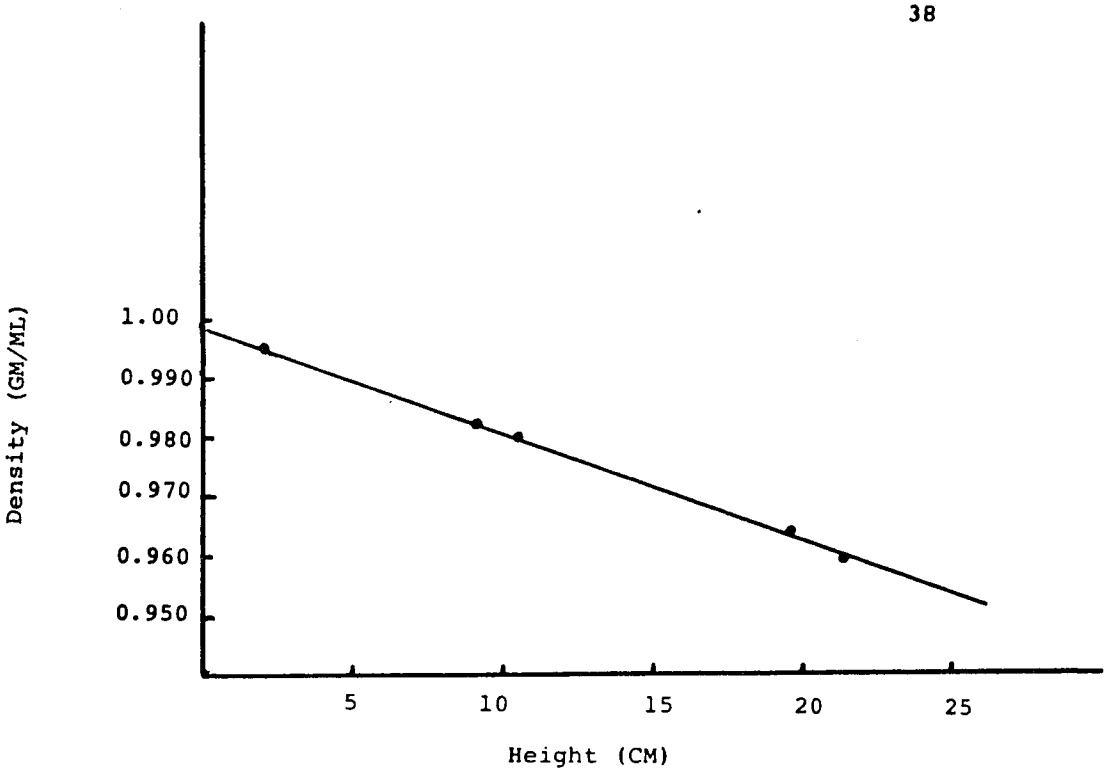

Fig. 11. Typical Calibration Curve of Density Gradient Column: The Points are the Positions of the Calibrated Floats (Floats with Densities 0.9584, 0.9643, 0.9800, 0.9826 and 0.995 g/ml were used)

Differential Scanning Calorimetry (DSC): Measurements were made with a DuPont 900 thermal analyzer with 2-5 mg at comparatively high instrumental sensitivities. The temperature indicated by the analyzer were checked by comparing the melting point of purified and dried benzoic acid crystals. The absolute error in the temperature is estimated to be ±1°C. A scanning speed of 10°C min^{-1} was used in all the experiments. This speed was high enough to avoid recrystallization phenomena during the heating up. The heat of fusion (ΔH) was also measured by using time base at 0.25 min cm^{-1}. The peak area was used to calculate ΔH by substitution in the following equation as shown in the instruction manual.

$$\Delta H = \frac{A}{m} \times 60\ BE\ \Delta q_s$$

A: peak area in cm^2

m: sample mass in grams

B: time base setting in min/cm

E: cell calibration coefficient

Δq_s: Y-axis range setting in Mv/cm

ΔH: Heat of fusion in J/Kg

Epoxidation and Proton NMR Analyses: Reaction of the double bonds at the surface of wet crystal structures in suspension was carried out in amyl acetate at 0.05 to

1% (w/v) of TPI crystals corresponding to original weight of sample at 0°C with enough m-chloroperbenzoic acid (Aldrich Chemical Company, Inc. with 85% peracid content) present to react with about 80% of the total double bond. 0.01% (w/v) of 2,2'-methylene bis(4-methyl-6-tertiary-butyl)phenol was used as antioxidant. After reaction for a particular time period the epoxidized crystals were filtered, washed first with amyl acetate, then with ether and dried at 0°C in vacuum. The degree of epoxidation of the polymer in $CDCl_3$ solution was monitored from the relative integral intensity using a JEOLCO 100 MHz proton NMR spectrum. The relative intensity of a peak was measured by xeroxing the spectral plot, cutting it and weighing.

III. RESULTS

Morphological Characterization with Microscopy: It was realized early in this study that maximum information can only be obtained by microscopic examination of the structures being formed while they are still in the liquid suspension. In the case of multilayer crystals this method affords a means of seeing the same crystals in different projection without distortion resulting from the sedimentation and drying down processes. In addition, in the case of more complex objects, the presence of a liquid medium also removes disturbing scattering effects, and clear features may arise in what can appear as a collapsed opaque mass in the dried state. Both interference contrast and the crossed polaroid techniques were used for recording the salient features of crystals photographically. A number of factors which influence the morphological form were varied as given below:

1. The influence of crystallization temperature and/or molecular weight: The effect of apparent crystallization temperature was investigated in the -15°C to +32°C region using three molecular weight fractions ($\bar{M}_n$'s of 2.4×10^4, 1.0×10^5 and 2.5×10^5) from amyl acetate solution. A concentration of 1% (w/v) was used for all but one preparation which was 3% (w/v). The morphologies

obtained were classified in terms of the appearance under interference contrast optics, the behavior when examined with polarized light as shown in Fig. 12., and the crystal form as found from X-ray diffraction and DSC endotherm temperatures.

The various structures observed are classified into six types and discussed in the following:

Type I: The simplest hedrites in α crystal form

For the lowest molecular weight (LMW fraction) with $\overline{M}_n = 2.4 \times 10^4$ used, a large number of these hedrites are formed at 15°C (Fig. 12-C) and only this type exists at 20°C (Fig. 12-B) and 30°C (Fig. 12-A). The high molecular weight (HMW fraction) with $\overline{M}_n = 2.5 \times 10^5$ has only a few of this type of hedrites at 32°C. These crystals are predominately in a "flat on" orientation with an elliptical structure that has a long axis of about 10-20 μM after sedimentation onto a glass slide; some splaying in an "edge-on" direction can be observed for these structures while floating in liquid suspension. The observation with crossed polaroids shows little, if any, birefringence in the "flat-on" direction, but a strong birefringence from the "edge-on" direction. These crystals are too thick to obtain much information using electron microscopy. At 32°C the LMW fraction has a high solubility and a more concentrated

solution, 3% (w/v), must be used to obtain crystalline structures.

Fig. 12: Photomicrographs for the Simplest Hedrites in α Crystal Form (Type I)

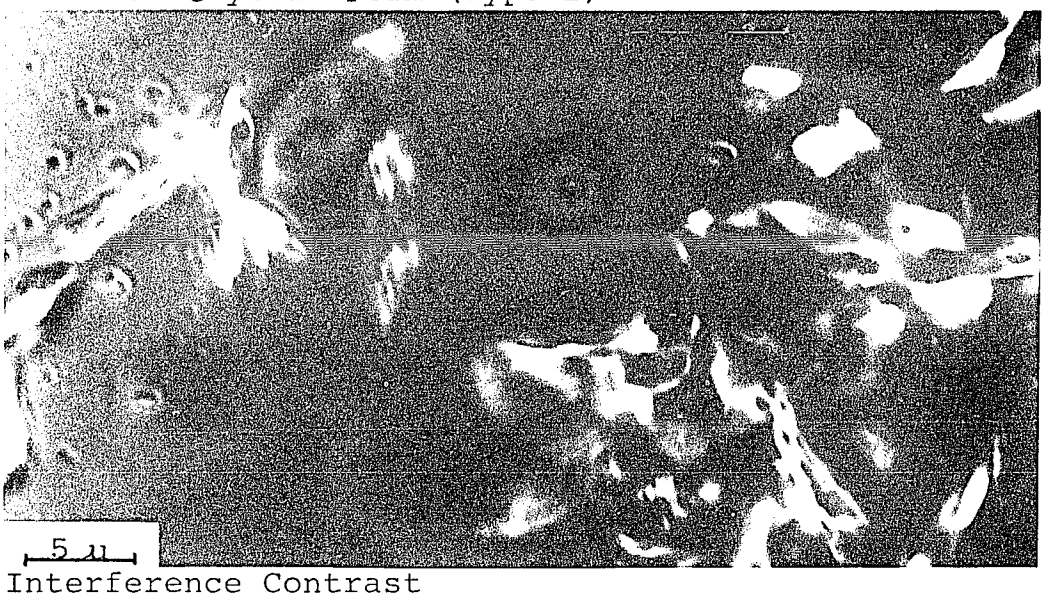

A: Interference Contrast

$\overline{M}_n = 2.4 \times 10^4$, $T_C = 32°C$ in 3% (w/v) Amyl Acetate

Crossed Polaroids of A.

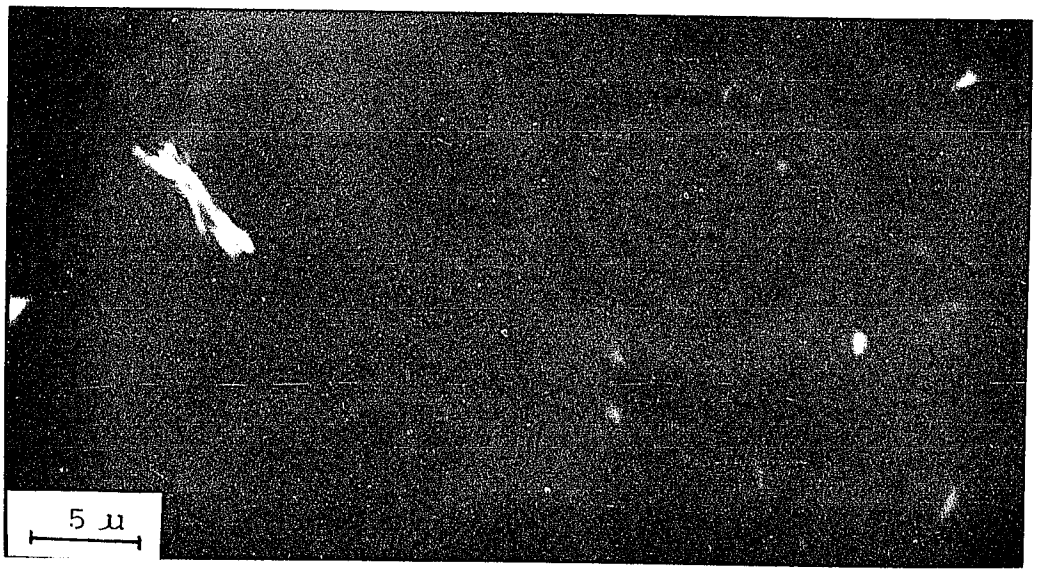

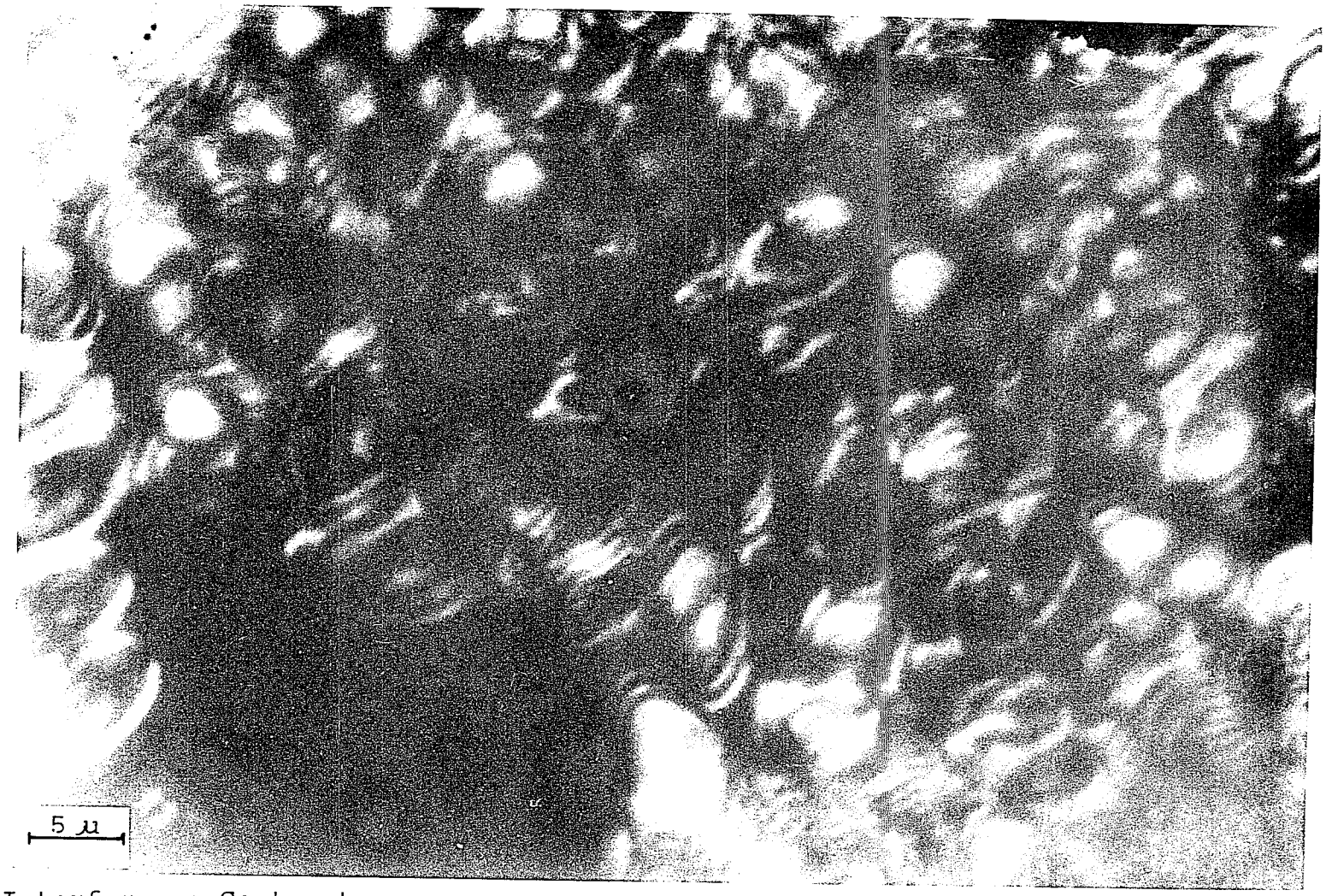

B-1: Interference Contrast

$\bar{M}_n = 2.4 \times 10^4$, $T_C = 20°C$ in 1% (w/v) Amyl Acetate

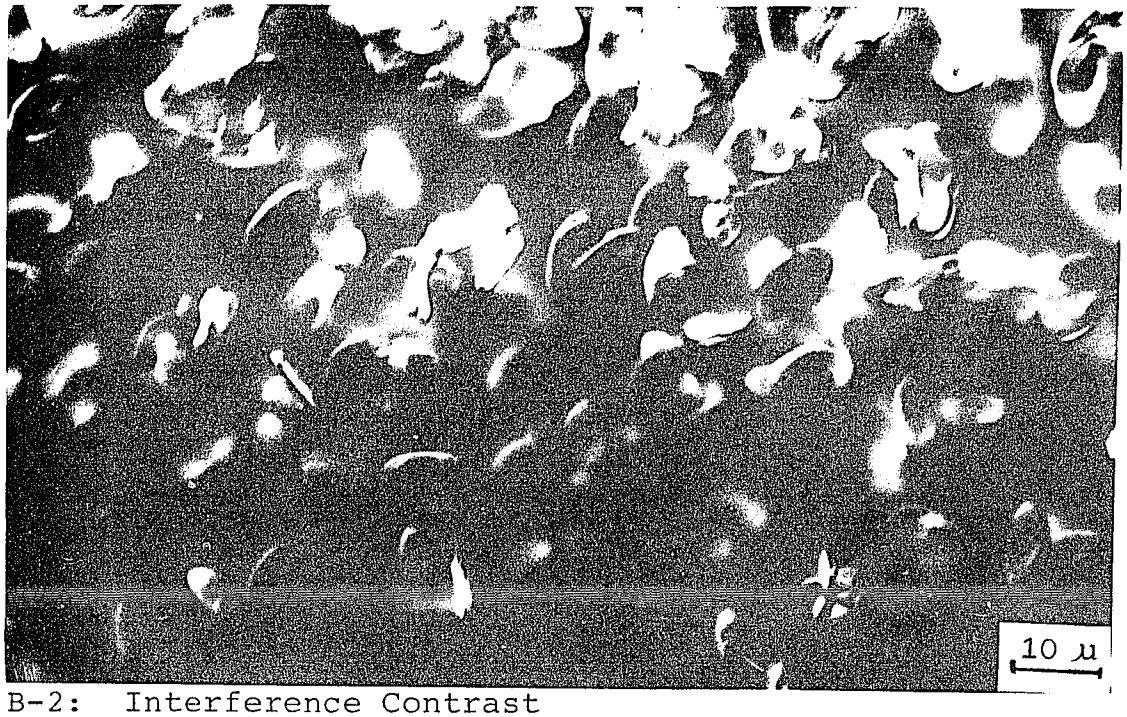

B-2: Interference Contrast

$\bar{M}_n = 2.4 \times 10^4$, $T_C = 20°C$ in 1% (w/v) Amyl Acetate

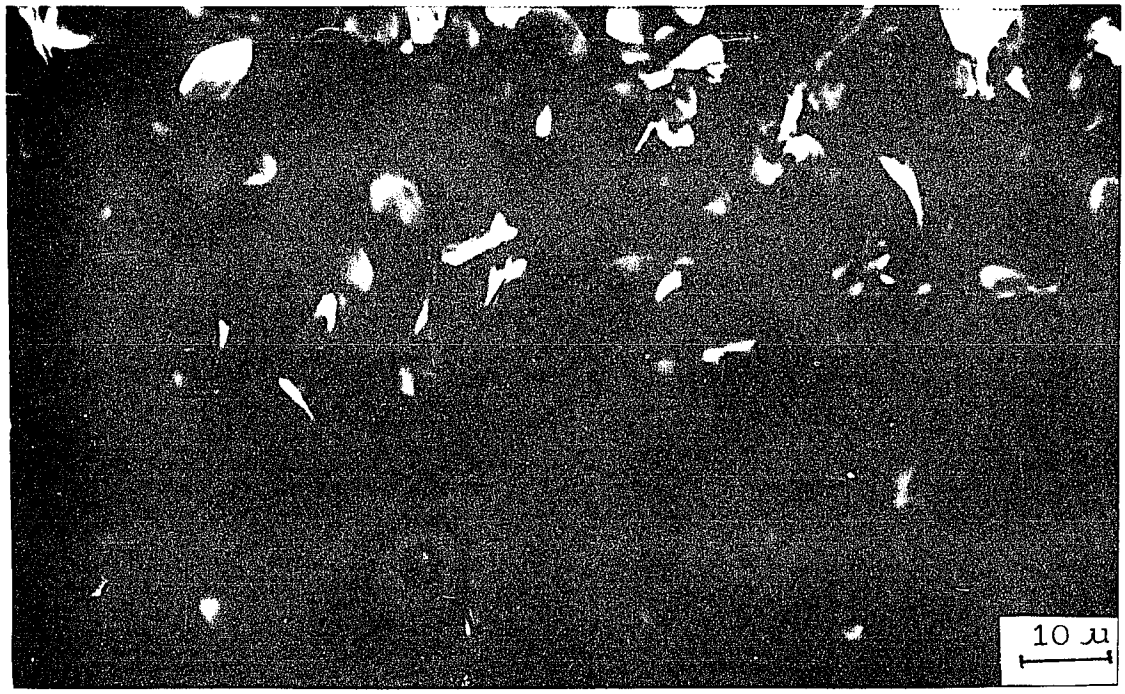

Crossed Polaroids of B-2

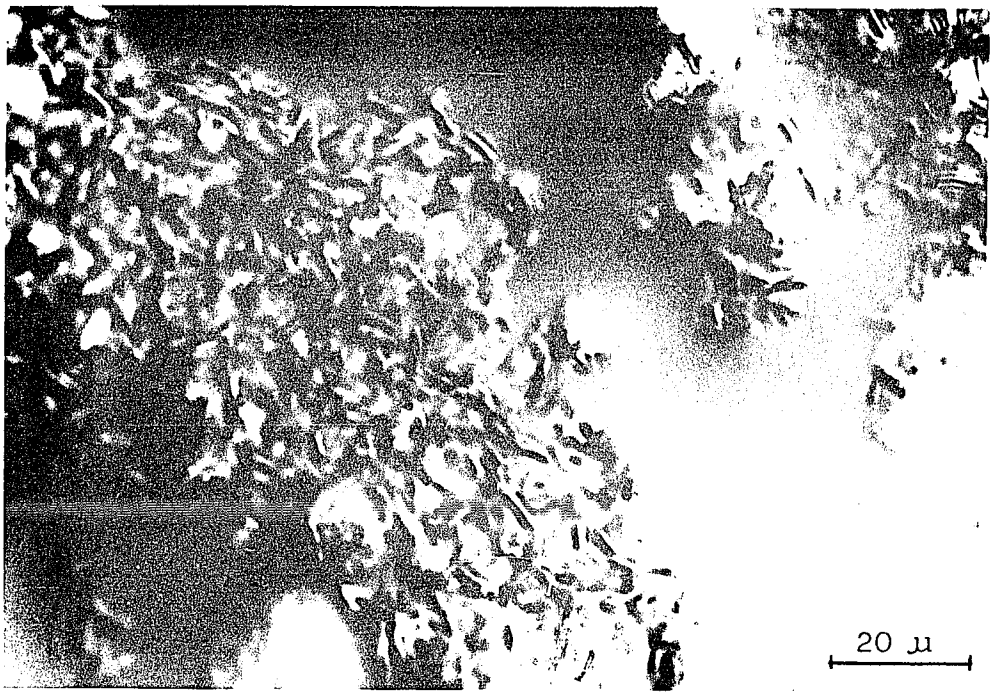

C: Interference Contrast

$\bar{M}_n = 2.4 \times 10^4$, $T_C = 15°C$ in 1% (w/v) Amyl Acetate

Type II: Sheaflike hedrites with weak briefringence and α form structure.

The structure obtained from the high molecular weight (HMW fraction) with $\bar{M}_n = 2.5 \times 10^5$ at high temperature, 32°C, (Fig. 13 A-1 and A-2) or grown from the medium molecular weight (MMW fraction) with $\bar{M}_n = 1.0 \times 10^5$ at medium temperature, 20°C, (Fig. 13-B) with clearly splaying branches are sheaflike and are predominately in the α structure; these also show a weak birefringence when observed with crossed polaroids.

Fig. 13. Photomicrographs for the Sheaflike Hedrites with Weak Birefringence and α Form Structure

A-1: Inference Contrast

$\bar{M}_n = 2.5 \times 10^5$, $T_C = 32°C$ in 1% (w/v) Amyl Acetate

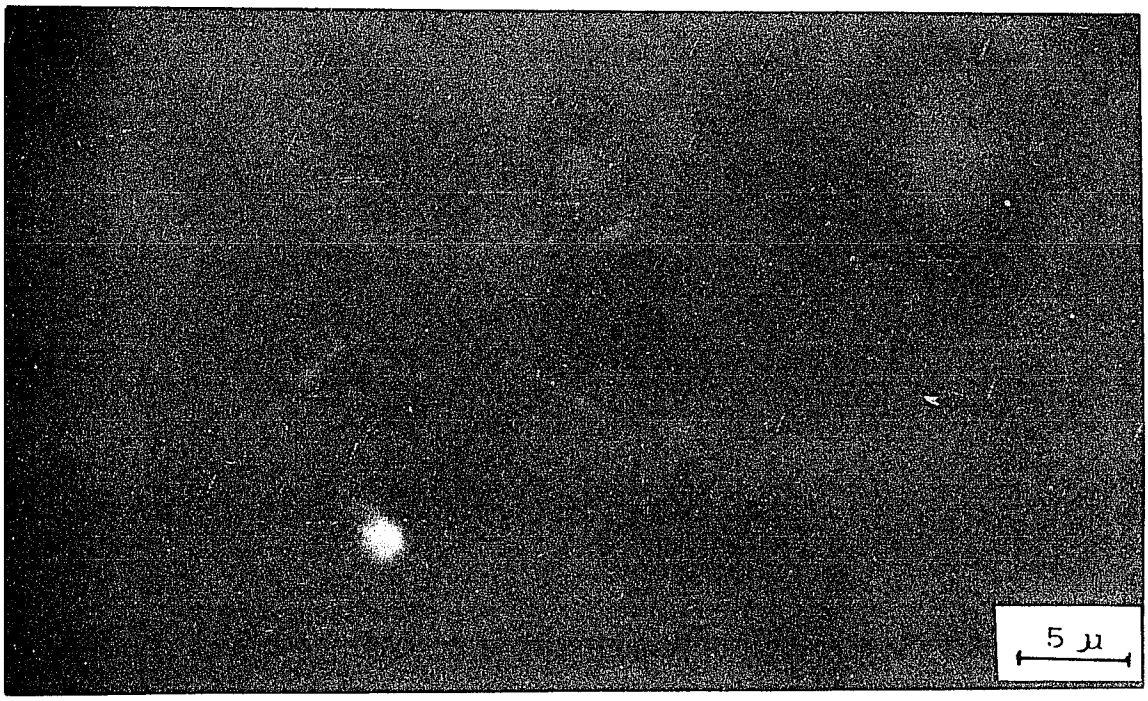

Crossed Polaroids of A-1

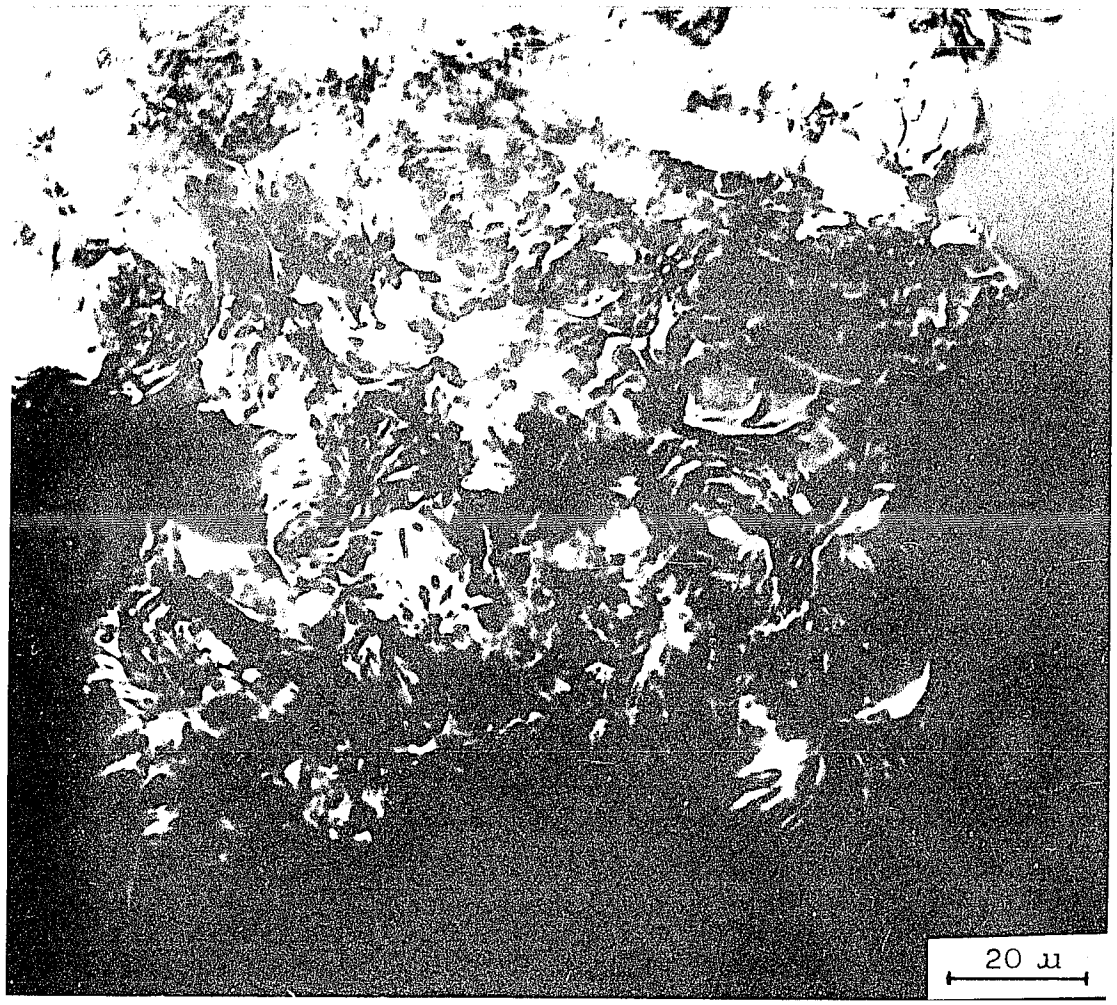

A-2: Interference Contrast

$\bar{M}_n = 2.5 \times 10^5$, $T_C = 32°C$ in 1% (w/v) Amyl Acetate

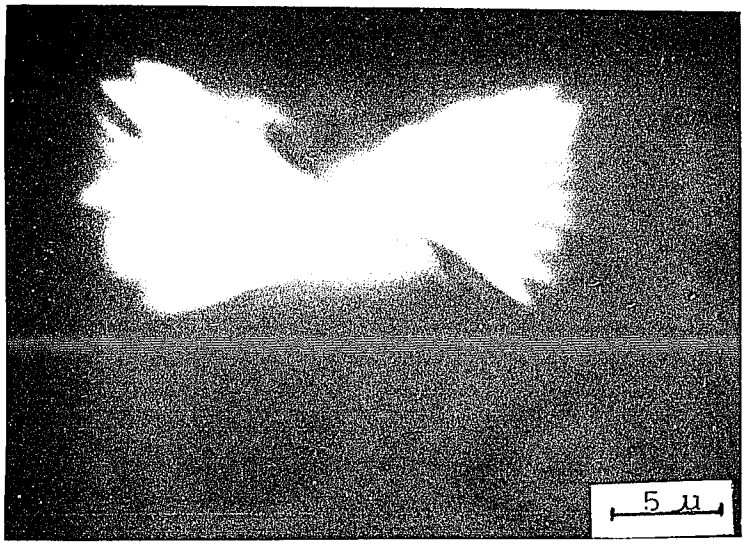

B: Interference Contrast

$\bar{M}_n = 1.0 \times 10^5$, $T_C = 20°C$ in 1% (w/v) Amyl Acetate

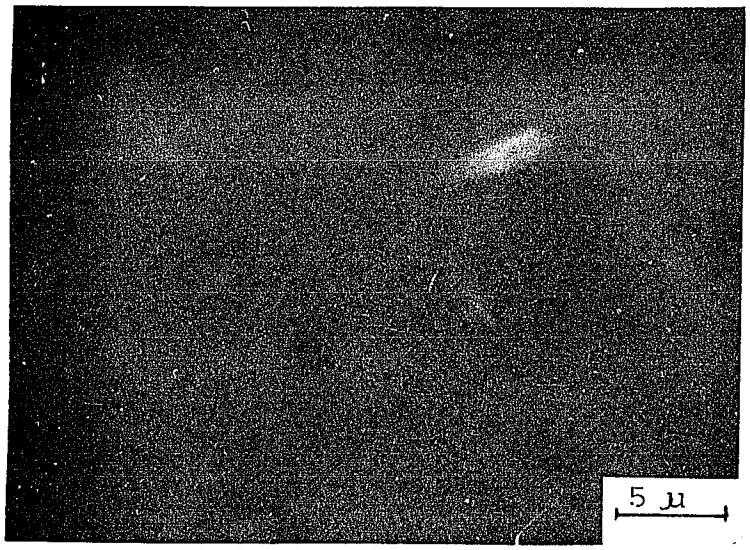

Crossed Polaroids of B

Type III and Type IV: Sheaflike hedrites with distinct birefringence, Type-III-β form and Type-IV-α form.

These can be prepared from different molecular weight fractions depending on the crystallization temperature. Low molecular weight (LMW fraction) with $\bar{M}_n = 2.4 \times 10^4$ at T_C's of 10,0,-15°C (Fig. 14-A,B,C) and medium molecular weight (MMW fraction with $\bar{M}_n = 1.0 \times 10^5$ at T_C of 10°C, show large more complex structures in the β form. High molecular weight (HMW fraction) with $\bar{M}_n = 2.5 \times 10^5$ at T_C of 15, 20°C show similar morphologies in the α form (14-D,E), a mixture of two forms is formed at T_C = 15°C for the MMW fraction (Fig. 14-F). These appear similar to the transitional multilayered hedrite structures which develop during the early stages as studied by Keith (22) in the growth of polyethylene spherulites. Rotating these crystals shows a radiating array of ribbons in an edge-on view and a bundle of chain-folded lamellae with rectangular shapes in a flat-on view.

These structures are not spherically symmetrical but apparently are precusors of spherulites. The numbers of arms in the birefringence pattern are changed by rotating the microscope stage. When the longer axis of the sheaflike crystals is in the direction of the polarizer or analyzer, birefringence with two equal arms is

observed as shown schematically in Fig. 15. When the field is rotating through 45° in the plane of the microscope stage with the longer axis now in the direction of the polarizer or analyzer one large arm and two small arms are observed. An example of the birefringence changes taking place at T_C = 20°C for a HMW fraction structure are given in Fig. 16.

From the flat-on view the structures with rectangular (close to oval) shape appear thin in the center by interference contrast microscopy observation. A similar extinction behavior due to the same cause is shown by the Type-I structures. However, we can not exclude the possibility that the molecular axis of TPI is oriented perpendicular to the rectangular plane in the central region. The coarseness of fibril structure increases with increasing crystallization temperature in the range of molecular weight used.

LMW fraction crystals grown at -15°C (Fig. 12-C) have a coarser and smaller structure than the same fraction grown at 0 or 10°C (Fig. 14-A,B). This may be due to a large nucleation density caused by the larger supercooling. This is consistent with the results of unfractionated TPI melt crystallization reported by Davies and Long (51) at similar supercoolings.

Fig. 14. Photomicrographs for Sheaflike hedrites with Distinct Birefringence (Type III and Type IV)

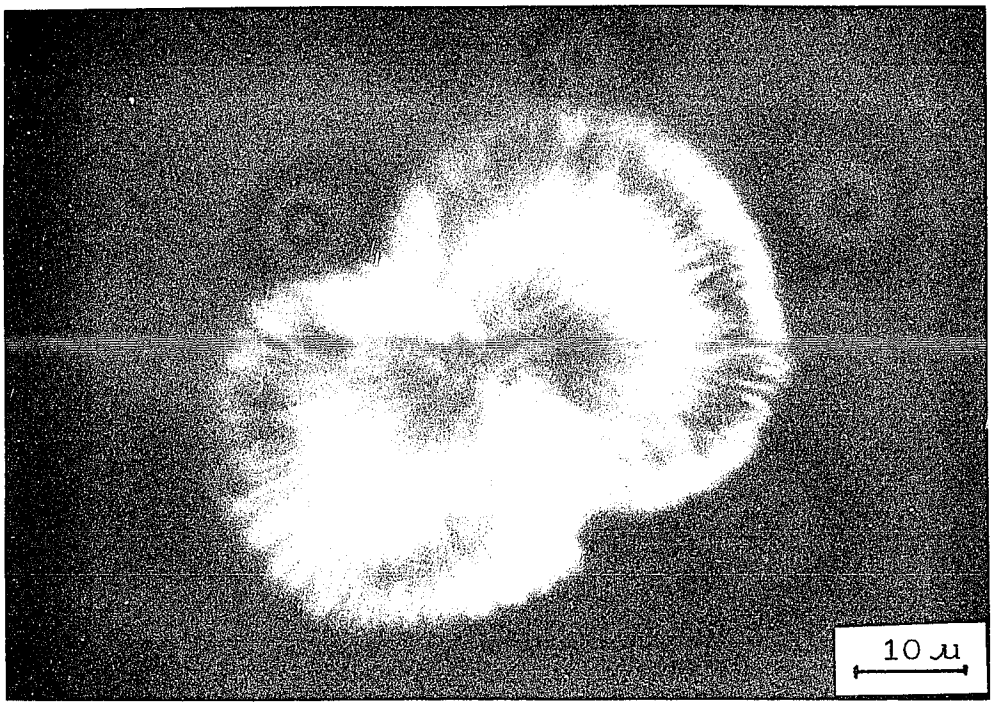

A-1: Interference Contrast

$\bar{M}_n = 2.4 \times 10^4$, $T_C = 10°C$ in 1% (w/v) Amyl Acetate

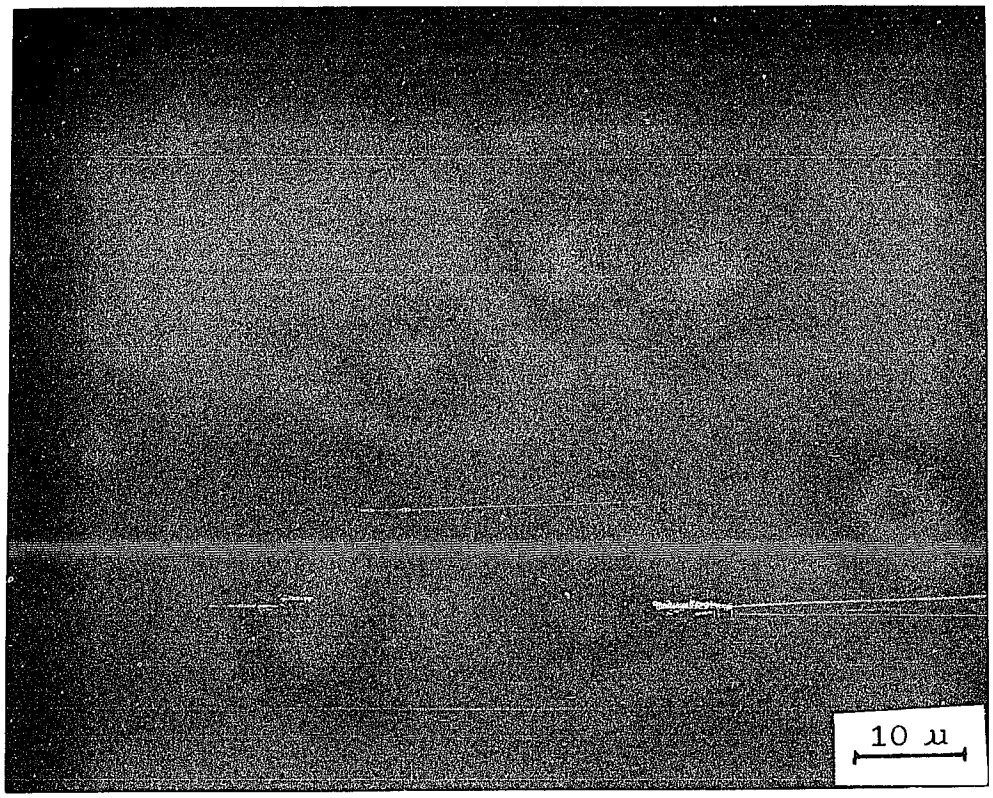

Crossed Polaroids of A-1

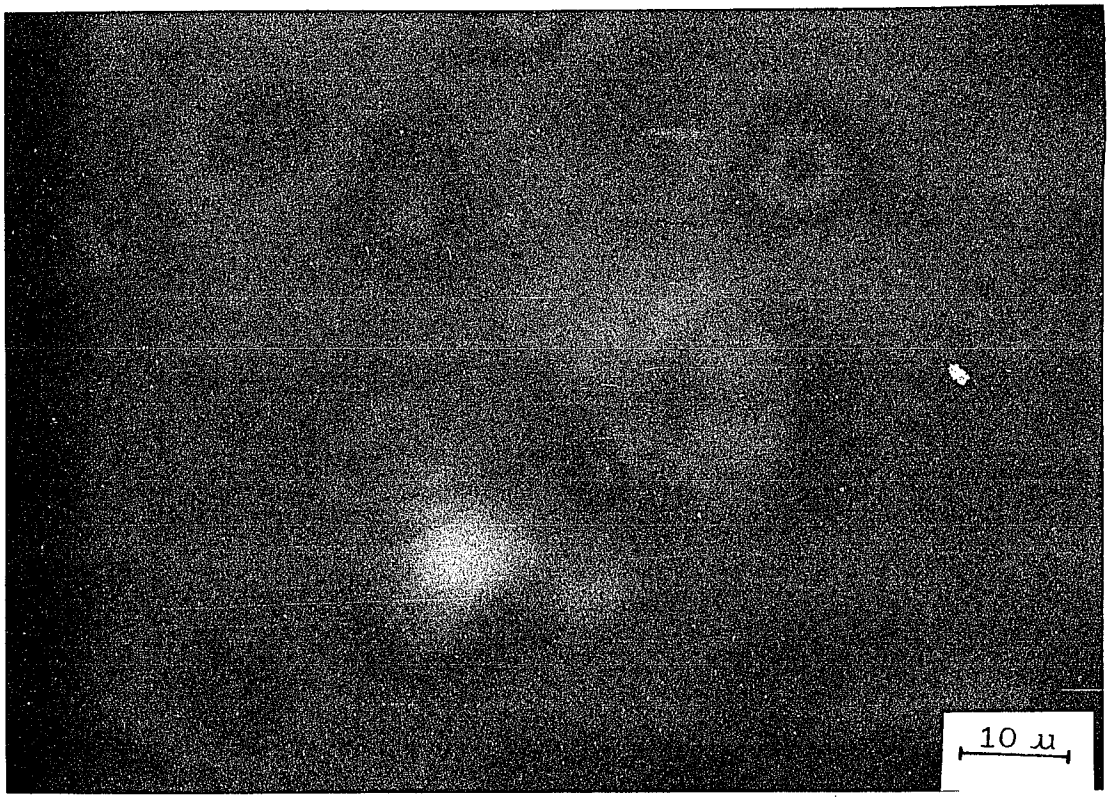

Interference Contrast

Forcus Change of A-1

A-2: Interference Contrast

$\overline{M}_n = 2.4 \times 10^4$, $T_C = 10°C$ in 1% (w/v) Amyl Acetate

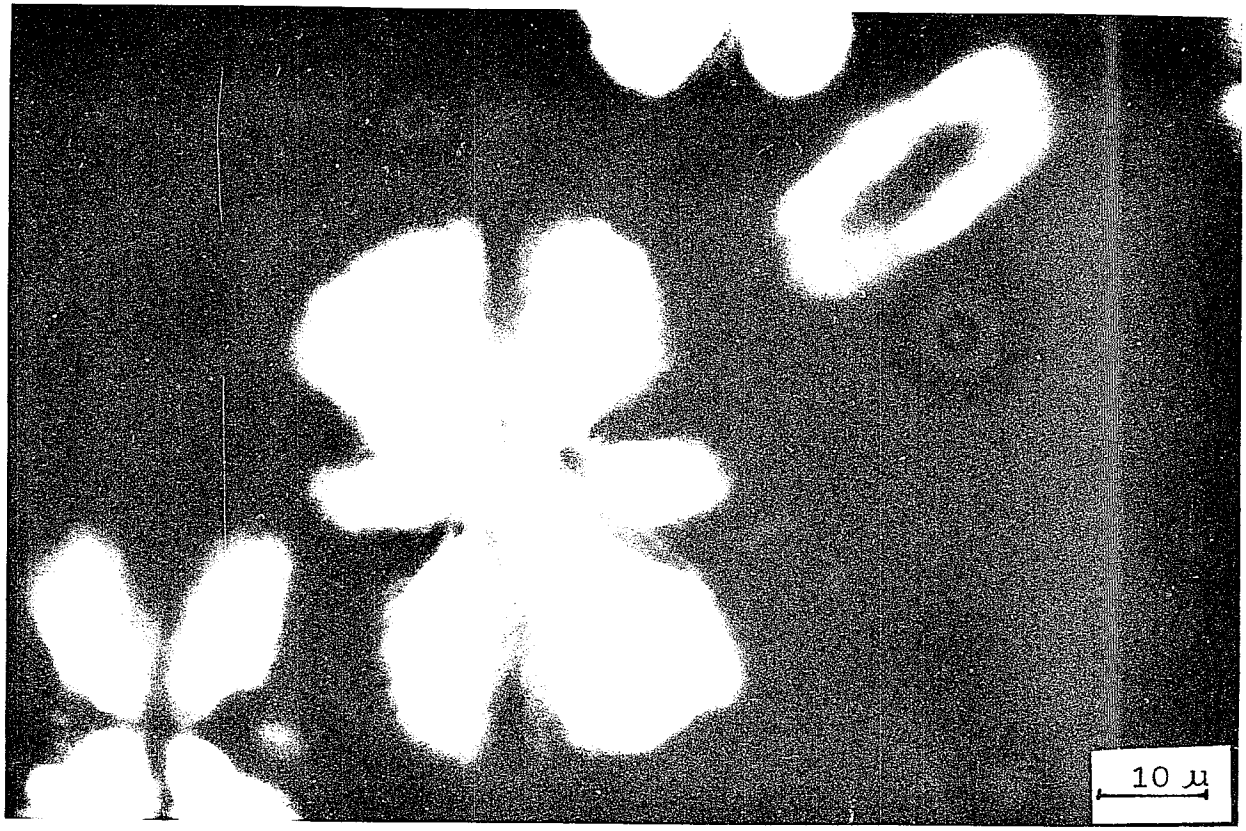

Crossed Polaroids of A-2

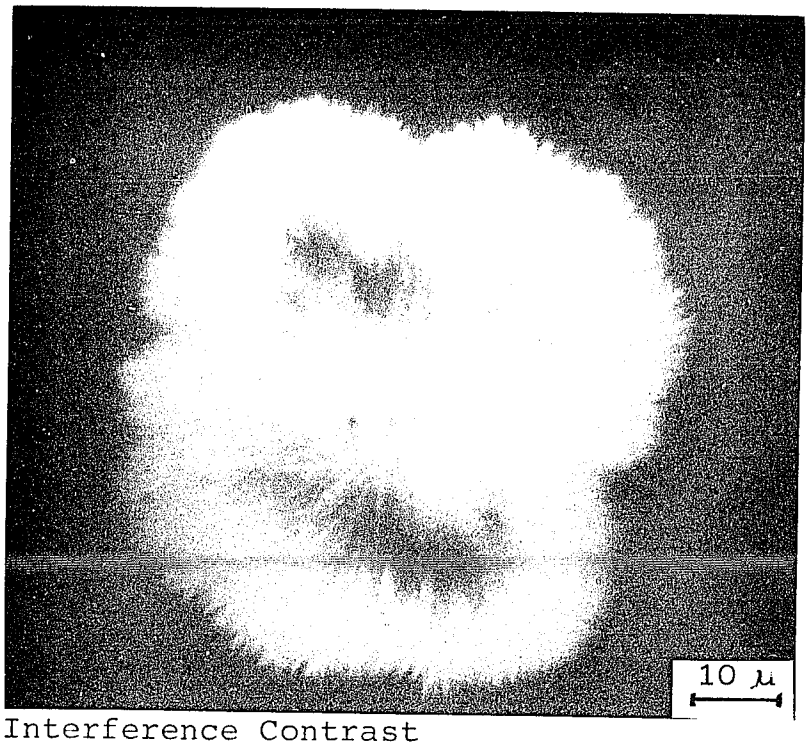

B-1: Interference Contrast

$\overline{M}_n = 2.4 \times 10^4$, $T_C = 0°C$ in 1% (w/v) Amyl Acetate

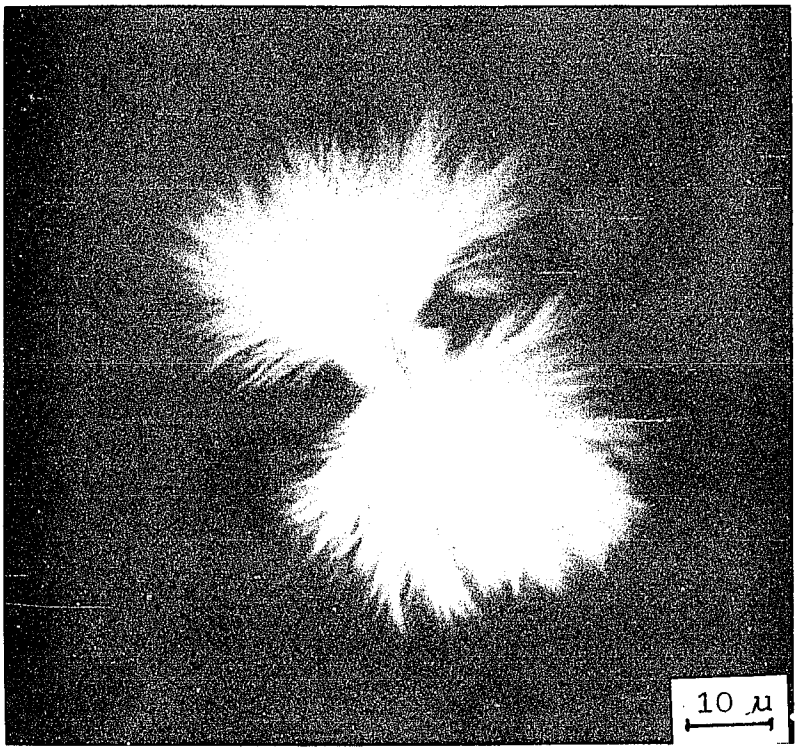

B-2: Interference Contrast

$\overline{M}_n = 2.4 \times 10^4$, $T_C = 0°C$ in 1% (w/v) Amyl Acetate

C: Interference Contrast

$\bar{M}_n = 2.4 \times 10^4$, $T_C = -15°C$, in the 1% (w/v) Amyl Acetate

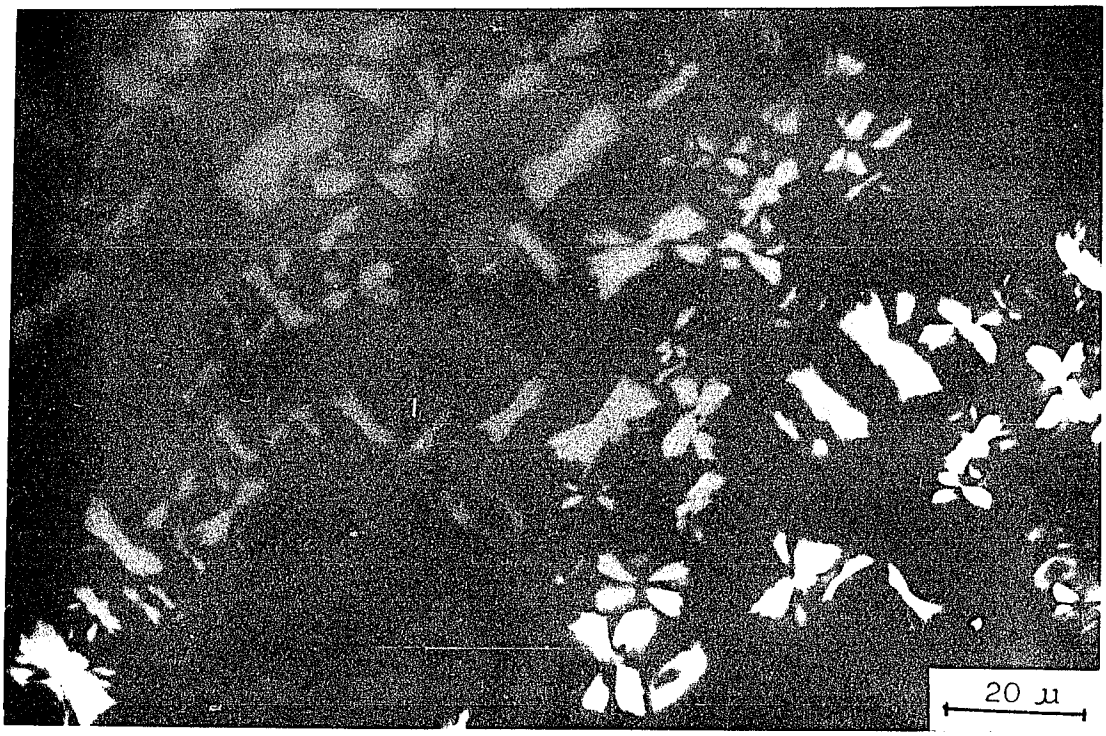

Crossed Polaroids of C

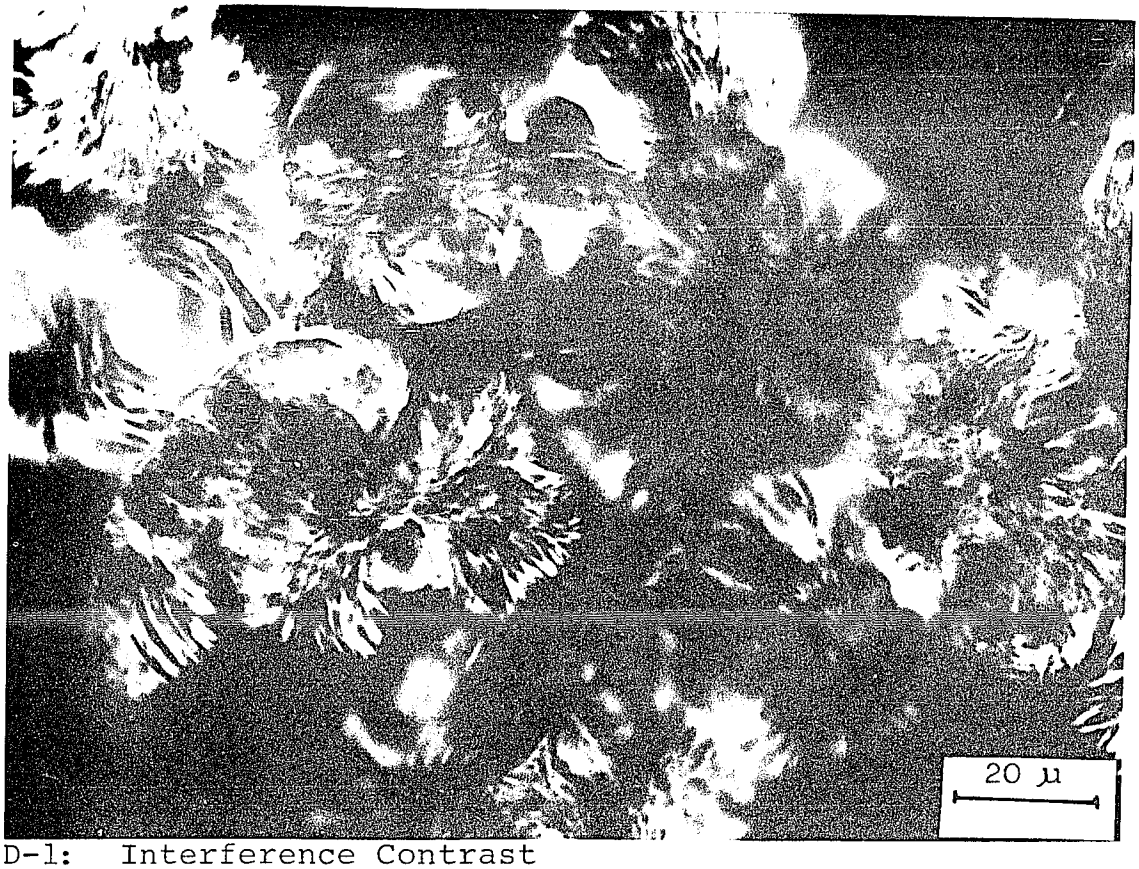

D-1: Interference Contrast

$\bar{M}_n = 2.5 \times 10^5$, $T_C = 20°C$ in 1% (w/v) Amyl Acetate

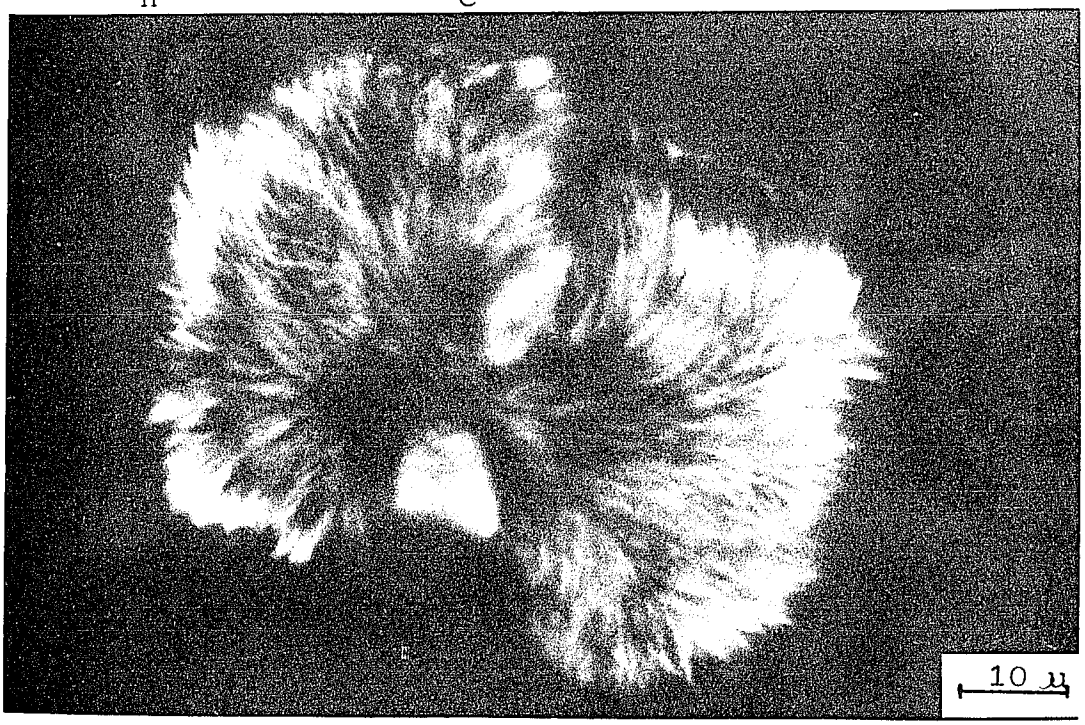

D-2: Interference Contrast

$\bar{M}_n = 2.5 \times 10^5$, $T_C = 20°C$ in 1% (w/v) Amyl Acetate

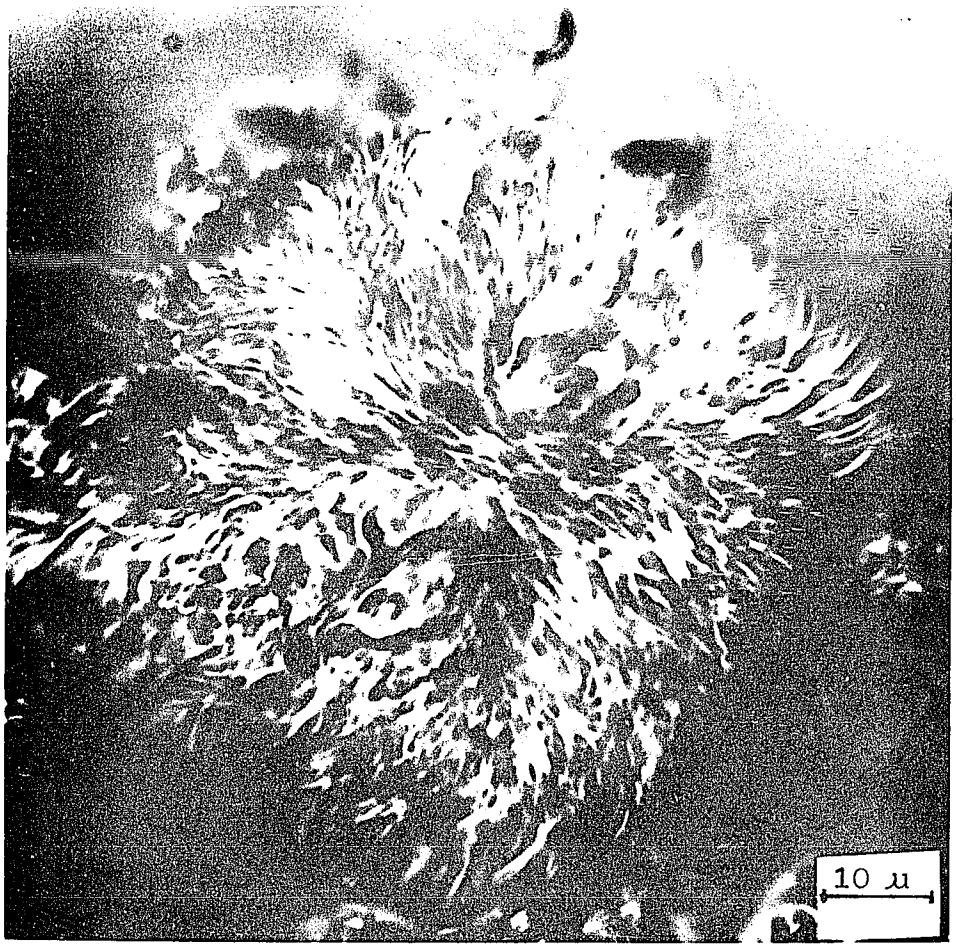

E: Interference Contrast

$\overline{M}_n = 2.5 \times 10^5$, $T_C = 15°C$ in 1% (w/v) Amyl Acetate

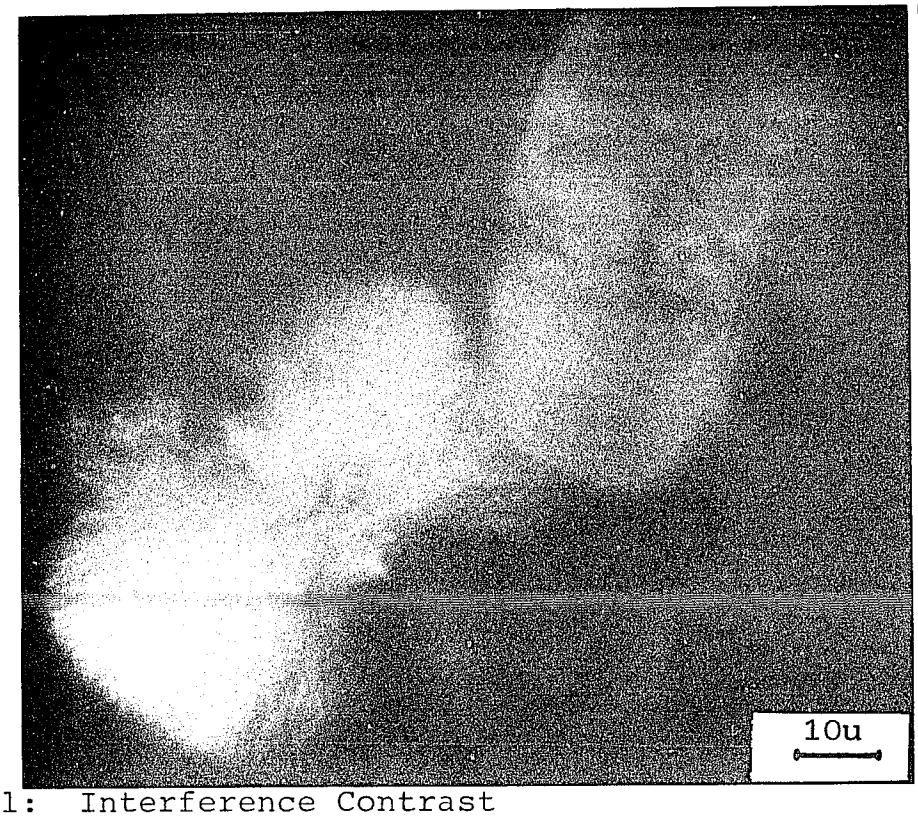

F-1: Interference Contrast

$\overline{M}_n = 1.0 \times 10^5$, $T_C = 15°C$ in 1% (w/v) Amyl Acetate

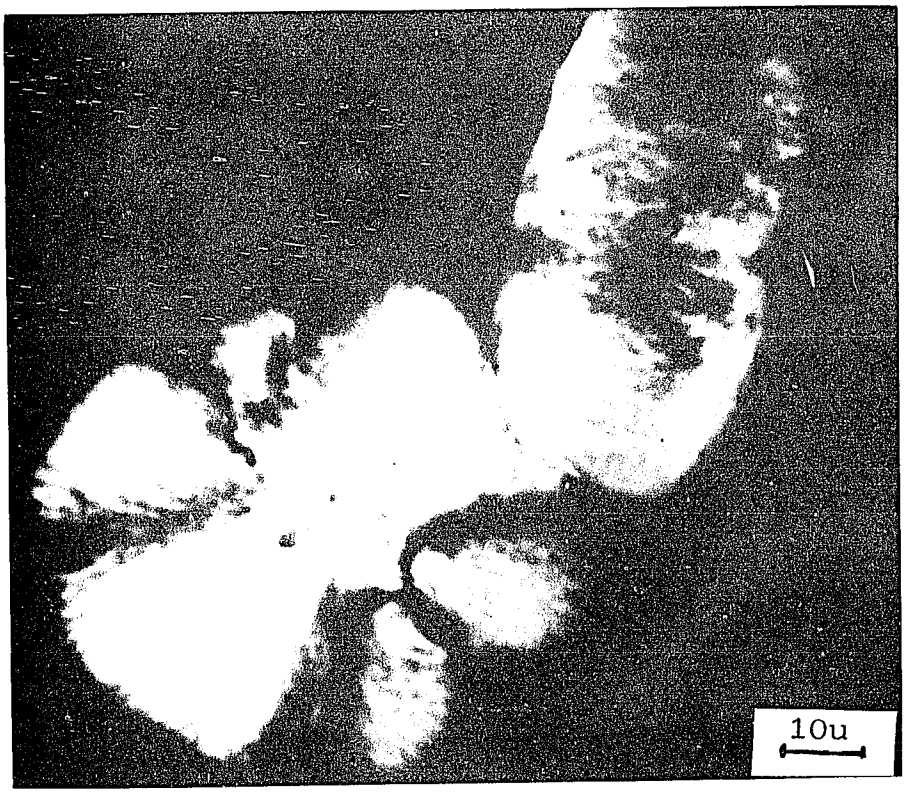

Crossed Polaroids of F-1

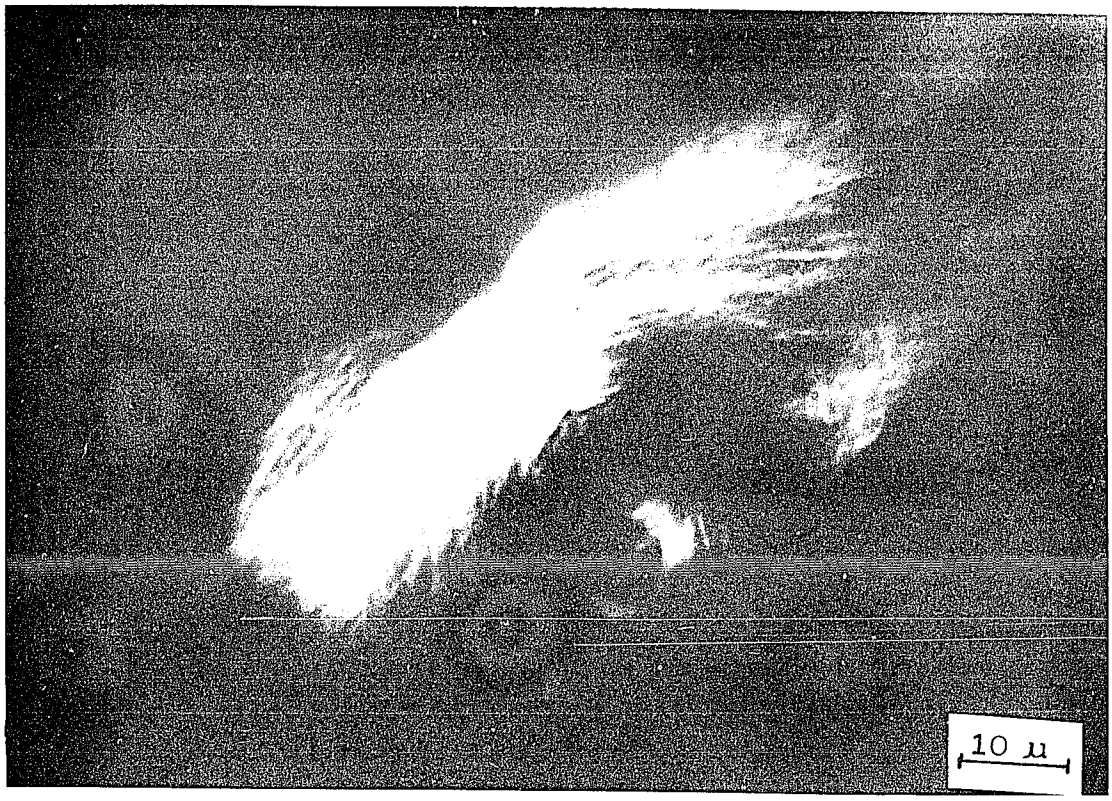

F-2: Interference Contrast

$\overline{M}_n = 1.0 \times 10^5$, T_C = 15°C in 1% (w/v) Amyl Acetate

F-3: Interference Contrast

$\overline{M}_n = 1.0 \times 10^5$, T_C = 15°C in 1% (w/v) Amyl Acetate

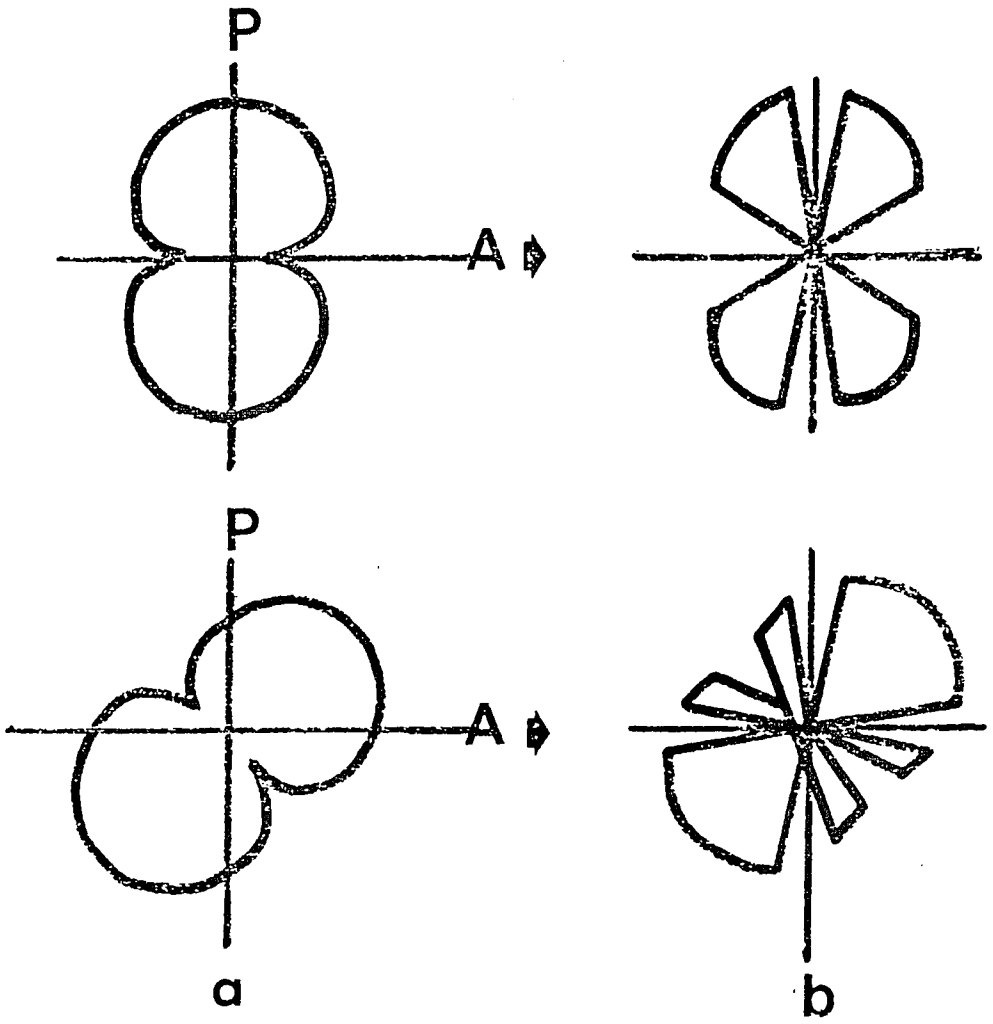

Fig. 15. Schematic Drawing of a) hedrites like those in Fig. 14 at two orientations with respect to analyzer (A) and polarizer (P) directions and b) the birefringence patterns arising from them.

Fig. 16. Photomicrographs for α-TPI Hedrites (Type IV) from 1% (w/v) Amyl Acetate Solution, $\overline{M}_n = 2.5 \times 10^5$, $T_C = 20°C$

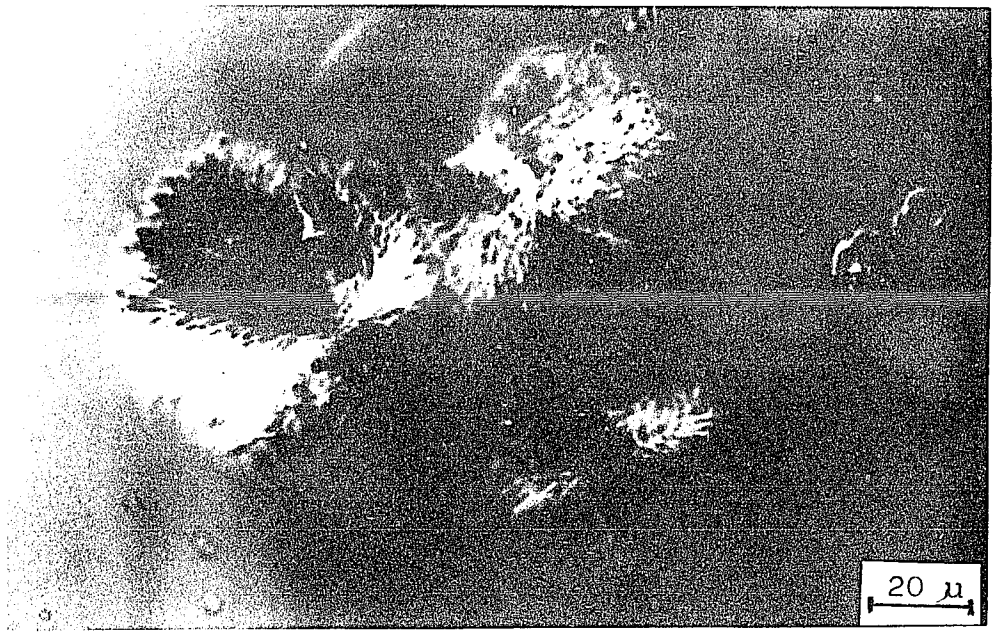

A. Interference Contrast

B. Crossed Polaroids, the Same Microscope Stage Orientation as A.

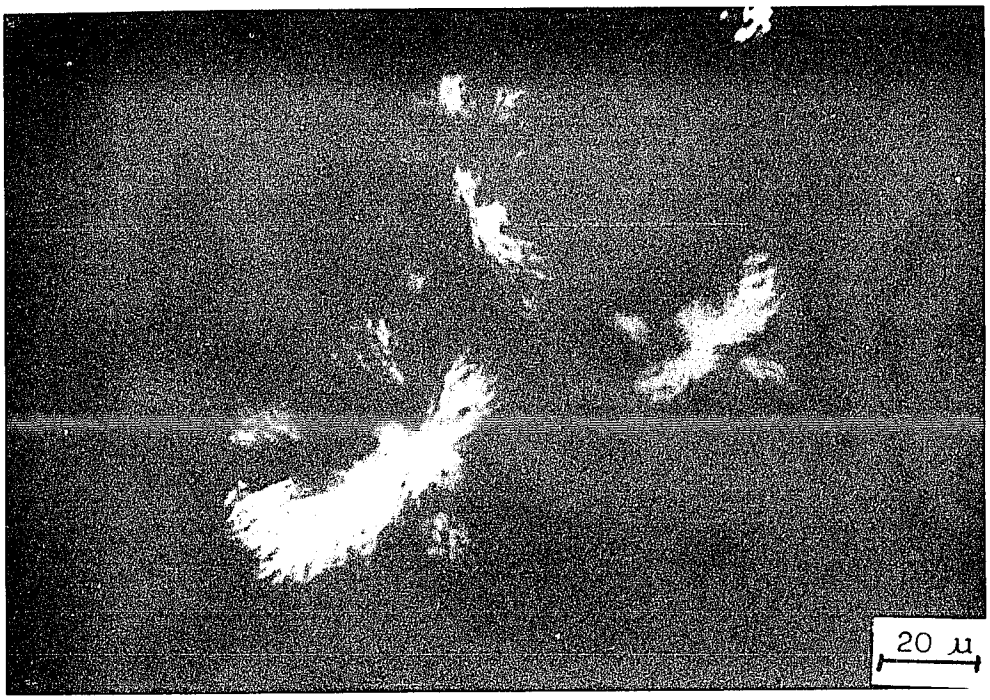

C: Stage Rotated 45° from Setting for B

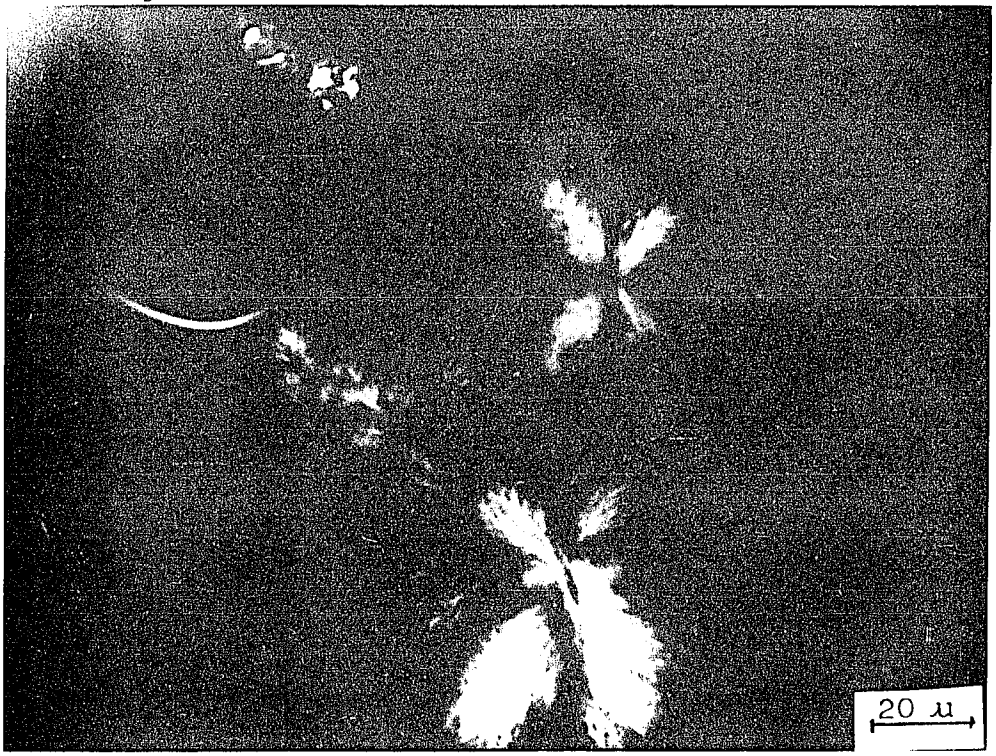

D: Stage Rotated 90° from Setting for B

Type V: Spherulites with Strong Birefringence in the β Form.

The crystal aggregates grown from HMW fraction with $\bar{M}_n = 2.5 \times 10^5$ at 10°C (Fig. 17-A) or MMW fraction with $\bar{M}_n = 1.0 \times 10^5$ at 0°C (Fig. 17-B) show almost a spherical symmetry and an apparent twisted stalk in the center. These look like typical twisted sheaf spherulites of Gutta percha as grown from the melt and reported by Keller and Warning (41).

Therefore, a larger supercooling cause a change from a hedrite to a spherulite morphology. The birefringence observed with crossed-nicols give a deviation from the Maltese Cross type pattern. However, the morphology with the radial orientation and fibrillar habit especially the incidence of low angle noncrystallographic branching yields the ultimate spherical symmetry of these crystals.

Fig. 17. Photomicrographs from Spherulites with Strong Birefringence in the β Form.

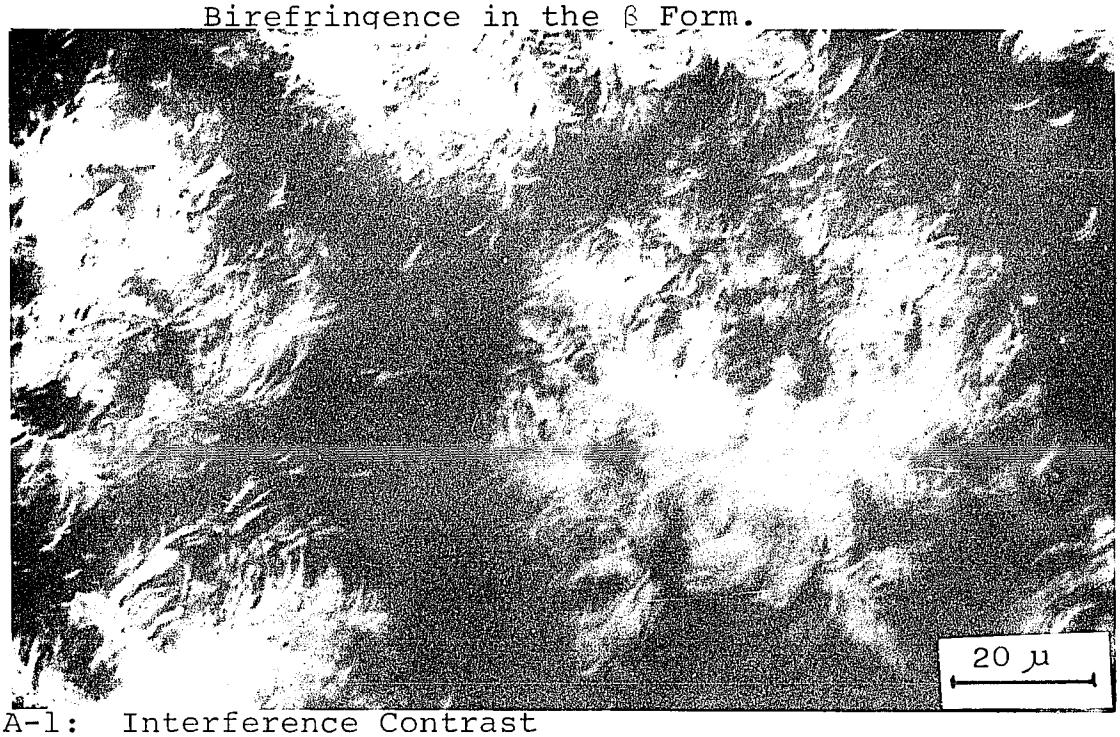

A-1: Interference Contrast

$\bar{M}_n = 2.5 \times 10^5$, $T_C = 10°C$ in 1% (w/v) Amyl Acetate

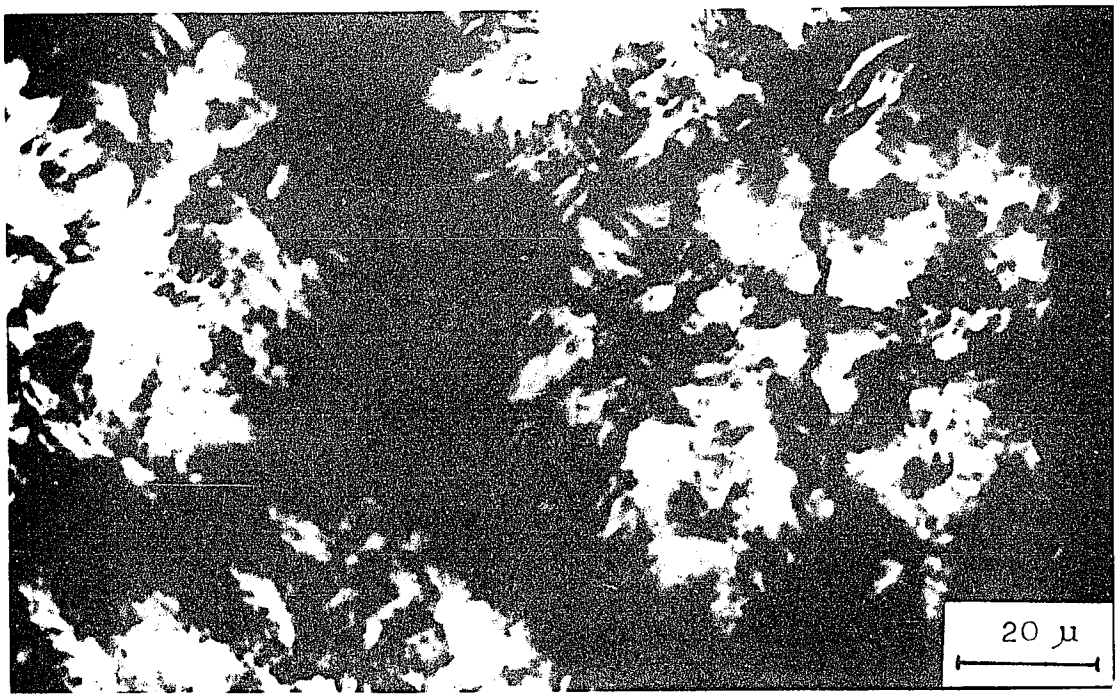

Crossed Polaroids of A-1

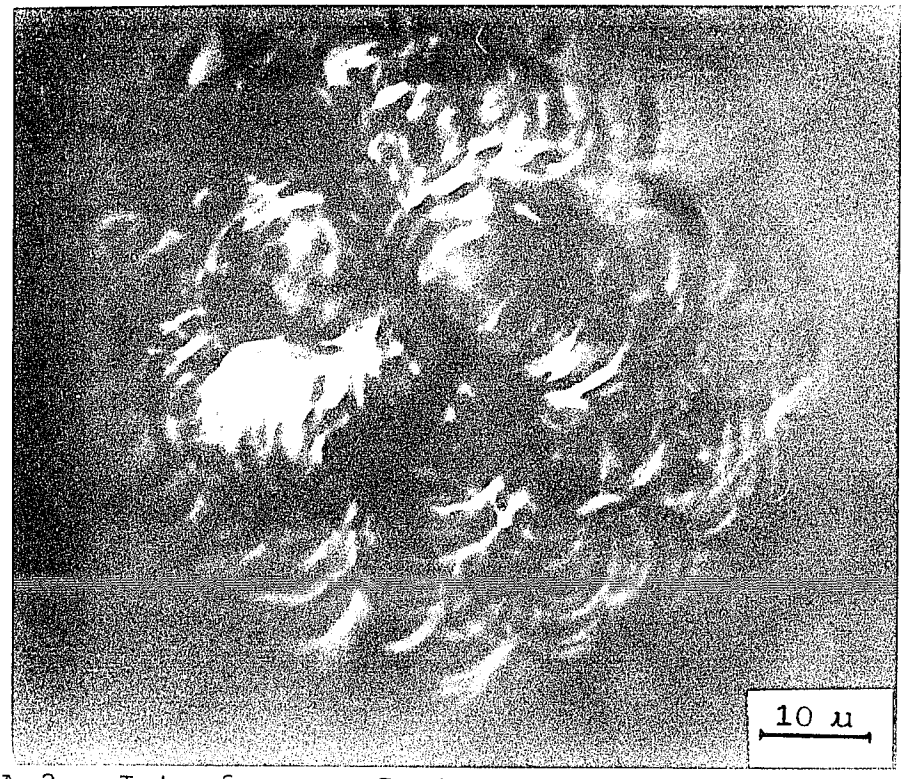

A-2: Interference Contrast

$\overline{M}_n = 2.5 \times 10^5$, $T_C = 10°C$ in 1% (w/v) Amyl Acetate

A-3: Interference Contrast

$\overline{M}_n = 2.5 \times 10^5$, $T_C = 5°C$ in 1% (w/v) Amyl Acetate

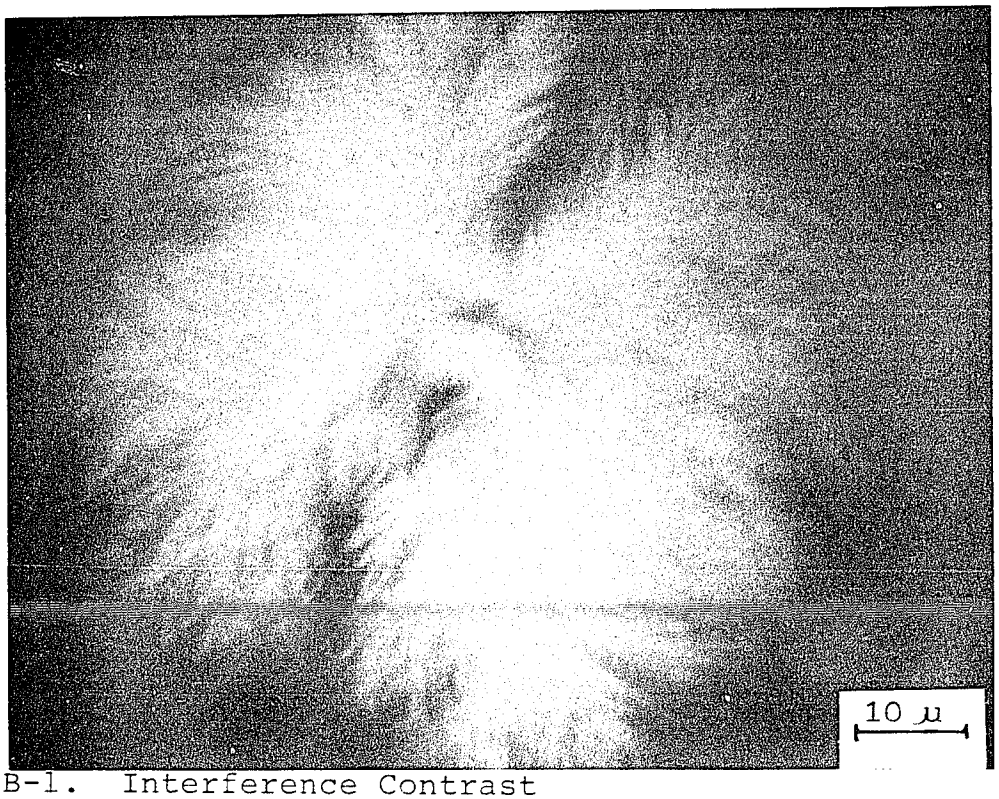

B-1. Interference Contrast

$\bar{M}_n = 1.0 \times 10^5$, $T_C = 0°C$ in 1% (w/v) Amyl Acetate

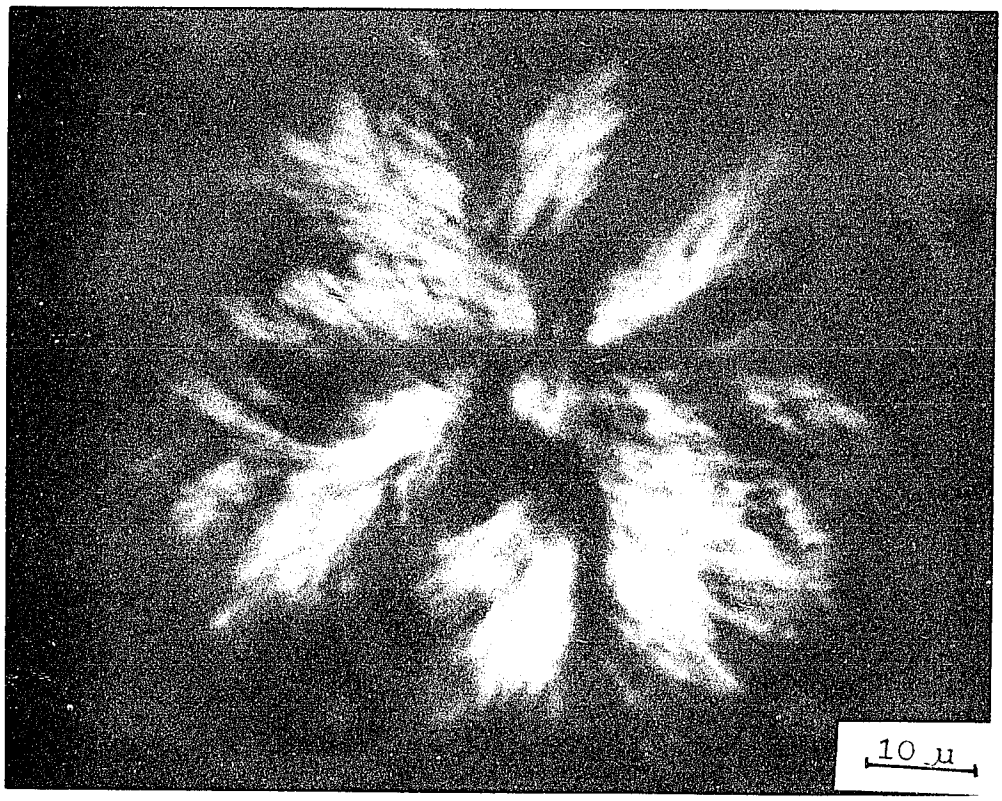

Crossed Polaroids of B-1

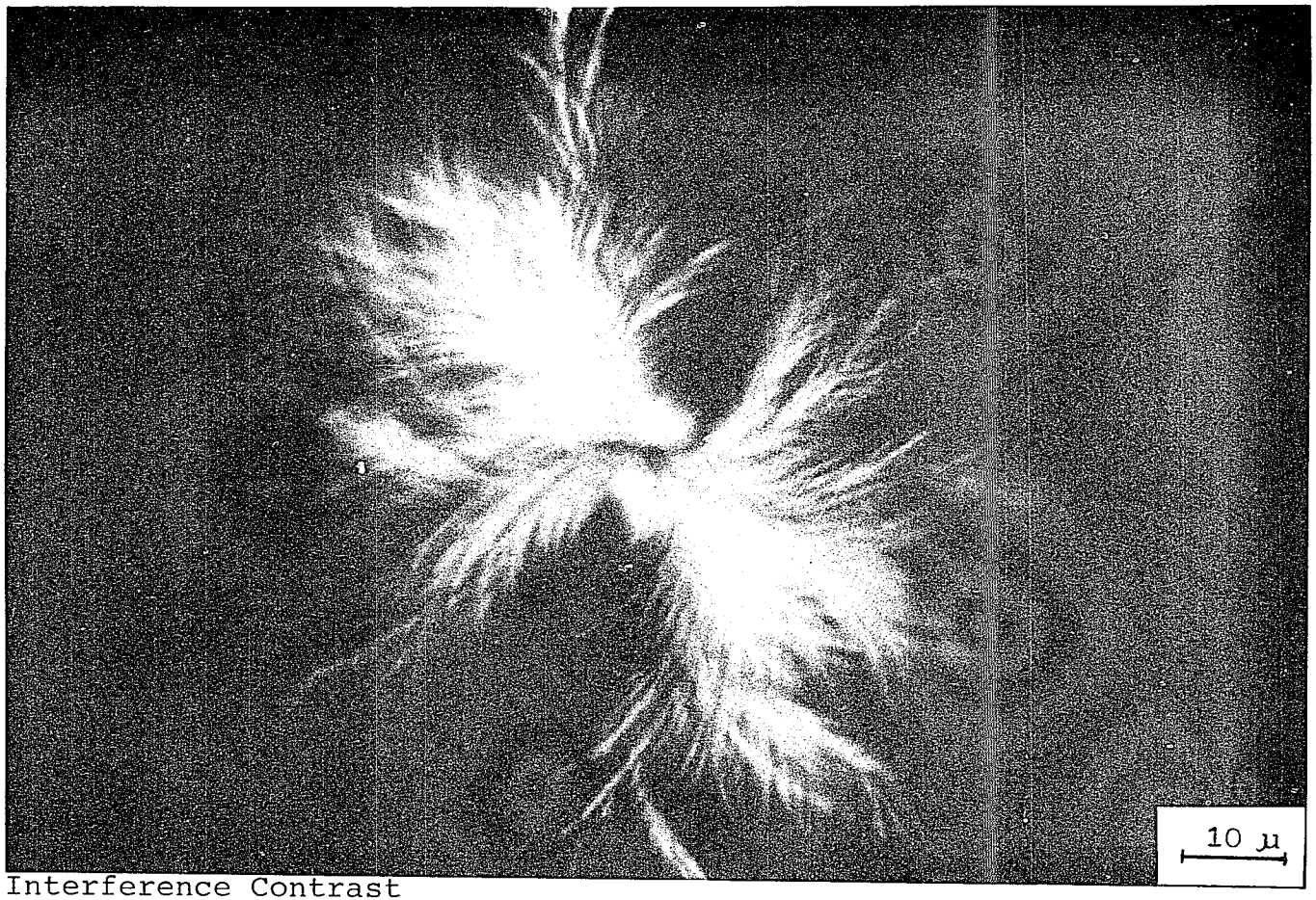

B-2: Interference Contrast

$\overline{M}_n = 1.0 \times 10^5$, $T_C = 0°C$ in 1% (w/v) Amyl Acetate

Type-VI: Cup-shaped Lamellar Aggregates with the β Form

The HMW fraction with the bath temperature at 0°C or the MMW fraction with a bath temperature of -15°C precipitate rapidly and produce complex arrays of curved chain-folded lamellae (Fig. 18-A,B). The top most layers in the center curl up and present the appearance of strong birefringence ; only weak birefringence exists at the edge of these curved lamellae. After fixing with O_sO_4 and drying, all the curved lamellae are flattened out and the birefringence disappears. The aggregates obtained from 1% (w/v) solutions are thick and show little detail in the transmission electron microscope. However, similar aggregates with a few curved layers grown from 0.05% (w/v) amyl acetate solution have been examined as discussed below. When Type-V spherulites grown from the HMW fraction at T_C = 10°C are subjected to the same O_sO_4 fixing technique, the birefringence still exists.

The HMW fraction grown at high supercooling with an apparent T_C of -15°C shows individual globules with a size of 2-5 μm mixed with cup-shaped lamellar aggregates (Fig. 18-C). This crystal habit was also found for poly(4-methylene pentene-1) (62,63), polyoxymethylene (64) and polychlorotrifluorethylene (65) crystallized at relatively large supercoolings. Surprisingly, a strong Maltese Cross like birefringence was observed while it was viewed

flat-on, i.e., along the central axis of the globules. However, the pattern and intensity of birefringence give somewhat change depending on the orientation of crystals.

When the structures are fixed with O_sO_4 and examined under the electron microscope as shown in Fig. 17., they exhibit, due to the thickness, an overall opacity to the electron beam and little detail can be observed.

Fig. 18. Photomicrographs of Cup-shaped Lamellar Aggregates from 1% (w/v) Amyl Acetate. $\bar{M}_n = 2.5 \times 10^5$ at $T_C = 0°C$.

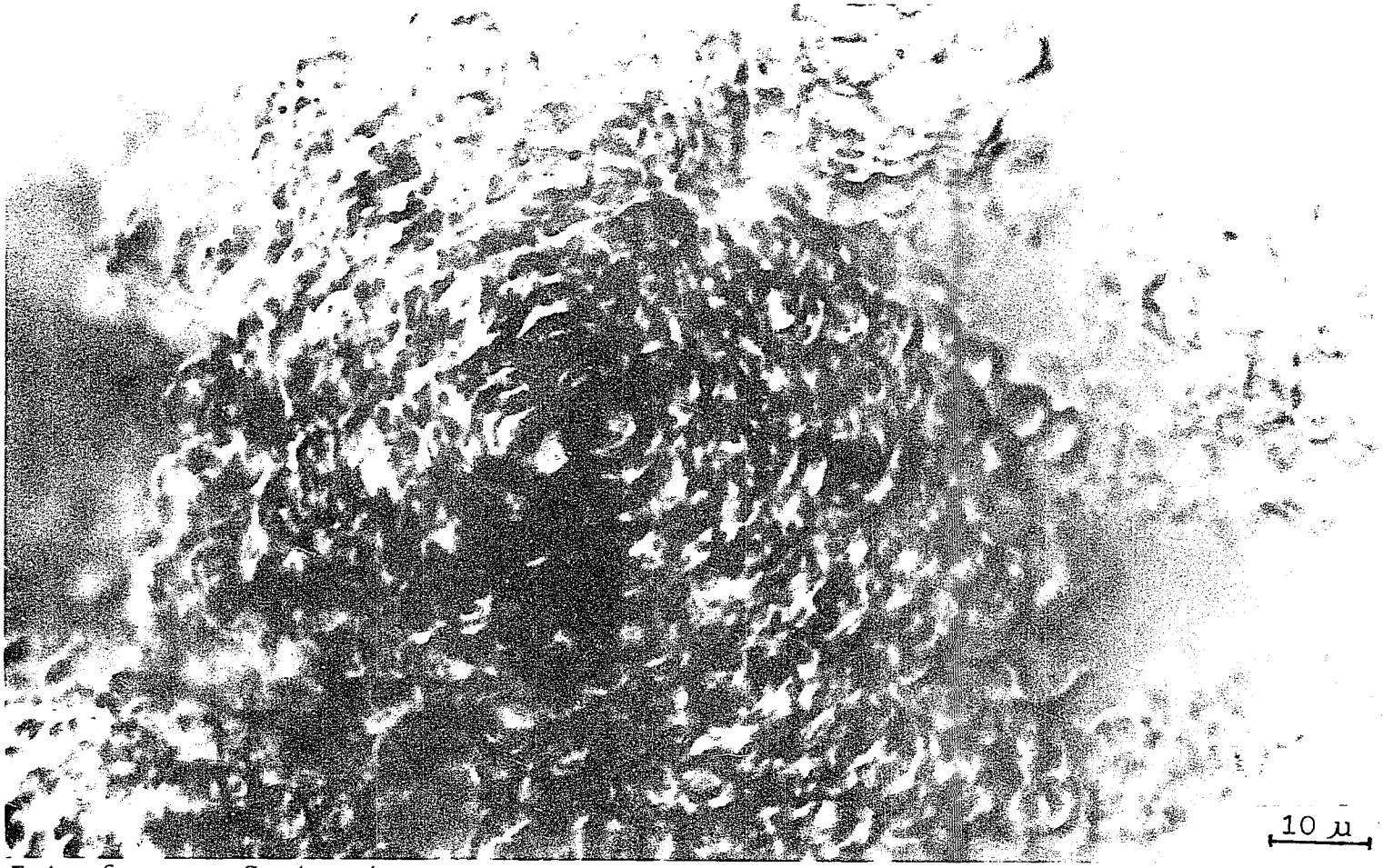

A-1: Interference Contrast

$\bar{M}_n = 2.5 \times 10^5$, $T_C = 0°C$ in 1% (w/v) Amyl Acetate

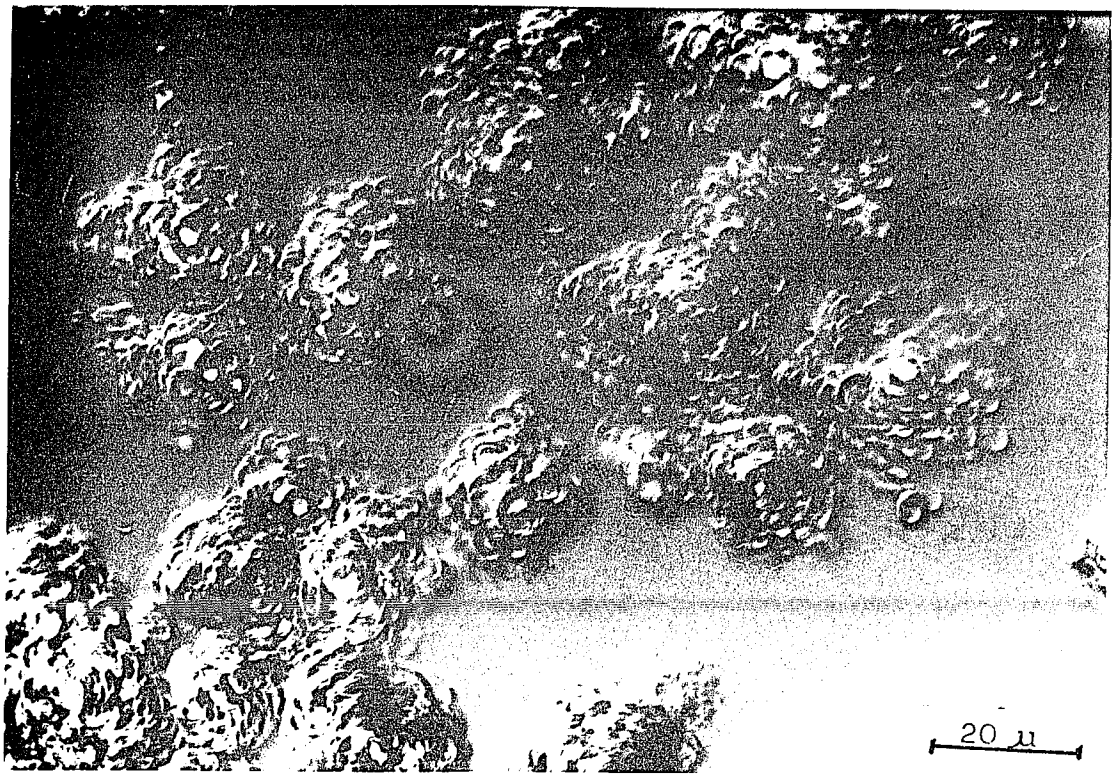

A-2: Interference Contrast

$\bar{M}_n = 2.5 \times 10^5$, $T_c = 0°C$ in 1% (w/v) Amyl Acetate

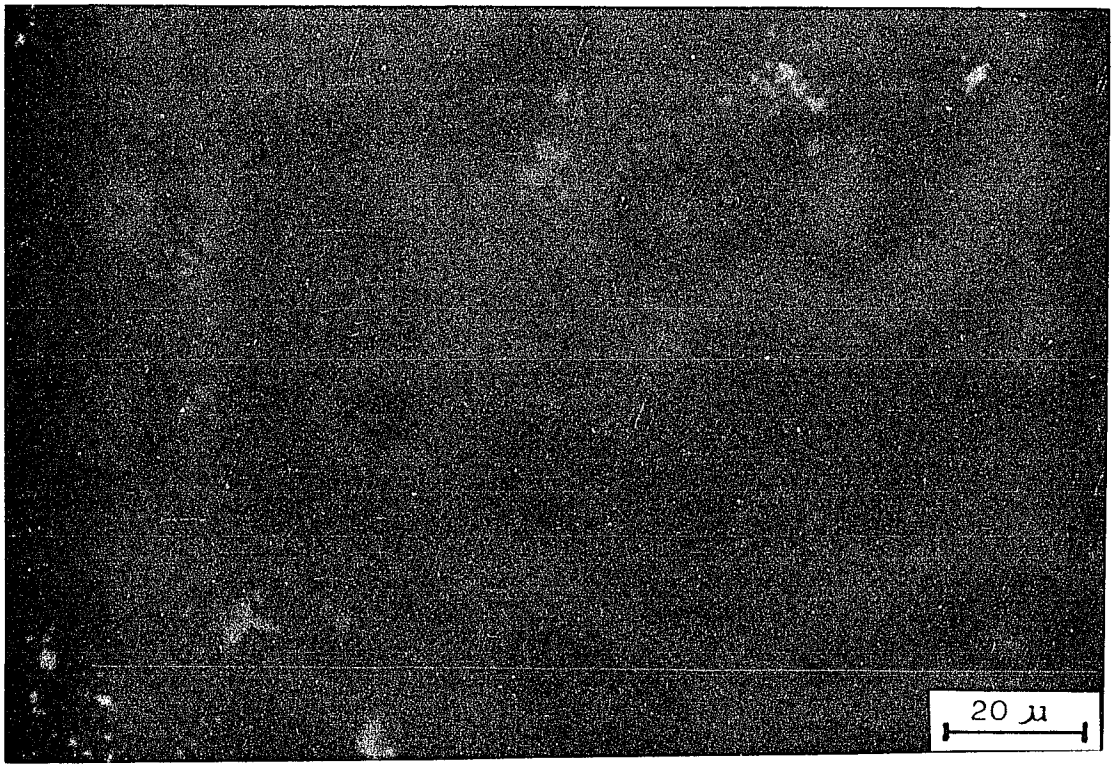

Crossed Polaroids of A-2

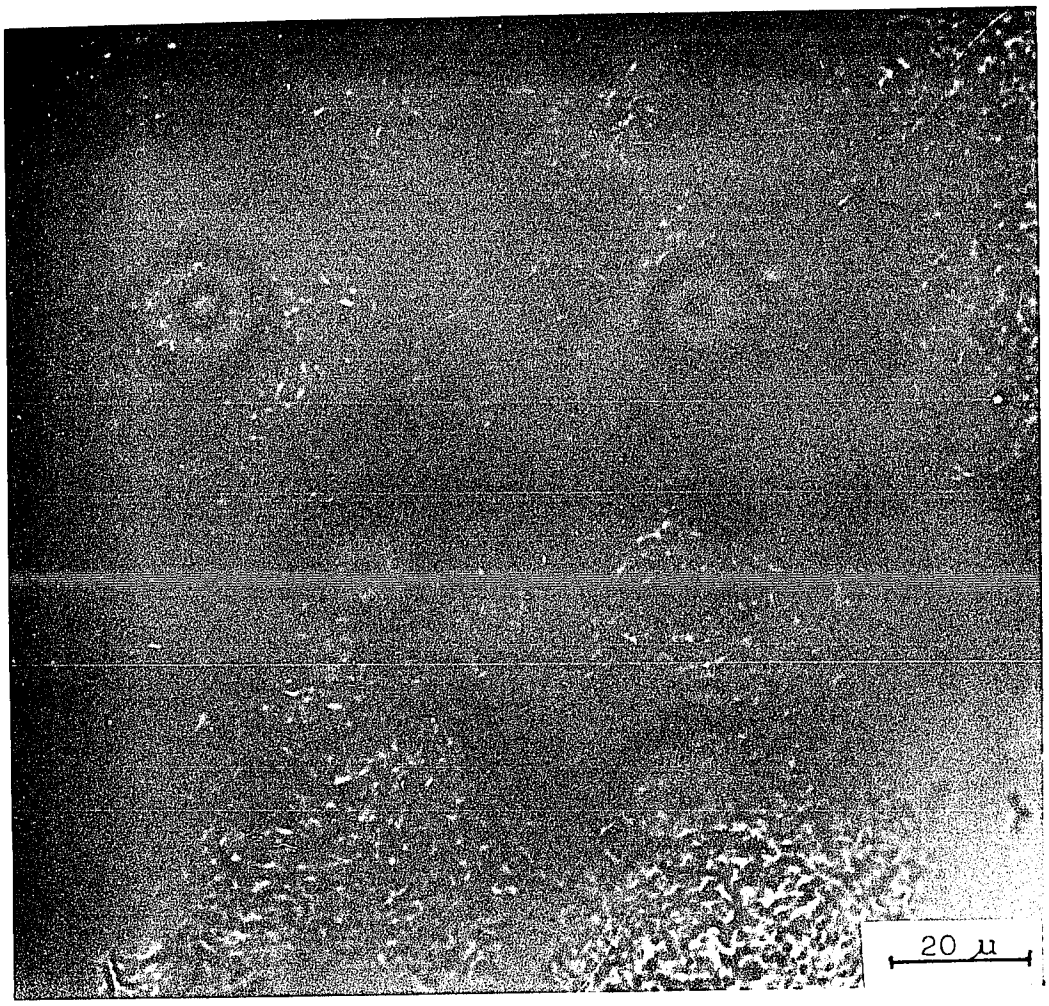

B: Interference Contrast

$\bar{M}_n = 1.0 \times 10^5$, $T_C = -15°C$

(Water Condensed on the Slide Surface)

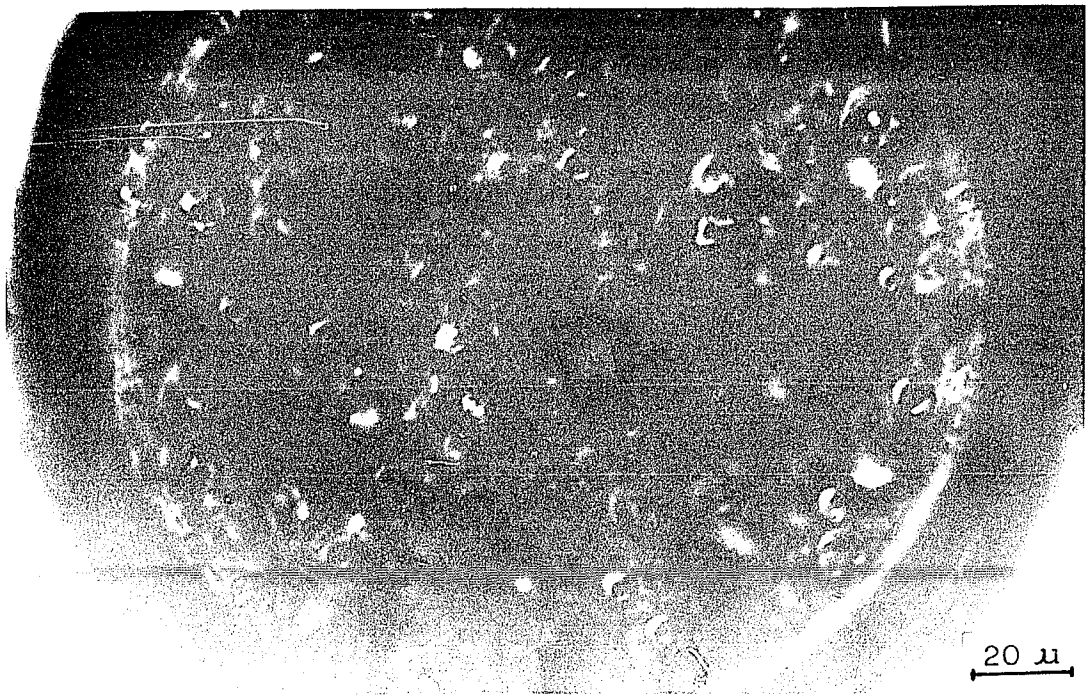

C: Interference Contrast

$\bar{M}_n = 2.5 \times 10^5$, $T_C = 15°C$ in 1% (w/v) Amyl Acetate

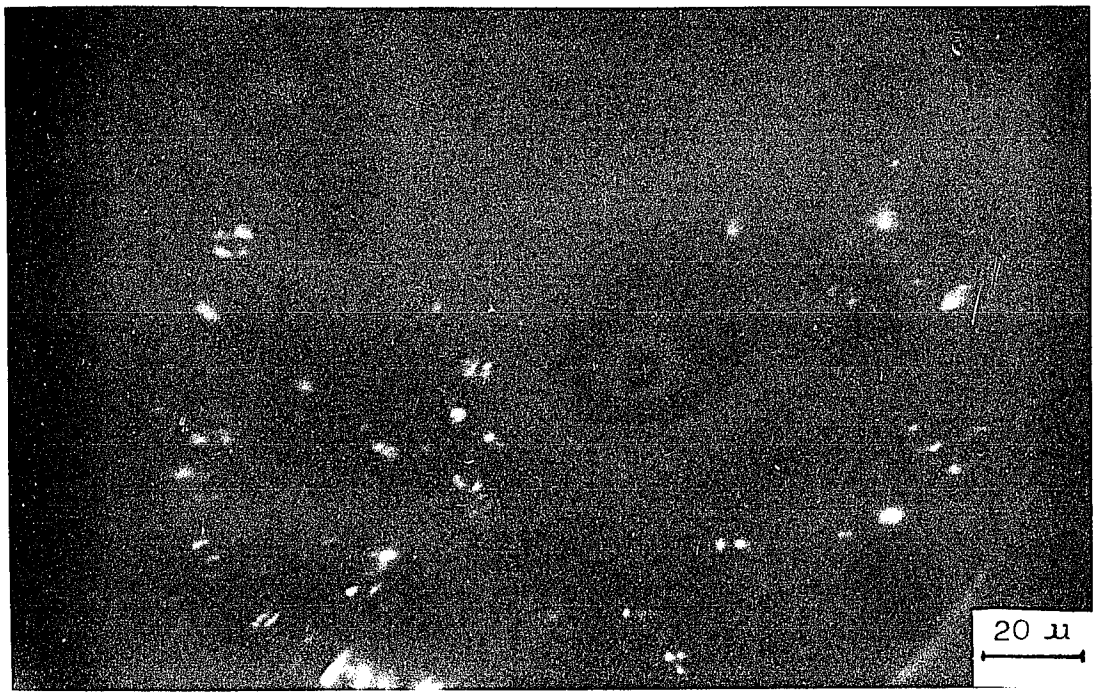

Crossed Polaroids of C

Fig. 19. Electron Micrographs of Cup-shaped Lamellar Aggregates at the Edge Grown from 1% (w/v) Amyl Acetate with $\bar{M}_n = 2.5 \times 10^5$ at $T_C = -15°C$

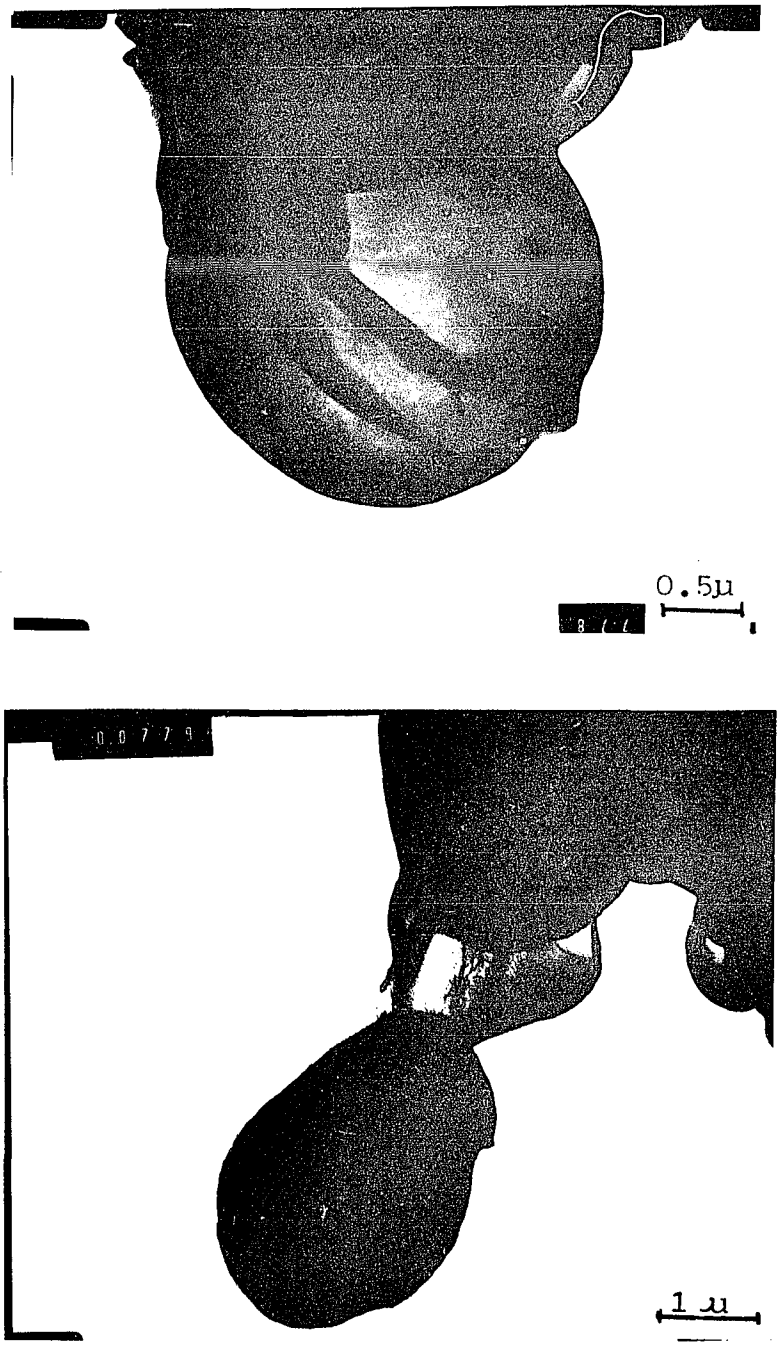

A summary of the morphological features is given in Table 3. For trans-1,4-polyisoprene crystals grown by the direct crystallization method from 1% (w/v) amyl acetate solution, the morphologies described above have been classified as:

Type-I: small elliptical hedrites with strong birefringence from the side in α form.

Type-II: sheaflike hedrites with weak birefringence in α form.

Type-III: sheaflike hedrites with strong distinct birefringence in the β form.

Type-IV: sheaflike hedrites with strong distinct birefringence in the α form.

Type-V: spherulites with strong scattered birefringence in the β form.

Type-VI: aggregates of cup-shaped lamellae with weak birefringence in the β form.

An important feature is the fact that the morphology or morphological changes are continuous with respect to either molecular weight or temperature. The changes from one morphological form to another occurs over a small range of conditions, consequently samples characterized near the boundary of two forms are difficult to identify precisely.

Table 3. Morphological Classification as a Function of Crystallization Temperature and Molecular Weight

High molecular weight fraction (HMW), $\bar{M}_w = 3.42 \times 10^5$, $\bar{M}_n = 2.54 \times 10^5$, $\bar{M}_w/\bar{M}_n = 1.34$.

Medium molecular weight fraction (MMW), $\bar{M}_w = 1.60 \times 10^5$, $\bar{M}_n = 1.03 \times 10^5$, $\bar{M}_w/\bar{M}_n = 1.56$.

Low molecular weight fraction (LMW), $\bar{M}_w = 3.6 \times 10^4$, $\bar{M}_n = 2.4 \times 10^4$, $\bar{M}_w/\bar{M}_n = 1.51$.

Crystallization Condition: T_D = 100°C in 1% (w/v) amyl acetate, time = 1 day.

$\bar{M}_n$	2.4×10^4	1.0×10^5	2.5×10^5
T_C (°C)	(LMW)	(MMW)	(HMW)
32	I‡	-	II + I
20-21	I	II	IV
15	I + III	III + IV	IV
10	III	III	V
0	III	V	VI
-15	III	VI	VI

‡: Crystallized in 3% (w/v) Amyl Acetate Solution

2. Effect of Concentration on TPI Crystallization:

Generally, the morphological texture of multilayers is found to become more open with a greater splaying of layers when direct crystallization is carried out from dilute polymer solution in amy acetate. Examples of crystallization from 0.3 and 0.05% (w/v) solutions in Fig. 20 and Fig. 21. Structures grown from the HMW fraction at a concentration of 1% (w/v) in amyl acetate at 10°C shows Type-V spherulites (Fig. 17-A), while Type-III (or Type-IV) hedrites (Fig. 20) are formed from 0.05% (w/v) amyl acetate solution at the same temperature. This suggests that the early stages of the spherulic structures are a sheaflike hedrite. Upon lowering the crystallization concentration from 1% to 0.3% (w/v) in amyl acetate, the crystals, grown from the LMW fraction at 0°C, show a rapid decrease in the number of layers, a more open hedrite (Type-II) structure is observed (Fig. 21-A); however, the simplest hedrites (Type-I) are formed from 0.05% (w/v) solution.

Fig. 20. Optical Micrographs of High Molecular Weight Fraction Crystals from Dilute Solution

A: Interference Contrast

$\bar{M}_n = 2.5 \times 10^5$, $T_c = 10°C$ in 0.05% (w/v) Amyl Acetate

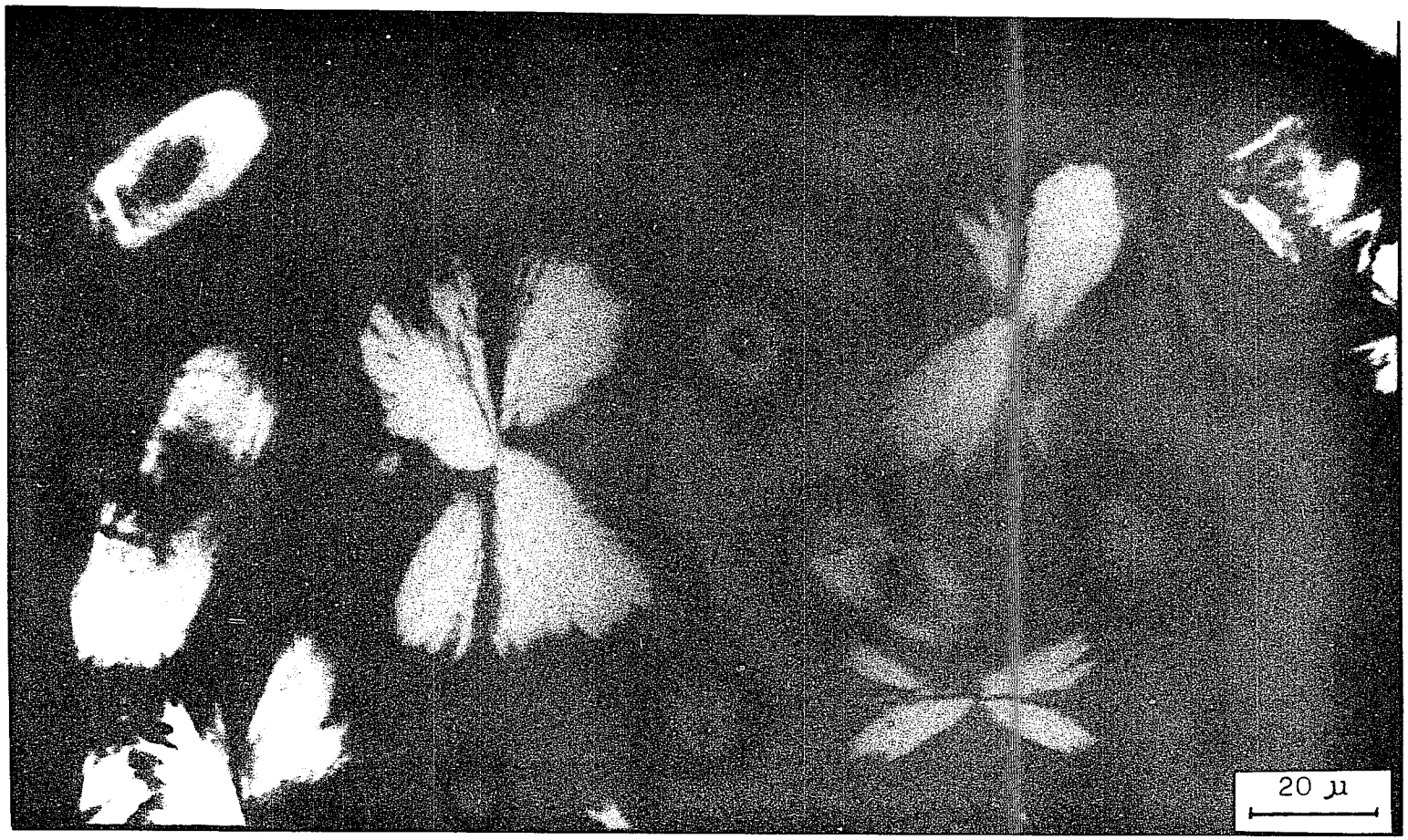

Crossed Polaroids of A

B-1: Interference Contrast

$\bar{M}_n = 2.5 \times 10^5$, $T_C = 20°C$ in 0.05% (w/v) Amyl Acetate

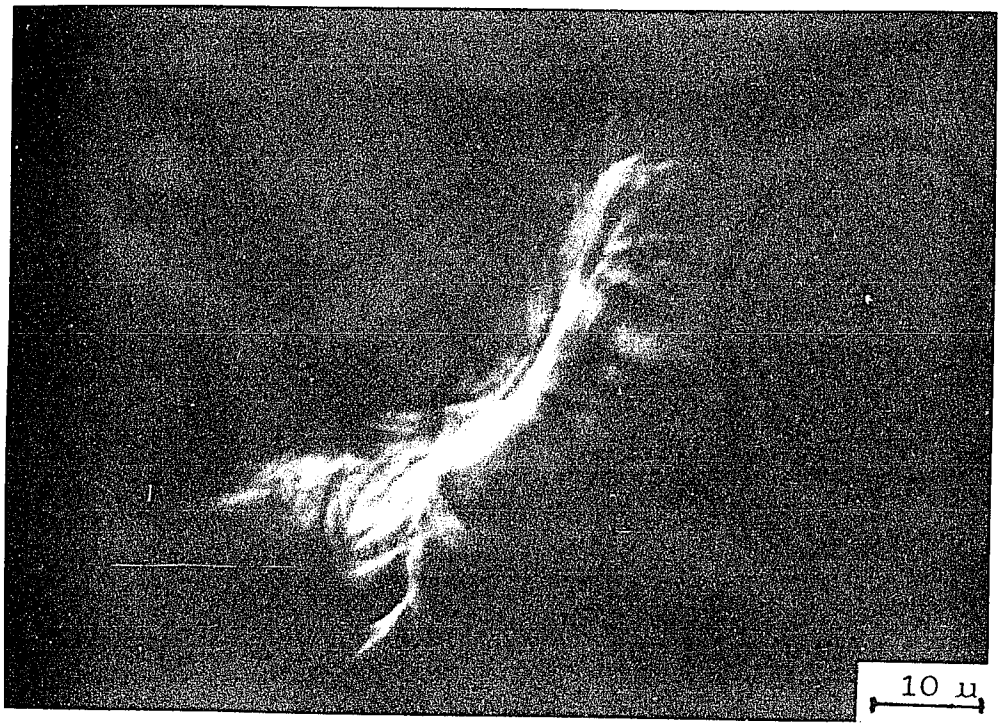

B-2: Interference Contrast

$\bar{M}_n = 2.5 \times 10^5$, $T_C = 20°C$, in 0.05% (w/v) Amyl Acetate

Fig. 21. Optical Micrographs of Low Molecular Weight Fraction Crystals from Dilute Solution

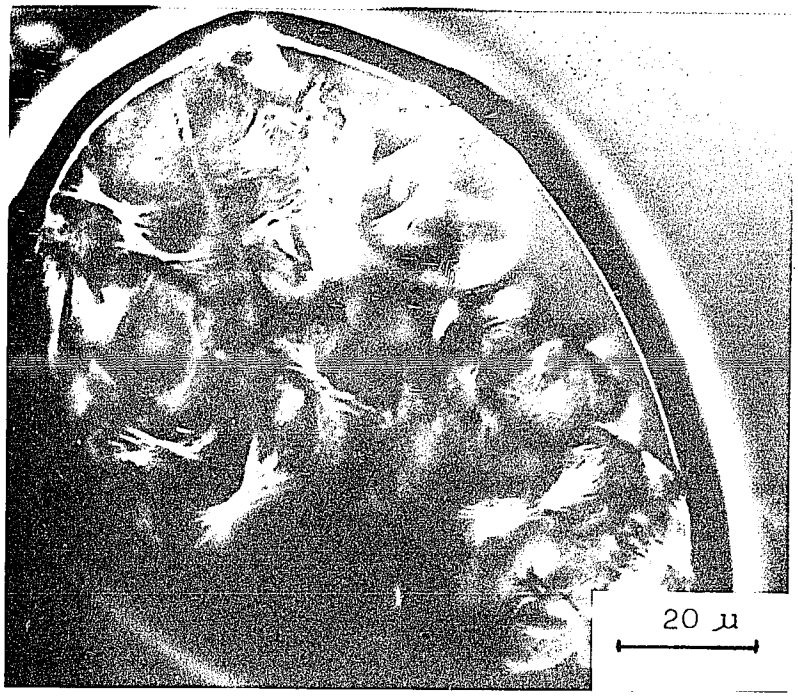

A: Interference Contrast

$\bar{M}_n = 2.4 \times 10^4$, $T_C = 0°C$ in 0.3% (w/v) Amyl Acetate

B: Interference Contrast

$\bar{M}_n = 2.4 \times 10^4$, $T_C = 0°C$ in 0.05% (w/v) Amyl Acetate

It was found that cup-shaped lamellar aggregates from dilute solution, 0.05% (w/v), were less complicated and easier to be investigated by optical and electron microscopy. An optical microscope photograph is shown in Fig. 22-A for cup-shaped lamellar aggregates grown from the HMW fraction at 0.05% (w/v) amyl acetate at 0°C. At the onset of crystallization cup-shaped lamellae appear in the optical microscope followed by growth of other such lamellae about the initial one.

Because these aggregates collapse easily in the drying process (Fig. 22-B), osmium tetroxide was successfully used to fix them in amyl acetate suspension at 0°C. the mixture was also washed and dried at the same temperature and the optical and electron microscopy were then carried out. The photograph of the O_sO_4 fixed and dried aggregates as shown in Fig. 22-C show that the aggregates look like a cluster of globules which become flattened on the glass slide and some evidence of lamellar strips connecting the cup-shaped lamellae is found. However, no birefringence is observed.

Although the central region of the aggregates is too thick to observe in transmission electron microscopy, cup-shaped lamellae as shown in Fig. 23 are found at the edge of the aggregates.

Fig. 22. Optical Micrographs of Cup-Shaped Lamellar Aggregates Grown from 0.05% (w/v) Amyl Acetate TPI Solution at 0°C with $\bar{M}_n = 2.5 \times 10^5$

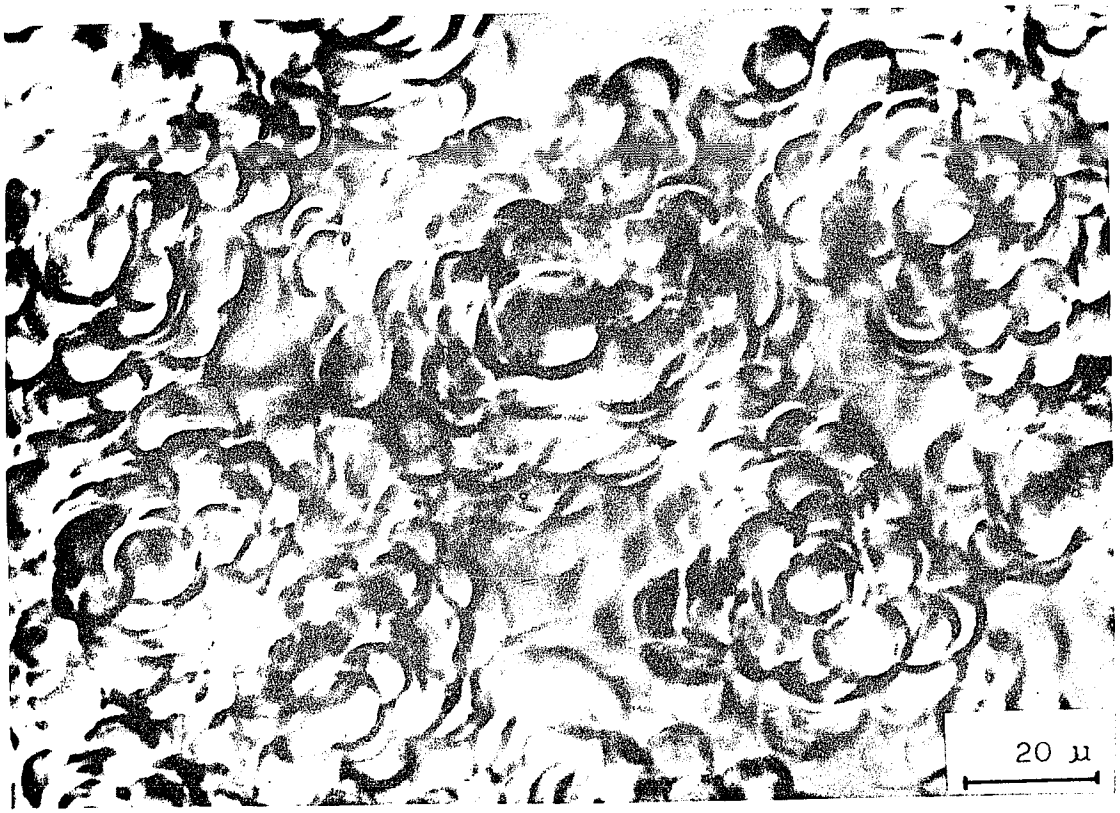

A: Interference Contrast in Amyl Acetate Suspension.

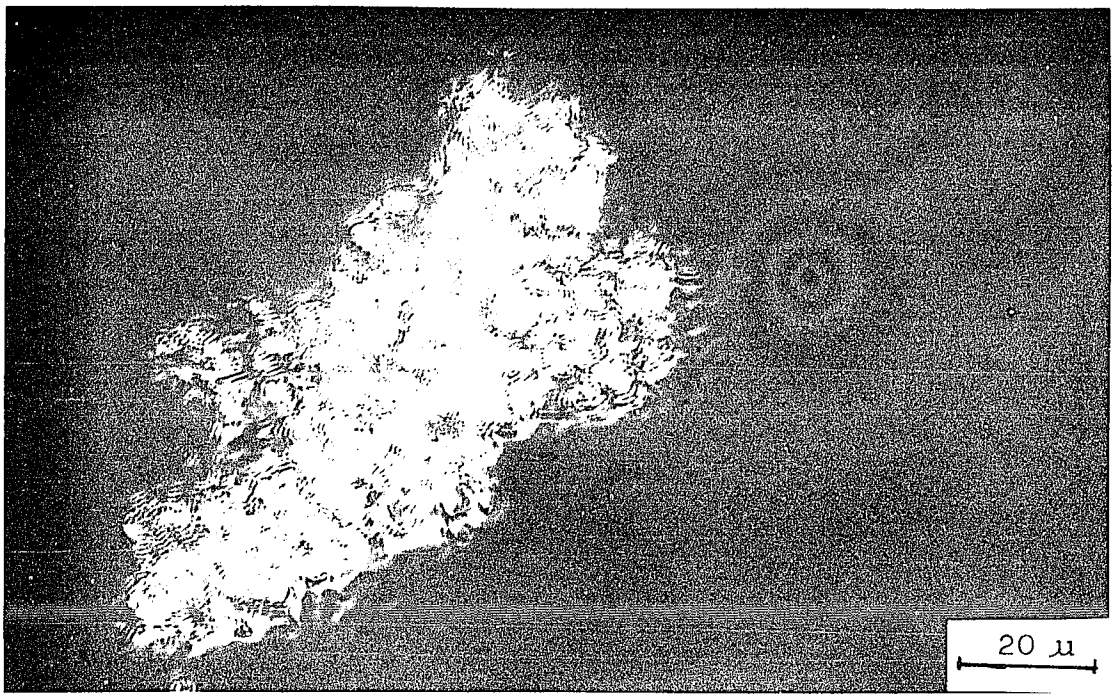

B: Interference Contrast in Dried State

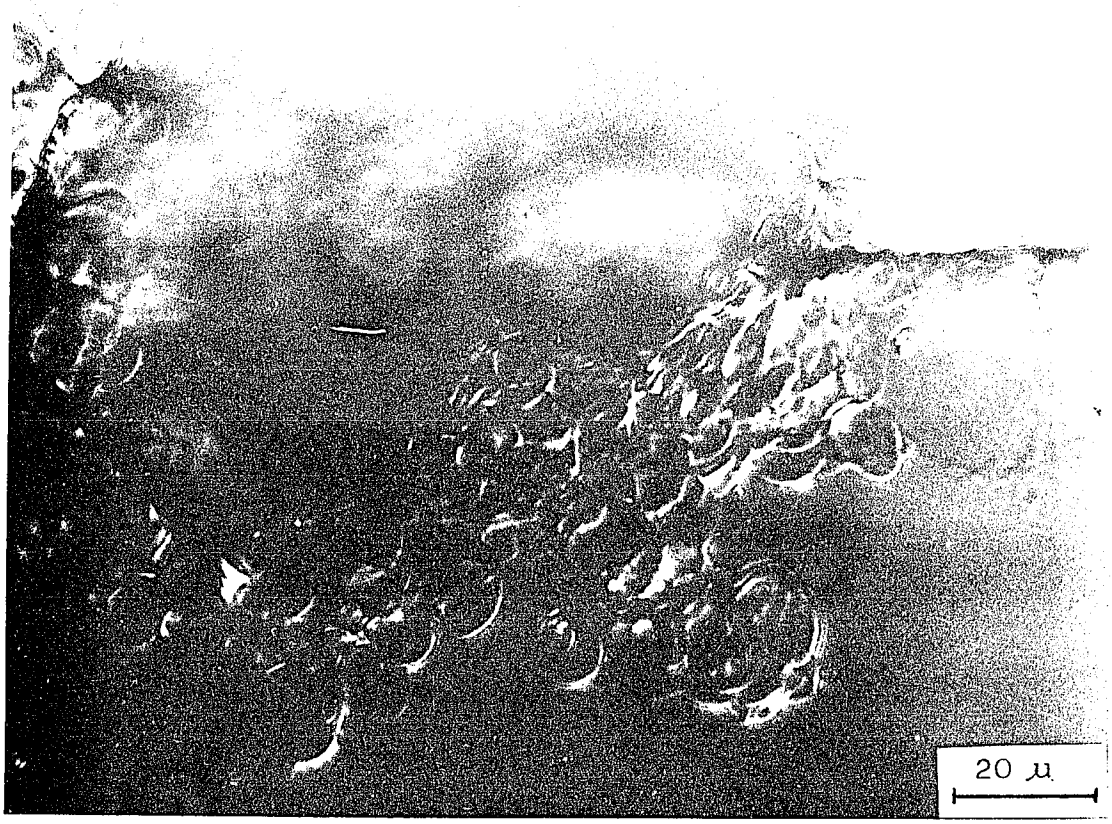

C: Interference Contrast

O_sO_4 Fixed and Dried Aggregates

Fig. 23. Electron Micrographs of TPI Cup-Shaped Lamellar Aggregates Growing from 0.05% (w/v) Amyl Acetate Solution at 0°C with $\bar{M}_n = 2.5 \times 10^5$ after O_sO_4 Treatment

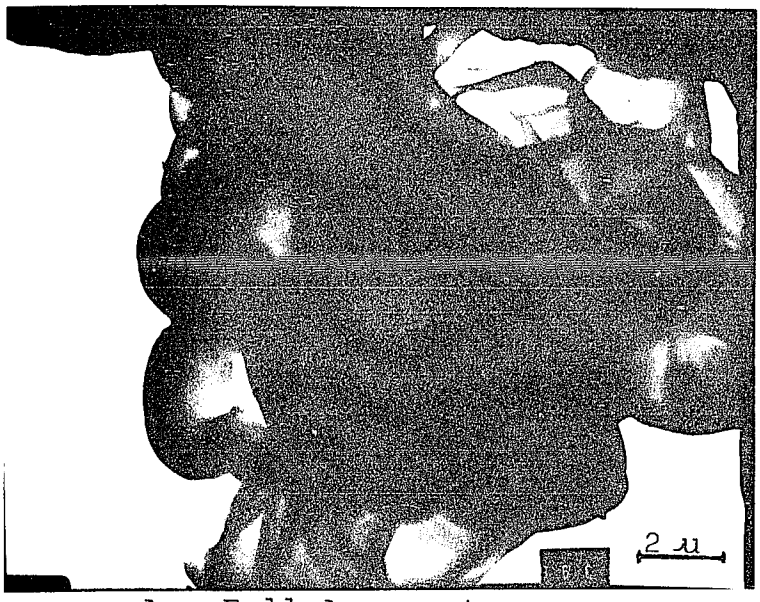

A. Full Aggregate

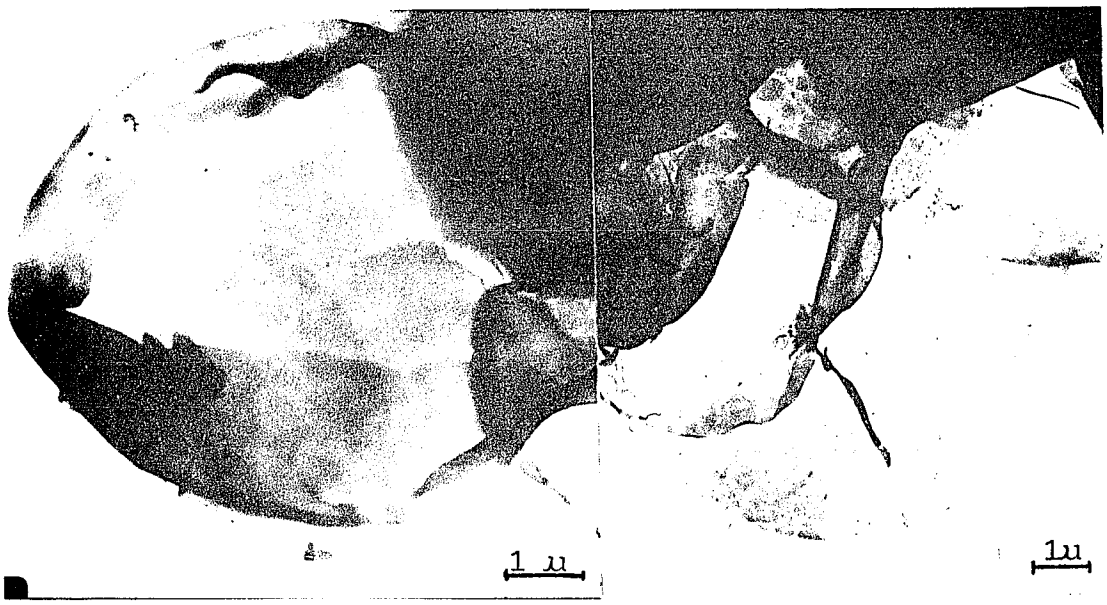

B. Edge of Aggregate

C. Edge of Aggregate

3. The Effect of Molecular Weight Distribution on TPI Crystallization:

In Section III-1, it was concluded that the morphology of crystals growing at the same crystallization temperature depends on the molecular weight. Turning to the consideration of the effect of molecular weight distribution, generally speaking, it should be noted that the fractionation according to molecular weight, i.e. chain length, occurs during the crystallization of polymer from solution (66,67,68) and that the chains of shorter length tend to remain in solution more readily than longer ones. However, the HMW fraction ($\overline{M}_n = 2.5 \times 10^5$, $\overline{M}_w/\overline{M}_n = 1.3$) crystallized in 1% (w/v) amyl acetate at 30°C shows relatively little change in molecular weight distribution by GPC analysis.

The crystallization of TPI obtained by the column fraction method with a narrow molecular weight distribution ($\overline{M}_w/\overline{M}_n = 1.2\text{-}1.3$) has also been carried out. The morphological structures shown in Fig. 24 are consistent with the result shown in Table 3. Therefore, in the range $\overline{M}_w/\overline{M}_n$ of 1.2 to 1.6, the molecular weight distribution does not have a noticeable effect on the morphological texture.

A blend of the HMW fraction with 10% (w/w) LMW fraction was made in 1% (w/v) amyl acetate solution and this

then crystallized at 10°C. It shows a similar morphology to the Type-III hedrites as shown in Fig. 25. The change of morphology from Type-V spherulite to Type-III hedrite with the decrease of average molecular weight is expected from the morphological map in Table 3.

Fig. 24. Optical Micrographs of TPI Crystals with a Narrow Molecular Weight Distribution

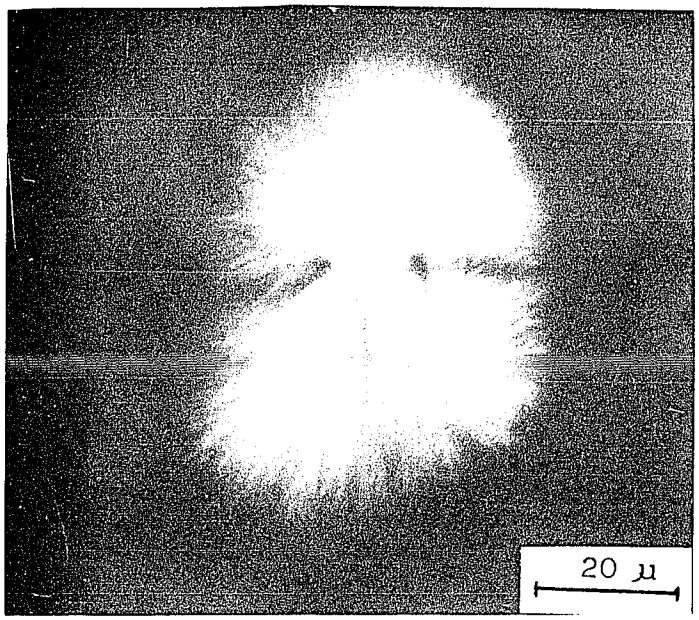

A. Interference Contrast

$\bar{M}_n = 1.2 \times 10^5$, $\bar{M}_w/\bar{M}_n = 1.24$, $T_c = 20°C$ in 1% (w/v) Amyl Acetate

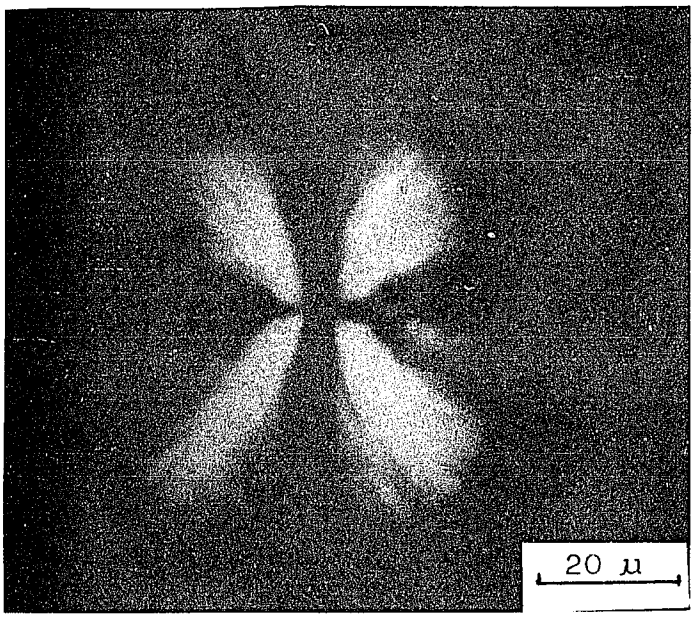

Crossed polaroids of A

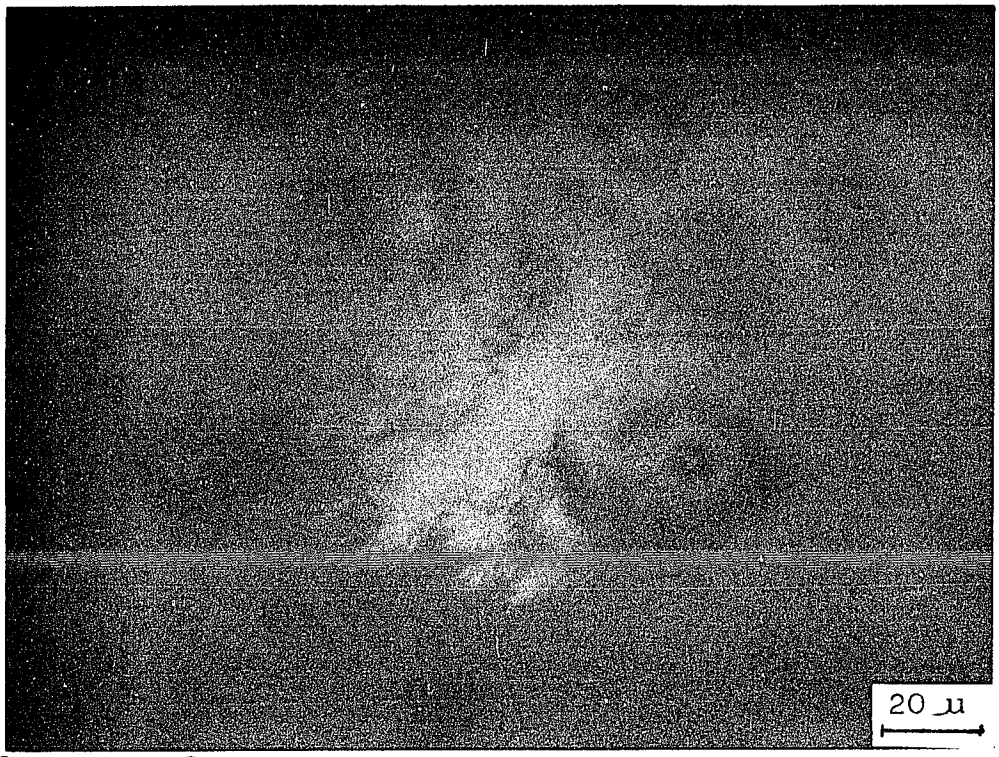

B-1. Interference Contrast

$\bar{M}_n = 1.2 \times 10^5$, $\bar{M}_w/\bar{M}_n = 1.24$ in 1% (w/v) Amyl Acetate, $T_c = 0°C$

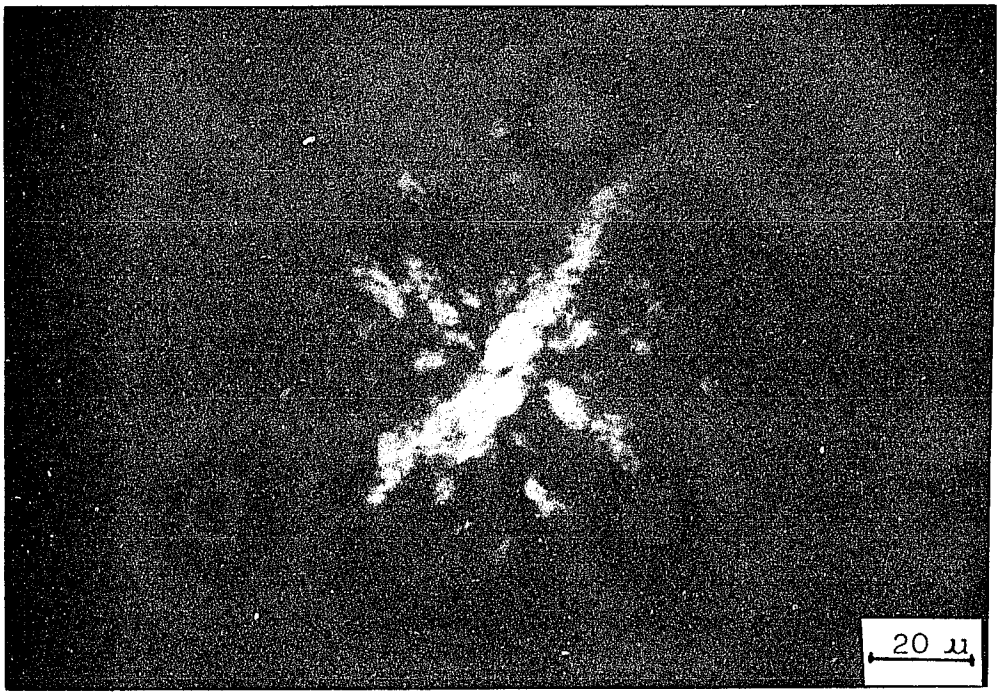

Crossed polaroids of B-1

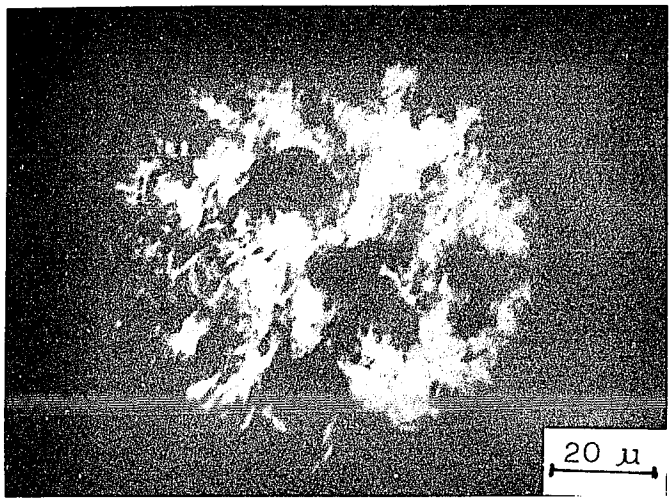

B-2. Interference Contrast

$\bar{M}_n = 1.2 \times 10^5$, $\bar{M}_w/\bar{M}_n = 1.24$ in 1% (w/v) Amyl Acetate, $T_c = 0\,°C$.

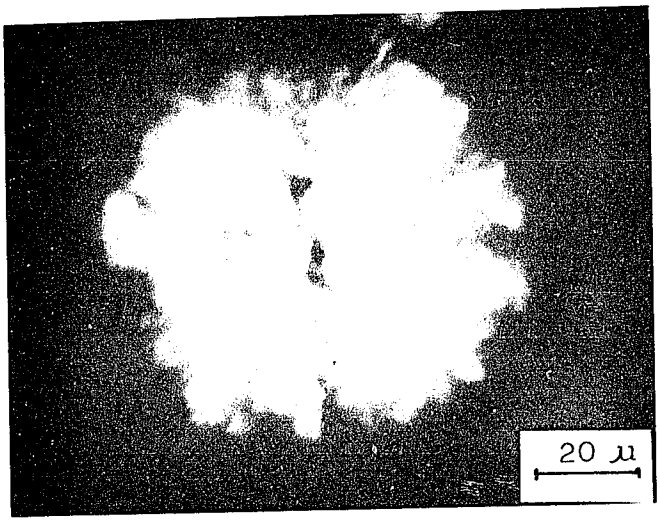

Crossed polaroids of B-2

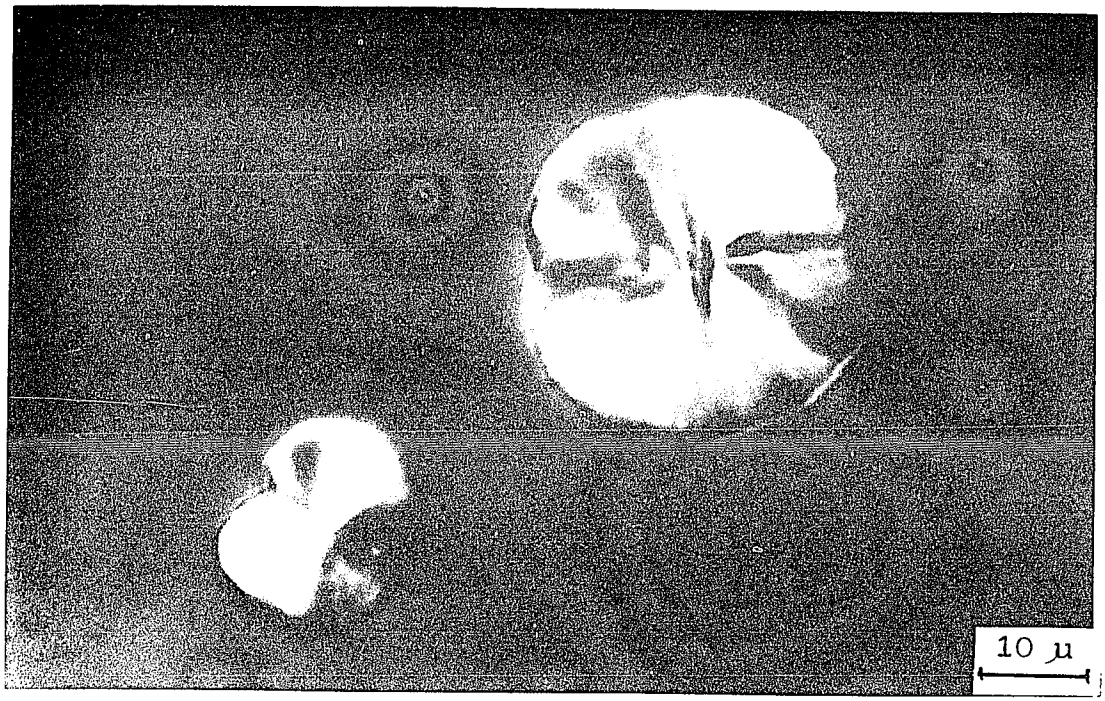

C. Interference Contrast

$\bar{M}_n = 2.3 \times 10^4$, $\bar{M}_w/\bar{M}_n = 1.27$, $T_c = 10°C$ in 1% (w/v)

Amyl Acetate

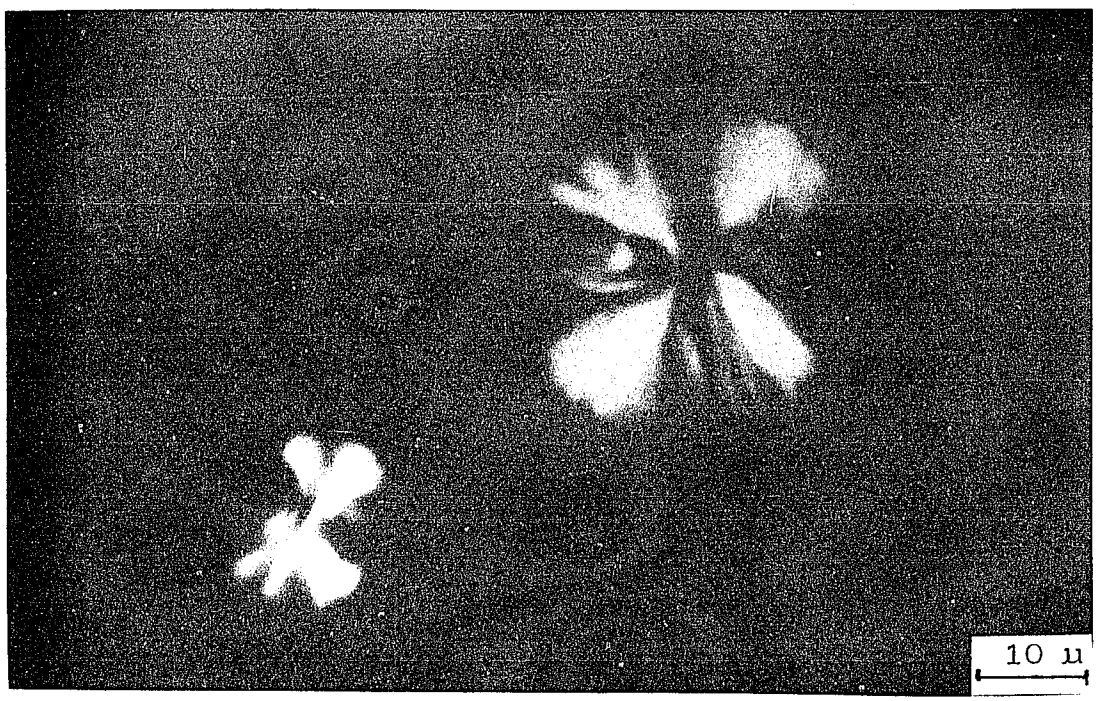

Crossed polaroids of C.

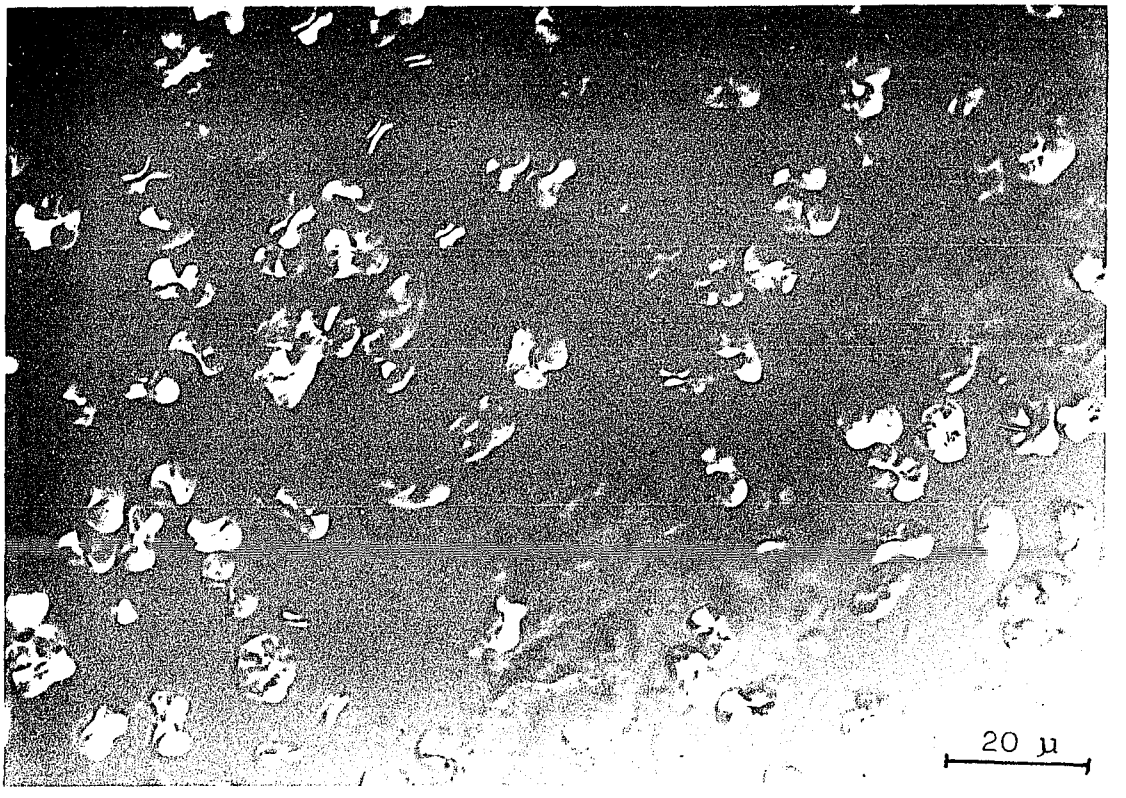

D. Interference Contrast

$\bar{M}_n = 4.9 \times 10^3$, $\bar{M}_w/\bar{M}_n = 1.25$, $T_C = 10°C$ in 1% (w/v) Amyl Acetate

Fig. 25. Optical Micrograph of Crystals Grown from TPI Blend of a HMW Fraction ($\bar{M}_n = 2.5 \times 10^5$) with 10% (w/w) LMW Fraction ($\bar{M}_n = 2.4 \times 10^4$) in 1% (w/v) Amyl Acetate Solution at 10°C

Interference Contrast

4. Effect of Solvent on TPI Crystallization:

With regard to our choice of amyl acetate as solvent for crystallization, it should be pointed out that in this solvent the trans-1,4-polyisoprene dissolves readily at a high temperature but is only sparingly soluble at the crystallization temperature used.

A few experiments were carried out using crystallization liquids other than amyl acetate. Direct crystallization from heptane or from dibutyl ether with $\bar{M}_n = 2.5 \times 10^5$ in 1% (w/v) at $T_C = 0°C$ yielded spherically symmetrical structures in the α crystal form as shown in Fig. 26-A, C, these structures have strong scattered birefringence and are classified as Type-VII spherulites. When the LMW fraction with $\bar{M}_n = 2.4 \times 10^4$ was employed with heptane as solvent, sheaflike structures as shown in Fig. 26-B in the β form appeared; these are similar to Type-III hedrites grown from amyl acetate. When a poor solvent such as n-butyl acetate was used for the HMW fraction at $T_C = 0°C$, Type-VI cup-shaped lamellar aggregates with some single crystal like individual globules as shown in Fig. 26-D coexisted. The birefringence exhibited had the same pattern as the Type-VI aggregates grown from the HMW fraction at -15°C in 1% (w/v) amyl acetate. All the optical microscopes are shown in Fig. 26.

Fig. 26. Optical Micrographs of TPI Crystals Grown from Dibutyl Ether, Heptane and N-Butyl Acetate

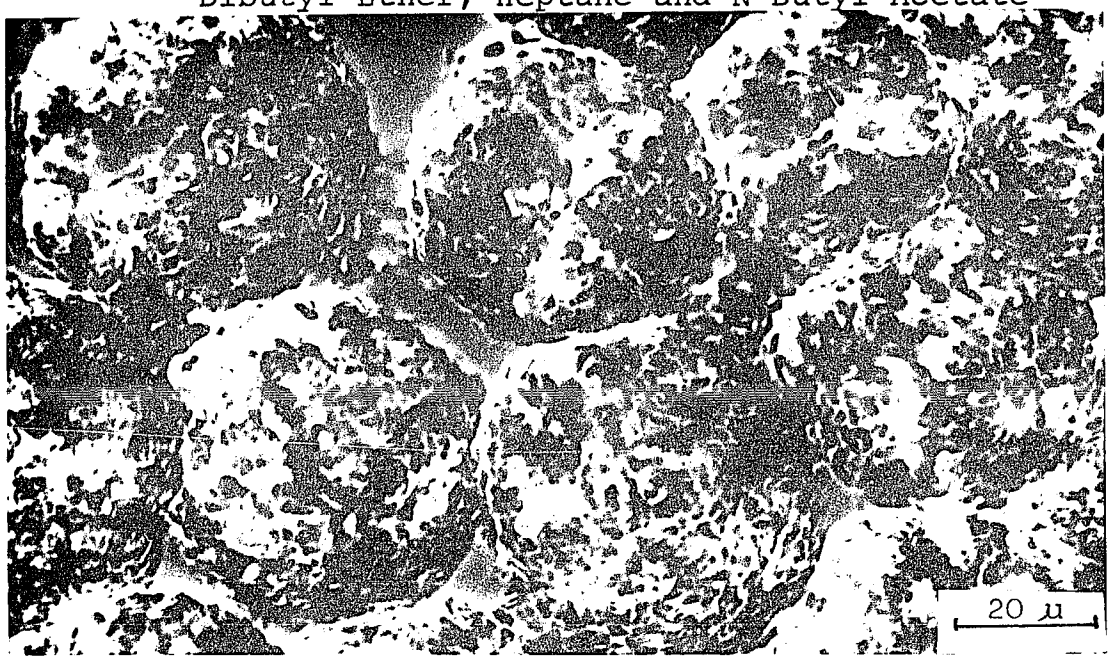

A. Interference Contrast

$\bar{M}_n = 2.5 \times 10^5$, $T_c = 0°C$ in 1% (w/v) Butyl Ether

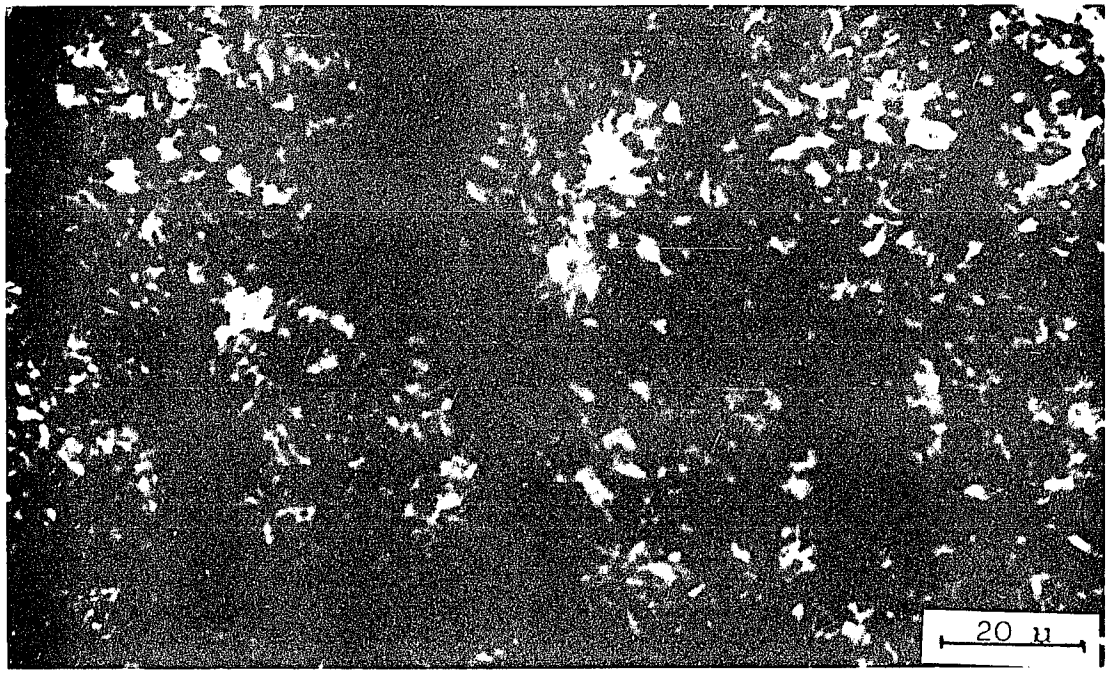

Crossed Polaroids of A

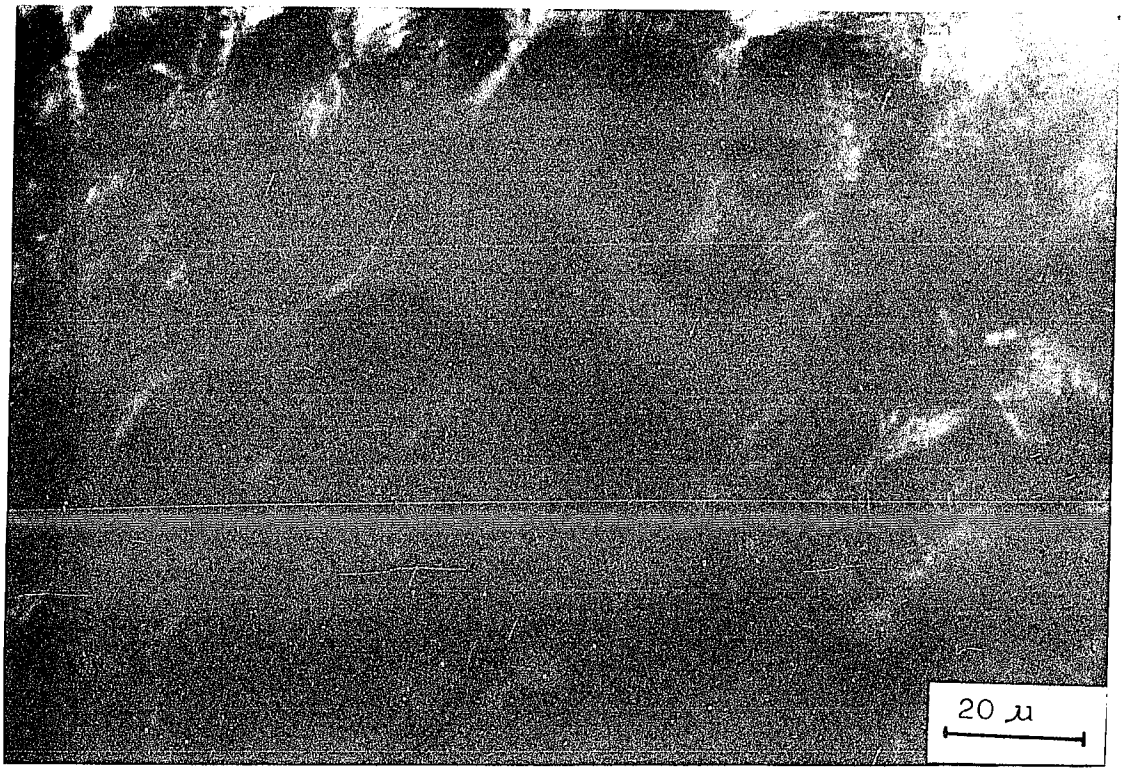

B. Interference Contrast

$\bar{M}_n = 2.4 \times 10^4$, $T_C = 0°C$ in 1% (w/v) Heptane

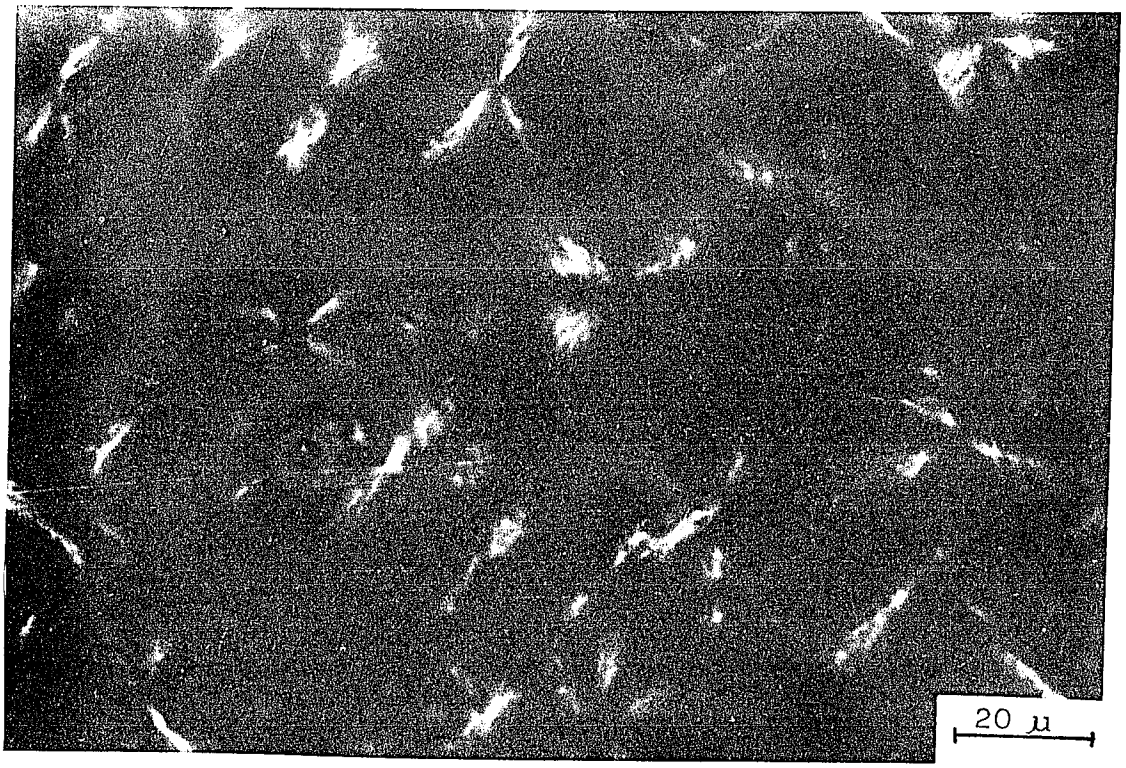

Crossed Polaroids of B

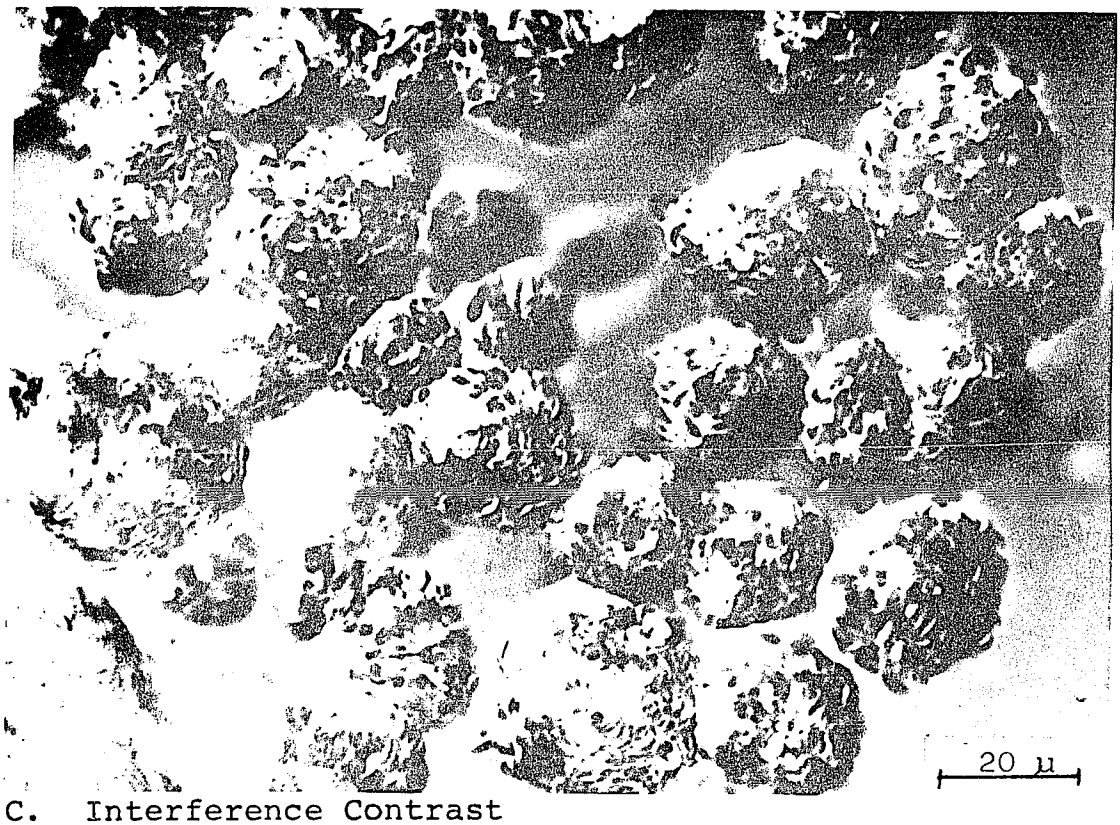

C. Interference Contrast

$\bar{M}_n = 2.5 \times 10^5$, $T_C = 0°C$ in 1% (w/v) Heptane

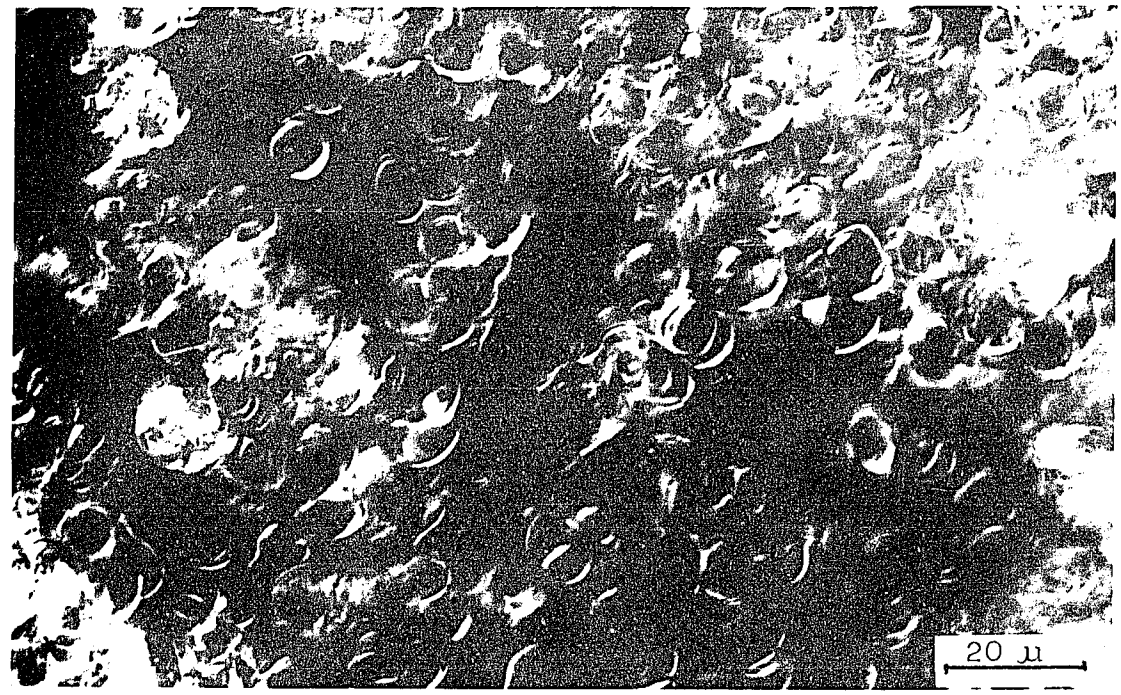

D. Interference Contrast

$\bar{M}_n = 2.5 \times 10^5$, $T_C = 0°C$ in 1% (w/v) N-Butyl Acetate

With heptane as solvent, the crystal form (α or β) is dependent on the molecular weight used; when crystallization is carried out at 0°C from 1% (w/v) heptane by the direct method, only the low molecular weight fraction formed the β modification. The results from x-ray diffraction. DSC and density measurement are summarized in Table 4.

Table 4. Effect of Molecular Weight on Crystal Form for Structures Grown from 1% (w/v) Heptane at Tc = 0°C

$\bar{M}_n$	$\bar{M}_w/\bar{M}_n$	Crystal form(a)	Tm (°C)(b)	Density(c) (g/cm^3)
2.5×10^5	1.3		62	0.965
9.7×10^4	1.6		61.5	0.967
2.4×10^4	1.6		54 (63) [20: 1]	0.969

(a) from wide angle x-ray diffraction

(b) melting endotherms from DSC measurement

(c) from density gradient column

5. TPI Morphology Using Other Crystallization Methods

A) Precooling method: The self-seeding technique is probably the most widely used method of growing single-layer crystals of polymers because the entire population is composed of similar crystals. Briefly, the method involves first the preparation of a crystal suspension by fully dissolving a polymer solution at a dissolution temperature (T_D), and then quenching to a precipitation temperature (T_P) to crystallize. This process usually results in crystals which have a predominantly multilayer morphology. The suspension is then warmed up to a redissolution temperature (T_R). It has been found that within a limited range above the clearing point, the solution retains a memory of the previous crystallization (18) when crystallizing at T_C. Following this method, single crystals grown from 1% (w/v) amyl acetate have been investigated under the electron microscope as shown in Fig. 27.

Fig. 27. Electron Micrographs of TPI Single Crystals Grown from 1% (w/v) Amyl Acetate with $\bar{M}_n$ = 2.5×10^5 at T_D = 100°C, T_P = 0°C and T_R = 45°C

Heating rate from T_P to T_R = 0.2°C/min.

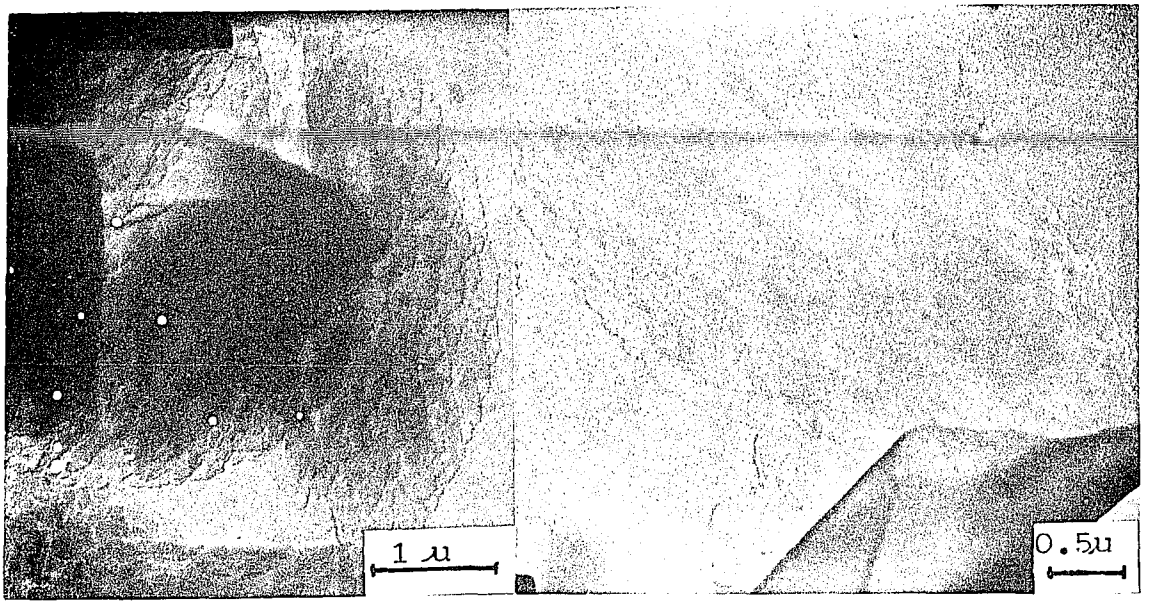

A. T_C = 10°C
Lamellar Thickness = 82 Å ± 5 Å

B. T_C = 20°C
Lamellar Thickness = 93 ± 2 Å

From DSC measurement and wide angle X-ray diffraction, these single crystals grown by the precooling method were found to be in the α form, whereas the multilayer crystals crystallized at the precipitation temperature (T_P = 0°C) were predominantly in the β form.

A modified method used to obtain lamellae in the form starts with precipitation at 20°C, and then, these

multilayer crystals with α form were heated up to the clearing temperature, i.e. redissolution temperature T_R, and crystallized at 30°C. In this case, no crystal form transition occurs during the heating. The electron micrographs compared with crystallization at T_P = 0°C are shown in Fig. 28. Single crystals grown from higher T_P exhibit a larger size.

Fig. 28. Electron Micrograph of TPI Single Crystals Grown from Different Precipitation Temperature and Redissolution Temperature in 1% (w/v) Amyl Acetate with $\bar{M}_n = 2.5 \times 10^5$

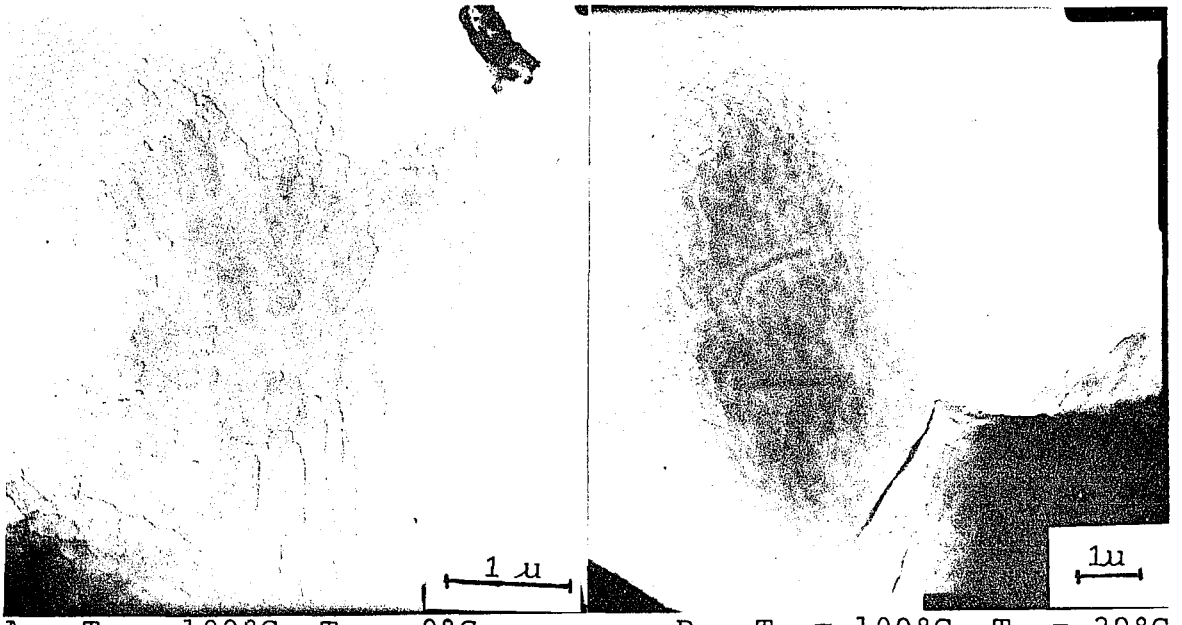

A. T_D = 100°C, T_P = 0°C
T_R = 45°C, T_C = 30°C
Heating rate from T_P to T_R: 0.2°C/min.

B. T_D = 100°C, T_P = 20°C
T_R = 50°C, T_C = 30°C
Heating rate from T_P to T_R: 0.2°C/min.

For the LMW fraction with $\bar{M}_n = 2.4 \times 10^4$ 1% (w/v)amyl acetate solution was heated to 100°C, and then cooled to 0°C. At a heating rate of 0.2°C/min, the suspension cleared at 38°C, i.e. clearing point. When $T_R = 40°C$ and $T_C = 20°C$, single crystals were formed. However, if a higher redissolution temperature ($T_R = 45°$) is used, hedrites, as shown in Fig. 29 were formed.

Fig. 29. Optical Micrograph of TPI Crystals Grown by the Precooling Method at Higher Redissolution Temperature in Interference Contrast $\bar{M}_n = 2.4 \times 10^4$, in 1%(w/v) Amyl Acetate $T_D = 100$, $T_P = 0$, $T_R = 45$ and $T_C = 20°C$, Heating Rate from T_P to T_R: 0.2°C/min

The rate of heating to T_R after an initial crystallization at T_P is of some importance. The effect of heating rate on the initial morphology with cup-shaped lamellar aggregates precipitated at 0°C from 1% (w/v) amyl acetate solution with $\bar{M}_n = 2.5 \times 10^5$ was investigated. The results are summarized in Table 5.

Table 5. The Influence of Heating Rate on Morphology

	T_D (°C)	T_P (°C)	T_R (°C)	Heating Rate from T_P to T_R (°C/min)	T_C (°C)	Crystal Form[b]	T_M (°C)[c]	Morphology[d]
1	100	0	45	0.2	20	α	61	single crystal
2	100	0	45	0.5-0.6	20	-	-	Type-I hedrite
3	100	0	45	rapidly[a]	20	α	60	Type-IV hedrite
4	100	0	44	0.2	0	α	58	Single crystal
5	100	0	44	rapidly[a]	0	β+α(e)	50 (59)	Cup-shaped lamellar aggregate
6	100	0	30	0.2-0.3	30	β	55	Cup-shaped lamellar aggregate
7.	100	0	30	rapidly[a]	30	α	65	Single crystal

(a) immediately placed in water bath at constant temperature
(b) from wide angle X-ray diffraction
(c) from differential scanning calorimetry
(d) from optical microscopy
(e) mainly in the β form

Experiments 1 to 3 in Table 4 indicate that the morphology of crystals change from simple crystals to multilayer hedrites by increasing the heating rate. Fig. 30 shows a hedrite

crystallized according to experiment 2. In experiments 3 and 5, the aggregates are dissolved due to the rapid heating rate, and therefore the same morphologies are obtained as by the direct crystallization method. Experiment 4 is for a normal precooling crystallization. Experiment 6 indicates that the morphology is not changed by solution annealing, if the heating rate is slow enough and if the temperature is lower than the temperature at which the aggregates finally dissolve. In experiment 7, single crystal structures are formed which means that the cup-shaped lamellar aggregates with β form are in a metastable state; these aggregates can be dissolved by increasing the temperature rapidly and then single lamellae can crystallize in the α form at the same temperature.

Fig. 30. Optical Micrograph with Hedrite Structure by Precooling Method at a Heating Rate of 0.5-0.6°C/min from T_P to T_R

$\bar{M}_n = 2.5 \times 10^5$ in 1% (w/v) Amyl Acetate at T_C = 20°C by Interference Contrast

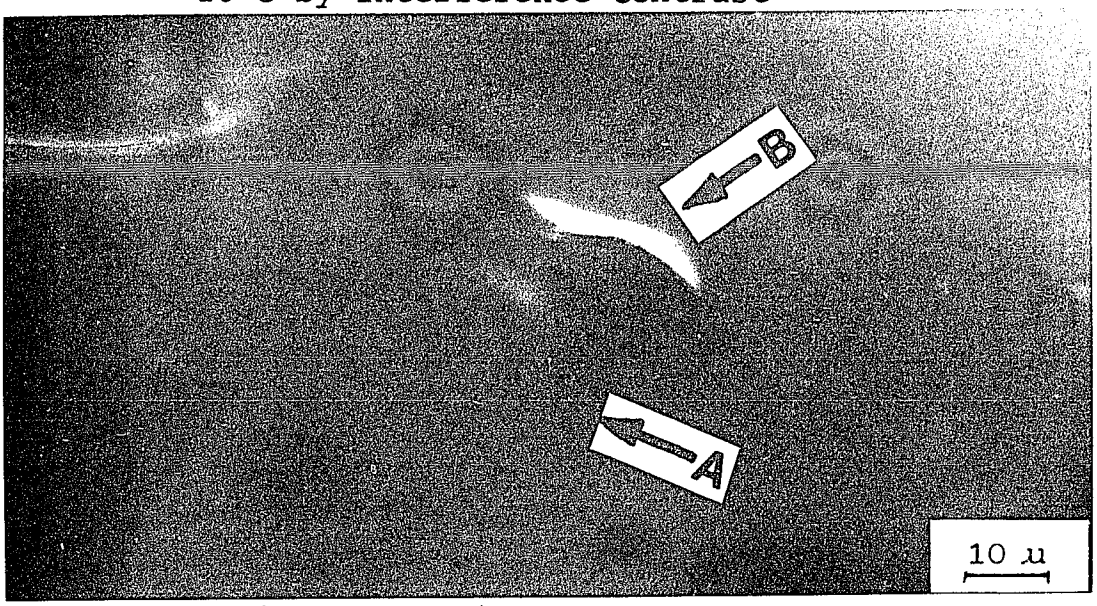

A. Flat-on view of hedrite

B. Edge-on view of hedrite

B. Surface Crystallization by Solvent Evaporation from a Polymer Solution

A thin film of TPI was made by evaporating the solvent from a 1% (w/v)TIP/benzene solution on the surface of grease-free deionized water at room temperature. However, the crystals are too small to be observed under the optical microscope. Ideally, if an amyl acetate solution is precooled to produce a constant amount of nuclei in solution, and then, placed dropwise on a glass slide and the solvent allowed to

evaporate, large crystals with multilayers can be promoted. Optical micrographs for a few trial results are shown in Fig. 31. Roughly, spherulitic (Fig. 31-A), dendritic (Fig. 31-B) and hedritic like (Fig. 31-C) structures are obtained depending on crystallization temperature and molecular weight.

Fig. 31. Optical Micrographs of Thin Films Made by the Evaporation of 1% (w/v) TPI Amyl Acetate Solution

20 μ

A. Interference Contrast

$\bar{M}_n = 2.5 \times 10^5$, $T_c = 32°C$ (2 hours) in 1% (w/v) Amyl Acetate

B-1. Interference Contrast

$\bar{M}_n = 2.5 \times 10^5$, $T_C = 20°C$ (1 hour) in 1% (w/v) Amyl

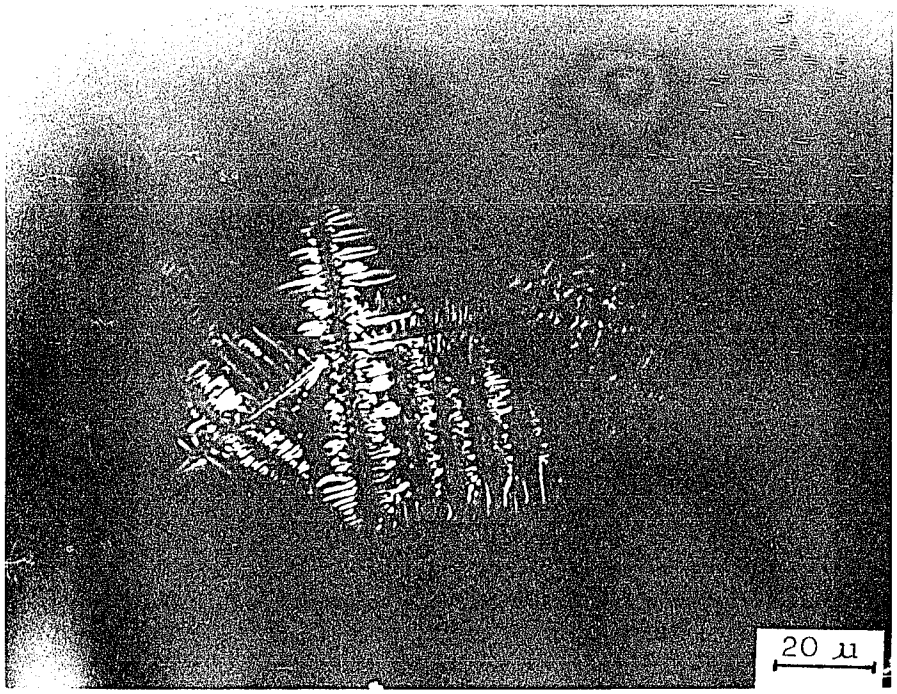

B-2. Interference Contrast

The Same as B-1 Condition

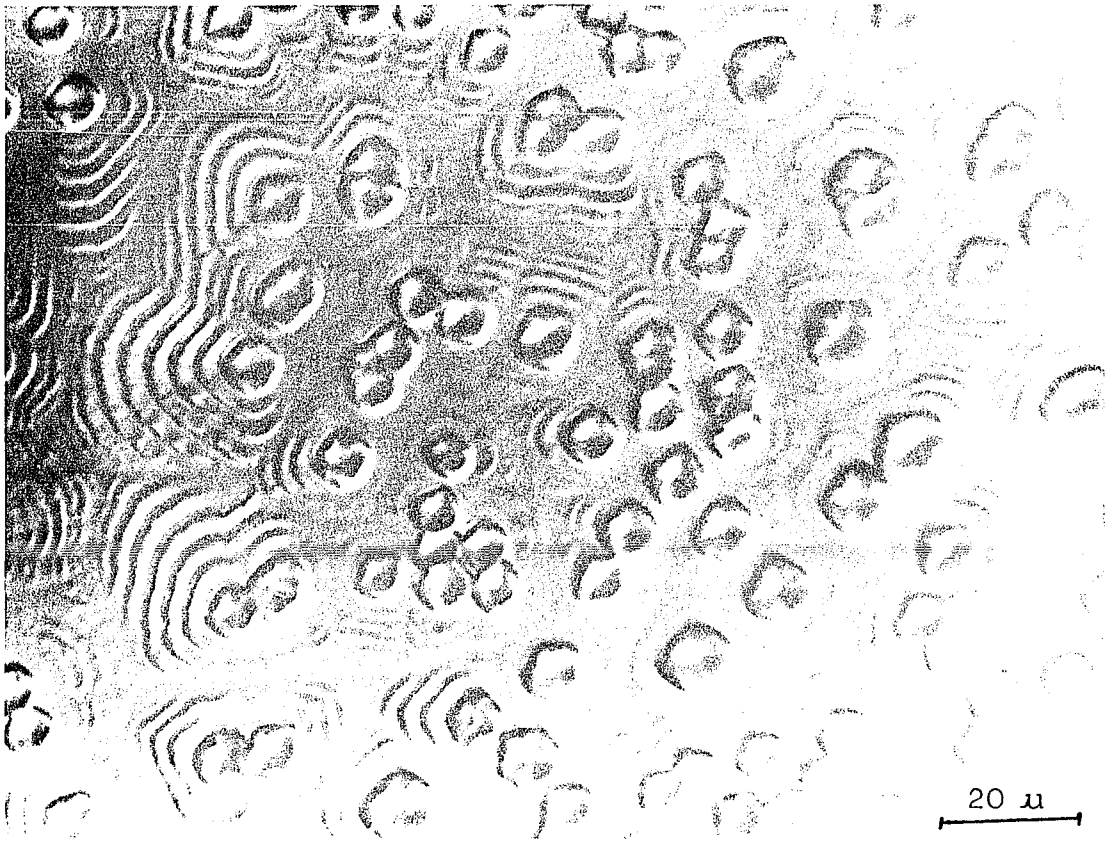

C. Interference Contrast

$\bar{M}_n = 4.9 \times 10^3$, T_c = 20°C (12 hours) in 1% (w/v) Amyl Acetate

C. Crystallization from Melt:

When TPI thin films were crystallized isothermally from the melt and viewed under cross-polaroids in the optical microscope, two forms of spherulites could be distinguished. The first form displayed a characteristic Maltese Cross pattern with the directions of the arms of the cross parallel to directions of the polarizer and analyzer (Fig. 32-A). These Maltese Cross spherulites were generally observed at a temperature below 35°C. At higher temperatures the second

form which exhibited a characteristic dendritic pattern (Fig. 32-B) was obtained. Evidence of crosslinking and/or degradation during crystallization was found from the analysis of molecular weight distribution by GPC; also recrystallization in presence of solvents during chemical reaction was observed.

Fig. 32. Optical Micrographs of TPI Crystallized from Melt

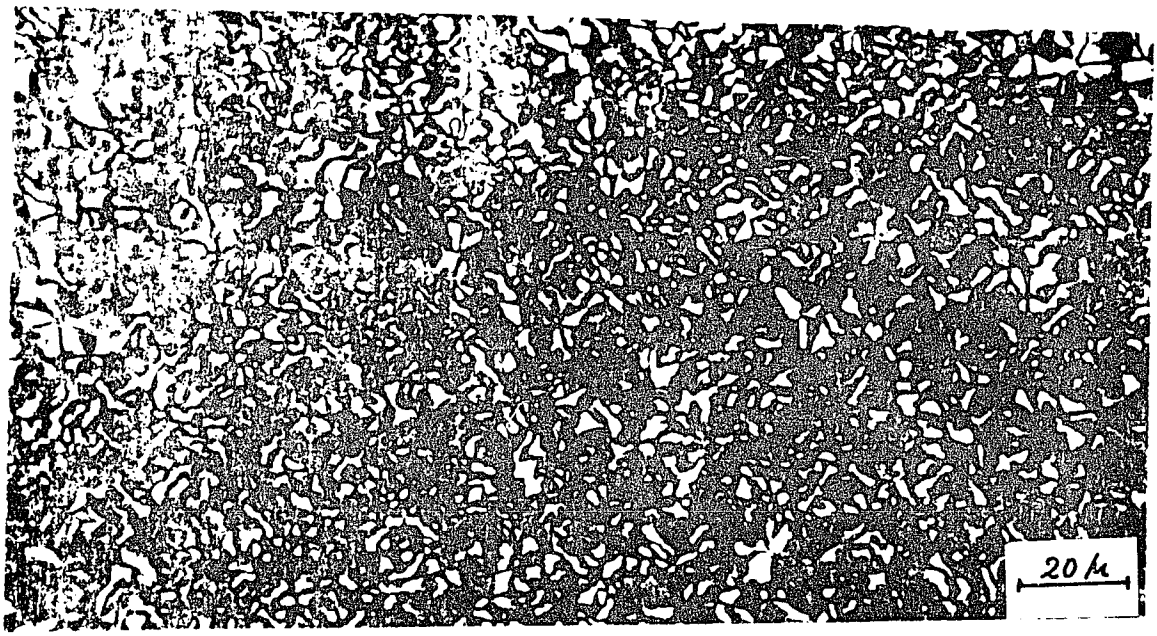

A. Crossed Polaroids of Fractionated Gutta Percha

$\bar{M}_n = 5.8 \times 10^4$, $\bar{M}_w/\bar{M}_n = 1.93$, $T_D = 100°C$, $T_C = 0°C$

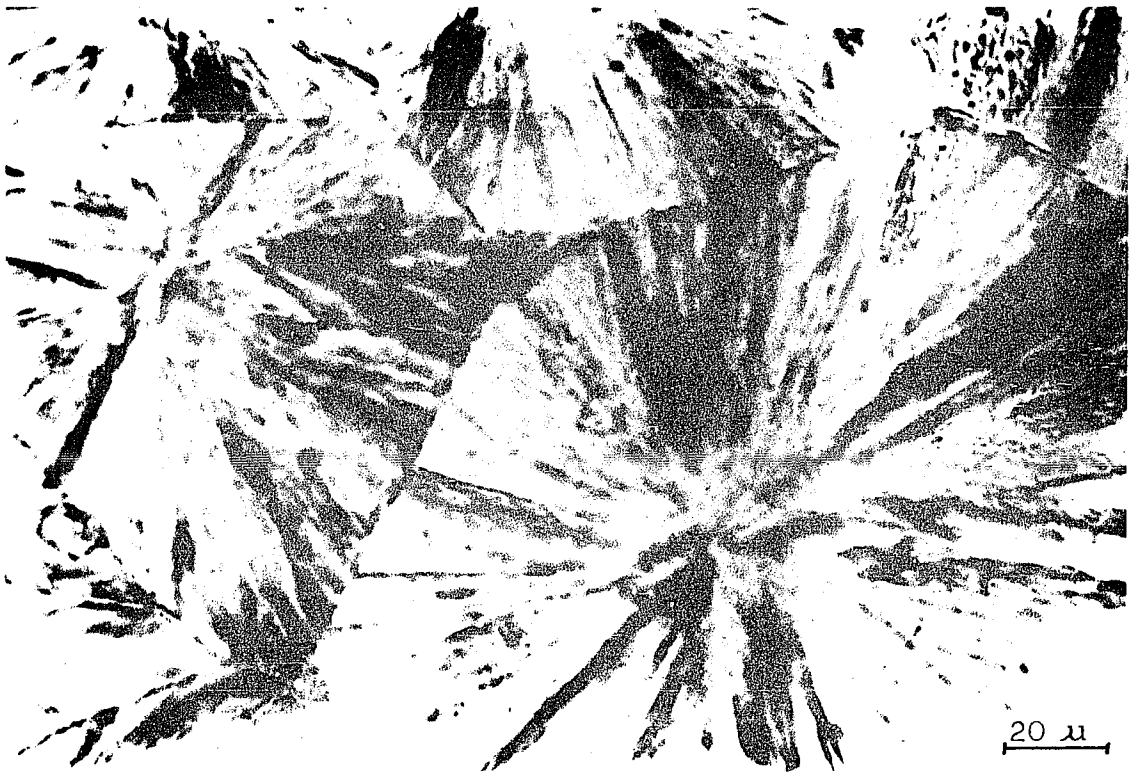

B. Interference Contrast of Unfractionated and Purified Balata

$\bar{M}_n = 1.4 \times 10^5$, $\bar{M}_w/\bar{M}_n = 1.96$, $T_D = 100°C$, $T_C = 55°C$ for Two Weeks

Determination of Crystal Form:

1. Wide Angle X-ray Diffraction:

Assuming that crystals of TPI grown from solution show the same lattice packing as melt grown crystals, the X-ray technique used in this study primarily provides one method to determine the crystal modification, either α or β. However, in this work, a series of structures with different morphology grown from fractionated Gutta Percha under different crystallization conditions have been subjected to X-ray diffration study. A comparison of d-spacing for four samples in this work with the values reported by Takahashi et al. (50) for α form and with the value reported by Bunn (48) and Fisher (49) for the β form is shown in Table 6 and Table 7 respectively. The results suggest that within the experimental precision ($\pm$ 0.15) of the d-spacing measurement, a large difference in the X-ray diffraction pattern cannot be found at least for the α form.

Table 6. d-spacing of α-TPI for the First Six Lines

Morphology	A	B	C	D
T_M (Endotherm) °C	Single Crystal	Hedrite (Type-II)	Spherulite	Spherulite
d-spacing (Å)	58	66	60	-
100	7.88	7.79	7.74	7.81
110	4.90	4.79	4.79	4.90
200	3.94	3.76	3.70	3.90
210	3.26	3.04	3.07	3.32
120	2.87	2.68	2.69	2.92
121	2.52	2.42	2.40	2.70

A: $\bar{M}_n = 2.5 \times 10^5$, 1% (w/v) amyl acetate solution

$T_D = 100°C$, $T_C = 32°C$

B. $\bar{M}_n = 2.5 \times 10^5$, 1% (w/v) amyl acetate solution

$T_D = 100°C$, $T_C = 32°C$

C. $\bar{M}_n = 2.5 \times 10^5$, melt crystallization

$T_D = 100°C$, $T_C = 50°C$

D. Unfractionated Gutta Percha by melt crystallization calculated by Takahashi et al. (50)

$a = 7.98$ Å, $b = 6.29$ Å, $c = 8.77$ Å, $\alpha = \gamma = 90°$, $\beta = 102.0°$

$$\frac{1}{d^2} = \frac{1}{\sin^2\beta}\left(\frac{h^2}{a^2} + \frac{k^2\sin^2\beta}{b^2} + \frac{l^2}{c^2} - \frac{2hl\cos\beta}{ac}\right)$$

Table 7. d-spacing of β-TPI for the First Six Lines

	A		B (Bunn)		C (Fisher)	
	Aggregates of Curved Lamellae		Spherulite		Spherulite	
	d-spaciing (Å)	Intensity	d-spacing (Å)	Intensity	d-spacing (Å)	Intensity
120	4.59	VS	4.69	VS	4.73	VS
200	3.69	VS	3.89	VS	3.92	VS
040	3.04	MS	2.94	MW	2.97	M
230	2.72	M	2,76	MS	2.79	MW
140			2.75	W	2.78	
201	-	-	3.00		3.03	-
211			2.91		2.93	
320	2.48	W	2.37		2.39	M

VS: very strong, MS: medium strong, M: medium, W: weak

A: $\bar{M}_n = 2.5 \times 10^5$, 1% (w/v) amyl acetate solution

$T_D = 100°C$, $T_C = 0°C$

B: Unfractionated Gutta Percha, rapid cooling reported by Bunn (48)

$a = 7.78$ Å, $b = 11.78$ Å, $c = 4.72$ Å, $\alpha = \beta = \gamma = 90°$

$$\frac{1}{d^2} = \frac{h^2}{a^2} + \frac{k^2}{b^2} + \frac{l^2}{c^2}$$

C: Unfractionated Gutta Percha, thin film casted from benzene solution reportedly by Fisher (49)

$a = 7.83$ Å, $b = 11.87$ Å, $C = 4.75$ Å. $\alpha = \beta = \gamma = 90°$

The crystal growth habit (either α or β modification) has been investigated for melt crystallized samples obtained at various temperatures [51]. In the present study X-ray diffraction was carried out on samples with molecular weights from 9.9×10^3 to 2.5×10^5 which were crystallized in 1% (w/v) amyl acetate by the direct crystallization method. The crystal form changed from β to α as the crystallization temperature was increased. The β form was present at crystallization temperatures from -15 to 10°C and the α form appeared predominantly at 15 to 32°C. The crystalline form doesn't vary with the molecular weight or the morphology.

Some X-ray determinations were made on structures obtained from a different solvent, heptane. TIP fractions with molecular weight 2.4×10^4, 9.7×10^4 and 2.5×10^5 were crystallized in 1% (w/v) heptane at $T_C = 0°C$; the crystals grown from the higher molecular weight fractions were in the α form and those grown from $\bar{M}_n = 2.4 \times 10^4$ were in the β form. These results were also confirmed by DSC measurements as presented above and are summarized in Table 4.

A change in the crystallization procedure also affects the crystal modification. All the samples grown by the precooling method were in the α form. The β form was present when the direct cooling method at low crystallization temperature was used. One example are the structures obtained from material with $\bar{M}_n = 2.5 \times 10^5$ grown from 10°C. The X-ray

patterns are shown in Fig. 33.

Fig. 33. Dependence of X-ray Diffraction Patterns on Crystallization Procedure‡

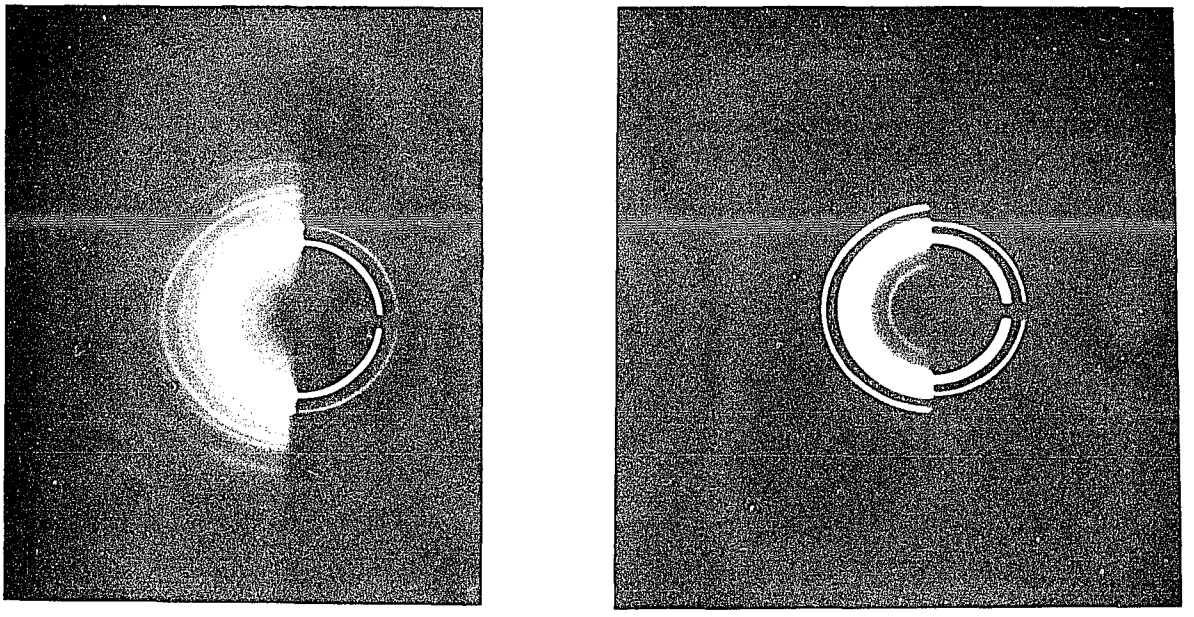

A. $\bar{M}_n = 2.5 \times 10^5$, in 1% (w/v) Amyl Acetate
$T_D = 100°C$, $T_C = 10°C$

B. $\bar{M}_n = 2.5 \times 10^5$, in 1% (w/v) Amyl Acetate
$T_D = 100°C$, $T_P = -78°C$,
$T_R = 45°C$, $T_C = 10°C$

‡ The left side of the X-ray patterns in both A and B are for longer exposure times.

In this work, randomly oriented polycrystalline samples were mainly used. Only one sample with cup-shaped lamellar aggregate ($\bar{M}_n = 2.5 \times 10^5$ growing in 1% (w/v) amyl acetate at $T_D = 100$ and $T_C = 0°C$) was investigated which was purposely oriented. A mat of cup-shaped lamellar aggregates was made

by filtration in a perpendicular cylinder connected to a filter holder with slow sedimentation at 0°C. The X-ray diffraction pictures were taken from both an "edge-on" view and a "flat-on" view of the aggregates. A strong (040) index was found from edge-on diffraction, but this index disappeared or became unclear in the flat-on diffraction. This indicates that the lamellae in the aggregate are not distributed in random style but are oriented with the b-axis parallel to the edge of the mat. The reason for this is still unknown.

2. DSC Measurements:

Crystallization from amyl acetate solution by the precooling method at constant temperature T_c from 0 to 25°C yields one crystal form only as evidenced by the appearance of a single DSC endotherm. An endotherm in the 56 to 63°C region have been identified previously with unfractionated α-TPI (55). This is also consistent with wide angle X-ray diffraction analyses.

Crystallization by the direct method at constant T_c from -15 to 32°C shows a large range of melting endotherm depending on the crystal form. DSC scans for some of the preparations from 1% (w/v) amyl acetate solution for a sample with $\overline{M}_n$ = 2.5×10^5 are given in Fig. 34, where curves for both direct and precooled crystallizations at T_c = 10, 20 and 25°C are shown. It is seen that direct crystallization at 10°C leads to an endotherm at 50°C indicative of the β form, while

direct crystallization at 25°C gives an endotherm at 62°C indicative of the α form. At an intermediate crystallization temperatures (15°C) both α and β forms may coexist. These results and those for other preparations studied are summarized in Table 8. The X-ray results summarized above and density measurements presented below are also included.

It can be seen from Table 8 that the precooling and direct crystallization methods at a particular T_c yield samples with similar endotherm temperatures if the same crystalline form results. Although care was taken to remove all of the amyl acetate from those samples at T_c before any tests were made, it is possible that some recrystallization due to the presence of amyl acetate occurred, thereby causing some of the variation in the DSC endotherms observed. An apparent example is the cup-shaped lamellar aggregates with $\bar{M}_n = 2.5 \times 10^5$ grown from 1% (w/v) amyl acetate solution at 0°C which showed two endotherms (50 and 59°C) with almost the same intensity from DSC analysis. The endotherm at 59°C is indicative of the α form recrystallizing from the β form (endotherm of 50°C) in amyl acetate. Annealing of these aggregates at 10°C for 12 hours yielded only a single β form endotherm at 52°C.

Fig. 34 DSC Scans for the HMW Fraction from Amyl Acetate Solution with $\bar{M}n = 2.5 \times 10^5$.

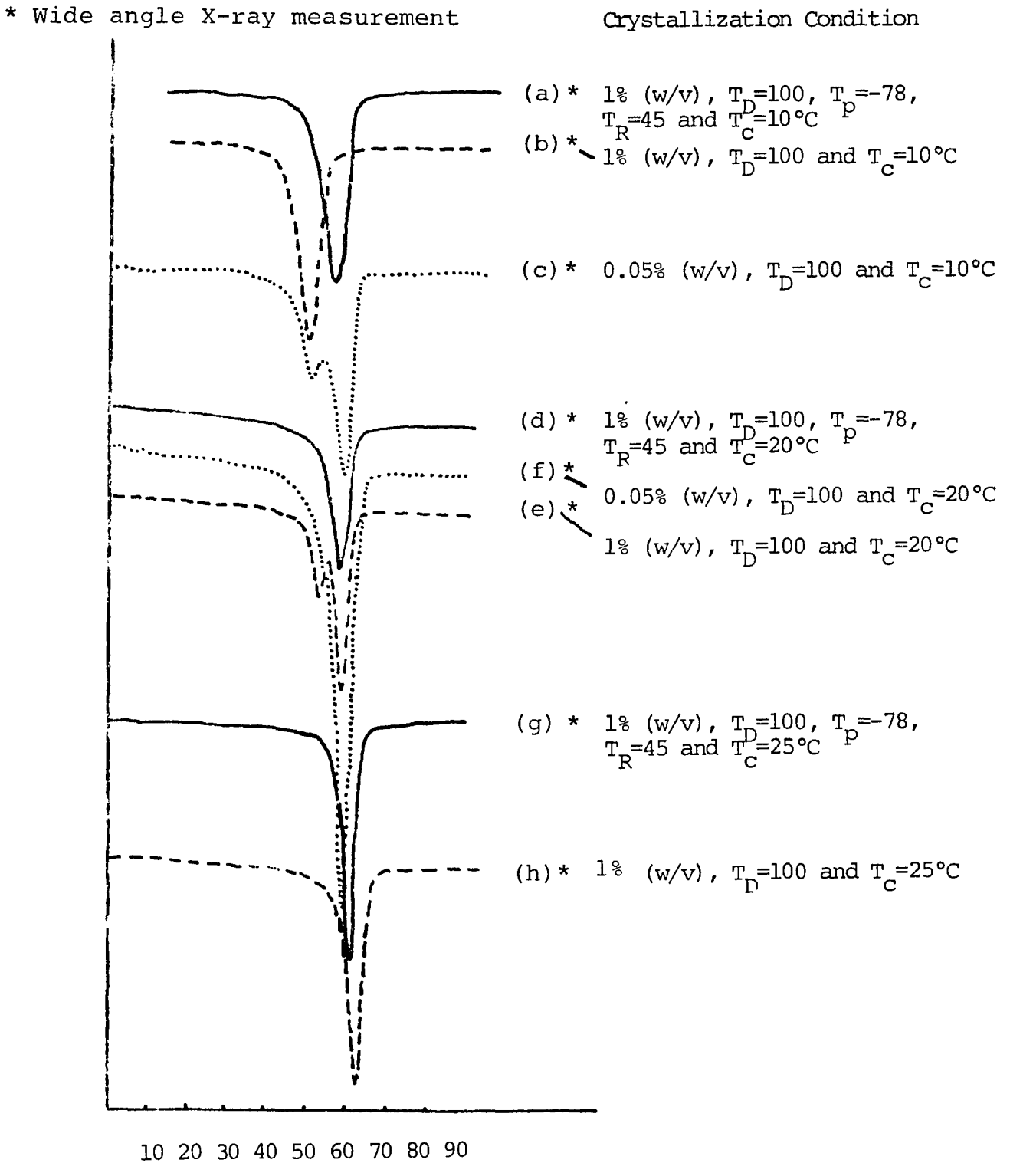

Table 8. DSC, Density and X-ray Results for TPI Fractions Crystallized from Amyl Acetate

$\bar{M}_n$	$\bar{M}_w/\bar{M}_n$	Conc. % w/v	Crystallization Condition (°C) T_P	T_S	T_C	DSC Endotherm (°C) [c] Direct Crystallization	Precooling	Crystal Forms	Density [b] g/cm^3
2.5×10^5	1.34	1	-	-	32	67	-	α	0.972
		1	0	45	30	-	64.5	α [a]	0.972
		1	20	50	30	-	65	α [a]	0.974
		1	-	-	25	62	-	α [a]	0.969
		1	-78	45	25	-	63	α	0.968
		1	0	45	25	-	63	α	0.968
		1	-	-	21	56(w),61	-	α	0.968
		1	-	-	20	54(w),59	-	α [a]	0.969
		1	-78	45	20	-	58	α	0.968
		0.05	-	-	20	60	-	α [a]	0.972
		1	-	-	15	54(b)	-	α + β [a]	0.968
		1	0	45	15	-	59	α	0.967

Table 8 (continued)

		1	-	-	10	50	-	β^a	0.964
		1	-78	45	10	-	57	α^a	0.964
		1	0	45	10	-	56	α	0.963
		0.05	-	-	10	51,59	-	$\underline{\alpha+\beta}^a$	0.965
		1	-	-	0	50,59	-	$\alpha+\underline{\beta}^a$	0.963
		1	-78	45	0	-	58	α^a	0.968
		1	0	45	0	-	58	α	0.964
		0.05	-	-	0	51,58(w)	-	β	0.964
		1	-	-	-15	43(s),51,59(w)	-	β^a	0.958
1.0×10^4	1.56	1	-	-	25	62.5	-	α	0.975
		1	-	-	20	60	-	α	0.973
		1	-	-	15	52,56.5	-	$\alpha+\beta^a$	0.972
		1	-	-	10	49,60(w)	-	β^a	0.966
		1	-	-	0	43,50,60(w)	-	β	0.966
2.4×10^4	1.51	3	-	-	32	65	-	α	0.973
		1	-	-	21	55(s),60,64(w)	-	α^a	0.972

Table 8 (continued)

		1	-	-	20	54(s),58,63(w)	-	α	0.972
		1	-78	40	20	-	59(b),62(w)	α	0.976
		1	-	-	15	51,56,62(w)	-	α + β	0.972
		1	-	-	10	48,54	-	$\underline{\beta} + \alpha$ [a]	0.967
		1	-	-	0	42,53	-	β [a]	0.966
9.9×10^3	2.0	8	-	-	30	63	-	α	0.979
		1	-	-	20	59	-	α	0.983
		1	-78	38	20	-	59	α	0.980
		2 [d]	-	-	20	62	-	α	0.979
		10 [d]	-	-	20	62	-	α	0.974
		1	-	-	10	47,53,5,61(w)	-	β + α	0.965

a: determined by wide angle X-ray diffraction; underscoring of α or β indicates the predominate crystal structure

b: measured on ethanol/H_2O density gradient column

c: endotherms from DSC: (w): weak, (s) shoulder, (b): broad

d. crystallized from heptane

The double melting points of crystals grown from the lower molecular weight fractions at low T_C, such as $\bar{M}_n = 1.0 \times 10^5$, $T_C = 0°C$ or $\bar{M}_n = 2.4 \times 10^4$, $T_C = 0$ or 10°C by direct crystallization method suggests the presence of two different lamellar thicknesses. The possibility of a mixture of α and β crystals is excluded because the presence of the β form only has been confirmed by X-ray diffraction. In a study of morphology, type-III hedrite structures of two sizes were observed, one about 70 μm, the other much smaller (about 30 μm) in sheaf length for $\bar{M}_n = 2.4 \times 10^4$ at 1% (w/v) amyl acetate solution, $T_C = 0°C$. These crystals were washed and suspended and then placed on a glass slide, dried at T_C under vaccum, and the melting observed with polarizing microscope equipped with a hot stage. At an approximately heating rate of 10°C/min., the melting temperature of the small hedrite was 45°C and that for the large hedrite was 57°C by observing the disappearance of birefringence from crossed polaroids. Fig. 35 shows the absence of the small structures at 50°C. This is essentially consistent with the DSC measurement.

The DSC thermogram obtained from the crystals grown under the above conditions, as a function of crystallization time is shown in Fig. 36. For short crystallization time (15 min.) only one melting endotherm at 53°C was observed. However, at longer crystallization time a second melting endotherm at 42°C developed. After one day, a double endotherm with equal inten-

sity has been observed. Less than 50% by weight of the material crystallized during the first 15 minutes. It was found that at least 30 minutes were necessary to cool 10 ml of amyl acetate in a test tube from 100°C to 0°C. Obviously, the double endotherms observed in the crystallizations are due to nonisothermal crystallization. A sharp fraction of TPI with $\overline{M}_n$ = 4.9×10^3, $\overline{M}_w/\overline{M}_n$ = 1.25 gave double endotherms for the same crystallization conditions.

Fig. 35. Melting of Hedrites Grown from 1% (w/v) Amyl Acetate with $\overline{M}_n = 2.4 \times 10^4$ at $T_C = 0°C$ from Optical Microscope Heating Rate 10°C/min

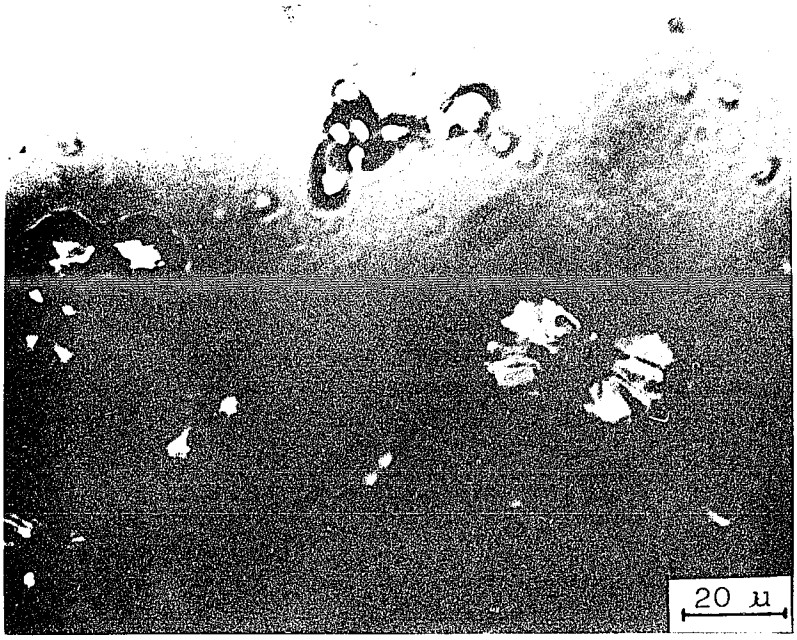

A. Dried Crystals Before Heating

Interference Contrast

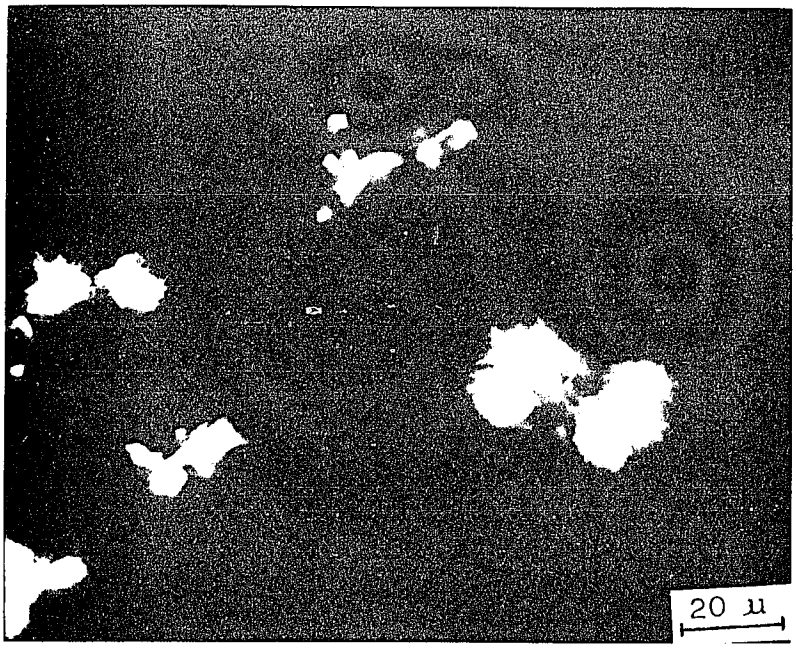

B. Dried Crystals Before Heating

Crossed Polaroids

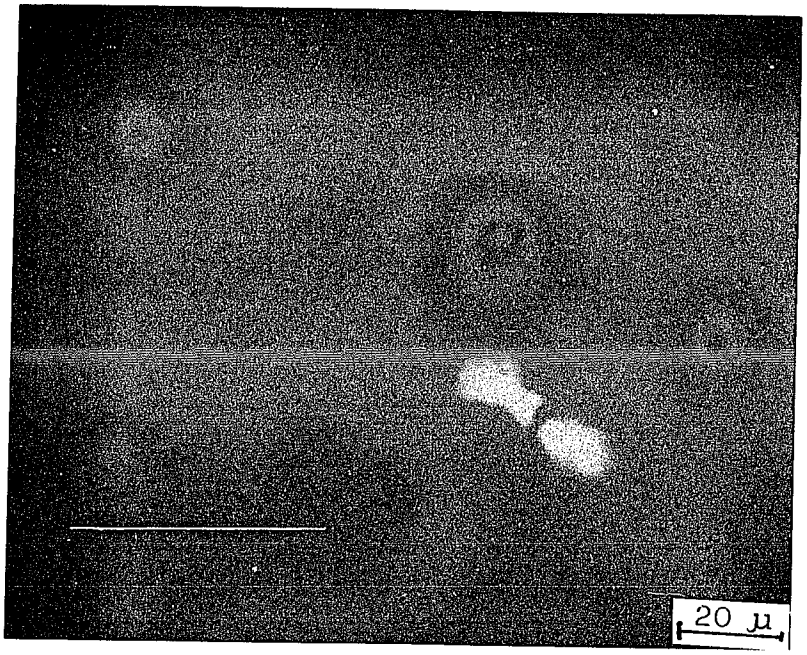

C. Dried Crystals Heated to 50°C

Crossed Polaroids

Fig. 36. Thermograms of LMW TPI as a Function of Crystallization Time

$\bar{M}_n = 2.4 \times 10^4$, $T_D = 100°C$, $T_C = 0°C$ in 1% (w/v) Amyl Acetate

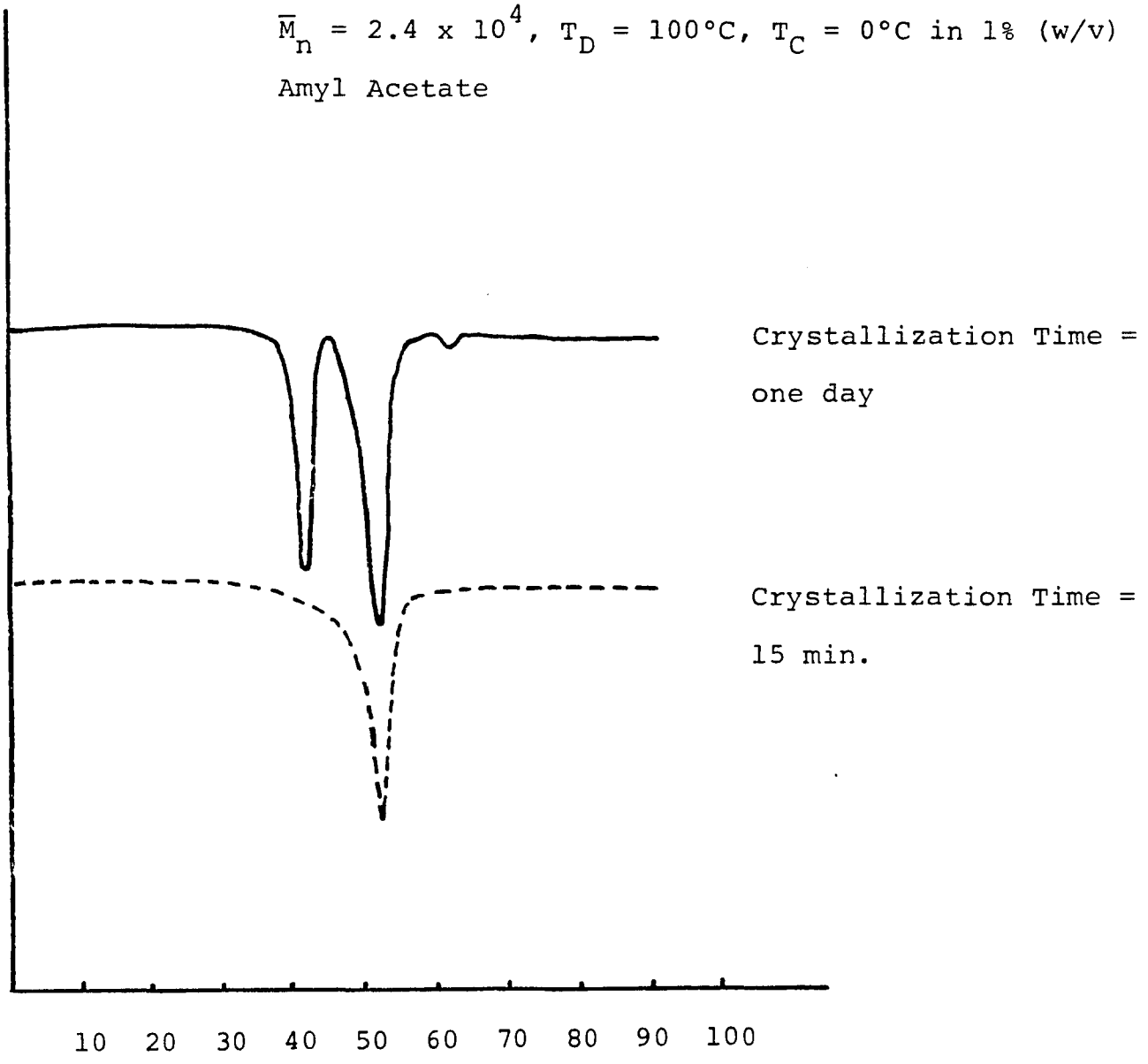

Stability of Cup-Shaped Lamellar Aggregates in Suspension

The structures grown with high supercooling from the high molecular weight fraction ($\overline{M}_n$ = 2.5 x 10^5, T_c = 0°C) at concentrations from 0.05 to 1% (w/v) amyl acetate solution, as discussed above, are cup-shaped lamellar aggregates. This aggregate dissolves if heated rapidly in suspension to room temperature, also the suspension becomes clear in one minute or less and then becomes cloudy again if ether is added at 0°C. The cloudiness is due to the presence of single lamellae as shown in the electron micrograph in Fig. 37. X-ray diffraction and DSC (Fig. 38) showed the presence of the α modification.

Fig. 37. Micrographs of Ether Washed Precipitate from Cup-Shaped Lamellar Aggregates

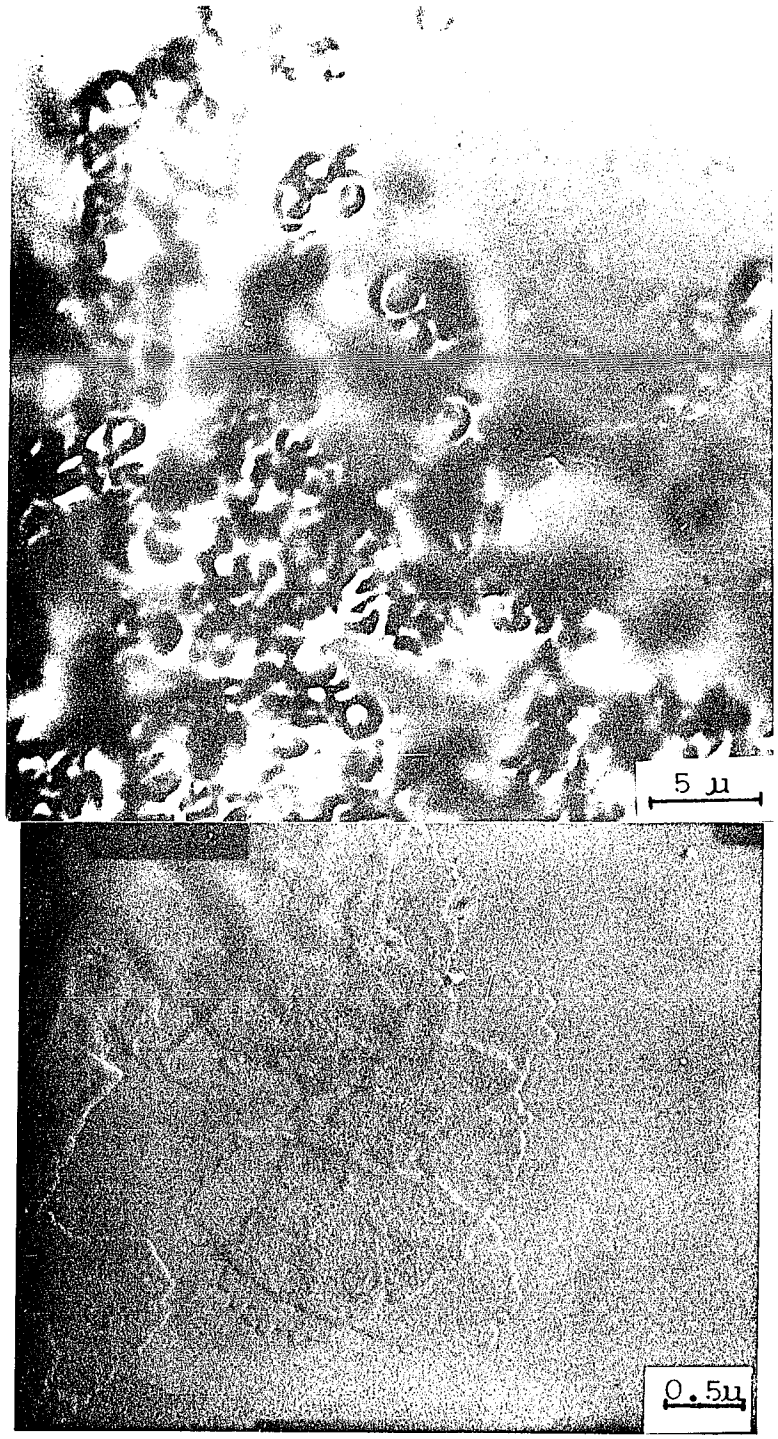

A. From Interference Contrast Microscopy (wet state)

B. From Electron Microscopy (dried state)

Fig. 38. DSC Thermograms for Cup-Shaped Lamellar Aggregates Grown from Amyl Acetate Solution with $\bar{M}_n = 2.5 \times 10^5$, at 0°C and Treated with Ether

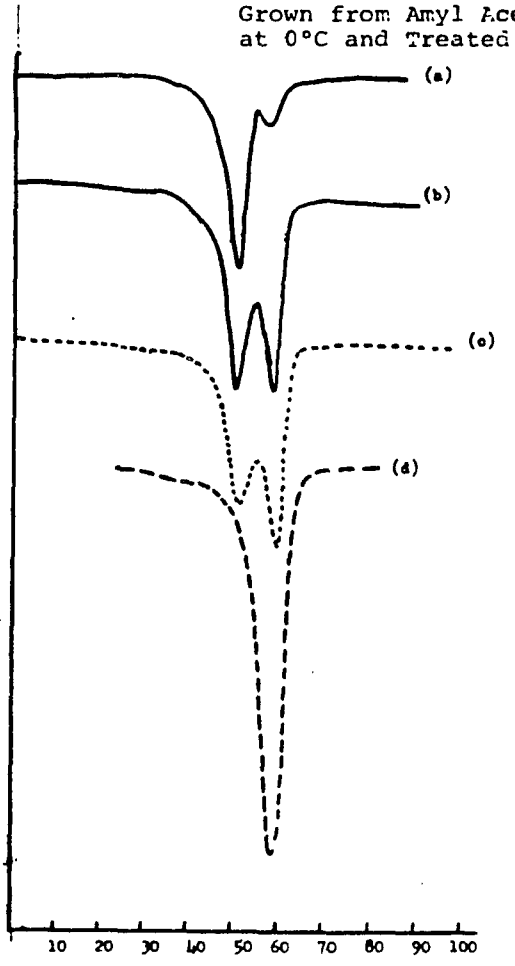

(a): 0.05% (w/v) endotherm: 51, 58°C
(b): 1% (w/v) endotherm: 50, 59°C
(c): ether washed (a) incompletely at 0°C
endotherm: 50, 59°C
(d): ether washed (a) and permeated over one hour
endotherm: 59°

Since these aggregates are so sensitive to temperature and solvent there was initially considerable doubt as to whether or not the aggregate was at all crystalline.

Turning to some other phenomena, the original cup-shaped lamellar aggregates can exist at room temperature, if the temperature is slowly increased from 0°C. Heating the aggregates at a rate of 0.2-0.3°C/min gave a clearing point as high as 44°C. This indicates that a lamellar thickening has occurred.

Some studies carried out to investigate these structures are discussed below:

1). Annealing in Solution:

Four separate samples of the aggregates grown from 1% (w/v) amyl acetate at 0°C with $\bar{M}_n = 2.5 \times 10^5$ were heated to 10, 20, 30 and 35°C at a rate of 0.2-0.3°C/min., and then placed in an isothermal water bath at the particular annealing temperature (T_A) for twelve hours. No apparent change in morphology was observed with the optical microscope while keeping the annealing temperature at or below 30°C as shown in Fig. 39. The melting endotherm increases from 50 to 55°C due to lamellar thickening (Fig. 40). X-ray diffraction showed retention of the β form. However, a strong endotherm at 59°C (Fig. 38) indicative of the α form, which existed for the original aggregates before annealing, almost disappears. This endotherm had been attributed to recrystallization during

the drying process. Thickening of the lamellae should stabilize the aggregates and lead to a higher melting temperature for the β form crystallites.

While heating these β form aggregates to 35°C at a rate of 0.2-0.3°C/min., the suspension becomes partially clear (it is totally clear at about 44°C). The aggregates become smaller at 35°C but still survive, although the surface shows damage as observed in Fig. 41 (A-position). Upon keeping the partially dissolved suspension for twelve hours at the same constant temperature (35°C), a lot of new single crystals (B-position, Fig. 41) are observed. The X-ray diffraction pattern shows only the α structure and DSC measurement also shows a sharp melting endotherm (curve e, Fig. 40) indicative of the α form.

Fig. 39. Morphology of Cup-Shaped Lamellar Aggregates with $\bar{M}_n = 2.5 \times 10^5$ after Annealing in Amyl Acetate Suspension

Crystallization Condition: $T_D = 100°C$, $T_C = 0°C$ in 1% (w/v) amyl acetate

Annealing Condition: Heating Rate 0.2-0.3°C/min.

$T_A = 30°C$, $t_a = 12$ hours

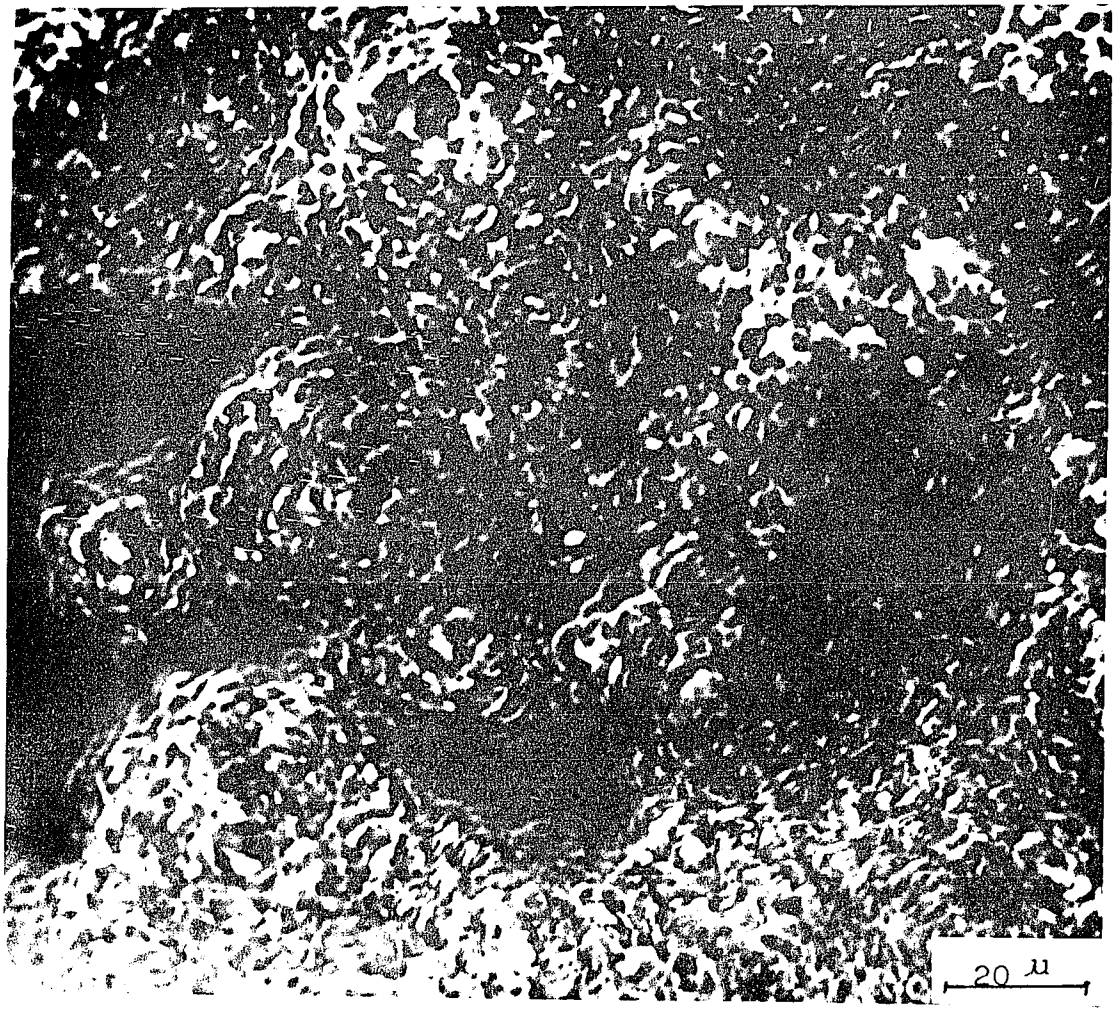

Fig. 40. Effect of Annealing on the Melting Endotherms for TPI Cup-Shaped Lamellar Aggregates in Amyl Acetate Suspension

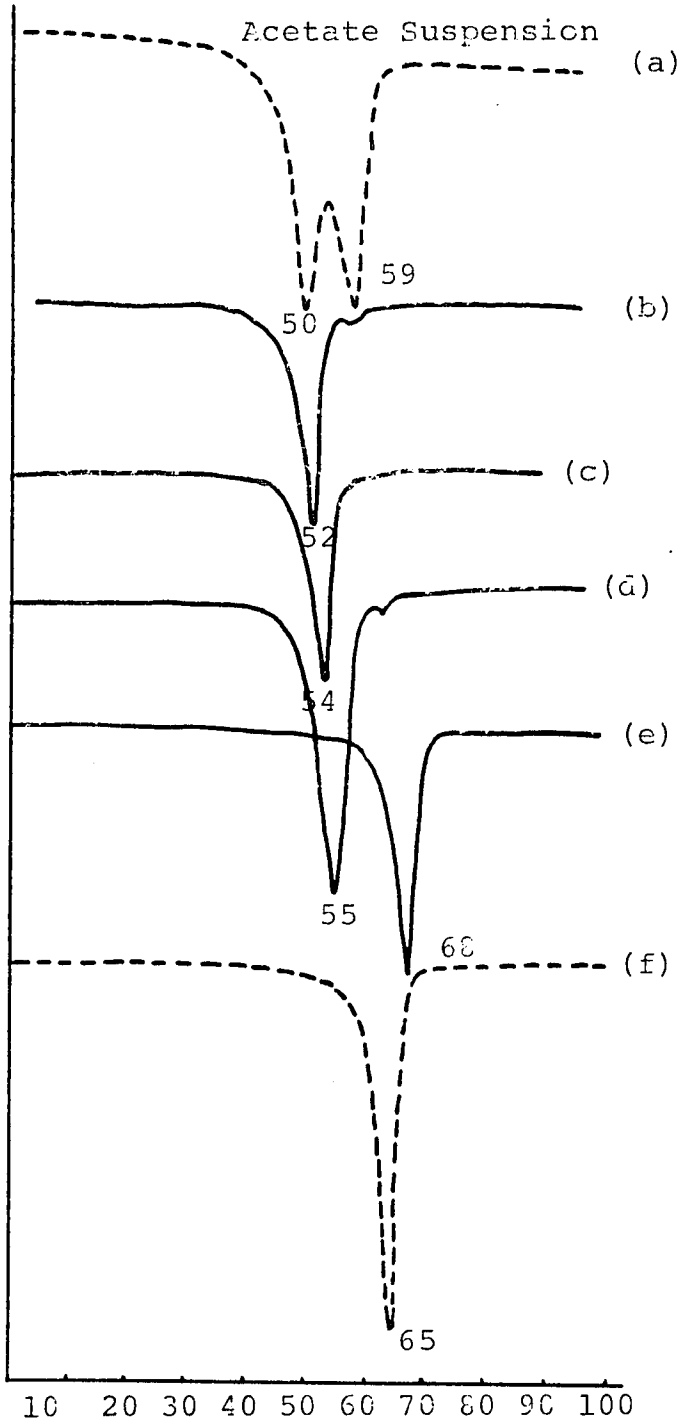

(a) Original aggregates with $\bar{M}_n = 2.5 \times 10^5$ Crystallized from 1% (w/v) Amyl Acetate Solution at $T_D = 100°C$, $T_C = 0°C$.

(b) - (e): Annealing of (a), at a Heating Rate of 0.2-0.3°C/min. for 12 hours

(b) $T_A = 10°C$ (c) $T_A = 20°C$ (d) $T_A = 30°C$ (e) $T_A = 35°C$

(f) $T_A = 30°C$ at a Rapid Heating, $t_a = 12$ hours

Fig. 41. Optical Micrographs of Cup-Shaped Lamellar Aggregates, Annealing to 35°C at a Heating Rate of 0.2-0.3°C min^{-1} and Crystallizing at the Same Temperature for Twelve Hours

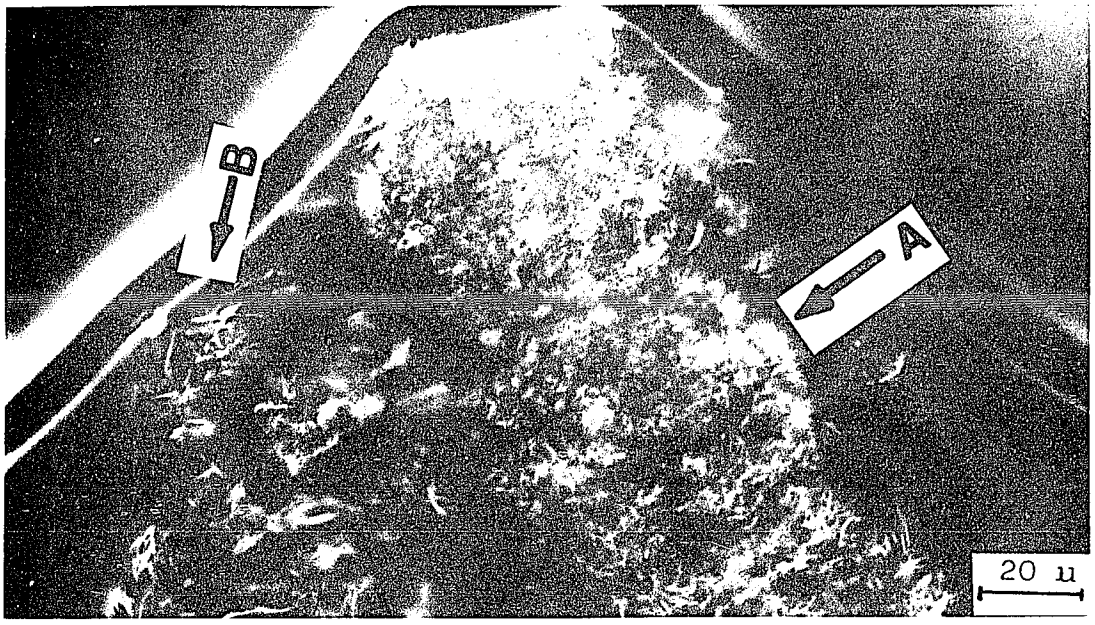

A. Interference Contrast

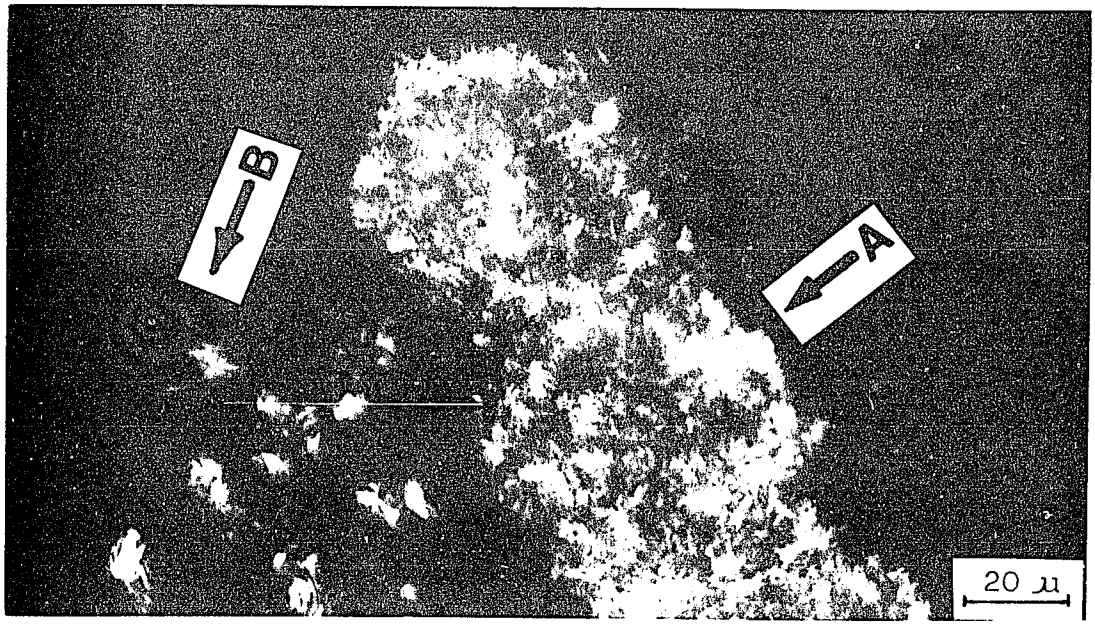

Crossed Polaroids of A

(The overgrown single crystals in position B have moved, the real birefringence is weak in an edge-on view.)

The morphology, crystal form, crystallinity, melting endotherm and heat of fusion from X-ray diffusion, density and DSC measurements are summarized in Table 9.

Table 9. Effect of Annealing Cup-Shaped Lamellar Aggregates in Suspension

Morphology	T_A (°C)	Crystal Form from X-Ray Diffraction	Crystallinity from Density Wc %	DSC Measurement Endotherm (°C)	DSC Measurement ΔH_f cal/mol
Type-VI[(a)]	-	$\beta + \alpha$	56	50,59	-
Type-VI	10	β	58	52	1114.4
Type-VI	20	β	60	54	1196.7
Type-VI	30	β	63	55	1287.7
Partially dissolved Type-VI and single crystals	35	α	54	68	-
Single crystals	30 (rapidly)	α	54	65	-

(a) Original aggregates grown from 1% (w/v) amyl acetate at T_D=100°C and T_C = 0°C.

Some other morphological changes that take place when the heating rate to the annealing temperature is rapid are shown in Fig. 42. Generally, surface damage of the aggregate increases and the birefringence becomes weak with increasing T_A. At T_A = 25°C almost all the aggregates dissolve and recrystallize as single lamellae.

Fig. 42. Morphological Changes Due to Rapid Heating Rates from Optical and Electron Microscopy

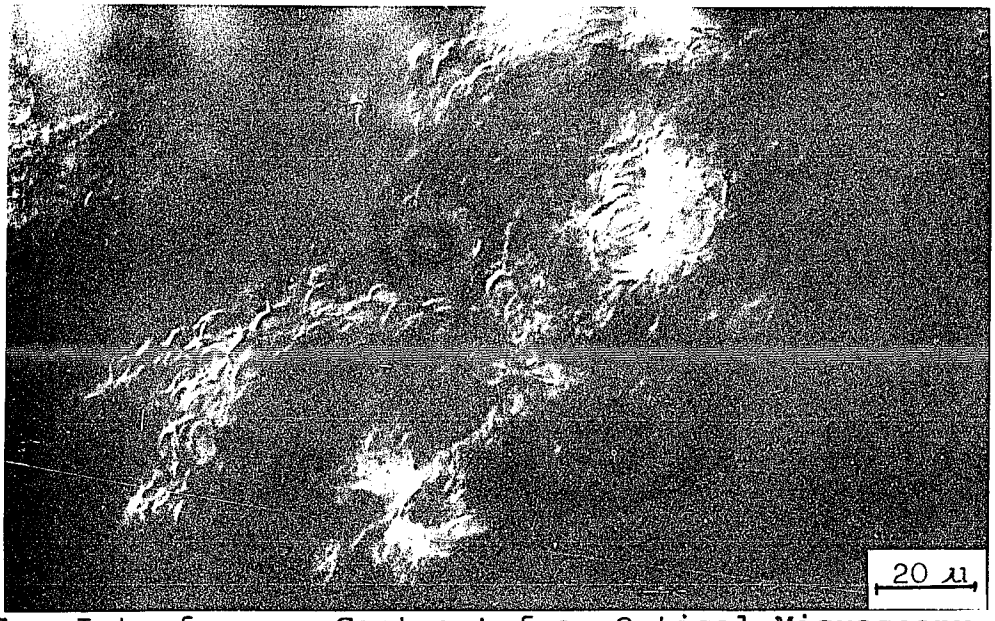

A. Interference Contrast from Optical Microscopy

T_A = 15°C (Rapidly) for 12 hours

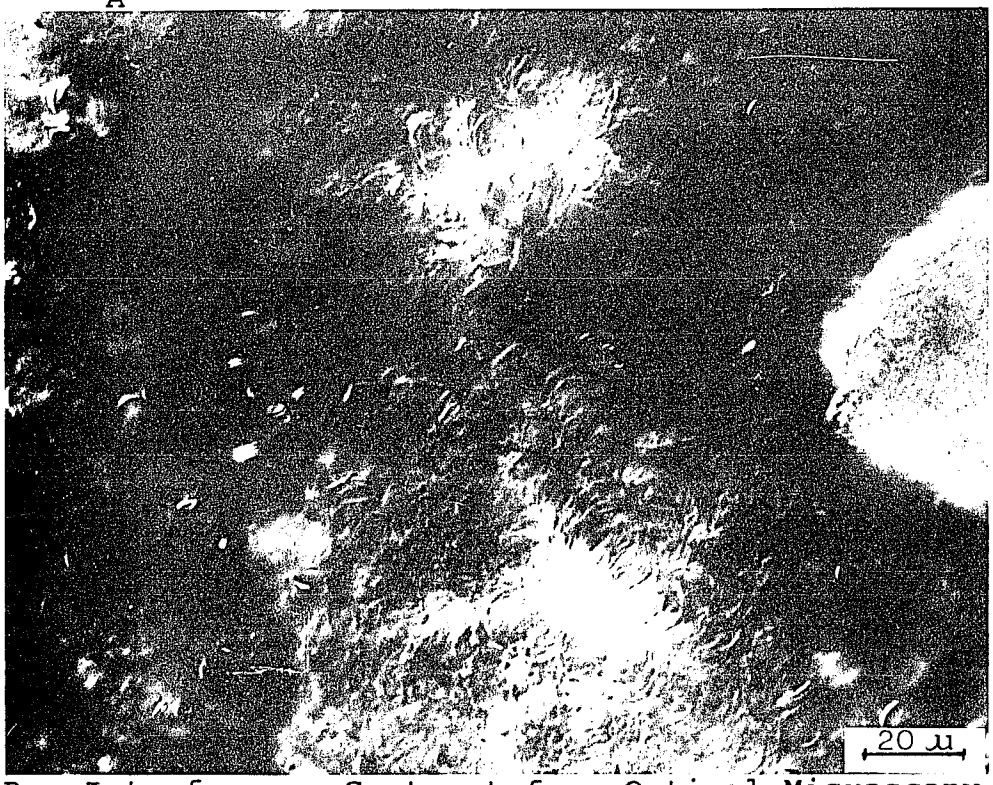

B. Interference Contrast from Optical Microscopy

T_A = 20°C (Rapidly) for 12 hours

C. Interference Contrast from Optical Microscopy

T_A = 25°C (Rapidly) for 12 Hours

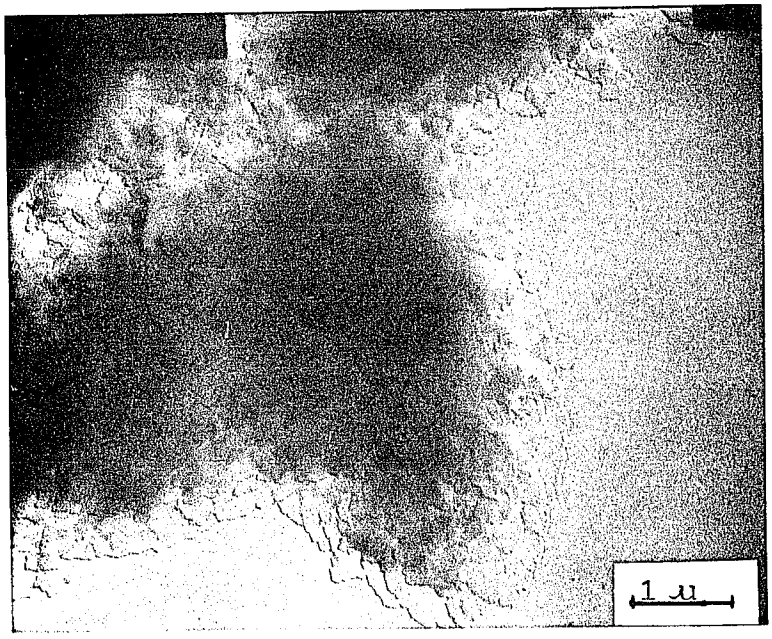

D. Electron Micrographs of (C)

2) Other Changes:

Aggregates grown from 1% (w/v) amyl acetate at 0°C with $\bar{M}_n = 2.5 \times 10^5$ were filtered and washed carefully at 0°C to remove all the soluble material in the solution. The aggregates were then permeated with pure amyl acetate at -15°C for 15 hours. The DSC thermogram as shown in Fig. 43-C indicates a strong new endotherm at 45°C along with the endotherms at 50 and 59°C. The endotherm at 59°C, which is due to recrystallization during drying becomes smaller. It is expected that the amorphous chains or parts of chains crystallize when the temperature is decreased. However, the morphology as observed by optical microscopy did not show any change. The same result was also observed when washing with ethyl acetate, a poorer solvent than amyl acetate, was carried out at 0°C (See Fig. 43-d). For O_sO_4 fixed aggregates, the endotherm was a little higher than for unfixed aggregates due to the fact that the double bonds of the mobile phase and the chain fold regions were reacted and the chains crosslinked (see Fig. 43-b).

Fig. 43. The Effect of Various Treatments on the DSC

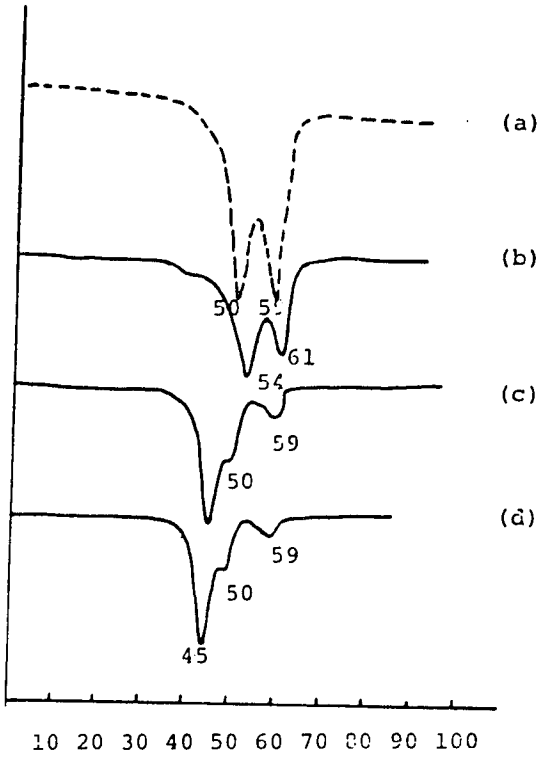

(a) Before treatment

$\bar{M}_n = 2.5 \times 10^5$ grown from 1% (w/v) amyl acetate at $T_c = 0°C$

(b) C_sC_4 fixed for 2 days

(c) Cooling to -15°C for 15 hours

(d) Treatment with ethyl acetate at 0°C for 15 hours

DSC scans for the crystallization from MW fraction, from other solvents and from the melt are summarized in Fig. 44, Fig. 45 and Fig. 46 respectively.

Fig. 44. DSC Thermograms of TPI Crystals from the MMW fraction ($\bar{M}_n$ = 1.0 x 10^5) grown from 1% (w/v) Amyl Acetate by the Direct Crystallization Method

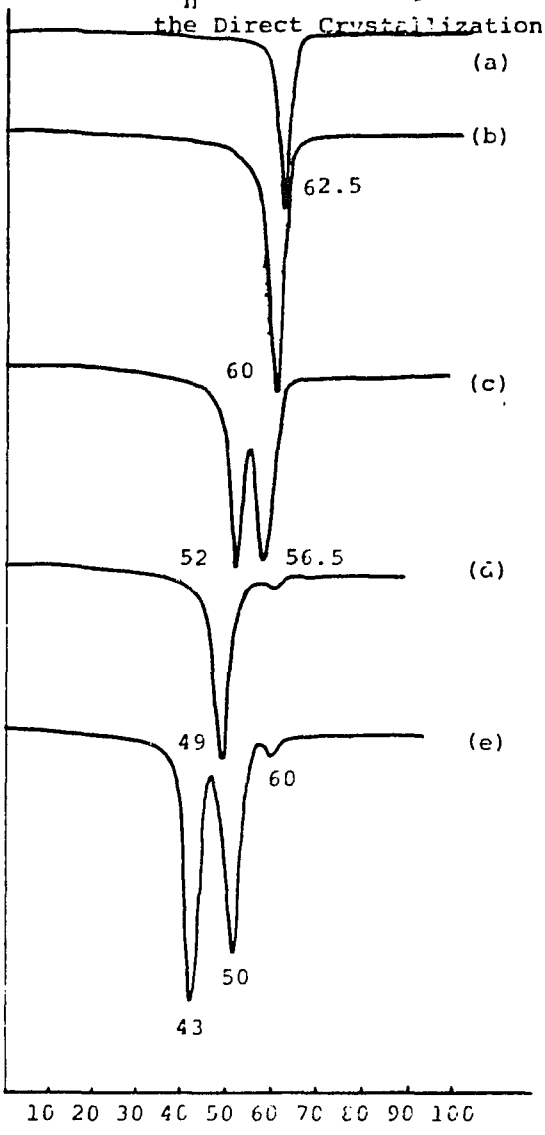

(a) T_C = 25°C

(b) T_C = 20°C

(c) T_C = 15°C

(d) T_C = 10°C

(e) T_C = 0°C

Fig. 45. DSC Thermograms of TPI Crystals from Different Solvents

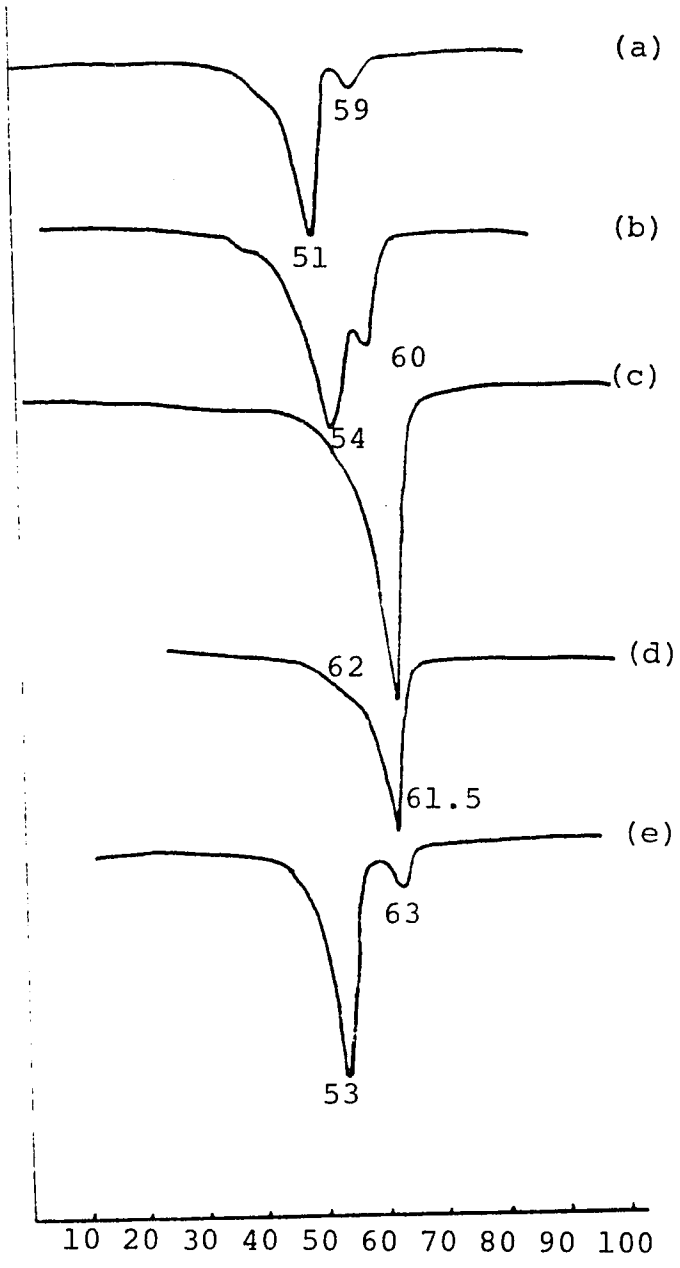

(a) 1% (w/v) butylacetate with $\bar{M}_n = 2.5 \times 10^5$ at $T_c = 0°C$

(b) 1% (w/v) dibutyl ether with $\bar{M}_n = 2.5 \times 10^5$ at $T_c = 0°C$

(c) 1% (w/v) heptane with $\bar{M}_n = 2.5 \times 10^5$ at $T_c = 0°C$

(d) 1% (w/v) heptane with $\bar{M}_n = 9.7 \times 10^4$ at $T_c = 0°C$

(e) 1% (w/v) heptane with $\bar{M}_n = 2.4 \times 10^4$ at $T_c = 0°C$

Fig. 46 DSC Thermograms of TPI Crstallized from the Melt
(a) - (e): Balata, $\bar{M}n = 1.4 \times 10^5$
(f), (g) : Synthetic TPI

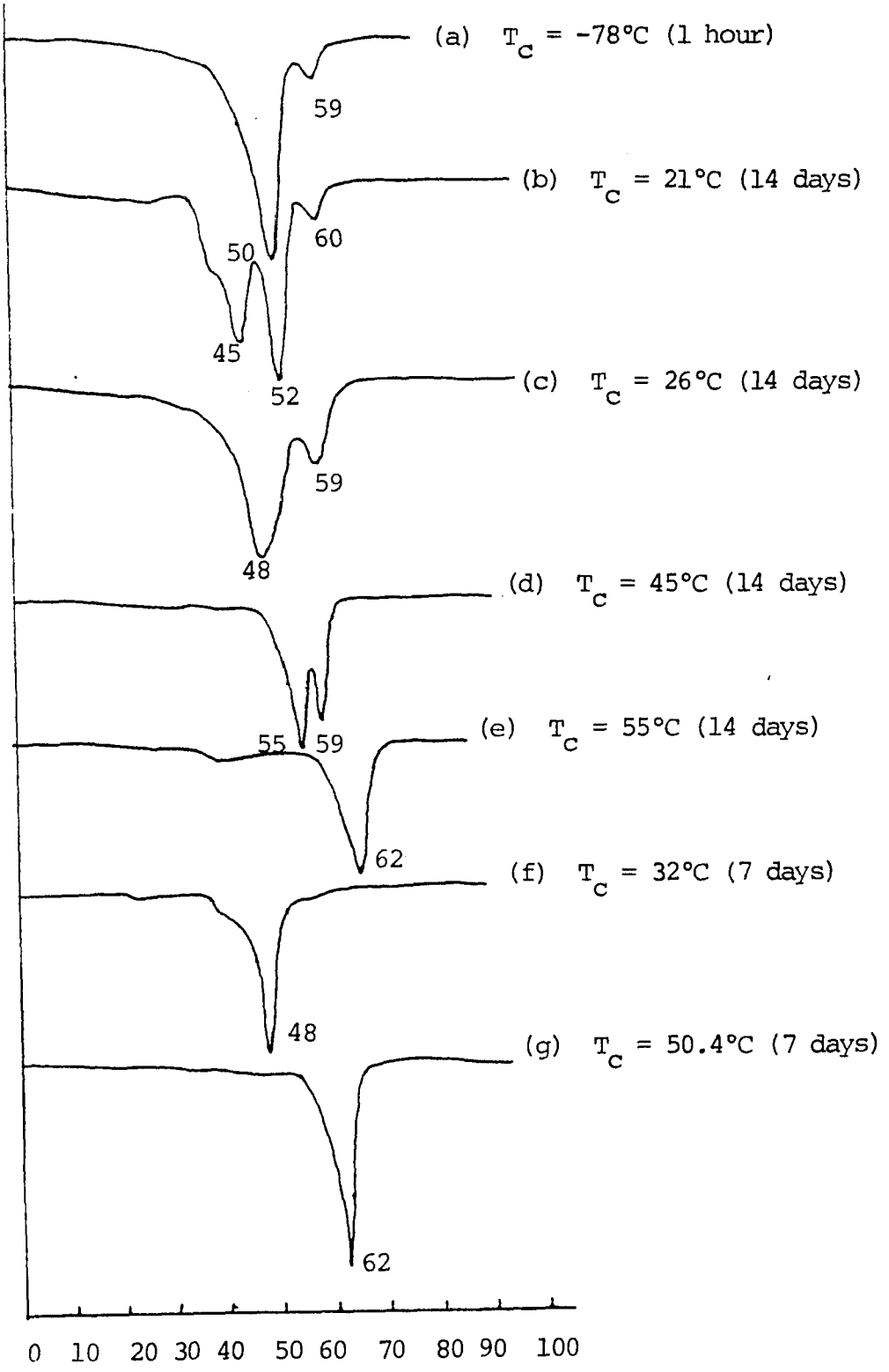

Determination of Noncrystalline Content in TPI Structures from Solution:

1) Density Measurement:

The density is a basic macroscopic quantity of a crystal and is linked directly to the unit cell parameters (48) (49) (50). For TPI, the crystal density is 1.02 g/cm^3 for the β form and 1.05 g/cm^3 for the α form at 25°C and the density of amorphons TPI at 25°C is extrapolated from the melt and is 0.905 g/cm^3 as established by dilatometry (69). Assuming that macromolecules crystallize only partially, the semi-crystalline sample is thought to consist of two positions: a crystalline portion, to be described by the crystal structure, and noncrystalline one, as described by the melt. The weight fraction crystallinity W_c is calculated by the following formula (29)

$$W_c = \frac{\rho_c}{\rho} \frac{(\rho - \rho a)}{(\rho c - \rho a)}$$

where ρ_a: density of 100% noncrystalline sample

ρ_c: density of 100% crystalline sample

ρ: sample density

The experimental results from the density measurements are summarized in Table 8, and plotted as a function of crystallization temperature in Fig. 47. Generally, the density increases in an irregular fashion with increasing T_c and

decreases with an increase in concentration from 0.05 to 1.0% (w/v) and with an increase in molecular weight. With increasing molecular weight at constant T_c using the direct crystallization method, the density first decreases, then remains constant, then decreases further. Very little, if any, consistent change in the density is found for sample preparation by the direct or by the precooling method. As noted in Table 3 in the 10 to 20°C region for directly crystallized samples a mixture of two different crystal structures with different densities can result. Density measurements were also made on (dried) cup-shaped lamellar crystal aggregates directly crystallized from 1% (w/v) amyl acetate solution at 0°C using TPI with $\bar{M}_n = 2.5 \times 10^5$ and subsequently annealed in the crystallization liquid at 10, 20 and $_{30}$°C. Two values for the rate of heating to the annealing temperature of 30°C were used, 0.2-0.3°C/min (slow) and immediate immersion at 30°C (fast), the former giving the β form and latter the α form. The densities obtained were 0.966, 0.968 and 0.972 g/cm^3 for a heating rate of 0.2-0.3°C/min to 10, 20 and 30°C while a value of 0.975 g/cm^3 upon fast heating to 30°C was measured.

Density at 25°C vs Crystallization Temperature T_c for TPI

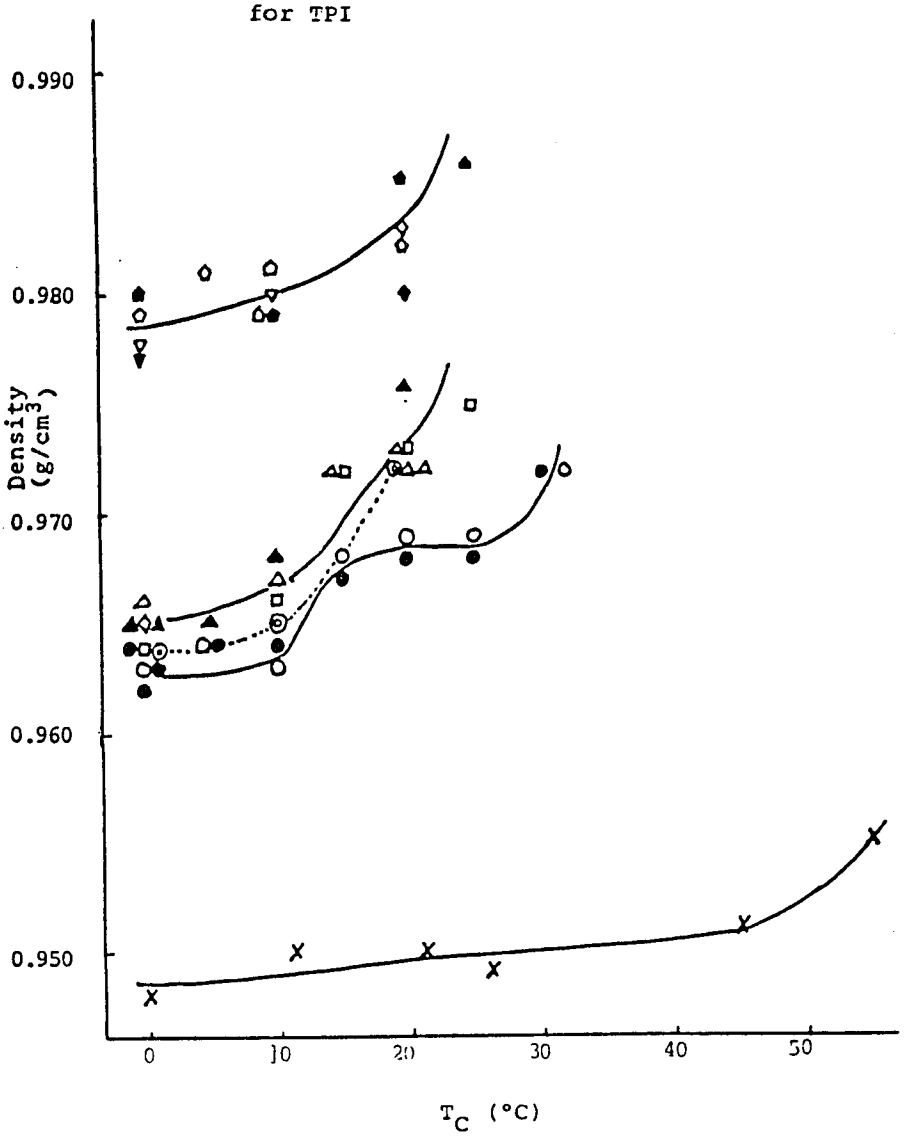

concentration: 1% (w/v) amyl acetate by direct crystallization (○) $\bar{M}_n$ = 2.5 x 10^5, (□) $\bar{M}_n$ = 1.0 x 10^5, (△) $\bar{M}_n$ = 2.4 x 10^4, (◇) $\bar{M}_n$ = 9.9 x 10^3, (▽) $\bar{M}_n$ = 4.9 x 10^3, (⬡) $\bar{M}_n$ = 4.7 x 10^3; precooling crystallization: (●) = 2.5 x 10^5, (▲) $\bar{M}_n$ = 2.4 x 10^4, (◆) $\bar{M}_n$ = 9.9 x 10^3, (⬟) $\bar{M}_n$ = 4.7 x 10^3
Concentration: 0.05% (w/v) amyl acetate by direct crystallization (⊙) $\bar{M}_n$ = 2.5 x 10^5
Melt Crystallization: (X): Nonfractionated Balata $\bar{M}_n$ = 1.4 x 10^5

Weight fraction crystallinities calculated from the density values obtained in this study are given in Table 10 for the preparations that yielded a crystalline portion completely in either the α or the β form. At the top of the table the crystal forms prepared are indicated. At the lower temperatures (0 and 10°C) direct crystallization yields β and the precooling technique gives α. It is to be noted that at any temperature used the samples in the β form show a significantly larger crystallinity than those in the α form.

Table 10. Weight Fraction Crystallinity of TPI Structures from Solution[a]

T_c - °C	32	30	0/30 slow[b]	0/30 fast[b]	25	20	0/20 slow	10	0/10 slow	5	0
$\bar{M}_n$ crystal method / crystal form	α	α	β	α	α	α	β	β or α	β	β or α	β or α
2.5×10^5											
direct	0.52	----	0.63	0.54	0.50	0.49	0.60	0.56(β)	0.58	0.56(β)	----
precooled	----	0.52	----	----	0.49	0.49	----	0.45(α)	----	0.46(α)	0.46(α)
1.0×10^5											
direct					0.54	0.52		0.54(β)			0.56(β)
2.4×10^4											
direct	0.52[c]					0.52		----			0.58(β)
precooled	----					0.55		0.49(α)		0.47(α)	0.47(α)
0.99×10^4											
direct	----	0.57[d]				0.60					
precooled	----	----				0.57					
0.49×10^4											
direct								0.70(β)			0.68(β)
0.47×10^4											
direct						0.59[c]		0.69(β)			0.69(β)
precooled					0.62	0.61		0.57(α)			0.57(α)

[a] 1% w/v amyl acetate except where noted

[b] slow and fast refer to heating rate from 0° to 30°C (see text)

[c] 3% w/v

[d] 8% w/v

2). Heat of Fusion Measurements:

Heats of fusion as obtained from DSC are shown in Table 11. Values were obtained for crystals of the high molecular weight fraction with $\bar{M}_n = 2.5 \times 10^5$ grown by the direct and precooling crystallization methods at 10°C in 1% (w/v) amyl acetate. If the heat of fusion at 100% crystallinity is chosen as 3070 $\pm$ 250 cal mol^{-1} (12.8 $\pm$ 1.1 KJ mol^{-1}) for the α form while the heat of fusion for the β form was found to be about one-half to three-fourths this value, i.e. 1540-2300 cal mol^{-1} (6.4-9.6 KJ mol^{-1}) reported by Mandelkern et al. (69), an apparent crystallinity can be obtained. These show a smaller value by about 10% than those from density measurement but the relative order is the same. If a reverse calculation of heat of fusion at 100% crystallinity from DSC and density results in Table 8 is carried out, the heat of fusion with 2690 cal mol^{-1} (11.3 KJ mol^{-1}) for the α form and 2050 cal mol^{-1} (8.3 KJ mol^{-1}) for the β form are obtained. The heats of fusion for annealed cup-shaped lamellar aggregates increase by increasing the annealing temperature (T_A) from 10 to 30°C; the melting endotherm value also increases with increasing T_A. These results are summarized in Table 9.

Table 11. Thermodynamic and Density Data of β and α-TPI Grown by Direct and Precooling Crystallization at T_C = 10°C

Crystallization Condition				DSC Measurement						Density Measurement		
T_D (°C)	T_P (°C)	T_R (°C)	T_C (°C)	Endotherm (°C)	T_M (°C)	Form	ΔH_f cal mol^{-1}	ΔS_f eu mol^{-1}	Crystallinity W_c % ‡	D g cm^{-3}	V^c %	W^c %
100	0	45	10	56	54	α	1233.3	3.77	40.2	0.964	42.1	45.9
100	-	-	10	50	48	β	1159.1	3.61	50.4	0.964	53.6	56.7

‡ 100% crystallinity is chosen as 3070 cal mol^{-1} for the α form and 2300 cal mol^{-1} for the β form

3. Epoxidation and Proton NMR Analyses:

The epoxidizing agent m-chloro perbenzoic acid (McPBA) has been found to react rapidly and quantitatively with double bond containing polymers. It has been used extensively for the determination of the total unsaturation in various types of polymers (70). Moreover, it has greater stability than perbenzoic acid in solution: The reaction occurring is

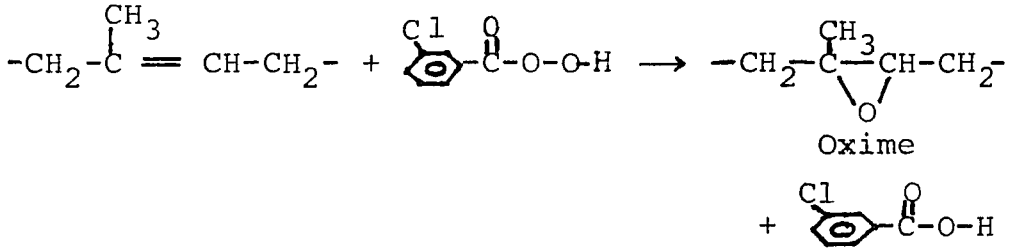

In our work, the epoxidation was to be carried out on solution crystallized samples suspended in the same liquid as the crystallization solvent which can dissolve McPBA and penetrate into the amorphous regions of the samples without affecting the crystalline portions. Generally low solvent polarity is preferable so as to minimize the effect on the epoxidation reaction. Epoxidation at low temperature is desirable to prevent side reactions. The solubility of TPI was tested in amyl acetate and found to be less than 1.0×10^{-3}g/ 100 ml at 0°C. This is considered low enough to be neglected in our epoxidation systems.

The 'H NMR spectrum of partly-epoxidized TPI crystals

as shown in Fig. 48 indicates that the signals are assignable to the protons of the unmodified monomer unit and the epoxidized unit produced in the reaction. The degree of epoxidation is obtained from the relative integral intensity of 'H NMR spectrum in the $CDCl_3$ solution by cutting out the spectral peaks and weighing. Peak assignments and symbols used are as follows:

S_I: Integral intensity of olefinic proton signal (δ = 5.14 ppm)

S_{II}: Integral intensity of epoxy methine proton signal (δ = 2.74 ppm)

The degree of epoxidation can be calculated from:

$$DE_1 = \frac{S_I}{S_I + S_{II}} \times 100$$

The chemical shift signal of the methyl protons in the neighborhood of the double bond has an overlap with the signal of the methylene protons in the neighborhood of epoxy group as has been explained by Tutorskii et al. (71) from studies on partly epoxidized polyisoprene and squalene. The remaining signals in a partly epoxidized trans-1, 4-polyisoprene are as follows:

S_{III}: Integral intensity of methylene proton signal in the neighborhood of a double bond (δ = 2.03 ppm)

S_{IV}: Total integral intensity of both the methyl proton signal in the neighborhood of the double bond and the methylene proton signal in the neighborhood of the epoxy group (δ = 1.62 ppm), and

S_V: Integral intensity of methyl proton signal in the neighborhood of the epoxy group (δ = 1.28 ppm)

Four kinds of calculation methods were considered to measure the integral intensity of the methyl proton signal and the methylene proton signal more exactly. Obviously, the integral intensity of methylene proton signal in the neighborhood of the double bond (δ = 2.03 ppm) is equal to four thirds of the integral intensity of the methyl proton signal in the neighborhood of the double bond (δ = 1.62 ppm). However, since the combination of S_{III}, S_{IV} and S_V integral intensities can be regarded as a total intensity of both methylene and methyl protons in the partly epoxidized samples, the intensity of methyl protons in the neighborhood of a double bond will be equal to three sevenths of the sum of S_{III}, S_{IV} and S_V. The degree of epoxidation can also be expressed by the following formulas:

$$DE_2 = \frac{S_V}{\frac{3}{4} S_{III} + S_V} \times 100$$

$$DE_3 = \frac{S_V}{\frac{3}{7} (S_{III} + S_{IV} + S_V)} \times 100$$

$$DE_4 = \frac{S_V}{S_{IV} - \frac{4}{3} S_V + S_V} \times 100 = \frac{S_V}{S_{IV} - \frac{1}{3} S_V} \times 100$$

$$DE_5 = \frac{S_{IV} - \frac{3}{4} S_{III}}{S_{IV} - \frac{3}{4} S_{IV} + S_{III}} \times 100 = \frac{S_{IV} - \frac{3}{4} S_{III}}{S_{IV} + \frac{1}{4} S_{III}} \times 100$$

All values obtained with the above equations show a precision within $\pm$ 2%. Mainly, the methine proton signal was used to calculate the degree of epoxidation in this work.

Fig. 48. ^{1}H NMR Spectra of TPI and Epoxidized TPI in $CDCl_3$

A. Before epoxidation—fractionated Gutta Percha with $\overline{M}_n = 2.5 \times 10^5$

B. Partly epoxidized TIP—Crystals were grown from 1% (w/v) amyl acetate with $\overline{M}_n = 2.5 \times 10^5$, $T_D = 100$ and $T_C = 21°C$ epoxidation condition: $[McPBA]_{t=0} = 1.02$ g/100ml, $T_E = 0°C$, $t_e = 21$ days, $\overline{DE} = 55.4\%$

C. Completely epoxidized TPI—Crystals were grown from 1% (w/v) amyl acetate with $\overline{M}_n = 2.5 \times 10^5$, $T_D = 100$ and $T_C = 0°C$ epoxidation condition: the same as (B), $\overline{DE} = 100\%$

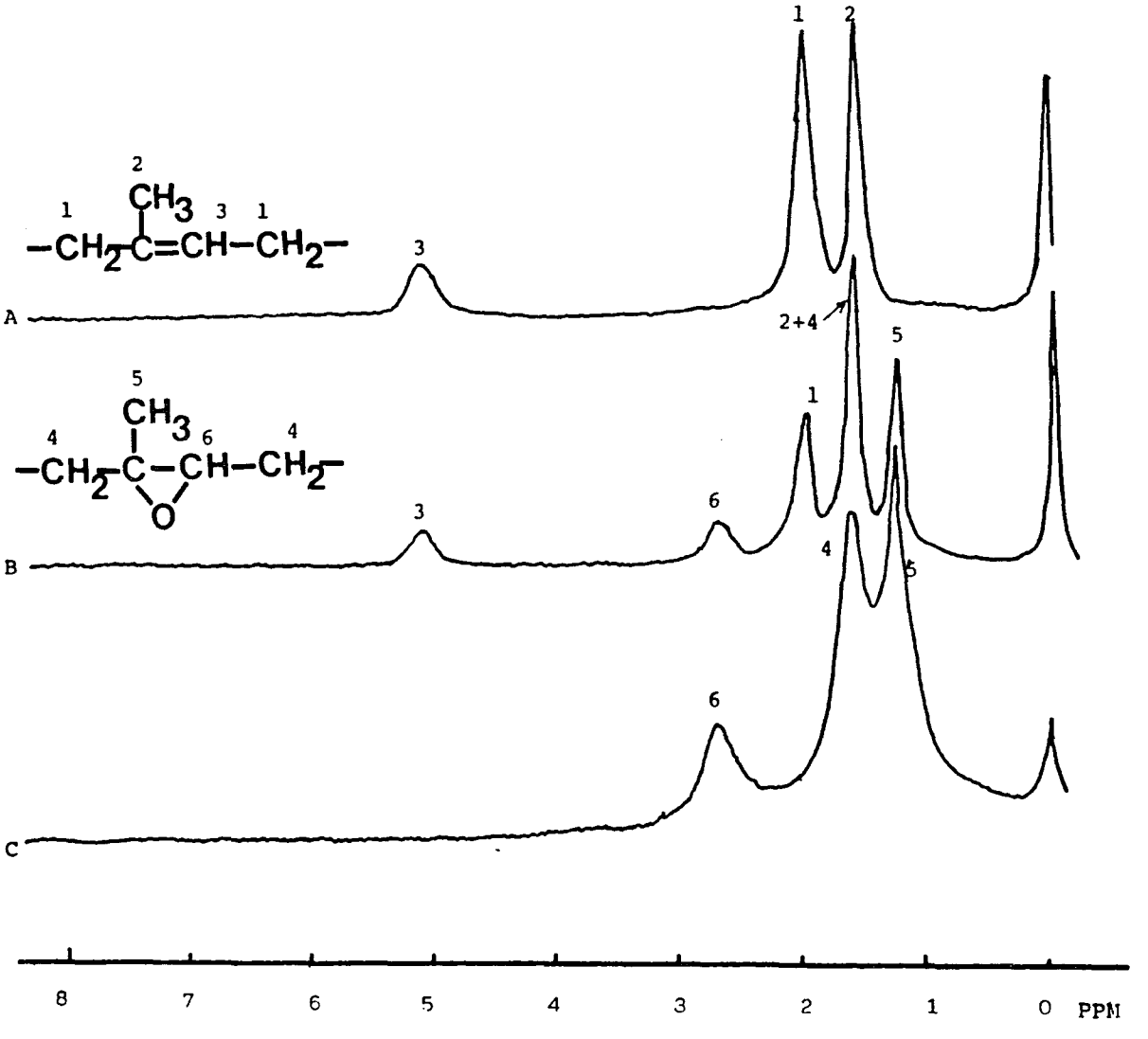
1
2
2
CH3
1
3
1
–CH2–C=CH–CH2–
3
A
2+4
5
5
CH3
1
4
6
4
–CH2–C–CH–CH2–
O
3
6
B
4
5
6
C
8
7
6
5
4
3
2
1
0
PPM

In the first experiments epoxidation of a particular Type-IV TPI hedrites was run at different concentrations of MCPBA as shown in Fig. 49. These results indicate that the degree of epoxidation (DE) is dependent on the concentration of MCPBA used. The time to reach equilibrium is also dependent on the concentration of MCPBA. In both cases shown in Fig. 49, a rapid initial epoxidation is followed by a slower epoxidation step apparently linear with time. At low concentration, [MCPBA] = 0.203 g/100 ml, the double bonds epoxidized reach a constant value after 60 hours (curve A). A longer time is necessary to reach equilibrium at higher concentration, [MCPBA] = 2.032 g/100 ml (curve B). The increase in available double bonds with concentration of epoxidizing agent observed could be due to either penetration of additional amorphous regions or reaction of double bonds in the crystalline regions. A limiting value for the amount of reaction is always reached with time at constant concentration of MCPBA with MCPBA still present. Recently, Woodward and coworkers (30)-(34) in the investigation of the noncrystalline component at the surfaces of solution grown trans-1,4-polybutadiene single crystals by the epoxidation method found that the total number of double bonds available for epoxidation increases with reaction temperature and that the total noncrystalline fraction, as calculated from density measurement, is larger than the fraction available

for epoxidation on the crystal surface at the epoxidation temperature, 6°C. However, for crystals of TPI with $\bar{M}_n = 2.5 \times 10^5$, $T_C = 21°C$, $[MCPBA]_{t=0} = 0.105$ g/100ml, $T_E = 0°C$ and $t_e = 22$ days in amyl acetate, the degree of epoxidation for both single crystals and hedrites (Type-IV) indicates a higher value, as shown in Table 12, than the noncrystalline fraction from density measurement.

Fig. 49. Degree of Epoxidation vs. Expoxidation Time for TPI Grown from 1% (w/v) Amyl Acetate, $T_D = 100$, $T_C = 20°C$, and $\bar{M}_n = 1.3 \times 10^5$

(O): $[MCPBA]_{t=0} = 0.203$ g/100ml, $T_E = 0°C$

(X): $[MCPBA]_{t=0} = 2.032$ g/100ml, $T_E = 0°C$

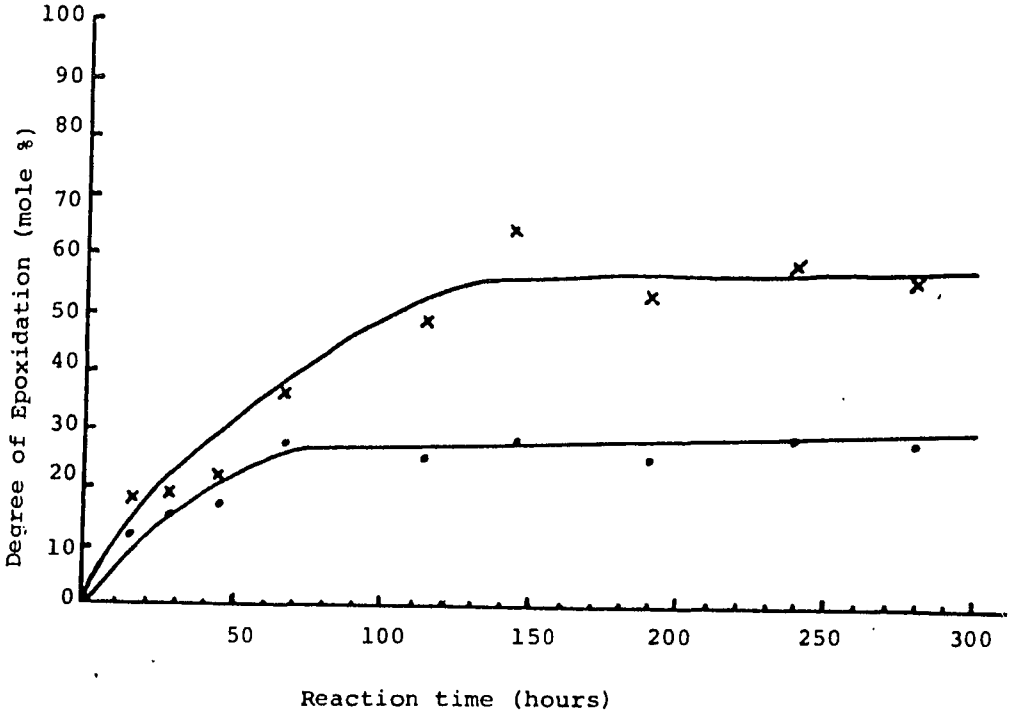

Table 12. Noncrystalline Content from Density and Degree of Epoxidation Measurement for HMW Fraction TPI Crystals Grown from 1% (w/v) Amyl Acetate with $\bar{M}_n = 2.5 \times 10^5$

Crystallization Condition								
T_D (°C)	T_P (°C)	T_R (°C)	T_C (°C)	Morphology	Density	W_c	$1-W_c$	Degree of Epoxidation (mole %)
100	-	-	21	hedrites (Type-IV)	0.968	0.49	0.51	55.4
100	0	44	21	Single crystals	0.968	0.49	0.51	57.8

Three other TPI fractions with number average molecular weights from 9.7×10^4 to 2.5×10^5 crystallized from 1% (w/v) amyl acetate at 20-21°C were epoxidized to various times at various m-chloroperbenzoic acid concentrations. The degree of epoxidation taking place is given in Table 13.

For the epoxidation of the fraction with $\bar{M}_n = 9.7 \times 10^4$ shown in Table 13, the concentration of MCPBA in the range of 1.015 to 2.032 g/100ml, shows a little change in the non-crystalline fraction available for epoxidation at the crystal surface. Surprisingly, single crystals show higher available double bonds for epoxidation than any hedrite structures.

For the multilayered TPI crystals grown from solution, the morphology of epoxidized crystals did not show any change under the optical microscope. Turning to a study of surface damage of epoxidized single crystals by electron microscopy, in Fig. 50, the TPI single crystals remain the same size as before the epoxidation. Some damage, involving less than 10% of the surface available was found in the epoxidized single crystal surface with 53.6% epoxidized double bonds, the wide angle X-ray diffraction patterns indicate that the same crystal structure prevails as before the epoxidation. This evidence suggests that the reaction of double bonds takes place mainly on the crystal surface.

Table 13. Epoxidation Data

Crystallization Concentration: 1% (w/v) Amyl Acetate

Epoxidation Temperature: 0°C in Amyl Acetate

Amount of MCPBA: Moles MCPBA/Moles Double Bonds > 0.80

		Crystallization				Epoxidation		
$\bar{M}n$	$\frac{\bar{M}w}{\bar{M}n}$	T_P (°C)	T_R (°C)	T_C (°C)	Morphology	[MCPBA] g/100 ml	Time (days)	Degree of Epoxidation Mole %
		-	-	21	Hedrite-Type II	2.032	10	40.9
		-	-	21	=	2.032	21	51.3
		-	-	21	=	1.624	10	42.0
		-	-	21	=	1.624	21	45.7
9.7×10^4	1.58	-	-	21	=	1.015	10	42.2
		-	-	21	=	1.015	21	46.8
		-	-	21	=	0.609	10	30.5
		-	-	21	=	0.203	10	21.8
		-	-	21	=	0.203	16	22.3
		0	44	21	Single Crystal	1.015	10	53.6
		0	44	21	=	0.203	10	35.5
		-	-	20	Hedrite-Type II	0.203	8	26.0
		-	-	20	=	2.032	8	53.3
1.3×10^5	1.53	-	-	20	=	0.203	10	28.6
		-	-	20	=	2.032	10	58.5
		-	-	20	=	0.203	12	28.2
		-	-	20	=	2.032	12	56.8
		-	-	21	Hedrite-Type IV	1.015	22	55.4
2.5×10^5	1.34	0	44	21	Single Crystal	1.015	22	57.8
		-	-	20	Hedrite-Type IV	1.015	21	56.3
		-	-	20	=	0.102	28	44.6

Fig. 50. Electron Micrographs of TPI Single Crystals Before and After Epoxidation

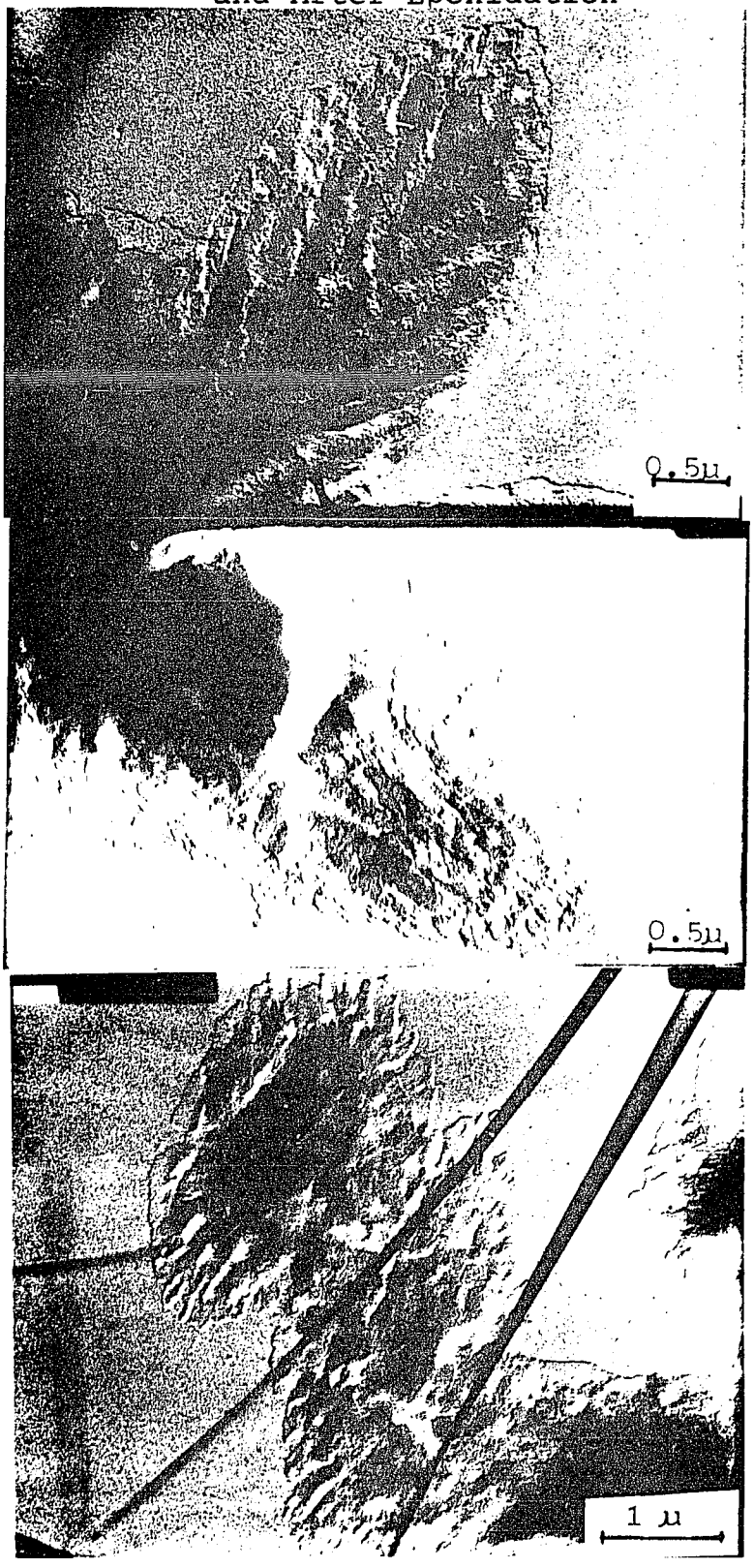

Crystallization Condition:

1% (w/v) Amyl Acetate with $\bar{M}_n = 9.7 \times 10^4$ at $T_D = 100$, $T_P = 0$, $T_R = 44$ and $T_C = 20°C$

A. Before Epoxidation

B. After Epoxidation for Five Days $[MCPBA]_{t=0}$ = 1.015 g/100ml

C. After Epoxidation for Ten Days $[MCPBA]_{t=0}$ = 1.015 g/100ml

The epoxidation reaction had been also tried for TPI structures grown by melt crystallization, however, the spherulites are apparently attacked by amyl acetate at 0°C, as observable in Fig. 51, indicating that melt grown crystals are not suitable for this reaction.

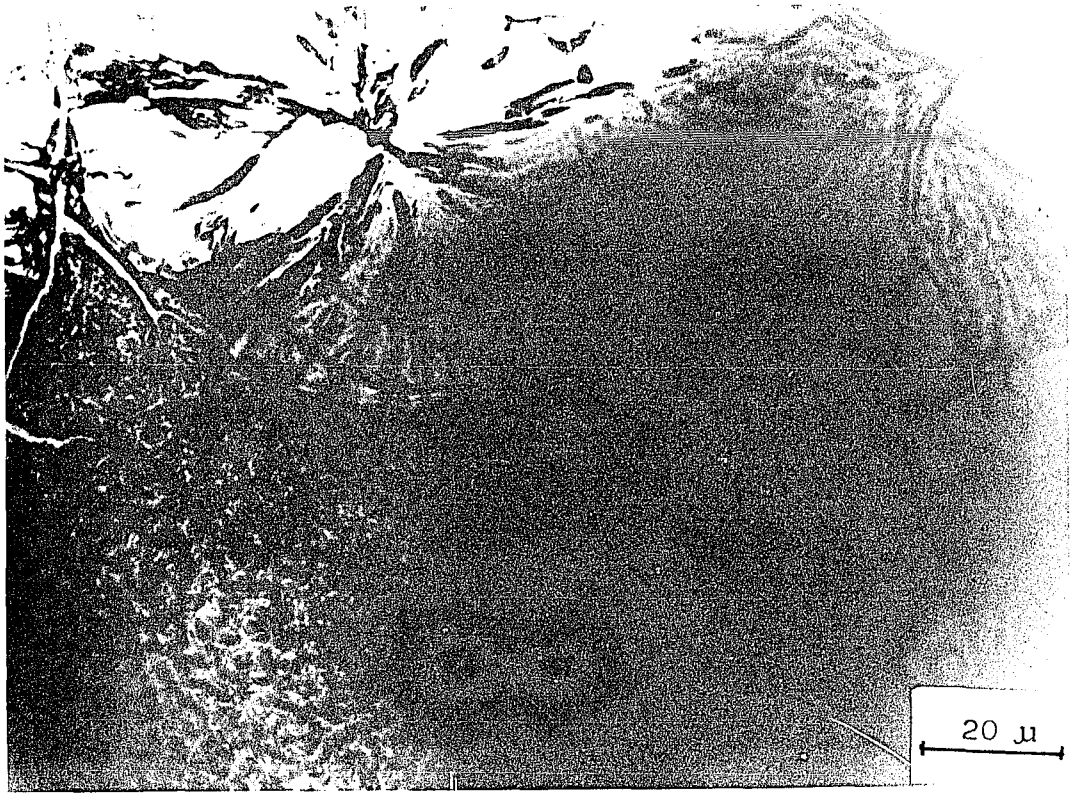

Fig. 51. Erosive Action of Amyl Acetate at 0°C on TPI Spherulites Grown from the Melt

IV. DISCUSSION

The morphologies of multilayer crystals:

High polymers are known to exhibit several different types of crystalline morphology. For solution grown polyethylene crystals, monolayered pyramid-shaped single crystals are typically predominant at low undercooling from dilute solution (2) but multilayered dendrites (72) or axialites (17) are formed at higher undercooling from concentrated solution. In conventional lamellar crystals, spiral terraces associated with a screw dislocation consist of continuous platelets situated at or near the center of the basal layer. There are further influences responsible for shaping the three-dimensional habits. Examination, even of comparatively simple multilayered aggregates grown from solution reveals a splaying apart of lamellar packets, which strongly resemble immature open spherulites grown from the melt (73). The origin of splaying itself is uncertain. An early and plausible suggestion is that this results from forces due to compression of cilia, i.e. those portions of otherwise crystallized molecules which remain outside lamellae and protrude from fold surfaces, e.g. chain-ends or long, loose loops. It is noteworthy that splaying of lamellar pockets in solution grown crystals leads to branched morphologies very similar to those found in melt grown systems. There the discussion

has been in terms of the relative probabilities of nucleating daughter fibrils at small but finite angles to the parents (28). Neither point of view excludes the other, but no systematic study of branching and its contributory factors appears to have been made. Splaying of solution grown lamellae is visible optically, but individual lamellae are only about 10 nm thick; therefore it follows that the mutually splaying entities must comprise groups or packets of lamellae. The obvious way to bring this about is to incorporate cilia from one lamella into its neighbors This has long been anticipated and would give rise to tie molecules, i.e. interlamellar links bridging fold surfaces and being crystallized in neighboring lamellae.

From the morphological point of view, there are only a few references concerning the relation with molecular weight of polymers (13)-(16), (74)-(77). Recently, from small angle light scattering studies it has been found that different morphologies can be developed in molecular weight fractions of linear polyethylene (74) and polyethylene oxide (16) grown from the melt. Spherulitic structures were not universally observed when a wide range in molecular weights were studied under different crystallization conditions (both by isothermal growth and under quenching conditions). Spherically symmetric birefringent structures, displaying a dark Maltese Cross when viewed under crossed

polarizers can be prepared. Depending on crystallization conditions and molecular constitution they can develop varying degrees of perfection and display typical four-fold symmetric Hv small angle light scattering patterns (74), the simplest hedrites are characterized by extinguished birefringence when viewed parallel to the basal plane. The small-angle light scattering pattern shows very little azimuthal dependence to the Hv. Intermediate states shows a gradual disappearance of the Maltese Cross. The morphological similarity between the polyethylene and the polyethylene oxide grown from the melt are summarized in Table 14.

Table 14. Comparison Between Supermolecular Structure of Polyethylene and Poly(ethylene oxide)

	Polyethylene[a]	Poly (ethylene oxide)[b]
Extreme quench and/or high molecular weight	Random	Random
Mild quench, $\Delta T > 25°$ for intermediate to high molecular weight	Spherulite	Spherulite
$\Delta T \simeq 20°C$ (isothermal) for intermediate molecular weight	Short rods	Hedrite (Intermediate state)
Small ΔT and/or low molecular weight	Long rods	Hedrite (No birefringence in flat-on view)

[a]Morphological designation according to refs (15, 74)

[b]Morphological designation according to refs (16, 75)

Both polymers show spherulitic structures whose degree of perfection vary systematically depending on molecular weight and crystallization temperature although these show some difference from solution grown crystals of these polymers. The range of dendritic and polyhedral lamellar growth of linear polyethylene has been explored for 0.1% O-xylene solution as a function of molecular weight and crystallization temperature by Wunderlich et al. (76). At increasingly lower temperature all intermediate stages from polyhedral lamellae to highly dendritic structures were observed. Rybnikar (77) reported that the unfractionated branched polyethylene crystallized at 50°C from a 0.05% (w/v) amyl acetate solution, formed leaf-like lamellae and globular structures in an approximately equal ratio. Using this solvent, molecular weight fractions with molecular weights of 1×10^4, 5.3×10^4 and 16.8×10^4 were crystallized at the same conditions; the low molecular weight fraction tended to crystallize in leaf-like lamellae whereas the high molecular fraction had the globular structures only. Besides, depending on the solvent power, a large variety of morphologies may be prepared.

It was demonstrated in this work that the morphology of TPI structures grown directly from solution depends on the crystallization temperature T_C, the TPI molecular weight and the solvent. Three structural types were observed:

hedrites--at all T_C's dependent on $\bar{M}_n$, spherulites--at medium and low T_C and medium $\bar{M}_n$, and aggregates of curved lamellae--at low T_C and medium $\bar{M}_n$. However, the morphological changes are continuous with respect to $\bar{M}_n$ and T_C.

The Type II, III and IV hedrites of TPI become larger and more crystagraphically perfect as the crystallization temperature decreases and/or the molecular weight increases for isothermal crystallization. As the temperature is decreased, the polymer solubility decreases and the crystallization rate increases. Both of these, but particularly the latter, would lead to the observed increase in hedrite size with decreasing temperature assuming little increase in nucleation rate. When T_C is 0°C or lower, nonisothermal crystallization occurs for all molecular weights studied leading to two sizes of crystals and double melting endotherms. Concerning the differences in birefringence observed in this work, an extinction cross (or double cross) was exhibited by some of the larger hedrite structures with an apparently larger polymer segment density; the structures giving these patterns are not spherically symmetrical.

Relatively thick elliptical and elongated hexagonal shaped crystal structures with the $_\alpha$ form have been previously grown either by slow diffusion of solvent or by cooling a supersaturated solution using Chicle Gutta, a

natural TPI with low molecular weight (1.6-1.8 x 10^4) (58). Similar crystals with β form had also been found from melt crystallization using unfractionated Gutta Percha (51); the birefringence of these structures changes from no extinction to complete extinction upon rotation of the crystals. When the longer axis of these elliptical crystals was at 45° to the direction of the polarizer or analyzer, maximum transmission of light was observed. When the same field of view was rotated through 45° with the longer axis of the elliptical crystal in the direction of the polarizer and analyzer, complete extinction of the birefringence of the crystal was observed. However, in the present work, changes in extinction upon rotation without complete extinction taking place were observed. The elliptical structures obtained in the present work splay out, at least when in contact with the crystallizing liquid, and the thinner center portion shows extinction when viewed flat on at all orientations.

The cup-shaped lamellar aggregate morphology, grown under nonisothermal conditions at low T_c and medium molecular weights differs apparently from the hedrite morphology (a precursor of a spherulite) or the spherulite structure found at the same temperatures for lower molecular weight fractions. From the knowledge of crystallization kinetics, spherulite or hedrite growth is nucleated at

the center followed by sufficient radiating growth and branching to occupy the outwardly increasing volume. At the onset of crystallization, cup-shaped lamellae appear in the optical microscope followed by growth of other such lamellae about the initial one. Some evidence of lamellar strips connecting the cup-shaped lamellae was found for $O_s O_4$ fixed aggregates in the optical micrograph (Fig. 22-C). Probably, the increased curvature in these aggregates and the undercooling prohibit the unlimited lamellar growth; in addition, other lamellae can not pack on the top of the first lamella which is one mechanism for development of multilayer crystals as shown in Fig. 3.

The formation of single and of aggregate cup-shaped lamellae has been cited previously for unfractionated poly (4-methyl-pentene-1), (62, 63) polyoxymethylene (64) and polychlorotrifluoroethylene (65) crystallized at relatively large supercoolings. For unfractionated P4MPI with $\bar{M}_n$ of 2.5×10^5 the morphology was found to change from square to curved as the supercooling increases. The model put forth to explain the increase in curvature of poly (4-methyl-pentene-1) crystals with increased supercooling contained the combined influence of two factors; these are a fold domain buckling due to chain fold bulkiness and the lateral size of fold domains in the multisectored lamellae formed (63). In the present work using trans-1,

4-polyisoprene the change is from (ribbonlike) multilamellar structures to connected cup-shaped lamellae; this is molecular weight dependent.

Influence of crystallization technique and conditions

A special problem arises in the crystallization of TPI by the precooling method. This polymer has been found to crystallize in two crystal forms from the melt (48, 49) or solution (55, 57). The α form is the stable one but only β form crystallizes at low temperatures. In addition, thermodynamic studies have revealed that the β form is metastable. It converts into the α form by a process of fusion and crystallization (61, 78). Heating the final crystallization aggregates with the β form from 1% (w/v) amyl acetate solution at T_P = 0°C to the redissolution temperature (T_R) slowly and then crystallizing at T_C of 0-25°C, yields overgrown single crystals. Obviously, the nuclei necessary to bring about crystallization have been transformed from the β to the α form in the heating procedure. We suggest that there are two possible ways that α-nuclei can form while the temperature is increased to T_R. The first possibility is that α-nuclei are produced by renucleation and recrystallization of dissolved material in the solution, the second possibility is that there is a crystal-crystal transition in the amyl acetate-swelled

β crystal with the α-nuclei being produced directly from the β crystal. Although no crystal-crystal transition was observed in β crystals grown from melt (61, 78). Leeper and Schlesinger (79) found that a liquid mixture of two volumes of ethyl acetate and one volume of benzene had converted β to α in 72 hours at 25°C due to swelling. Apparently the entry of solvent molecules into the crystalline structure of TPI will lower the energy requirement for the β to α transition.

Evidence for both mechanisms given above is found upon annealing cup-shaped lamellar aggregates crystallized from 1% (w/v) amyl acetate at 0°C. Early observation of faster annealing of polyethylene single crystals immersed in relatively poor solvents (ethylene glycol) or in the presence of even a small amount of good solvent (tetrachloroethylene) was reported by Statton (80) and Geil (81) respectively. More details of the annealing in contact with solvent were generated by studying the dissolution process. Basset and Keller (82) and Holland (83) showed by electron microscopy of solution-grown polyethylene single crystals (from 0.01 Wt% in xylene) dispersed in fresh solvent, that on slow heating, partial dissolution occurs somewhat above the crystallization temperature, this is followed by recrystallization in the form of a border around the original crystal and in the formation of new crystals of the same thickness as the border. Dendrites also showed similar partial

dissolution above their crystallization temperature, which was followed by recrystallization (84). Recently, Magill et al. gave new evidence on the lamellar thickening of polyethylene (85) and nylon-6.6 (86) single crystals due to solution annealing. The lamellar thickness from small angle X-ray scattering measurement was a function of annealing temperature in xylene with corresponding changes in melting temperature and heat of fusion for polyethylene single crystals grown at 70°C. In the course of crystallizing nylon-6,6 from solution, the lamellar thickness versus crystallization temperature curve joined up smoothly and with considerable overlap with the lamellar thickness versus annealing temperature.

When annealing is carried out in the presence of a solvent, there is a swelling of the amorphous layers. The swelling of the surface will remove interlamellar stresses and stresses in the surface layer itself may also be removed. As long as the solvent cannot enter the crystal, the chain diffusion process necessary for thickening the lamellae should be effected only through greater mobility in the folds. The retention of the cup-shaped morphology and of the β structure in TPI that usually takes place upon slow heating in the crystallization liquid is caused by recrystallization to form thicker, more thermodynamically stable, crystals with higher melting points (Fig. 39 and Fig. 40 curve (d)). If the annealing temperature

is high enough (T_A = 35°C) a solid state β to α transition occurs in part of structure while in other parts melting of the β form and recrystallization of the α form take place. Therefore, the survivors of the aggregates (Fig. 41-A) now with α form are due to a crystal-crystal transition in the amyl acetate and the formation of new overgrown single crystals (Fig. 41-B) with α form are due to the recrystallization of dissolved material in solution at 35°C. It appears evident that the crystal-crystal transition temperature ($T_{crys-crys}$) in amyl acetate at a heating rate of 0.2-0.3°C/min for $\bar{M}_n = 2.5 \times 10^5$ occurs between 30 and 35°C. However, the heating rate is an important factor in determining the apparent $T_{crys-crys}$, the transition occurs below 30°C when rapid heating to the annealing temperature is carried out (Fig. 40 curve (d)). Therefore, increasing of both the melting endotherm and crystallinity value with increasing annealing temperature is due to increasing the lamellar thickness of the cup-shaped lamellar aggregates.

Using the direct crystallization technique to grow multilayer crystals, the initial dissolution temperature (T_D) is not important (87) if the sample is dissolved completely. The TPI fraction with $\bar{M}_n = 2.5 \times 10^5$ was crystallized with T_D = 80, 90 or 100°C and with T_C = 20°C in 1% (w/v) amyl acetate solution, the same Type-IV hedrites were formed. When single crystals are grown by the pre-

cooling method, the initial precipitation temperature (T_P) is also not important as far as the morphology is concerned. Whether the fraction was precipitated at T_P = -78, 0 or 20°C with T_C = 20°C, the single crystals formed had the same shape under the microscope and the same melting endotherm from DSC measurement. When precipitation was carried out at 0° and 20°C with T_C = 30°C, the single crystals appearing at the higher T_P had a larger size (Fig. 28-B). However, with precipitation at -78 and at 0°C with T_C = 0°C, single crystals with the same endotherm (58°C) and the same morphology but with a small difference in density (see Table 8) are formed.

In the precooling crystallization method the redissolution temperature (T_R) is an important factor, because the number of nuclei is mainly controlled by this temperature. Generally, in this work, T_R was at the clearing temperature of the suspension or 1-2 degrees higher. Blundell, Keller and Kovacs (88) indicated that the overall rate of crystallization for 1% (w/v) polyethylene xylene solution is strongly dependent on the redissolution temperature T_R in the condition of T_D = 120°C, T_P = 75°C, T_R = 98 to 120°C and $T_C < 98$°C, the rate decreased with increasing T_R up to a limiting redissolution temperature (T_{LR}) beyond which it remained constant. This reveals that a crystallization memory persists up to T_{LR}. Accordingly, there must

be centers surviving which hasten the subsequent crystallization. If T_R is higher than T_{LR}, no original nuclei survive. Nucleation therefore occurs as the solution is cooled to T_C or it occurs at T_C and this usually leads to multilayered crystals. However, single crystals can only be observed at $T_R \leq T_{LR}$. The number of nuclei is also dependent on the rate of heating to T_R after an initial crystallization at T_P. Normally, the number of nuclei per gram of polymer increases with decreasing heating rate. For experiments 3 and 5 in Table 5, the TPI aggregates with cup-shaped lamellae were dissolved completely due to the rapid heating rate to T_R with no nuclei surviving. This indicates that the limiting redissolution temperature (T_{LR}) decreases upon increasing the heating rate.

Keller and Willmouth (89) found that the high molecular weight fraction of polyethylene was particularly active in self-nucleation. The temperature which gave for the indicated molecular weight fractions of polyethylene ($\bar{M}_w/\bar{M}_n$ = 1.1) the same number of nuclei (2.4×10^{12} g^{-1}) in xylene were

$\bar{M}_n$	T_R (°C)
2.6×10^6	105.5
2.4×10^5	102
7.6×10^4	98.5
6.8×10^3	95

Addition of an increasing amount of a polymer with a high molecular weight to the solution increases linearly the number of nuclei. A similar molecular weight effect on the redissolution temperature were also found in this work. The clearing temperature of aggregates initially crystallized at 0°C at a heating rate of 0.2°C/min decreased from 45 to 35 $\pm$ 0.5°C when the molecular weight was decreased from $\bar{M}_n = 2.5 \times 10^5$ to 4.7×10^3. The clearing temperature also decreases with decreasing concentration of polymer.

Crystal form determination:

Wide angle X-ray diffraction is a simple method to identify the pure crystal form (α or β) from the diffraction pattern, although it is somewhat difficult to identify the preparation with an α and β mixture. Differential scanning calorimetry is a supplementary method using the values of the melting endotherms. Lovering and Wooden (78, 90) reported melting endotherms for fractionated TPI crystallized from the melt. Their results indicate that the β form melts between 45 and 53°C and the α form is above 57°C. Within experimental error, melting endotherms were found to be independent of molecular weight above a number average molecular weight of 3.3×10^4.

In this work, the crystallization of TPI from 1% (w/v)

amyl acetate solution by the precooling technique with T_C in the 0-25°C range leads exclusively to the formation of the α form, whereas the β form appears at low T_C and α form at higher T_C when the direct crystallization technique is employed. The molecular weight does not have a big influence on the crystal form while growing the crystals in amyl acetate. However, with heptane as solvent an apparent molecular weight effect was found (see Table 4). Crystallization from heptane solution at 0°C is noniso-thermal, probably the formation of nuclei for the high molecular weight fraction starts early, i.e. nucleation begins at a higher temperature than T_C, with formation of the α form for the reason of a faster crystallization rate and lower solubility.

Density and Crystallinity:

The density of TPI crystals increases with increasing crystallization temperature using either the precooling or direct crystallization methods. Assuming that these TPI crystals are composed of chain folding lamellae with crystalline and amorphous noncrystalline phases, the in-creasing in density is caused mainly by the decrease in the amount of surface area (noncrystalline phase) in a crystal due to the following: 1) larger lamellar thickness 2) fewer and/or shorter chain ends 3) tighter and/or more

adjacent folds 4) fewer intralamellar defects and 5) shorter or fewer interlamellar links. If the intralamellar defect is negligibly small and the subunit cell density does not vary significantly, the noncrystalline component is expected to consist of chain folds, chain ends and interlamellar links.

DSC measurements show that the higher the T_c the higher the melting endotherms with the same crystal form, indicating an increase in the lamellar thickness. The crystallinity calculated from density measurement (Table 10) shows little, if any change with a change in TPI morphology from hedrites (direct crystallization) to single but overgrown lamellae (precooled preparations) at constant molecular weight and crystallization temperature. This suggests that any interlamellar links present in the multilamellar structures contain about the same average number of monomer units as found in a fold.

It was found in this study that spherulites, Type-III hedrites and cup-shaped lamellar aggregates in the β form have a significantly higher crystallinity than hedrites or overgrown lamellae in the α form when the same final (crystallization or annealing) temperature is used. The difference as shown in Table 10 is found to be about 20% and suggests that the lamellar thickness for crystals in the β form is larger than those in the α form. The

measured thickness for β lamellae (L_β) grown from the melt using nonfractionated TPI were reported by Davies and Long (53) as larger than those for α-form lameallae (L_α) grown at the same T_C; at a T_C of 50°C $(L_\beta - L_\alpha)/L_\beta$ for melt crystallized TPI is about 20%, in agreement with the density difference cited above for solution grown crystals.

An increase in crystallinity of about 20 to 30% is found with decreasing molecular weight below about 10^5 down to 5000 for both the α and β forms. An increase in crystallinity with decreasing molecular weight down to about $\bar{M}_n = 10^4$ was reported for polyethylene (91, 92) and for various polyalkylene oxides (93-96) crystallized from the melt. For example, Maclaine and Booth (93) reported about a 50% increase in crystallinity for melt crystallized poly (ethylene oxide) fractions ranging in molecular weight from 2×10^4 to 1.6×10^6. Also Hamada and Wunderlich et al. (97) indicate that the crystallinity increases about 10% for polyethylene single crystals grown from 0.1% (w/v) p-xylene at 85°C while decreasing molecular weight from 5×10^5 to 10^4. However, at molecular weights below 10^4 a decrease in crystallinity occurs for a number of these polymers, including polyethylene (91, 92) poly (ethylene oxide) (94) and poly (hexamethylene oxide) (95). Also a decrease in crystallinity with decreasing molecular weight in the 5×10^3-3×10^4 range was reported for solution grown trans-1.4-polybutadiene single crystals (44, 45).

In this work, at T_C = 20-21°C a linear increase in crystallinity of about 20% is found with decreasing molecular weight $\bar{M}_n$ from 2.5 x 10^5 to 10^4. Lowering the concentration from 1% (w/v) to 0.05% (w/v) amyl acetate solution also shows an increase in density but the effect on the crystallinity is a small one. The near constancy of the crystalline fraction for structures in either the α or β form at 0°C for $\bar{M}_n$'s between 2.5 x 10^5 and 2.4 x 10^4 is apparently a consequence of the non-isothermal crystallization conditions.

A comparison can be made with the densities of nonfractionated but purified Balata (Natural TPI) grown by first melting at 100°C for one hour and then crystallizing at T_C for two weeks. The density measurement on these melt grown samples shows agreement with the result for Gutta Percha crystallized from the melt as reported by Cooper and Vaugham (61). However, the low weight crystallinity for samples from the melt (about 43% for β form and 39% for α form) indicates either a different crystallization mechanism, the high effect of chain entanglement in the viscous state or the presence of other factors still unknown.

The Calculation of the Average Number of Monomer Units in a Noncrystalline Chain Sequence:

The noncrystalline component is expected to consist of

chain folds, chain ends, interlamellar links and interlamellar defects. Assuming intralamellar defects to be negligibly small, the noncrystalline fraction is given by (44)

$$F_S = (UF + C)/\bar{N}_n \tag{1}$$

where U is the average number of monomer units per fold and interlamellar traverse combined, F is the number of folds and interlamellar traverses per chain with a number average DP of $\bar{N}_n$, and C is the average number of monomer units in the two chain ends. The crystalline fraction $1-F_S$, is related to the above parameters and to the crystalline stem length, L_C, by:

$$1-F_S = (L_C/R\bar{N}_n)(F + 1) \tag{2}$$

where R is the crystallographic repeat distance in the chain direction. Equations 1 and 2 can be combined to eliminate F, giving:

$$1-F_S = (L_C/R)(1 + (U-C)/\bar{N}_n)/(U + L_C/R) \tag{3}$$

At large $\bar{N}_n$, $(U-C)\bar{N}_n$ will be much smaller than 1 and the crystalline fraction $1-F_S$, will be independent of $\bar{N}_n$ and will be constant with changing $\bar{N}_n$ if L_C and U remain constant. At low $\bar{N}_n$, $1-F_S$ will change with a change in $\bar{N}_n$ and the direction of this will depend on the relative values of C and U. If C is greater than U, then $1-F_S$ decreases as $\bar{N}_n$ decreases

(at constant U and L_C/R), as was found for trans-1, 4-polybutadiene lamellae. (44) The observed increase in crystallinity, W_C, with decreasing molecular weight for α-TPI at T_C's of 10 to 30°C suggests that the average length of the noncrystallizing chain-ends, C/2, is small with respect to U/2. As discussed below the U-values for α-TPI structures prepared in this work range from nine to thirteen. Therefore the maximum molecular weight at which a change in crystallinity should occur with changing $\bar{M}_n$, with the crystallinity expressed to two significant figures, is about 9×10^4. However the results in Table 10 show a decrease in crystallinity as $\bar{M}_n$ increases up to 2.5×10^5 at T_C's of 20° and 25°C, suggesting that a change in U and also L_C/R is taking place at larger molecular weights. It was reported earlier (57) that α-TPI lamella grown from dilute amyl acetate solution using the precooling method show no constant change in crystallinity with molecular weight in the 3.8×10^5 to 6.9×10^4 range.

In order to analyze the crystallinity results in a more quantitative manner, U values are calculated for the structures with $\bar{M}_n$'s of 1.0×10^5 and above using the following expression, obtained from equation 3 when $\bar{N}_n$ is large: (44)

$$U = L_C/R \; [F_S/(1-F_S)] \qquad (4)$$

The $1-F_S$ values are taken as equal to the crystalline fraction as obtained from density. A value for the parameter L_C is also needed for this calculation; this is obtained from the lamellar thickness, L, measured by electron microscopy for dilute solution grown TPI lamellae. (50) Bassett and Keller (98) indicated that the low-angle X-ray diffraction spacing were independent of concentration and molecular weight for polyethylene crystal preparations from the same solvent at the same T_C although the crystal morphologies were not. Therefore the lamellar thickness of TPI single crystals grown from dilute (0.05% w/v) amyl acetate solution may be used here, using the relationship:

$$L_C = W_C \rho_A L / (W_C \rho_A + (1-W_C) \rho_C) \qquad (5)$$

Values of U and L_C obtained for α-TPI at T_C's of 10 to 30°C are given in Table 15. The U values are found to increase with increasing T_C, as reported earlier for dilute solution grown α-TPI lamellae. (57) A small increase in U with decreasing molecular weight, as suggested above, is also observed. To demonstrate that the variation of the crystallinity with molecular weight below $\bar{M}_n$ of 10^5 is principally due to replacement of chain folds by chain ends, equation 3 was used to calculate the crystallinity assuming U and L_C/R are constant and C is zero. The U and L_C values used were

those found at $\bar{M}_n$ of 1 x 10^5 for samples prepared at crystallization temperatures of 20 and 25°C (see Table 15) and at $\bar{M}_n$ of 2.4 x 10^4 for T_C = 10°C due to the lack of a value at $\bar{M}_n$ of 1 x 10^5. In Fig. 52 the W_C values calculated from equation 3, represented by solid lines, are compared with those calculated from the density. Density derived values for α-TPI crystallized from dilute solution by the precooling method (57) are also included. Except for the structures obtained using material with $\bar{M}_n$ of 2.5 x 10^5 at a 1% (w/v) concentration at all crystallization temperatures, the density-derived crystallinities are well represented by equation 3. Choice of a C value greater than zero would yield lower calculated values for W_C of structures with $\bar{M}_n$ below 10^5.

In order to explain the molecular weight dependence of the crystallinity for melt crystallized polyethylene, poly (ethylene oxide) and poly (hexamethylene oxide) using equation 3, a decrease in U with decreasing $\bar{N}_n$ at large $\bar{N}_n$ values must be postulated. This does not necessarily mean that the average number of monomer units per fold is decreasing since U is composed of two parts and changes may be occurring in the number and/or the length of the interlamellar traverses. The decrease in W_C with decreasing $\bar{M}_n$ at low $\bar{M}_n$ would occur if C is greater than U.

Table 15. Average Number of Monomer Units per Fold and Interlamellar Traverse, U, for α-TPI from 1% (w/v) Amyl Acetate Solution

T_C - °C	$\bar{M}_n$	L^a-nm	$L_C{}^b$-nm	U
10	2.5×10^5	7.8	3.2	9.0
20	1.0×10^5	9.0	4.4	9.2
	2.5×10^5	9.0	4.1	9.7
25	1.0×10^5	11.5	5.8	11
	2.5×10^5	11.5	5.2	12
30	2.5×10^5	12.5	6.0	13

a) lamellar thickness from electron microscopy (57)

b) crystal thickness from L using equation 5.

Fig. 52. Crystalline Fraction vs Log $\bar{M}_n$ for α-TPI Structures from Amyl Acetate at T_C of 10, 20 and 25°C. (X) Crystallized by Precooling Method from 1% (w/v) Solution. (●) Crystallized Directly from 1% (w/v) Solution. (■) Crystallized by Precooling Method from 0.05% (w/v) solution. (————) calculated with Equation 3.

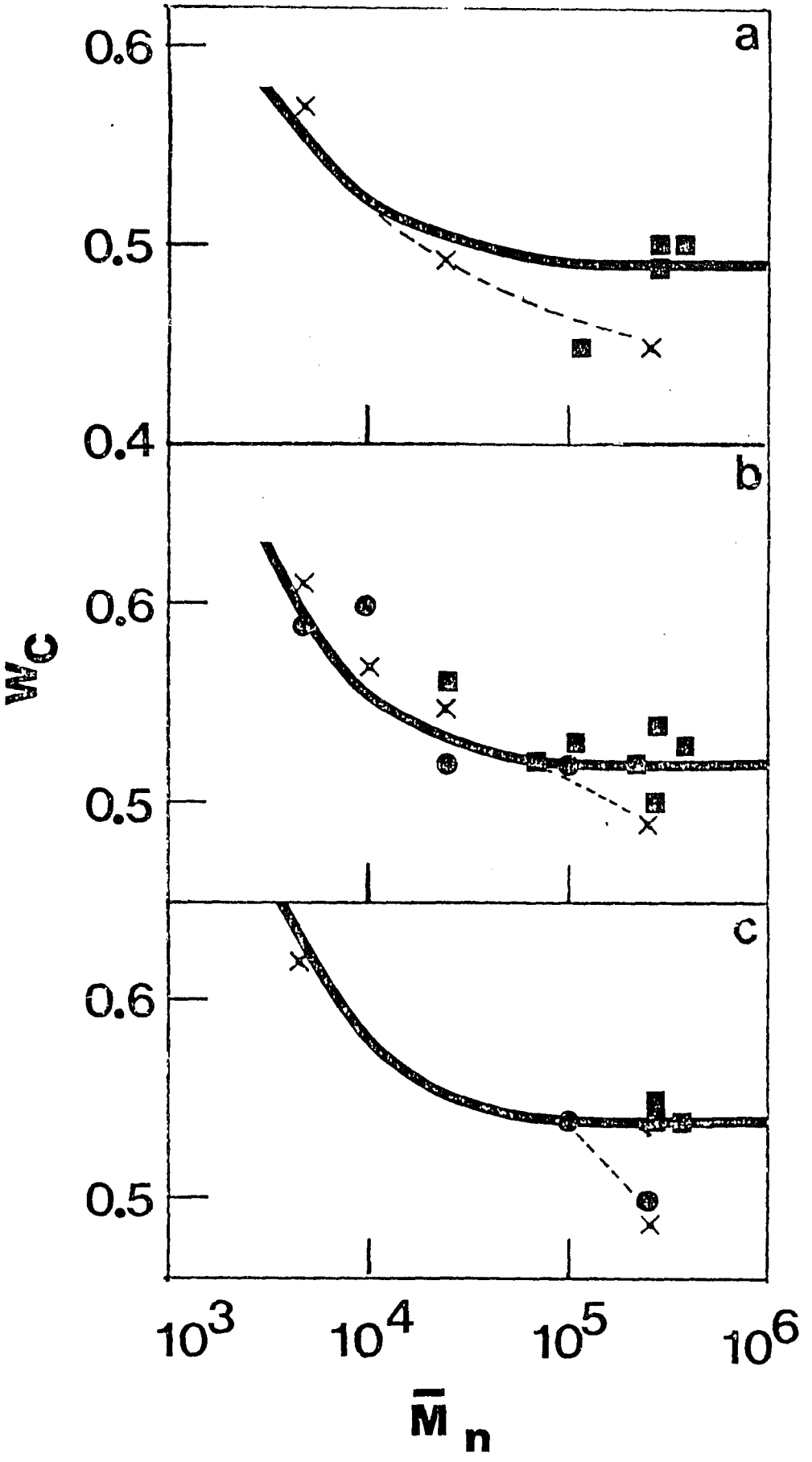
a
b
c
0.6
0.5
0.4
0.6
0.5
0.6
0.5
w_c
10^3
10^4
10^5
10^6
$\bar{M}_n$

A linear relationship between melting temperature and reciprocal of lamellar thickness of polymers has been suggested by Hoffman and Weeks (99). A superposition of results is also found for solution grown single crystals (100) and melt grown polyethylene (101) as regards the melting temperature (T_M) for a given value of lamellar thickness (L), a plot of T_M vs $\frac{1}{L}$ is linear. For TPI crystal grown from the melt, the lamellar thickness from electron microscopy and corresponding melting point data were obtained by Davis and Long (53). According to the above results for polyethylene, the lamellar thickness of TPI crystals grown from amyl acetate solution should show the same value as melt grown crystals if they have the same melting temperature.

The lamellar thickness obtained from the corresponding melting endotherm from Davis and Long's results are shown in Table 16 for the β-TPI samples grown by solution crystallization or by a solution annealing treatment with $\bar{M}_n = 2.5 \times 10^5$. The crystal thickness (L_c) and average number of monomer unit per fold and interlamellar traverse (U) are calculated from equation 5 and 4, respectively. The values of the non-crystalline fraction (F_s) from density measurement. L_c and U obtained for β-TPI at T_C or T_A's of 10 to 30°C are given in Table 16. The U values of β-TPI are found to be the same within experimental uncertainty as for β-TPI at a crystallization temperature of 10°C. The β structures annealed at

temperatures above T_C in the presence of the crystallization liquid increase in L_c with T_A but U stays essentially the same.

Table 16. Average Number of Monomer Units Per Fold and Interlamellar Traverse, U, for β-TPI from 1% (w/v) Amyl Acetate with $\bar{M}_n = 2.5 \times 10^5$

T_C (°C)	T_A (°C)	T_m (°C)	$L_{(nm)}$ [a]	$1-F_s$ [b]	F_s	$L_{c(nm)}$ [c]	U [d]
10	-	50	9.9	0.56	0.44	5.3	9
-	10	52	10.3	0.58	0.42	5.7	9
-	20	54	10.8	0.60	0.40	6.2	9
-	30	55	11.0	0.63	0.37	6.6	9

a. Lamellar thickness from ref. (53)

b. Crystalline Fraction from density measurement

c. Crystal thickness from equation 5

d. From equation 4

Epoxidation:

Epoxidation of dilute solution grown lamellae of trans-1, 4-polybutadiene and trans-1, 4-polyisoprene (TPI) in suspension at low temperature has been used to assess the average number of monomer units per fold indirectly from the fraction epoxidized and the lamellar thickness (41-45, 57) or directly by ^{13}C NMR analysis of the resulting block copolymer (102).

It was found earlier for TPBD lamellae grown from solution that F_s i.e. the degree of epoxidation was generally smaller than $1-W_c$ (from density measurement)(44). The possible causes given for that behavior were [1]: the existence of a lower density for the surface fraction as compared to the value extrapolated from the melt,[2]: the presence of partially or totally hidden folds or other defects within the crystals (103) [3]: shielding of the fold surface by absorbed polymer chains. For TPI single crystals a small decrease in total noncrystalline content does take place when these single crystals are washed repeatedly over a 1-2 month period, which suggests that either some desorption or further crystallization occurs (67). It was also found that prolonged washing of epoxidized crystals at 0°C had only a small effect on F_s although loss of material from the crystal edge was evident. Any polymer chains adsorbed on the crystals are expected to be epoxidized to a high content. Loss of these chains by desorption and removal during washing should cause a decrease in F_s. Since for epoxidized TPI lamellae F_s shows only a small decrease with extended washing, it is concluded that shielding of the surface by an adsorbed layer does not occur to any appreciate extent.

For the epoxidation method to give an accurate determination, all of the double bonds in the folds and between lamellae must react and penetration of the crystalline parts

must not occur. If the fraction epoxidized exceeds the non-crystalline fraction as determined by density, then crystal penetration has probably taken place. It is also assumed that penetration and reaction of the crystalline portion will be slower than reaction of the folds, chain ends, and interlamellar links and therefore should be detectable in a fraction of double bonds reacted vs time plot (Fig. 49).

From the results obtained in this investigation (Table 13) using hedrites in the α form, complete penetration at $[MCPBA]_{t=0}$ of 0.6 and below. At higher $[MCPBA]_{t=0}$ and polymer concentration penetration of the crystal core of at least some parts of the lamellae can take place during epoxidation.

The appreciable accessibility of double bonds within the crystals was also found on the chemical reaction of TPI single crystals by ozone degradation (55) and bromination (104). Keller and Martuscelli intended to degrade single crystals of Gutta Percha selectively by reaction with ozone and examined the resulting molecular weight distribution by GPC. From the IR analysis of the degraded material the intensity of the peak characteristics of the trans double bond, observed in the region of 750-960 cm^{-1}. Ozone reacts rapidly with the single crystals during the first 30 min. but thereafter the reaction levels off. The maximum percentage of the trans double bonds cut by the ozone is about

80%. This leads to the conclusion that about 15.2 double bonds are reacted for each fold. The bromination in carbon tetrachloride of the double bonds at the surface of suspended TPI single crystals, grown from 0.05% (w/v) amyl acetate, was also carried out at a concentration of about 0.4% polymer by weight at the temperature of 0°C and of -11°C (104). The amount of bromine disappearing was measured as a function of time using visible light absorbance measured with a spectrophotometer. The total noncrystalline fraction is about 5% higher than the values calculated from density measurement, and is consistent with our work on epoxidation at high $[MCPBA]_{t = 0}$ in the range 1.02-2.03 g/100ml amyl acetate solution epoxidized at 0°C. About 12 to 13 average numbers of monomer unit per fold have been epoxidized.

Because of the lower crystallinity (about 50%) in TPI crystals, the double bonds are attacked deep within the crystal without a clear distinction between the fold surface and the interior in contrast to the analogous studies involving polyethylene (105) and TPBD (41)-(45). The concentration is an important factor in the epoxidation reaction. It is concluded that essentially all of the noncrystalline material present can be reacted. Therefore the intramolecular defects are not appreciable and the density values can be used as a first approximation to calculate the average

number of monomer units in a non-crystalline chain sequence, U_{ℓ}, made up of folds and interlamellar links, as done above.

V. CONCLUSION

The main conclusions to be drawn from these results are as follows:

1. A morphological table of trans-1, 4-polyisoprene has been constructed as a function of molecular weight (from 2×10^4 to 3×10^5) and crystallization temperature, T_C (from -15 to 32°C), for crystallization from 1% (w/v) amyl acetate solution by a direct crystallization method. Hedrites appeared for all $\bar{M}_n$'s with degree of complexity dependent on T_C and $\bar{M}_n$. Spherulites were found at moderate T_C and high $\bar{M}_n$. Cup-shaped lamellar aggregates are found initially in trans-1,4-polyisoprene crystallization from solution under conditions of high supercooling and high or moderate $\bar{M}_n$

2. The trans-1,4-polyisoprene structures obtained from amyl acetate by the direct crystallization method are dependent on the concentration. A change of concentration from 1% (w/v) to 0.05% (w/v), causes a small increase in density and a change in morphology from spherulites to hedrites or from complex hedrites to simple hedrites.

3. The cup-shaped lamellar aggregates obtained at low T_C and high $\bar{M}_n$ after fixing with O_sO_4 were found to have a lamellar structure which is sensitive to the change of temperature or solvent. These aggregates are stabilized by

annealing in the crystallization liquid using a slow heating rate.

4. The crystal form (α or β) appearing depends on the crystallization method. The precooling crystallization method yields crystals in the α form at all temperatures, while the direct crystallization method leads to the formation of the β form at low T_C and the α modification at high T_C.

5. Normally, crystallization by the precooling technique shows a formation of single lamellae, even if from concentrated solution, and crystallization by direct crystallization technique yields multilayer crystals. However, increasing the heating rate to the redissolution temperature (T_R) after an initial crystallization can lower T_R and may result in the formation of multilayered crystals instead of seeded single lamellae. This suggests that the limiting redissolution temperature (T_{LR}) introduced by Blundell, Keller and Kovacs (88) is dependent on the molecular weight, on polymer concentration as well as on heating rate.

6. The increase in the melting endotherm temperature with increasing crystallization temperature (T_C) for α-TPI is characteristic of lamellar crystals for which the thickness increases with increasing T_C, generally, it is independent

of the crystallization method and molecular weight. The double endotherm always occurring for crystals grown at low temperatures with low molecular weight is due to the formation of different crystal thickness caused by nonisothermal crystallization. However, the double endotherm occurring for the cup-shaped lamellar aggregates is due to recrystallization during the drying process.

7. The crystallinity from density measurement is dependent on crystal form and molecular weight, but is not appreciably influenced by the crystallization method. Spherulites and cup-shaped lamellar aggregates in the β form has about 20% higher crystallinity than hedrites or overgrown lamellae in the α form when the same final (crystallization or annealing) temperature is used. An increase in crystallinity of about 20 to 30% is found with decreasing molecular weight from 2.5×10^5 to below about 10^4 for structures in both the α and β form. Crystals grown from the melt show lower crystallinity than solution grown crystals for both the α and β form.

8. Combined with #4 the crystal form is mainly changed by changing the crystallization temperature with pure α-TPI being formed at $T_C \geq 20°C$ and pure β-TPI at temperatures lower than 15°C. No evident molecular weight influence is found when amyl acetate is used as solvent. However, an

apparent molecular weight influence exists when heptane is the solvent.

9. The fraction of epoxidation occurring for TPI crystals in suspension has been quantitatively measured by 'H NMR. The degree of epoxidation found is dependent on the concentration of m-chloroperbenzoic and [MCPBA] used. The degree of epoxidation becomes constant with time in the presence of excess MCPBA but the value of this increases with increasing [MCPBA]. At high concentrations of MCPBA, the total non-crystalline fraction, as obtained from density measurement, was exceeded and damage of the crystals was noticed. The degree of epoxidation reached was also somewhat morphology dependent.

10. The average number of monomer unit per fold and inter-lamellar traverses combined (U) for α-TPI structures prepared in this work range from 9 to 13. The U values are increased with increasing T_C and a small increase in U with decreasing molecular weight. For cup-shaped lamellar aggregate β-TPI structures with $\bar{M}_n = 2.5 \times 10^5$ crystallized directly or upon annealing U value of nine was obtained.

Suggestion for further investigations:

1. A morphological table has been constructed for the first time as a function of molecular weight and crystallization temperature for solution grown crystals. It would be interesting to extend this study to other polymers such as polyethylene, trans-polybutadiene and polyethylene oxide. For solution grown crystals, it is easier to control the morphology (which can give single crystals, hedrites, spherulites or cup-shaped lamellar aggregates) than for melt grown crystals.

2. The O_sO_4 fixing technique used in this work for studying cup-shaped lamellar aggregates could be used to investigate the morphology of multilayered crystals. After O_sO_4 treatment and drying they could be investigated by scanning electron microscopy.

3. The suspension annealing method was used successfully to stabilize β-TPI aggregates without morphological damage or crystal form change. It should now be possible to study the noncrystalline fraction of the β-form by chemical methods.

4. The noncrystalline sequence length in epoxidized multilayered TPI crystals is still not well characterized; it is important to investigate the average number of monomer units per chain fold in detail. An examination by ^{13}C NMR spectra

for a series of epoxidized TPI multilayer crystals with α and β crystal structure over a wide range of molecular weight and crystallization condition would be useful in that regard.

5. Limited studies on TPI crystals grown by the evaporation of thin film from amyl acetate solution indicate that the morphology has a dependence on molecular weight and crystallization condition. This should be investigated in detail by optical and electron microscopy.

VI. REFERENCES

(1) Bryant, W. M. D., J. Polym. Sci., 2, 547 (1947).

(2) Keller, A., Phil. Mag., 2, 1171 (1957).

(3) Jaccodine, R., Nature, 176, 305 (1955).

(4) Fischer, E. W., Z. Naturforsch, 12a, 753 (1957).

(5) Till, P. H. Jr., J. Polym. Sci., 24, 301 (1957).

(6) Geil, P. H., "Polymer Single Crystals," Wiley, New York (1963).

(7) Niegisch, W. D. and Swan, P. R., J. Appl. Phys., 31, 1906 (1960).

(8) Bunn, C. W., Trans. Faraday Soc., 35, 482 (1939).

(9) Martin, G. M. and Passaglia, E., J. Res. Nat. Bur Std. (U.S.), 70A, 221 (1966).

(10) Peterlin, A., J. Macromal. Sci.Phys., B3, 19 (1969).

(11) Fischer, E. W., Goddar, H. and Schmidt, G. F. J. Polym. Sci., B5, 619 (1969).

(12) Keller, A., Martuscelli E., Priest, D. J. and Lldagawa Y., J. Polym. Sci., A2, 9, 1807 (1971).

(13) Go, S., Prudhomme, R., Stein, R. S. and Mandelkern, L., J. Polym. Sci., Polym, Phys. Ed., 12, 1185 (1974).

(14) Mandelkern, L., Go, S., Peiffer, D. and Stein, R. S., J. Polym. Sci., Polym Phys. Ed., 15, 1189 (1977).

(15) Maxfield, J. and Mandelkern, L., Macromolecules 10, 1141 (1977).

(16) Allen, R. C. and Mandelkern, L., J. Polym. Sci., Polym. Phys. Ed., 20, 1465 (1982).

(17) Bassett, D. C., Keller, A., Mitsuhasi, S. and Wills, H. H., J. Polym Sci., A, 1, 763 (1963).

(18) Blundell, D. J., Keller, A. and Kovacs, A. J., J. Polym. Sci., B 4, 481 (1966).

(19) Kovacs, A. J. and Gonthier, A., Kolloid Z. Z. Polym., 250, 530 (1972).

(20) Keller, A., Rep. Prog. Phys., part 2, 31, 623 (1968).

(21) Geil, P. H., "Growth and Perfection of Cyrstals," pp. 579-582.

(22) Keith, H. D., J. Polym. Sci., A 2, 4339 (1964).

(23) Keller, A. and Bassett, D. C., J. R. Microsc. Soc., 79, 243 (1960).

(24) Geil, P. H., J. Polym. Sci., 47, 65 (1960).

(25) Slichter, W. P., J. Appl. Phys., 31, 1865 (1961).

(26) Miller, R. L., "Crystalline Olefin Polymers," pp. 577, Wiley, New York (1965).

(27) Geil, P. H., Polym. Rev. 5 (1963).

(28) Bassett, D. C., "Principles of Polymer Morphology," Cambridge Univ. Press, London (1981).

(29) Wunderlich, B., "Macromolecular Physics," Vol. 1, Academic Press, New York (1973).

(30) Alexander, L. E., "X-Ray Diffraction Methods in Polymer Science," Wiley, New York (1969).

(31) Hamada, F., Wunderlich, B., Sumida, T., Hayashi, S. and Nakajima, A., J. Phys. Chem. 172, 178 (1968).

(32) Anderson, F. R. and Holland, V. F., J. Appl Phys., 31, 1516 (1960).

(33) Anderson, F. R., J. Appl. Phys., 34, 2371 (1963).

(34) Keller, A., Matreyek, W. and Winslow, F. H., J. Polym. Sci., 62, 291 (1962).

(35) Harrison, I. R. and Baer, E., J. Polym Sci., A-2, 9, 1305 (1971).

(36) Harrison, I. R. and Baer, E., J. Colloid Interface Sci., 31, 176 (1969).

(37) Nickerson, R. F. and Habrle, J. A., Ind. Eng. Chem., 39, 1507 (1947).

(38) Sharples, A., Trans. Faraday Soc., 52, 1003 (1956), 53, 913 (1957).

(39) Palmer, R. P. and Cobbold, A. J., Makromol. Chem. 74, 174 (1964).

(40) Priest, D. J., J. Polym. Sci., A-2, 9, 1977 (1971).

(41) Stellman, J. M. and Woodward, A. E., J. Polym. Sci., B, 7, 755 (1969), J. Polym. Sci., A-2, 9, 59 (1971).

(42) Hendrix, C., Whiting, D. A. and Woodward, A. E., Macromolecules, 4, 57 (1971).

(43) Wichacheewa, P. and Woodward, A. E., J. Polym. Sci., Polym. Phys. Ed., 16, 1849 (1978).

(44) Tseng, S., Herman, W., Woodward, A. E. and Newman, B. A., Macromolecules, 15, 338 (1982).

(45) Tseng, S. and Woodward, A. E., Macromolecules, 15, 343 (1982).

(46) Marchetti, A. and Martuscelli, F., J. Polym. Sci., Polym. Phys. Ed., 14, 151 (1976).

(47) Schuur, G., J. Polym. Sci., 11, 385 (1935).

(48) Bunn, C. W., Proc. Roy. Soc., Lond., A, 180, 40 (1942).

(49) Fisher, D., Proc. Phys. Soc., Lond., 66, 7 (1953).

(50) Takahashi, Y., Sata, T., Tadokoro, H. and Tanaka, Y., J. Polym. Sci., 11, 233 (1973).

(51) Davis, C. K. L. and Long, O. E., J. Mater, Sci., 12, 2165 (1977).

(52) Keller, A. and Warning, J. R. S., J. Polym. Sci., 17, 447 (1955).

(53) Davis, C. K. L. and Long, O. E., J. Mater. Sci. 14, 2529 (1979).

(54) Martuscelli, E., Makromol. Chem., 151, 159 (1972).

(55) Keller, A. and Martuscelli, E., Makromol. Chem., 151, 189 (1972).

(56) Litsunomiya, H., Mori, T., Imada, K. and Takayanago, M., Rep. Prog. Polymer Phys., Japan, 11, 153 (1968).

(57) Anandakumaran, K., Herman, W. and Woodward, A. E., Macromolecules, 16, 563 (1983).

(58) Schlesinger, W. and Leeper, H. M., J. Polym. Sci. 11, 203 (1953).

(59) Eirich, F. R., "Science and Technology of Rubber," Academic Press, New York (1978).

(60) Francis, P. S., Coake, R. C. Jr. and Elliott, J. H., J. Polymer Sci., 31, 453 (1958).

(61) Cooper, W. and Vaughan, G., Polymer, 4, 329 (1963).

(62) Woodward, A. E., 5, 293 (1964).

(63) Khoury, F. and Barnes, J. D., J. Res. Nat. Bur. Std. (U.S.), 76A, 225 (1972).

(64) Khoury, F. and Barnes, J. D., J. Res. Nat. Bur. Std. (U.S.) 78A, 95 (1974).

(65) Barnes, J. D. and Khoury, F., J. Res. Nat. Bur. Std. (U.S.) 78A, 363 (1974).

(66) Kawai, T. and Keller, A., J. Polym. Sci., B3, 333, 1964).

(67) Sadler, D. M., J. Polym. Sci., A-2 9, 779 (1971).

(68) Sanchez, I. C. and Dinancio, E. A., J. Res. Nat. Bur. Std. (U.S.) 76A, 213 (1972).

(69) Mandelkern, L., Quinn, J. A. and Roberts, D. E., J. Am. Chem. Soc., 78, 926 (1956).

(70) Dreyfuss and Kennedy, J. P., Anal. Chem., 47, 771 (1975).

(71) Tutorski, I. A., Khodzhayeva, I. D. and Dogadkin, B. A., Vysokomol Soyed, A16, 157 (1974).

(72) Wunderlich, B., and Sullivan, P., J. Polym. Soc., 61, 195 (1962).

(73) Keller, A., Kolloid, A. A., Polym. 219 118 (1967).

(74) Mandelkern, L., Glotin, M. and Benson, R. A., Macromolecules 14, 22 (1981).

(75) Mikailov, M., Nedkov, E. and Goshev, I., J. Macromel, Sci. Phys., B15, 313 (1978).

(76) Wunderlich, B., James, E. A. and Shu, T. W., J. Polym. Sci., A2, 2759 (1964).

(77) Rybnikar, F., J. Macromol., Sci. Phys., B11 329 (1975).

(78) Lovering, E. G. and Wooden, D.C., J. Polym. Sci., A2 7, 1639 (1969).

(79) Leeper, H. M. and Schlesinger, W., J. Polym. Sci., 11, 307 (1953).

(80) Statton, W. O., J. Appl. Phys., 32, 2332 (1961).

(81) Geil, P. H., "Plymer Single Crystals," Chapter V, Wiley, New York (1964).

(82) Bassett, D. C. and Keller, A., Phil. Mag., 7, 1553 (1962).

(83) Holland, V. F., J. Appl. Phys., 35, 59 (1964).

(84) Wunderlich, B. J., Polym. Sci., A1, 3581 (1963).

(85) Magill, J. H., J. Polym. Sci. Polym Letter Ed., 20, 1 (1982).

(86) Magill, J., Girolamo M. and Keller, A., Polymer 22, 43 (1981).

(87) Wunderlich, B., "Macromolecular Physics," Vol. 2, Academic Press, New York (1976).

(88) Blundel, D. J., Keller, A. and Kovacs, A. J., J. Polym. Sci., B4, 481 (1966).

(89) Keller, A. and Willmouth, F. M., J. Polym. Sci., A2, 8, 1443 (1970).

(90) Lovering, E. G. and Wooden, D. C., J. Polym. Sci., A2, 9, 175 (1971).

(91) Banks, W., Gordon, M., Roe, R. J. and Sharples, A., Polymer 4, 61 (1963).

(92) Fatou, J. G. and Mandelkern, L., J. Phys. Chem., 69. 447 (1965).

(93) Maclaine, J. Q. G. and Booth, C., Polymer, 16, 680 (1975).

(94) Se, K., Adachi, K. and Kotaka, T., Polymer J., 13, 1009 (1981).

(95) Marcro, C., Fatou, J. G. and Bello, A., Polymer 18, 1100 (1977).

(96) Macro, C., Fatou, J. T., Bello, A. and Blanco, A., Polymer 20, 1250 (1979).

(97) Hamada, F., Wunderlich, B., Sumida, T., Hayashi, S. and Nakajima, A., J. Phys. Chem, , 72, 178 (1968).

(98) Bassett, D. C. and Keller, A., Phil Mag., 7, 1553 (1962).

(99) Hoffman, J. D. and Weeks, J. J., J. Res. Nat'l. Bur. Stad. (U.S.) A66, 13 (1962).

(100) Huseby, T. W. and Bair, H. E. J. Appl. Phys., 39, 4969 (1968).

(101) Brown, R. G. and Eby, R. K., J. Appl. Phys., 35, 1156 (1964).

(102) Schilling, F. C., Bovey, F. A., Tseng, S. and Woodward, A. E., Macromolecules, 16 808 (1983).

(103) Patel, G. N. and Keller, A., J. Polym. Sci. Polym. Phys. Ed., 13, 2259 (1975).

(104) Taylor, M., Thesis Report, City College, New York, 1982.

(105) Patel, G. N., "Method of Experimental Physics," Vol. 16, Part 13, Academic Press (1980).